ผลกระทบจากแผ่นดินทรุดที่มีต่อฐานรากแพเสาเข็ม

นายจาน ทวน วาน

วิทยานิพนธ์นี้เป็นส่วนหนึ่งของการศึกษาตามหลักสูตรปริญญาวิศวกรรมศาสตร์ดุษฎีบัณฑิต
สาขาวิศวกรรมโยธา ภาควิชาวิศวกรรมโยธา
คณะวิศวกรรมศาสตร์ จุฬาลงกรณ์มหาวิทยาลัย
ปีการศึกษา 2555

EFFECT OF GROUND SUBSIDENCE ON PILED RAFT FOUNDATION

Mr. Tran Tuan Van

A Dissertation Submitted in Partial Fulfillment of the Requirements
for the Degree of Doctor of Philosophy Program in Civil Engineering
Department of Civil Engineering
Faculty of Engineering
Chulalongkorn University
Academic 2012

Thesis Title	EFFECT OF GROUND SUBSIDENCE ON PILED RAFT FOUNDATION
By	Mr. Tran Tuan Van
Field of Study	Civil Engineering
Thesis Advisor	Associate Professor Tirawat Boonyatee, D. Eng.
Thesis Co-advisor	Professor Makoto Kimura, D. Eng.

Accepted by the Faculty of Engineering, Chulalongkorn University in Partial Fulfillment of the Requirements for the Doctoral Degree

……Dean of the Faculty of Engineering
(Associate Professor Boonsom Lerdhirunwong, Dr. Ing.)

THESIS COMMITTEE

…….Chairman
(Associate Professor Wanchai Teparaksa, D. Eng.)

…….Thesis Advisor
(Associate Professor Tirawat Boonyatee, D. Eng.)

…….Thesis Co-advisor
(Professor Makoto Kimura, D. Eng.)

…….Examiner
(Associate Professor Suched Likitlersuang, Ph. D.)

……Examiner
(Associate Professor Boonchai Ukritchon, Sc. D.)

……External Examiner
(Associate Professor Noppadol Phien-wej, Sc. D.)

จาน ทวน วาน: ผลกระทบจากแผ่นดินทรุดที่มีต่อฐานรากแพเสาเข็ม (EFFECT OF GROUND SUBSIDENCE ON PILED RAFT FOUNDATION). อ.ที่ปรึกษาวิทยานิพนธ์หลัก : รศ.ดร. ฐิรวัตร บุญญะฐี, อ.ที่ปรึกษาวิทยานิพนธ์ร่วม :ศ.ดร. มาโกโต คิมูระ, 172 หน้า.

ที่ผ่านมาได้มีการศึกษาวิจัยเกี่ยวกับฐานรากแพเสาเข็มเป็นจำนวนมากแต่การประเมินพฤติกรรมของฐานรากดังกล่าวในสภาพแผ่นดินทรุดก็ยังทำได้ยาก การศึกษานี้ได้ใช้แบบจำลองหมุนเหวี่ยงและระเบียบวิธีวิเคราะห์แบบไฟไนต์อิลิเมนต์ในการศึกษาผลกระทบจากแผ่นดินทรุดที่มีต่อฐานรากแพเสาเข็มโดยมุ่งเน้นไปยังการเปลี่ยนแปลงของการกระจายแรงระหว่างฐานรากแพและเสาเข็ม การทรุดตัวของฐานรากในขณะที่แผ่นดินทรุดและโมเมนต์และแรงเฉือนที่เกิดในฐานรากแพ

การทดสอบโดยแบบจำลองหมุนเหวี่ยงกระทำภายใต้แรงโน้มถ่วงเท่ากับ 50g โดยใช้แบบจำลองฐานรากสามแบบซึ่งได้แก่แบบจำลองฐานรากแพ ฐานรากแพเสาเข็มที่มีระยะห่างระหว่างเสาเข็มเท่ากับสองเท่าของเส้นผ่านศูนย์กลางเสาเข็ม และ ฐานรากแพเสาเข็มที่มีระยะห่างระหว่างเสาเข็มเท่ากับสี่เท่าของเส้นผ่านศูนย์กลางเสาเข็ม ในการศึกษานี้ได้ทดสอบโดยใช้แบบจำลองฐานรากทั้งสามแบบภายใต้สภาพชั้นดินสองแบบรวมเป็นการทดลองทั้งสิ้นหกกรณี จากผลการทดลองพบว่าการทรุดตัวของฐานรากมีค่าเพิ่มขึ้นเป็นสัดส่วนกับการทรุดตัวของชั้นดิน และเมื่อระยะห่างระหว่างเสาเข็มเพิ่มมากขึ้น การทรุดตัวของฐานรากจะมีค่าเพิ่มขึ้นโดยที่หน่วยแรงที่เกิดขึ้นภายในเสาเข็มจะมีค่าเพิ่มขึ้นด้วย นอกจากนี้ยังพบว่าแรงเสียดทานผิวเชิงลบที่เกิดขึ้นกับเสาเข็มแบบแบกทานมีค่าสูงกว่าแรงเสียดทานผิวเชิงลบที่เกิดในเสาเข็มเสียดทานเป็นอย่างมาก

นอกจากการทดสอบด้วยแบบจำลองหมุนเหวี่ยงแล้ว ยังได้ศึกษาเชิงพารามิเตอร์ด้วยระเบียบวิธีไฟไนต์อิลิเมนต์โดยใช้โปรแกรม Plaxis 3D ในการศึกษาครั้งนี้ได้จำลองพฤติกรรมภายใต้สภาพระบายน้ำโดยใช้พารามิเตอร์แบบหน่วยแรงประสิทธิผล สำหรับแบบจำลองที่ใช้ประกอบด้วยแบบจำลองของการทดสอบหมุนเหวี่ยงและแบบจำลองของฐานรากแพเสาเข็มที่มีความลึกของชั้นใต้ดินแตกต่างกันอีก 3 แบบ จากการวิเคราะห์พบว่าจำนวนเสาเข็มในฐานราก ค่าโมดูลัสของยังค์ของชั้นดิน รูปแบบของแรงกระทำ ความหนาของฐานรากแพ ระยะห่างระหว่างเสาเข็ม และการเปลี่ยนแปลงระดับน้ำใต้ดิน เป็นปัจจัยที่มีผลกระทบอย่างมากต่อการทรุดตัวของฐานราก การกระจายแรงระหว่างฐานรากแพและเสาเข็ม หน่วยแรงที่เกิดขึ้นในเสาเข็ม และลักษณะการทรุดตัวที่แตกต่างกันตามตำแหน่งต่างๆ ในฐานราก

ภาควิชา: วิศวกรรมโยธา ..... ลายมือชื่อนิสิต .....

สาขาวิชา: วิศวกรรมโยธา ..... ลายมือชื่ออาจารย์ที่ปรึกษาวิทยานิพนธ์หลัก .....

ปีการศึกษา: 2555 ..... ลายมือชื่ออาจารย์ที่ปรึกษาวิทยานิพนธ์ร่วม .....

5271853221: MAJOR CIVIL ENGINEERING
KEYWORDS: PILED RAFT/ SOFT SOIL/ GROUND SUBSIDENCE/ FE ANALYSIS / CENTRIFUGAL TEST

TRAN TUAN VAN: EFFECT OF GROUND SUBSIDENCE ON PILED RAFT FOUNDATION. ADVISOR: ASSOC. PROF. TIRAWAT BOONYATEE, D. Eng., CO-ADVISOR: PROF. MAKOTO KIMURA, D. Eng. 172 pp.

Extensive researches for piled rafts have been performed but the evaluation of their behavior in ground subsidence condition is still a challenge. In this study, centrifugal tests and finite element (FE) analyses were performed in order to investigate the effect of ground subsidence on load distribution between piles and raft, foundation settlement as well as moment and shear in raft.

Six cases of centrifugal tests consisted of group 1 (soil condition 1) with case 1: raft alone, case 2: piled raft (s = 2d), case 3: piled raft (s = 4d) and group 2 (soil condition 2) with case 4: raft alone, case 5: friction piled raft (s = 4d), case 6: end-bearing piled raft (s = 4d) were conducted under centrifugal force field of 50g. The centrifugal test results can be concluded as followed; 1) foundations settled almost linearly with ground subsidence, 2) as piled spacing increases, settlement of foundation increases and axial load of piles increases, 3) negative skin friction of end-bearing piled raft was much larger than that of friction piled raft in ground subsidence condition.

After centrifugal tests had been conducted, parametric studies were made for centrifugal piled raft models and three cases of piled rafts on Bangkok soil (case 1, case 3 and case 3 with levels of raft at -15 m, -7.5 m and + 0.0 m, respectively) under ground subsidence condition by a commercial finite element analysis program (Plaxis 3D). The calculations were done by drained, plastic analysis with effective parameters. Results showed that load-settlement curves, load distributions between piles and raft, axial force of piles, average and differential settlements, raft moment and shear were significantly affected by number of piles, Young's modulus of soil, pattern of loads, raft thickness, piled spacing and ground water levels.

Department: ……Civil engineering…..... Student's Signature ……..…...……
Field of Study: …Civil engineering……... Advisor's Signature ……..…….……...
Academic Year: ……2012…….……. Co-advisor's Signature ..…….……...

ACKNOWLEDGEMENTS

This study was carried out under the supervisions of Professor Makoto Kimura and Associate Professor Tirawat Boonyatee. I gratefully acknowledge the sharing of advisors' practical experiences for the study, and also permission to present the results. I would also like to acknowledge Dr. Le Ba Vinh for his assistance and encouragement in completing my research. I will also never forget the kind help of Professor Le Ba Luong, Dr. Vo Phan and Dr. Chau Ngoc An who introduced me to AUN/SEED-Net scholarship throughout this research.

I would like to thank Dr. Wanchai Teparaksa, Dr. Boonchai Ukritchon, Dr. Suched Likitlersuang, Dr. Noppadol Phien-wej and Dr. Supot Teachavorasinskun who gave an enthusiastic help and constructive comments during I performed the research and wrote the thesis as well. I would like to thank Mr. Teramoto Shuntaro who worked with me during centrifugal test and friends in Kimura's Lab who help me during the time I stayed in Japan.

Let me allow to thank Ms. Kalayaporn, Ms. Namba Sachiko and Ms. Maria Tsunosue who have helped me in communication. Their honest characteristics gave me good lessons in my lifestyle. I would like to thank all member of Geotechnical Lab in Chulalongkorn University for their willingness and patience to help me when I lived in Thailand. I would also like to thank people who established the AUN/SEED-Net program which gave me a good chance to study in Chulalongkorn University and Kyoto University.

Finally, I would like to thank my family and Vietnamese friends for giving encouragement and support to me. Without their encouragement and support, I would not be able to complete my research.

I would like to express my gratitude to Japan International Cooperation Agency (JICA) for the financial support and bringing me to Thailand and Japan.

CONTENTS

LIST OF TABLES

LIST OF FIGURES

LIST OF ABBREVIATIONS

a	Radius of circular raft
A_g	Total area covered by piled group
A_p	Sum of cross-sectional areas of piles in group
B	Width of rectangular raft
c_i	Correction factors for piled group efficiency exponent
d	Diameter of pile
d_{eq}	Diameter of equivalent pier
e	Exponent in calculation of piled group efficiency
E_{eq}	Young's modulus of equivalent pier
E_p	Young's modulus of piled (assumed solid)
E_r	Young's modulus of raft or piled cap
E_s	Young's modulus of soil
f	Parameter in modified hyperbolic stress-strain curves
F_D	Embedment correction factor for raft settlement
g	Parameter in modified hyperbolic stress-strain curves
G	Shear modulus of soil
G^*	Normalised modified shear modulus adjacent to piled shaft
G_{ave}	Average shear modulus of soil along pile length
G_b	Shear modulus of soil below piled base
G_l	Shear modulus of soil at full penetration of piled shaft
G_0	Initial tangent shear modulus of soil
h_i	Thickness of soil layer
I_D	Relative density
I_ρ	Influenced factor for vertical displacement (raft)
I_ε	Influence factor for calculation of vertical strain
k_i	Stiffness of i^{th} foundation unit (load divided by settlement)
k_p	Pile or pier stiffness (load divided by settlement)
k_{pr}	Piled raft stiffness (load divided by settlement)
k_r	Raft stiffness (load divided by settlement)

K_0	At rest earth pressure coefficient
K_{rc}	Relative raft-soil stiffness ratio for circular rafts
K_{rs}	Relative raft-soil stiffness ratio for rectangular rafts
l	Embedded length of pile
L	Length of rectangular raft
m	Parameter in parabolic load transfer curves
n	Number of piles in group
N	SPT blow-count
OCR	Overconsolidation ratio
p'	Mean effective stress
p_a	Atmospheric pressure (100 kPa)
P_{av}	Uniformly load on circled raft
P_b	Base load for single pile
P_p	Load carried by pile group
P_s	Shaft load for single pile
P_t	Total load at piled head
q	Applied pressure
q_b	Eng-bearing pressure
q_c	Cone resistance
Q_p	Ultimate base capacity
Q_s	Ultimate shaft capacity
Q_t	Ultimate pile capacity
r_c	Radius of piled cap (single pile)
r_m	Maximum radius of influence of pile
r_0	Piled radius
R	Aspect ratio of piled group
R^*	Normalised radius of zone of modified soil
R_f	Parameter in hyperbolic curve
R_s	Piled group settlement ratio
s	Centre-line spacing of piles
t	Thickness of raft

w_b	Displacement of piled base
w_p	Average displacement of piled group
w_r	Average displacement of raft
w_s	Displacement of piled shaft
w_t	Displacement of piled top
z	Depth co-ordinate
α_{ij}	Interaction factor between foundation units i and j
α_{pr}	Interaction factor between piled group and raft
α_{rp}	Interaction factor between raft and piled group
Δ	Increment
ζ	Load transfer parameter for pile shaft
η	Piled group efficiency; ratio of piled base radius to shaft radius
λ	Pile-soil stiffness ratio, E_p/G_l
μ	Parameter in solution for single pile response
ν	Poission's ratio of soil
ξ	Parameter for piled base flexibility
ρ	Parameter for relative homogeneity of soil modulus
σ'_{vo}	Vertical effective stress
τ	Shear stress
τ_ϕ	Failure shear stress
τ_o	Shear stress at pile-soil interface
τ_s	Limiting shaft friction
ψ	Parameter in non-linear load transfer response of piled shaft

CHAPTER I

INTRODUCTION

1.1 Background

Due to the pumping of large amount of ground water for water supply, ground subsidence has occurred at some cities such as Bangkok, Ho Chi Minh, Shanghai, Mexico, etc (Poulos, 2008). Effects of land subsidence from deep well pumping on differential settlement of many buildings in Bangkok area are reported in Phienwej et al. (2004). Comparison of ground water pumping rate and ground surface subsidence rate of Shanghai City and some results of ground subsidence observed in Ho Chi Minh area were presented in Le and Ho (2008).

A pile used in ground subsidence condition will be subjected to negative skin friction. As discussed by Poulos (2008) and Fellenius (1998, 2006), among many others, two key issues relating to negative skin friction are: (1) Additional axial forces (drag force) and (2) additional settlement (downdrag or drag settlement). Some suggestions for designing of piles and piled groups considering capacity, settlement and negative skin friction were presented in Goudreault et al. (1995).

Raft foundations are widely used for civil structures in construction industry such as industrial chimney (Turner, 2000), tower blocks (Morrison, 2000), buildings (Cracknell, 2000), immersed tube tunnel or foundation of mass rapid transit authority (Apted et al., 2000), etc. The use of raft foundation in soils with low bearing pressure gives some advantage (Gupta, 1997): (1) increasing ultimate bearing capacity with increasing width of the foundation. (2) Settlement decreases with increased depth. (3) Decreasing differential settlement. However, for high-rise buildings or civil structures where heavy loads are faced, the capacity of raft foundation may be unsatisfied or large settlements (average or differential settlements) of foundation need to be solved.

Nowadays, piled raft foundations have been used to support for many kinds of buildings in stiff soils (Frank et al., 2000) and in soft soils (Tan el al., 2004 and 2006). As pointed out in Katzenbach et al. (2000), the load-bearing behavior of a piled raft foundation is characterized by four interactions including: (1) soil – pile, (2) pile – pile, (3) soil – raft and (4) pile – raft. The interaction effects between adjacent piles and between the piles and raft are two principle factors which indicate that behavior of

the piles as part of a piled raft differs essentially from that of a comparable single isolated pile. Therefore, an important requirement for a reliable design of piled raft is in which both four above interactions should be taken account.

Several research works relating to interaction effects between adjacent piles in piled raft foundations such as Randolph (1994), Burland (1995), Katzenbach et al. (2000), Poulos (2000, 2001a and 2001b), Prakoso et al. (2001), Seo et al. (2003), Gobinath et al. (2010), etc, have been published during past decades.

Generally, the most economical design of piled raft, as presented by Randolph (1994), is that the raft itself can adequately support the loads of the structures and the piles are added to limit the total and differential settlements of the foundation within allowable margins. In other words, the piles should be designed so that their bearing capacity is fully mobilized at working load. Hemsley (2000) presents some examples of the use of piled raft with piles as settlement reducers in different types of soils.

In the regard of piles as settlement reducers, piled load share (load carried by the piles in piled raft) is the most important factor to estimate the settlement of the foundations. Some researched works (Vincenzo et al., 2008; Y. El-Mossallamy, 2008; Katzenbach et al., 2000, etc.) have presented and given explanations on this relationship. However, few experimental data can be found in literature and no many works focused on foundations under the effects of ground subsidence condition.

For cases where the piled raft are constructed on the soils subjecting to ground subsidence, the response of the foundation to the loads of superstructures may be changed because of changing in ground condition. Some components of capacity and settlements which influence on the response of the foundation are (1) load-settlement relationship, (2) axial forces in piles, (3) load distribution and average and differential settlements, (4) Bending moment and shear force in raft. Most of the recent research works has been performed for piled rafts on soils where ground subsidence has not occurred, and the reliable design of piled raft in which both four types of interactions are taken account in ground subsidence condition is still a challenge.

1.2 Objectives

The overall objective of this study is to investigate the effect of ground subsidence,

causing by pumping of ground water, on load distributions, settlements, and raft bending moment and shear of piled raft in ground subsidence condition.

In order to achieve the above objective, the following sub-objectives should be obtained.

(1) Review the use of simplified methods for analysis of response of piled raft in normal condition.
(2) Analysis of response of piled raft in ground subsidence condition using centrifugal test.
(3) Analysis of response of piled raft in ground subsidence condition using FE method.

1.3 Thesis Layout

The thesis is presented in the following five chapters.

Chapter 2 presents a brief review of previous research work on piles raft foundations. The review also presents the cases of foundations affected by ground subsidence causing by ground water pumping.

Chapter 3 presents the simplified methods for analysis of piled raft. Poulos-Davis-Randolph (PDR) method and Modifications of PDR method are presented in details.

Chapter 4 shows the results of centrifugal analysis of model piled raft in ground subsidence condition. Some results relating to load-settlement curves, distribution of axial force and distribution of pore water pressures is presented in detail.

Chapter 5 presents the numerical analyses of piled raft in ground subsidence condition. Geotechnical parameters assessment, verification analysis and applied numerical method to analysis three cases of piled raft in Bangkok soil are shown in details.

Chapter 6 summarizes the main conclusion drawn from this research work and recommends for future research work in this field.

CHAPTER II

LITERATURE REVIEW

2.1 Introduction

This chapter comes up with five parts. First part is a brief review of piled raft foundation which is included concept of piled raft, condition for selection piled raft, design philosophies, methods of analysis of piled raft and cases histories using of piled raft. Second part presents the review of ground surface subsidence problems. Third and fourth parts show the capacities of centrifugal test and FE analysis, respectively. Final part presents a case of piled raft in Bangkok soil.

2.2 Piled Raft Foundation

2.2.1 Concept of piled raft

When a raft does not satisfy the design requirements, the piles may be introduced to improve the ultimate load capacity, overall settlement and differential settlement, and the required thickness of the raft. Both the raft and the piles are used in such a foundation, and it is referred as a piled raft. This concept of piled raft has been described by Poulos (2001a, 2001b) as well as many other researchers, and can be schemed as in Figure 2.1. Figure 2.2 shows some examples of raft, piled raft and piled foundations in Frankfurt, Germany.

Piled raft is a geotechnical composite foundation composing of three bearing elements: piles, raft and subsoil. The bearing behavior of a piled raft, therefore, depends on the interaction between the elements of foundation and subsoil. Katzenbach et al. (2000) has defined four types of interaction as illustrated in Figure 2.3, and it is necessary to be taken into account in the analysis of behavior of piled rafts.

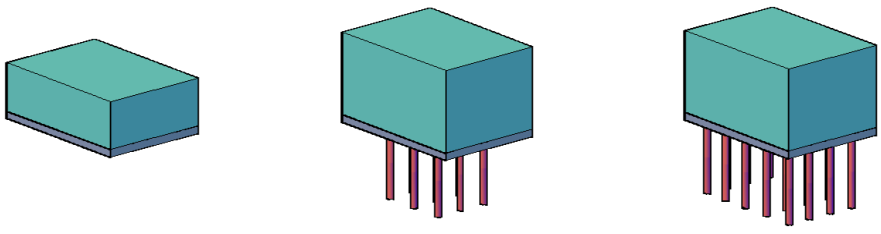

Raft foundation Piled raft foundation Piled foundation

Figure 2.1 Raft, piled raft and piled group foundations

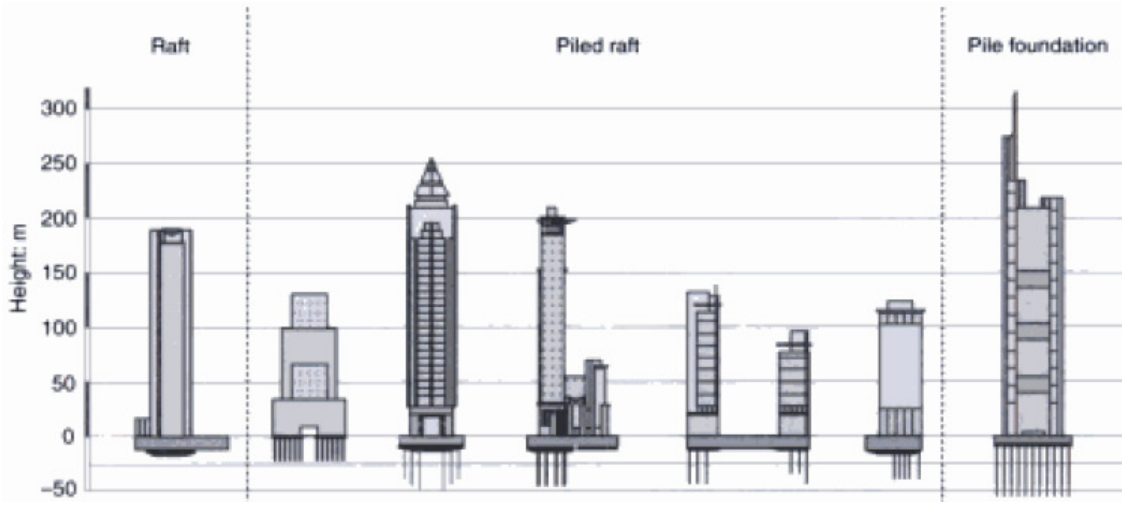

Figure 2.2 Raft, piled raft and piled foundations in Frankfurt, Germany (Frank et al., 2000)

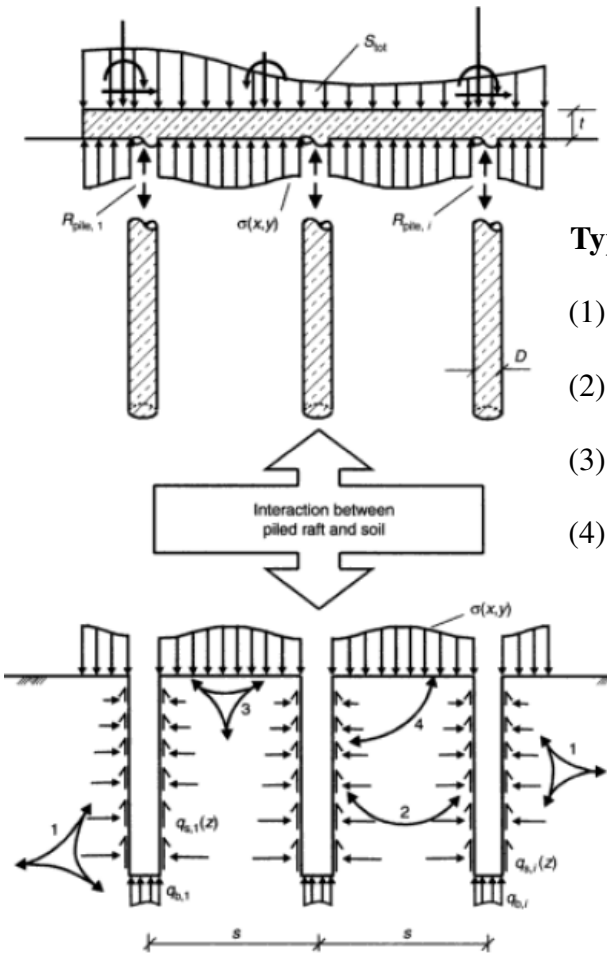

Types of interaction:

(1) soil-pile interaction

(2) pile-pile interaction

(3) soil-raft interaction

(4) pile-raft interaction

Figure 2.3 Soil-structure interaction for piled raft foundations (Katzenbach et al., 2000)

In design of piled rafts, five issues are necessary to be considered, including:

(1) Ultimate load capacity for vertical, lateral and moment loadings.
(2) Maximum settlement.
(3) Differential settlement.
(4) Raft moments and shears for the structural design of the raft.
(5) Pile loads and moments, for the structural design of the piles.

2.2.2 Conditions for selection of piled raft

Franke et al. (2000) suggests a procedure for selection of piled rafts as shown in Figure 2.4. The piled raft can be chosen if a raft alone has an inadequate factor of safety against failure, or would damage from excessive total or differential settlements.

Poulos (2000) points out the subsoil conditions where are favourable and unfavourable for piled rafts as below.

(1) For favourable situations
    (a) Soil profiles consisting of relatively stiff clays.
    (b) Soil profiles consisting of relatively dense sands.

(2) For unfavourable situations
    (a) Soil profiles containing soft clays near the surface.
    (b) Soil profiles containing loose sands near the surface.
    (c) Soil profiles which contain soft compressible layers at relatively shallow depths.
    (d) Soil profiles which are likely to undergo consolidation settlements due to external causes.
    (e) Soil profiles which are likely to undergo swelling movements due to external causes.

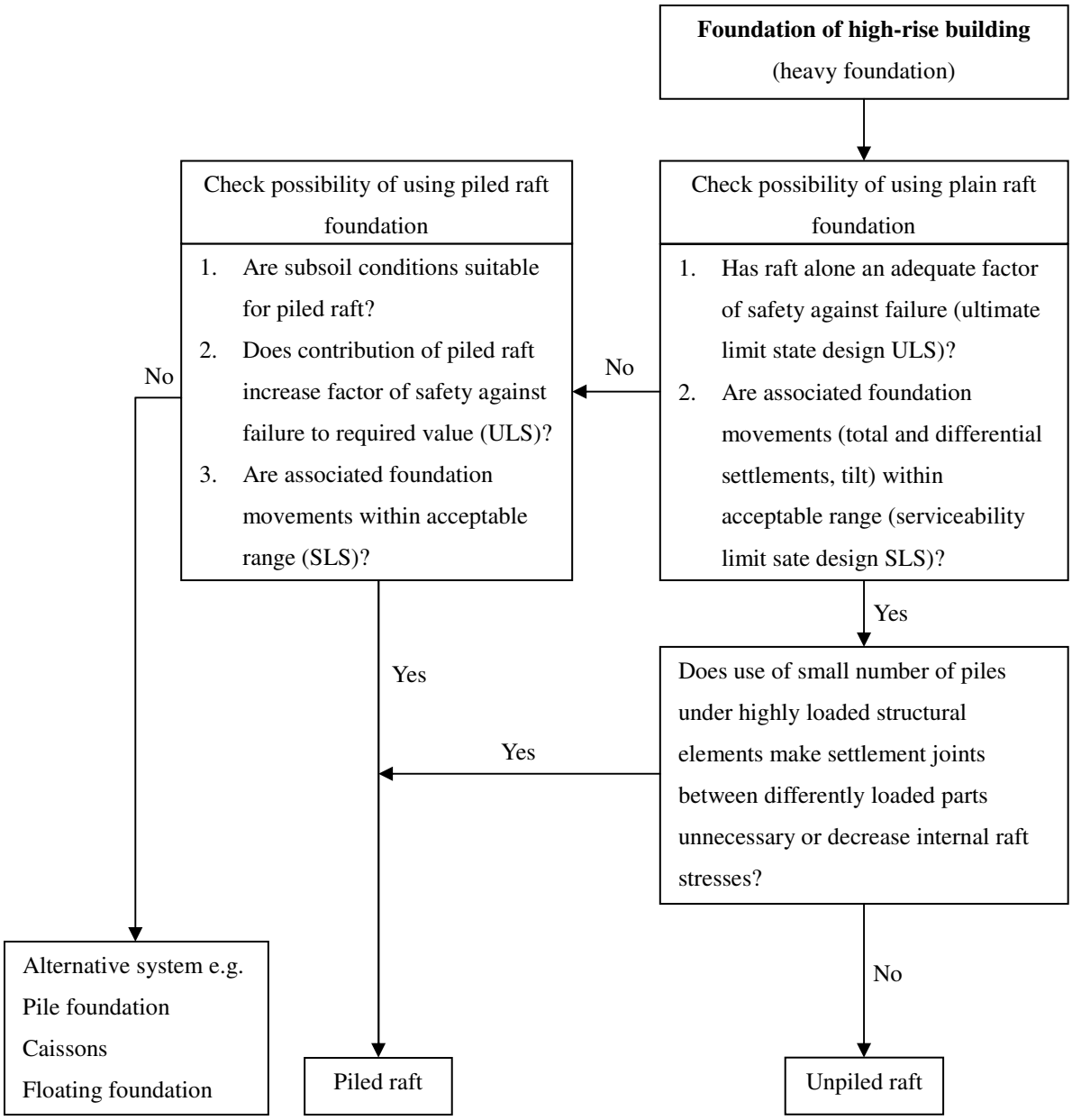

Figure 2.4 Selection procedure for design of plain and piled raft foundations (Franke et al., 2000)

2.2.3 Design philosophies

There are three different design philosophies for piled raft foundations summarized by Poulos (2000). He shows that the design of piles for supporting the raft can be based on conventional, creep piling or differential settlement control philosophies. He also notes the piles designed to act as settlement reducers (in creep piling philosophy) give the most economical solution.

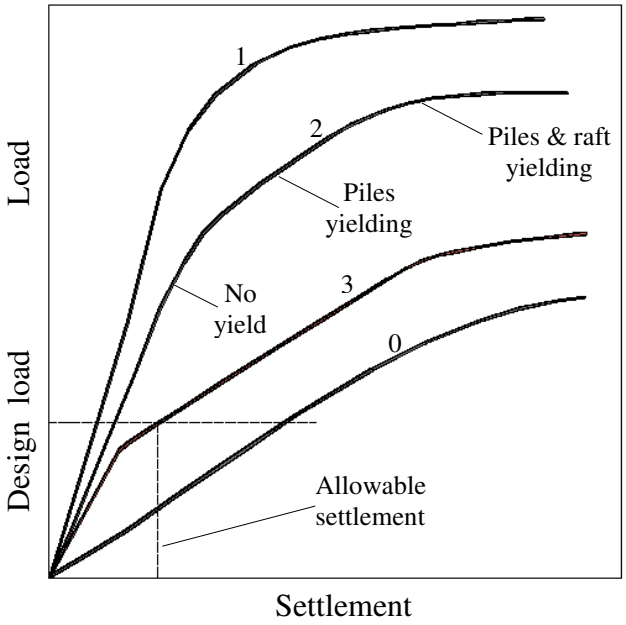

Figure 2.5 Load-settlement curves for piled rafts according to various design philosophies (Poulos, 2000)

The first two design strategies are shown in Figure 2.5, in which curve 3 presents the piles are designed as settlement reducers. The third strategy is explored by Randolph (1994), Horikoshi et al. (1996, 1998) and Ruel et al. (2004). An effective approach to reducing differential settlements for uniformly loaded raft is to locate a few piles over the central region 16-25% of the raft, discussed by Horikoshi et al. (1998). The use of piled rafts with different pile lengths gives an optimum design for the cases of non-uniform vertical loads, as suggested by Ruel et al. (2004).

Poulos (2001b) suggests a rational design process for piled rafts which includes three main stages:

(1) A preliminary stage to assess the feasibility to using a piled raft, and the required number of piles to satisfy design requirements.
(2) A second stage to assess where piles are required and the characteristics of the piles.
(3) A final detailed design stage to obtain the optimum number, location and configuration of the piles, and to compute detailed distributions of settlement, bending moment and shear in the raft, and the pile loads and moments.

2.2.4 Methods of analysis of piled raft

Several methods have been used for analysis of piled rafts, which can be divided into four categories:

1. Simplified calculation methods (e.g. Poulos-Davis-Randolph (PDR) (see Poulos, 2001a; Burland, 1995).
2. Approximate computer-based methods
   (a) Strip on Springs Approach (e.g. Poulos, 1991).
   (b) Plate on Springs Approach (e.g. Russo, 1998).
3. Rigorous computer-based methods.
   (a) Boundary element methods (BEM) (e.g. Butterfield, et al., 1971; Brown and Wiesner, 1975; Sinha, 1997).
   (b) Methods combining boundary element for the piles and finite element analysis for the raft (e.g. Hain and Lee, 1978; Ta and Small, 1996; Small and Zhang, 2002; Mendonca et al., 2003).
   (c) Finite element method (FEM) (e.g. Katzenbach et al., 2005; Sanctis et al., 2006; Ningombam Thoiba Singh et al., 2008; JinHyung Lee et al., 2010.

In this study, ***simplified method***, ***centrifugal tests*** and ***3D finite element method*** are used for model piled rafts on soft clay under the effects of ground surface subsidence.

2.2.5 Case histories using of piled raft

(a) Piled raft on stiff soils

Piled raft on Frankfurt clay is summed in Table 2.1. The general soil profile of Frankfurt city is shown in Figure 2.6. An example for previous analyses of project using piled raft on stiff soils is presented in Figure 2.7. The measured results are shown in Figure 2.8, Figure 2.9 and Figure 2.10. The numerical results are presented in Figure 2.11, Figure 2.12 and Figure 2.13. Other extensive analyses of projects using piled rafts on stiff soil can be seen in Katzenbach et al. (2000). Almost aspects of piled raft have been researched for stiff soils but for soft soils.

Table 2.1 Piled raft in Frankfurt clay, Katzenbach et al. (2000)

Building data	Torhaus	Messeturn	Westend 1	Eurotheum	Main Tower	American Express	Japan Centre	Congress Centre	Franfurter Welle
H (m)	130	256.5	208	110	198	74.7	115.3	51.6	55
P (MN)	2 × 200	1450	1140	450	1470	800	870	1440	500
A (m^2)	2 × 430	3457	2940	1830	3800	3570	1920	10200	25000
t_r (m)	2.5	6.0	4.5	2.5	3.8	2.0	3.5	2.7	2.2
z_r (m)	3.0	14	14	13	21	14	15.8	8.0	11.5
n	2 × 42	64	40	25	112	35	25	141	102
L_p (m)	20.0	26.9–34.9	30	25.0–30.0	20.0 & 30.0	20.0	22.0	12.5–34.5	20.0 & 25.0
d_p (m)	0.9	1.3	1.3	1.5	1.5	0.9	1.3	1.3	0.9
i/d_p	3.0–3.5	3.5–6.0	3.8–6.0	1.6–6.0	3.0–6.0	3.5	3.0–6.0	3.0–6.0	3.5
P_p (MN)	1.7–6.9	5.8–20.1	9.2–14.9	1.8–6.1	1.4–8.0	2.7–5.1	7.9–13.8	4.2–6.5	–
α_{pr}	0.8	0.55	0.5	0.3	0.85	–	0.4	0.4	–
s (mm)	150	144	110	32	25	55	60	40–60	–

H: max. height of building; P: effective load (total load minus uplift); A: area of raft; t_r: max. thickness of raft; z_r: max. depth of raft below the ground level; n: number of piles; L_p: pile length; d_p: pile diameter; i: average pile spacing; P_p: measured pile loads; α_{pr}: measured piled raft coefficient; s: max. measured settlements.

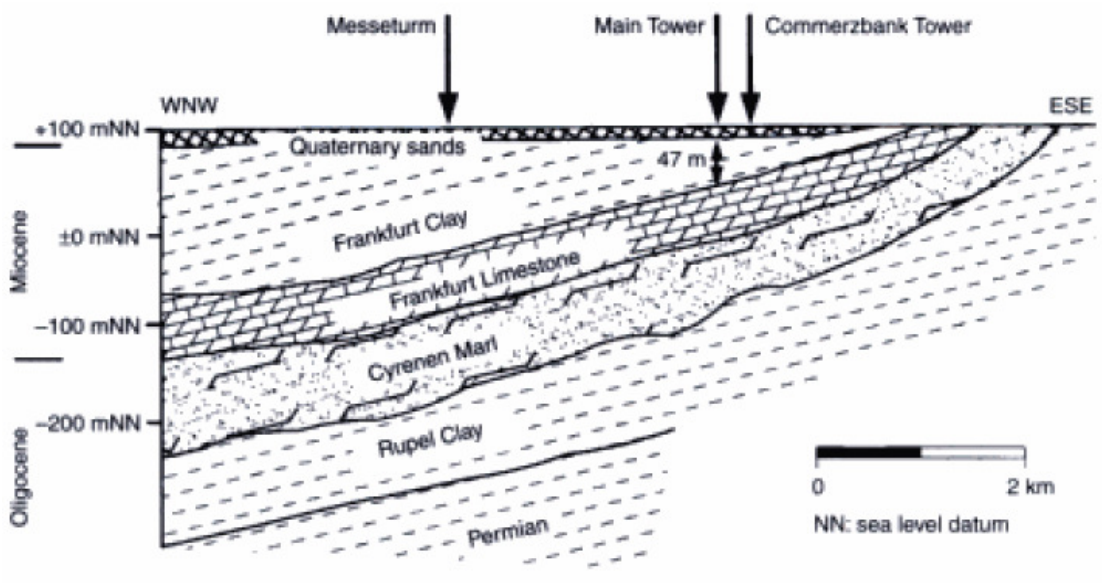

Figure 2.6 Soil profile beneath city of Frankfurt am Main (Katzenbach et al., 2000)

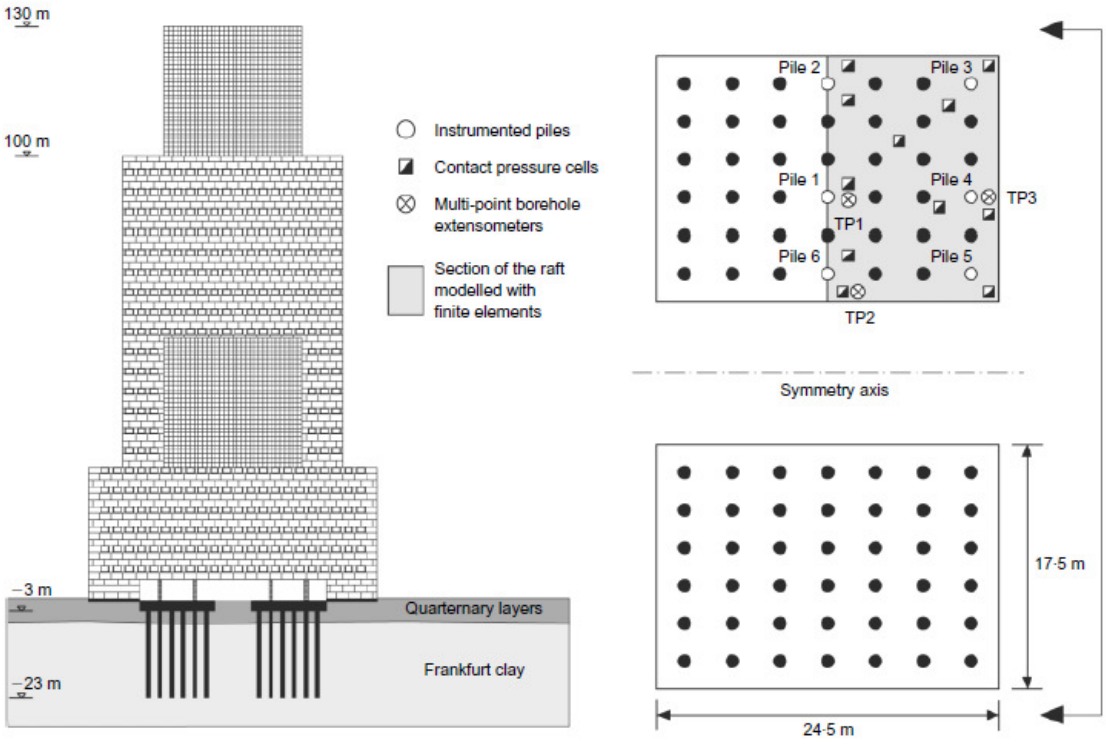

Figure 2.7 Torhaus: (a) profile view of the building, (b) ground plan of raft (Reul et al., 2003)

Measured results:

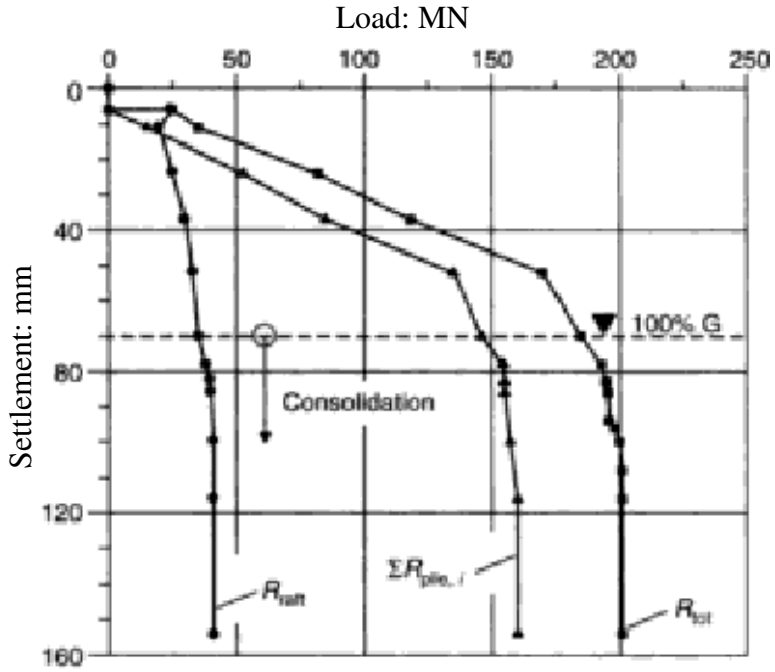

Figure 2.8 Measured load-settlement curves for Torhaus building (Katzenbach et al., 2000)

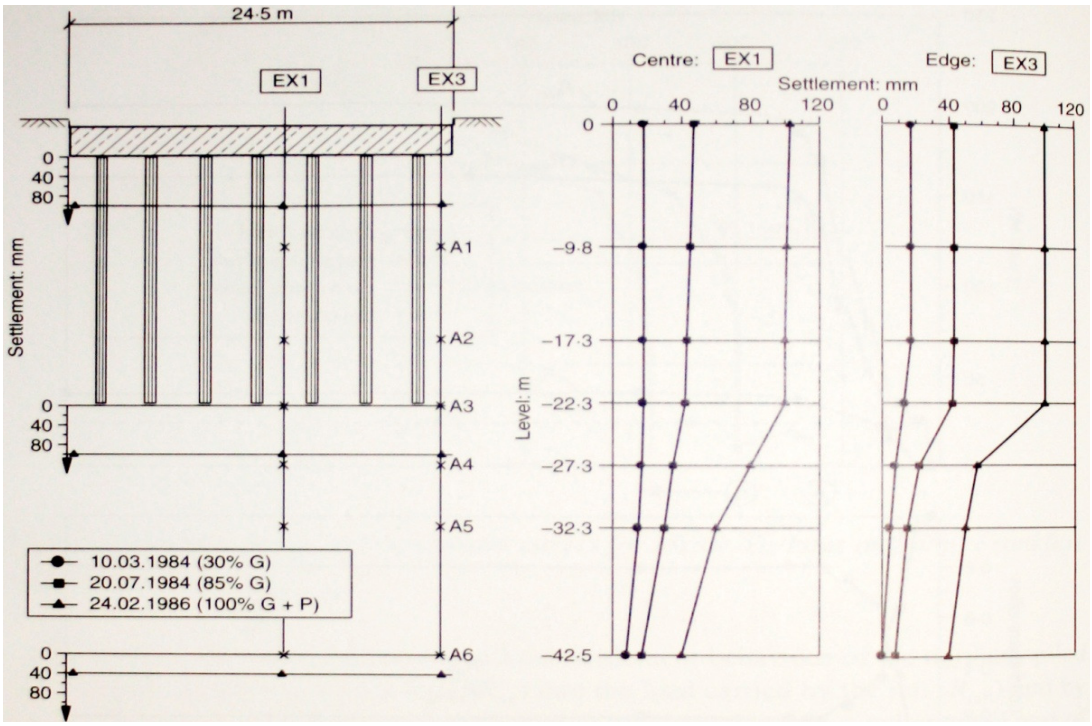

Figure 2.9 Measured settlement distribution with depth for Torhaus building (EX ≅ TP) (Katzenbach et al., 2000)

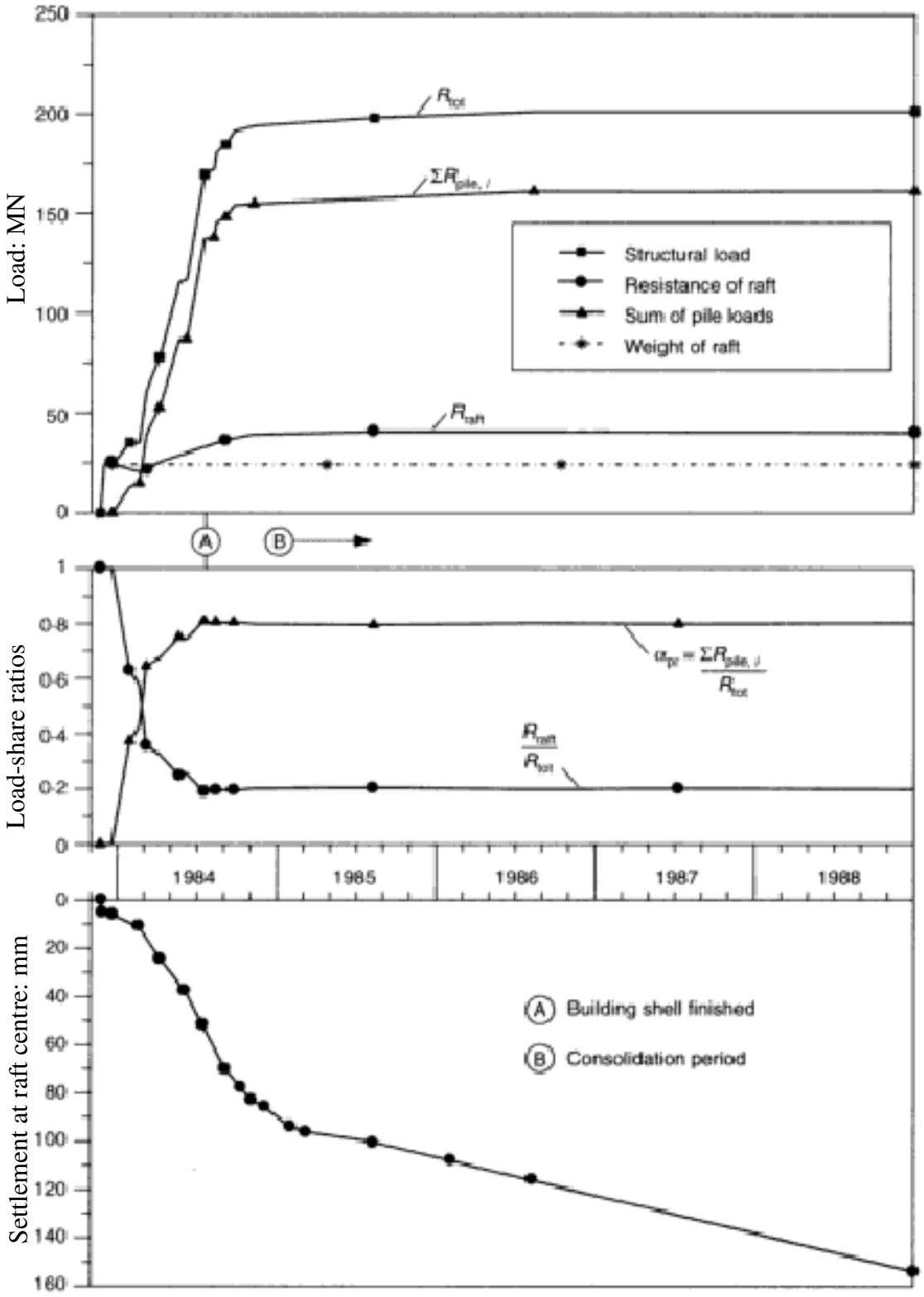

Figure 2.10 Observed time-dependent load-settlement behavior and load sharing for Torhaus building (Katzenbach et al., 2000)

Numerical results:

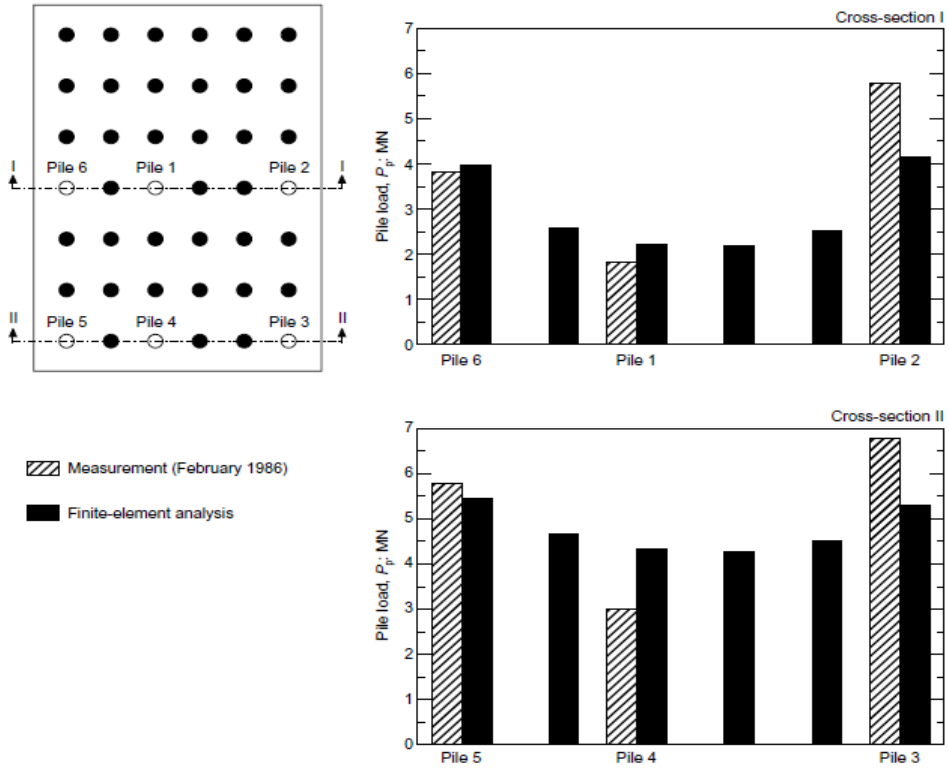

Figure 2.11 Torhaus: pile load. Measurement after Sommer (1991) and finite-element analysis (Reul et al., 2003)

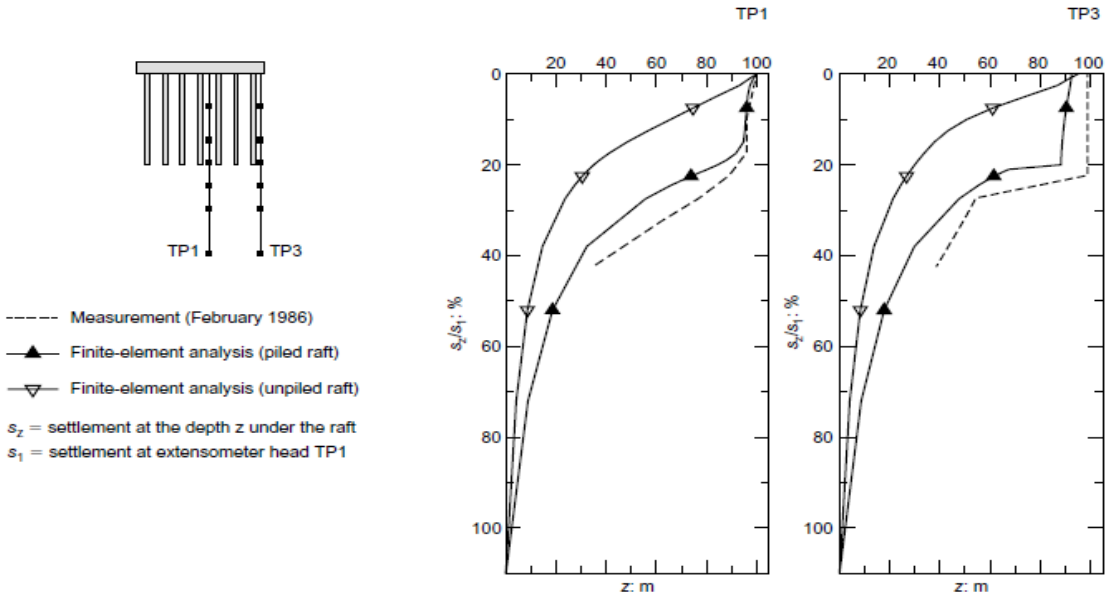

Figure 2.12 Torhaus: settlement profile. Measurement after Sommer (1991) and finite-element analysis (Reul et al., 2003)

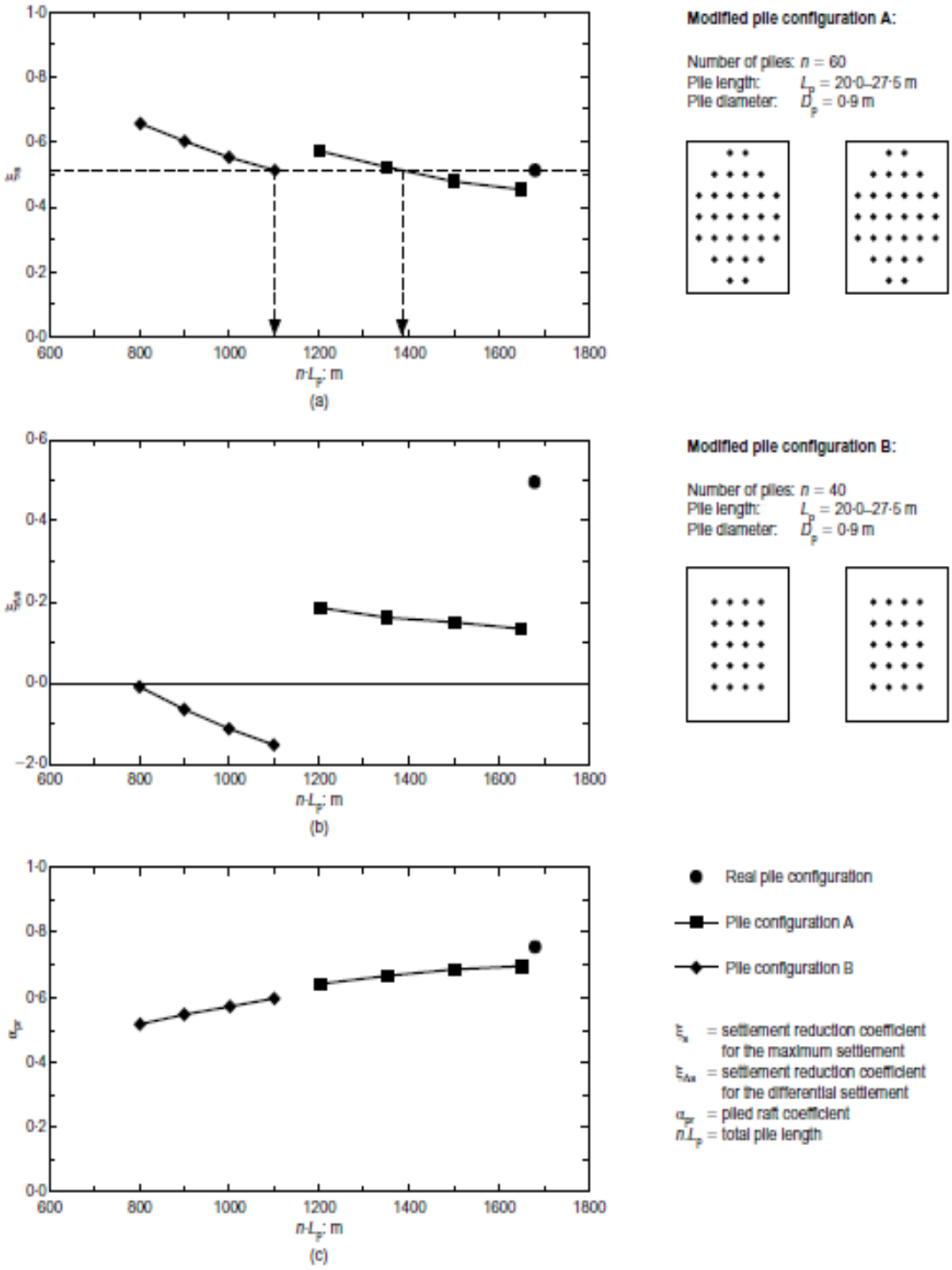

Figure 2.13 Torhaus: coefficient for maximum and differential settlement and piled raft coefficient depending on the total pile length (Reul et al., 2003).

There are some remarks on this group:

- The load carried by the raft is large.
- The average and differential settlements of the foundation are small.

(b) Piled raft on soft soils

Tan et al. (2004) reports a case of use of piled raft for 2-storey Terrace Houses on soft clay. The structures were built during 2002 - 2003 at Bukit Tinggi, Klang, Malaysia. The subsoil conditions include very soft to firm silty clay distributing up to 25m – 30 m which are underlain by a silty sand (Figure 2.14).

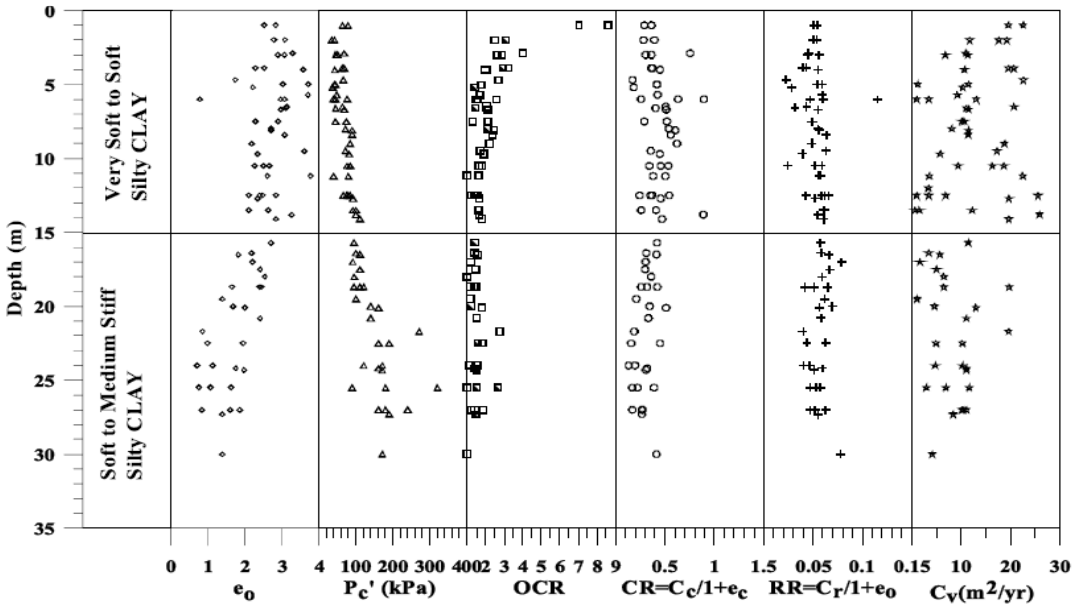

(a)

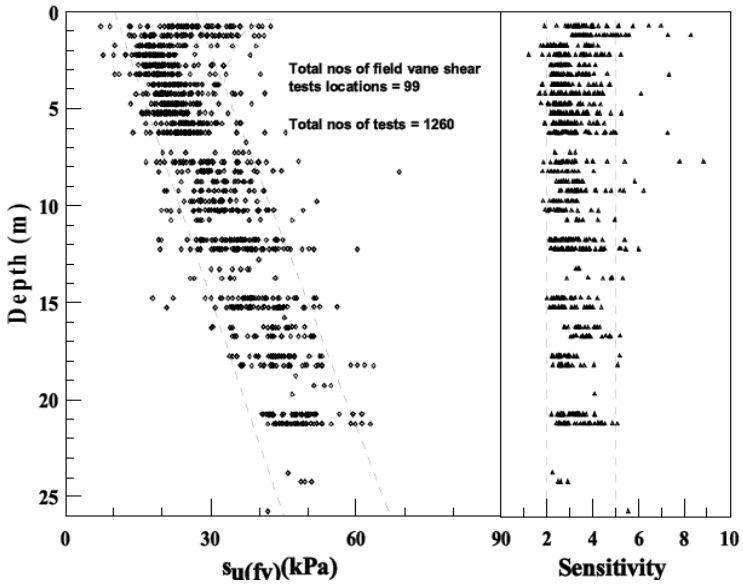

(b)

Figure 2.14 Properties of Klang Clay: (a) compressibility parameters, (b) undrained shear strength and sensitivity (Tan et al., 2004).

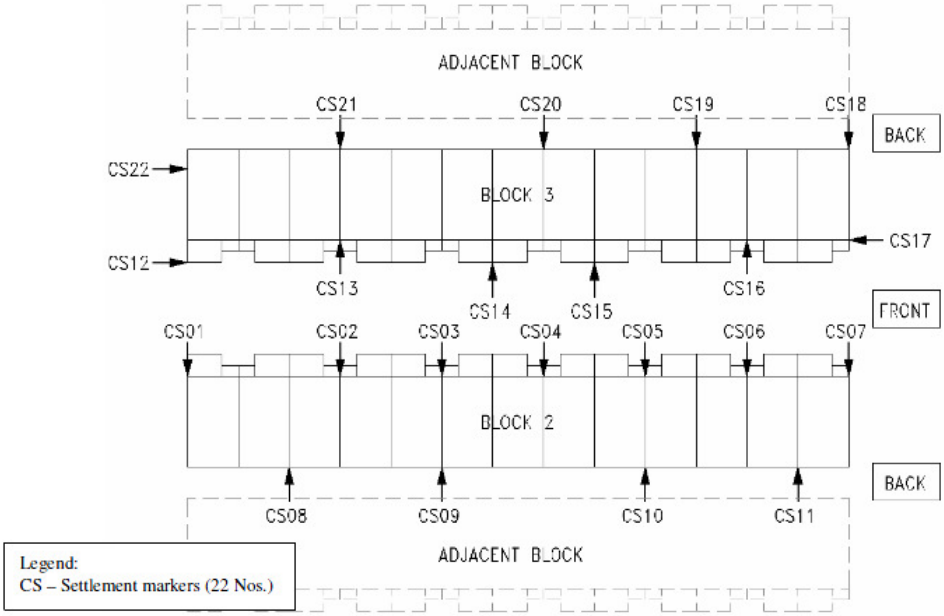

(a)

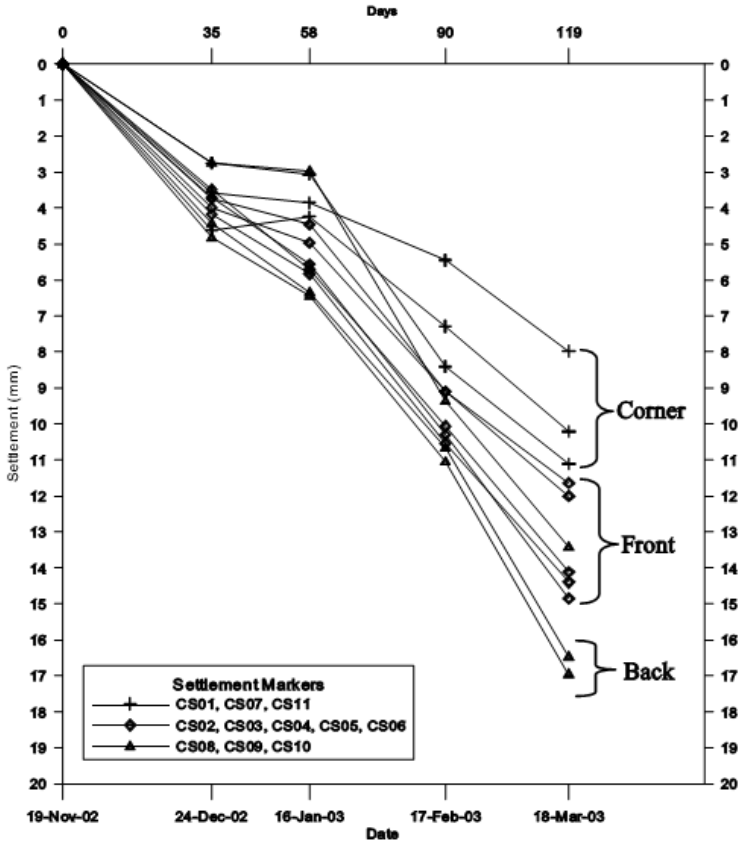

(b)

Figure 2.15 2-Storey Terrace Houses: (a) Locations of settlement markers, (b) Settlement monitoring results (Tan et al., 2004).

The maximum loads of 360 kN for column, 16 kN/m for line load and 3 kN/m^2 for live load. A 15 m x 80 m rectangular raft with 150 mm thickness is used and it is reinforced with 350 m x 600 mm strips. The 150 mm x 150 mm square piles with 9 m length are used as settlement reducers. Measured results during the construction period give 13 mm average settlement, 9 mm differential settlement and an angular distortion of 1/2850. Figure 2.15 shows the locations of settlement markers and settlement monitoring results.

Tan et al. (2006) presents completed 5-storey Apartments using piled raft on soft clay at the same site of 2-storey Terrace Houses. The maximum loads of 750 kN for column, 9 kN/m for line load and 2.7 kN/m^2 for live load. A 25 m x 70 m rectangular raft with 300 mm thickness is used and it is reinforced with 350 mm x 700 mm strips. The 200 mm x 200 mm square 'floating' piles with lengths vary from 18 m to 24 m are used. The total number of piles is 504. The results measured from construction of 3rd floor (9/2003) until 9 months after finishing the construction (10/2004) show 82 mm average settlement, 27 mm differential settlement and an angular distortion of 1/685. Figure 2.16 shows details of 5-storey Appartments.

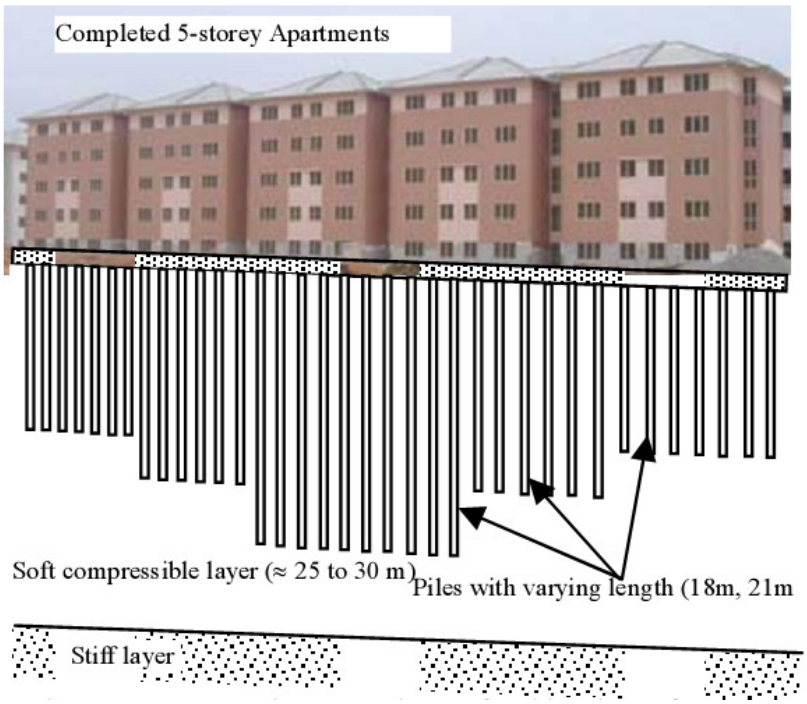

(a)

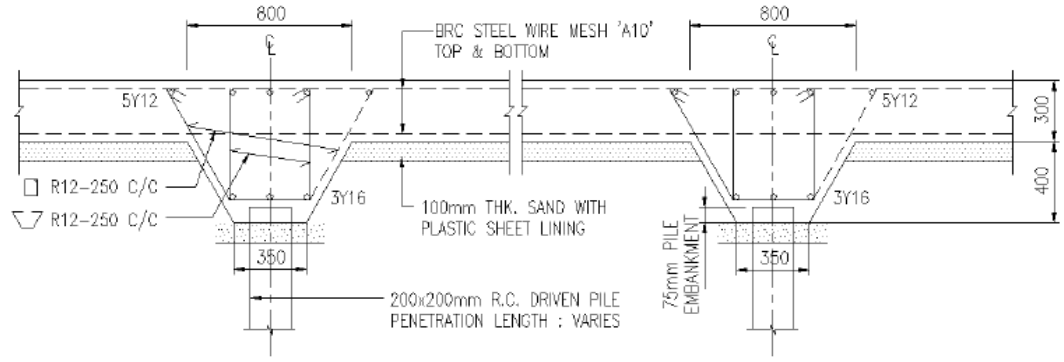

(b)

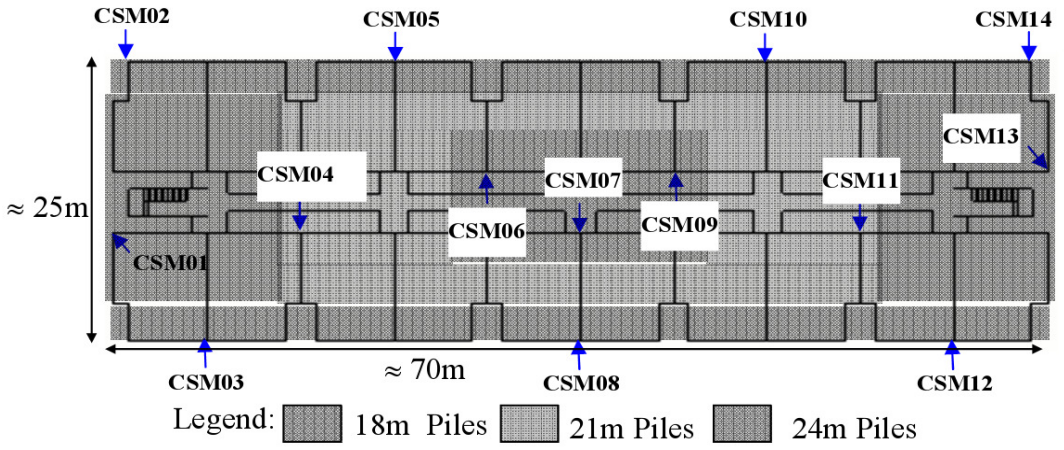

(c)

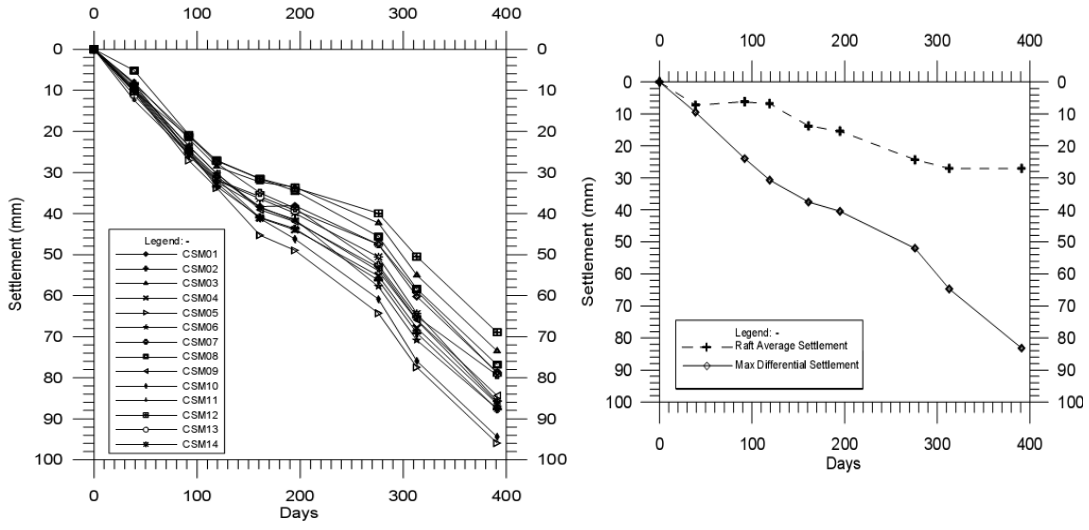

(d) (e)

Figure 2.16 5-Storey Apartments: (a) Schematic of piled raft system, (b) Typical cross-section of piled raft, (c) Location of settlement markers, (d) Settlement monitoring results, and (e) Raft average settlement and maximum differential settlement (Tan et al., 2006).

(c) Piled raft on soft soils and effected by ground subsidence

La Azteca building in Mexico city is a notable example of piled raft under ground surface subsidence. The building is constructed during 1954-55. The foundation is located on deep highly compressible volcanic clay which is subjected to land subsidence arising from groundwater extraction (Hemsley, 2000; Poulos, 2005). The soil profile is shown in Figure 2.17.

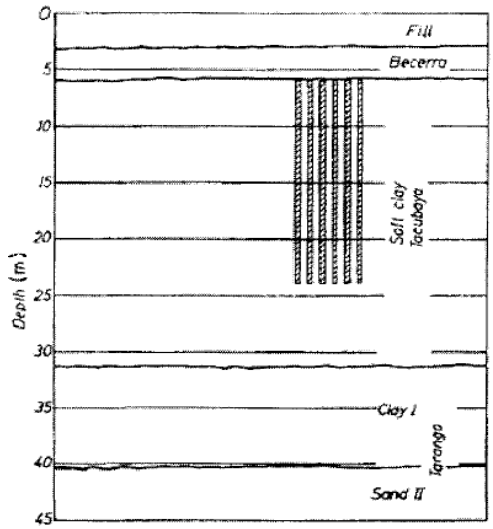

Figure 2.17 Soil profile of volcanic clay in Mexico City (Poulos, 2005)

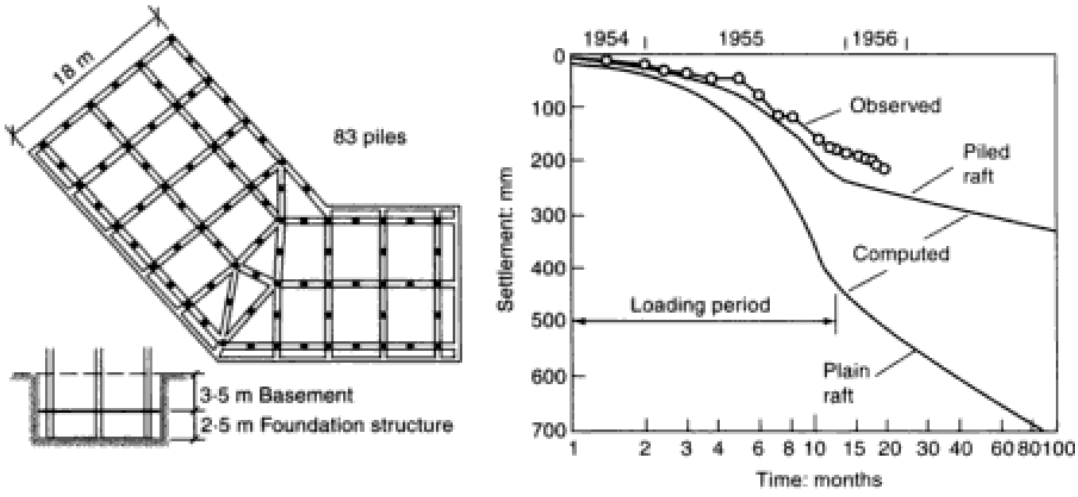

(a) (b)

Figure 2.18 Piled raft of La Azteca building after Zeevaert (1957): (a) foundation layout, (b) settlement curves (Hemsley, 2000)

The total load is 79.2 MN corresponding to an average applied pressure of 118 kPa. The 2.5 m thick raft is supported by 83 settlement reducing piles (0.4 m diameter, 18 m long), as shown in Figure 2.18(a). The piles are designed to carry 27 % of the total load. The final computed settlement is about 370 mm. The measured settlement at two years after the start of construction is 210 mm while differential settlement is smaller than 30 mm. Both measured and computed curves of settlement are presented in Figure 2.18(b). The method for calculation of settlements which is shown in Figure 2.18(b) is in traditional manner.

There are some remarks on this group:

- The load carried by the raft is small.
- The average and differential settlements of the foundation are very large.
- Use compensated friction piled raft to reduce the difference settlement between the foundation and the ground surface.

2.3 Ground Subsidence Problems

2.3.1 Sources of ground subsidence

Ground surface subsidence has been occurred in many cities because of some reasons:

- Heavy pumping of ground water: Bangkok, Mexico City, Tokyo, Houston and San Joan Valley (Zeevaert, 1973; Poulos, 2008); south Taiwan (Lee et al., 1998).
- Oil extraction: Long Beach, California and Maracaibo and Venezuela (Zeevaert, 1973).

2.3.2 Effects of ground subsidence on piled rafts

Ground surface subsidence induced by lowering the water table may cause some problems for piled raft foundation as below:

- Friction piles: shaft friction decreases due to negative friction.
- End-bearing piles: piles buckle due to shrinkage of the lateral supporting soil.
- Load sharing between raft and piles is changed.
- Large overall settlement is imposed due to the reduction of bearing capacity of the foundations.

- Large differential settlements occur because the reduction of bearing capacity of each pile is different.

Several examples which show the effects of ground surface subsidence on the foundation of structures can be seen in Zeevaert (1973) and Phienwej et al. (2004).

2.3.3 Mechanics of ground surface subsidence

Zeevaert (1973) proposed the following procedure for analyzing of ground surface subsidence arising from groundwater extraction.

(a) For an isotropic soil deposit of thickness H

The subsidence of ground at depth z of soil deposit can be calculated as

$$\delta_{sz} = m_v \gamma_w \cdot \frac{1}{2} i_z \left(H^2 - z^2 \right) \tag{2.1}$$

The ultimate ground surface subsidence at z = 0 is obtained as

$$\delta_s = m_v \left(\frac{1}{2} \gamma_w \lambda_0 \right) H \tag{2.2}$$

The rate of ultimate ground surface subsidence at z = 0 is given by

$$\frac{\partial \delta_s}{\partial t} = m_v . H . \left(\frac{1}{2} \gamma_w \frac{\partial \lambda_0}{\partial t} \right) \tag{2.3}$$

The rate of subsidence at any depth z is calculated by

$$\frac{\partial \delta_{sz}}{\partial t} = \frac{\partial \delta_s}{\partial t} \left[1 - \frac{z^2}{H^2} \right] \tag{2.4}$$

where

m_v is the coefficient of unit volume compressibility and γ_w is the unit weight water.

i_z is the hydraulic gradient at depth z and is defined as $i_z = \frac{\partial \lambda}{\partial z}$.

λ is the drop between piezometric water levels at distance z and λ_0 is the drop between surface and bottom of the deposit.

(b) For soil deposits are stratified and the mechanical properties of compressibility are not constant with depth

The total settlement at the ground surface is calculated by summing all the compressible strata as below

$$\delta_s = \frac{1}{2}\gamma_w \sum_{1}^{n} m_{vj}\left(\lambda_j + \lambda_{j+1}\right) d_j \tag{2.5}$$

The rate of subsidence is given by

$$\frac{\partial \delta_s}{\partial t} = \frac{1}{2}\gamma_w \sum_{1}^{n} m_{vj}\left(\frac{\partial \lambda_j}{\partial t} + \frac{\partial \lambda_{j+1}}{\partial t}\right) d_j \tag{2.6}$$

where

m_{vj} is the coefficient of unit volume compressibility of strata *j* and d_j is the thickness of strata *j*.

λ_j , λ_{j+1} are drops of piezometric water level when the water flows to the base of strata *j* and strata *j+1*, respectively.

2.4 Capacity of Centrifugal Test for Analysis of Piled Raft

Horikoshi et al. (1996) performs a series of centrifugal tests of model piled raft on clay to investigate the role of centred pile group in reducing the settlement of the raft. Conte et al. (2003) presents experimental research based on centrifuge test focusing on the problem of ultimate bearing capacity of piled raft on clay. Vincenzo Fioravante et al. (2008) carried out the centrifugal test to investigate the behavior of raft on settlement reducing piles on loose sand. Many successful results were archived through these researches, which are shown in figures 2.19 – 2.23 (*n*: number of piles in piled raft). The centrifugal test can be use for analysis behavior of model piled raft in this study.

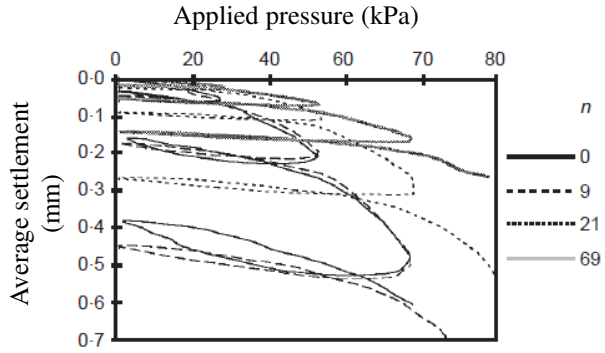

Figure 2.19 Average settlement of raft during loading test (Horikoshi et al., 1996).

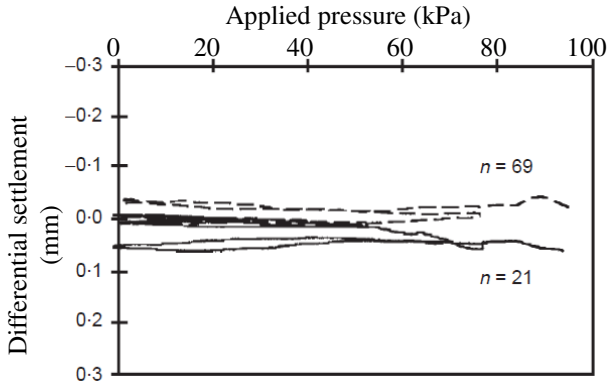

Figure 2.20 Differential settlement of raft during loading test (Horikoshi et al., 1996).

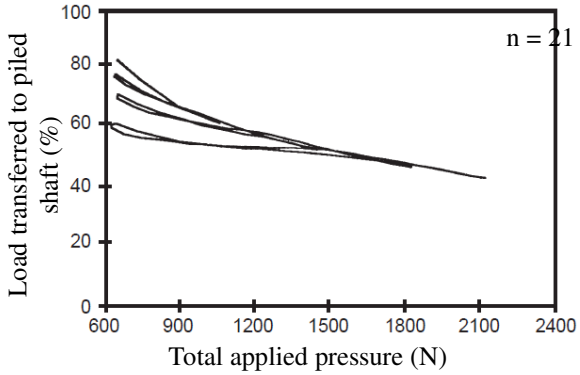

Figure 2.21 Percentage load transferred to piles (Horikoshi et al., 1996).

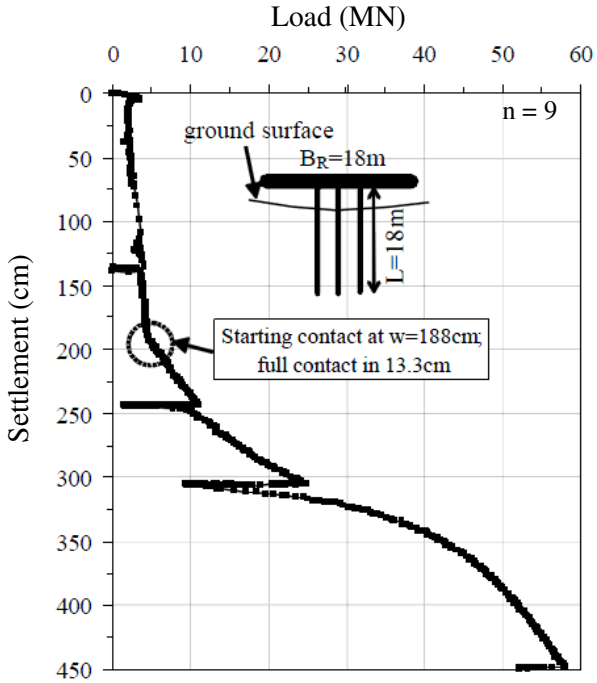

Figure 2.22 Load-settlement chart of a model piled raft (Conte et al., 2003).

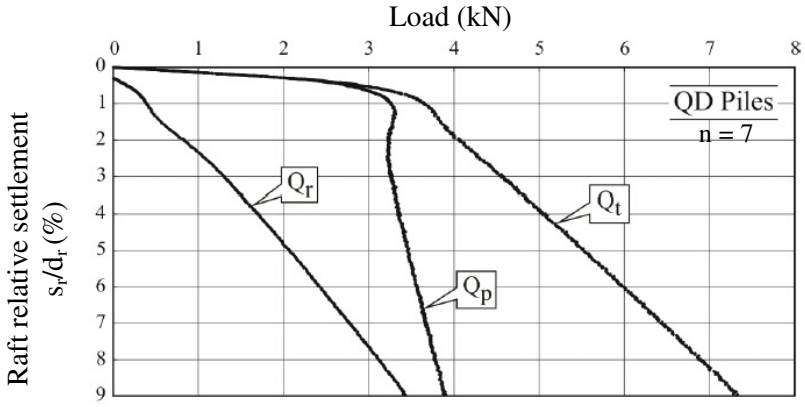

Figure 2.23 Load sharing mechanism of a model piled raft (Vincenzo Fioravante et al., 2008).

2.5 Capacity of Plaxis 3D Foundation for Analysis of Piled Raft

2.5.1 Plaxis 3D Foundation

Plaxis 3D Foundation is a finite element program which has been written for analysis foundations of structure including piled raft foundation. It can generate a large 3D finite element meshes. The mechanical behavior of soils can be modeled by several models (e.g. Mohr-Coulomb model) for different analyses. The interactions between piles, raft and soil can be simulated via this program. Extensive features of Plaxis 3D Foundation can be seen in Brinkgreve et al. (2007). A validated analysis of this program for piled raft in Frankfurt clay (Japan Centre building) has also been presented in Validation Manual. The results of the analysis are shown in Figure 2.24 and Figure 2.25.

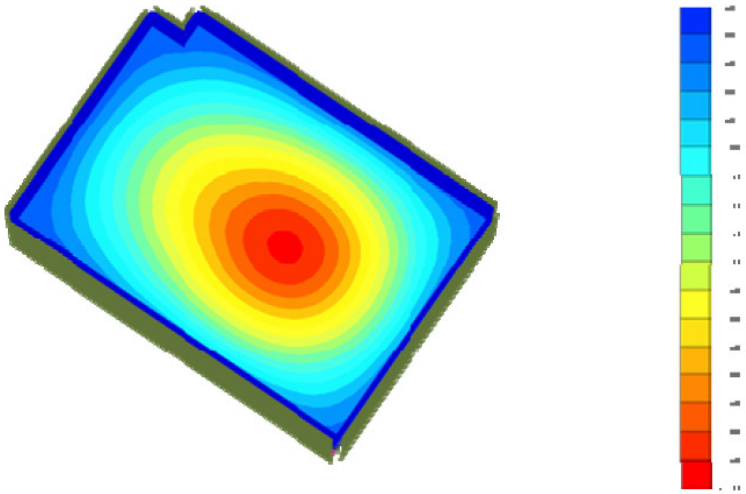

Figure 2.24 Foundation settlement under working load (Brinkgreve et al., 2007).

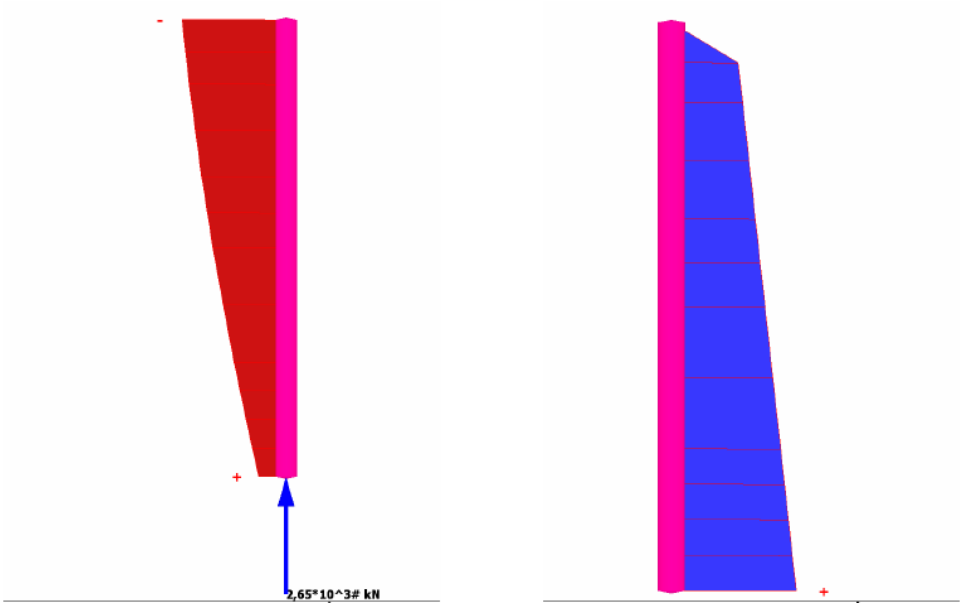

Axial force N (scaled up 500,00*10^{-6} times)
Max.Value = -2,66*10^{3} kN (Element 146 at node 26295)
Min.Value = -10,12*10^{3} kN (Element 141 at node 26283)

Skin friction T$_{skin}$ (scaled up 10,00*10^{-3} times)
Max.Value = 490,00 kN/m (Element 146 at node 26295)
Min.Value = -17,94*10^{-12} kN/m (Element 141 at node 26283)

Figure 2.25 Distributions of normal force and skin friction along a middle pile (Brinkgreve et al., 2007)

2.5.2 Model Formulations

Linear Elastic Model

This is the simplest model used for materials, which is based on the Hooke's law for isotropic linear elastic behavior. The relationship between effective stress and strain is expressed in term of the rate as below:

$$\dot{\sigma}' = D^e \dot{\varepsilon} \tag{2.7}$$

Where D^e is the elastic material stiffness matrix. Effective Young's modulus E and effective Poisson's ratio ν are used in this model, which are attached in D^e matrix. Linear elastic model is inappropriate to model behavior of the soils which have highly non-linear behavior. This model is suitable to simulate behavior of structures (e.g. piles, raft, floors or walls) where the strength properties of materials are very high compared to those of soils. In Plaxis, this model is usually used together with *Non-porous* type of material behavior to exclude pore pressures from these structural elements.

Mohr-Coulomb Model

The Mohr-Coulomb model is an elastic perfectly plastic model which is a constitutive model with a fixed yield surface and the behavior of points within the yield surface is purely elastic. Based on the basic principal of elastoplasticity, equation (2.7) can be written as:

$$\dot{\sigma}' = D^e \left(\dot{\varepsilon} - \dot{\varepsilon}^p \right) \tag{2.8}$$

Where $\dot{\varepsilon}^p$ is the plastic strain rate component which is defined by:

$$\dot{\varepsilon}^p = \lambda \frac{\partial g}{\partial \sigma'} \tag{2.9}$$

Where λ is the plastic multiplier which is defined from the yield function, *f*, as below:

$$\lambda = 0 \quad \text{for:} \quad f < 0 \quad \text{or:} \quad \frac{\partial f^T}{\partial \sigma'} D^e \dot{\varepsilon} \le 0 \quad \text{(Elasticity)} \tag{2.10}$$

$$\lambda > 0 \quad \text{for:} \quad f = 0 \quad \text{and:} \quad \frac{\partial f^T}{\partial \sigma'} D^e \dot{\varepsilon} > 0 \quad \text{(Plasticity)} \tag{2.11}$$

g is the plastic potential function which is introduced to fix the problem of theory of associated plasticity in estimating dilatancy. Non-associated plasticity is denoted as $g \neq f$.

Therefore, the relationship between effective stress rates and strain rates can be expressed as

$$\dot{\sigma}' = \left(D^e - \frac{\alpha}{d} D^e \frac{\partial g}{\partial \sigma'} \frac{\partial f^T}{\partial \sigma'} D^e \right) \dot{\varepsilon} \tag{2.12}$$

In which $\alpha = 0$ (elasticity) and $\alpha = 1$ (plasticity)

$$d = \frac{\partial f^T}{\partial \sigma'} D^e \frac{\partial g}{\partial \sigma'} \tag{2.13}$$

For multi surface yield contour, the above equations should be extended as:

$$\dot{\varepsilon}^p = \lambda_1 \frac{\partial g_1}{\partial \sigma'} + \lambda_2 \frac{\partial g_2}{\partial \sigma'} + \lambda_3 \frac{\partial g_3}{\partial \sigma'} + \ldots \tag{2.14}$$

Where λ_i (i = 1, 2, 3,…) can be defined from the yield functions f_i (i = 1, 2, 3,…), respectively.

The yield condition used in Mohr-Coulomb model is an extension of Coulomb's friction law to general states of stress. In principle stress space, this condition consists of six yield functions as below:

$$f_{1a} = \frac{1}{2}(\sigma'_2 - \sigma'_3) + \frac{1}{2}(\sigma'_2 + \sigma'_3)\sin\phi - c\cos\phi \le 0 \tag{2.15}$$

$$f_{1b} = \frac{1}{2}(\sigma'_3 - \sigma'_2) + \frac{1}{2}(\sigma'_3 + \sigma'_2)\sin\phi - c\cos\phi \le 0 \tag{2.16}$$

$$f_{2a} = \frac{1}{2}(\sigma'_3 - \sigma'_1) + \frac{1}{2}(\sigma'_3 + \sigma'_1)\sin\phi - c\cos\phi \le 0 \tag{2.17}$$

$$f_{2b} = \frac{1}{2}(\sigma'_1 - \sigma'_3) + \frac{1}{2}(\sigma'_1 + \sigma'_3)\sin\phi - c\cos\phi \le 0 \tag{2.18}$$

$$f_{3a} = \frac{1}{2}(\sigma'_1 - \sigma'_2) + \frac{1}{2}(\sigma'_1 + \sigma'_2)\sin\phi - c\cos\phi \le 0 \tag{2.19}$$

$$f_{3b} = \frac{1}{2}(\sigma'_2 - \sigma'_1) + \frac{1}{2}(\sigma'_2 + \sigma'_1)\sin\phi - c\cos\phi \le 0 \tag{2.20}$$

Where ϕ, c are the friction angle and cohesion of the soil respectively. The condition $f_i = 0$ for all yield functions together give a hexagonal cone as shown in Figure 2.26.

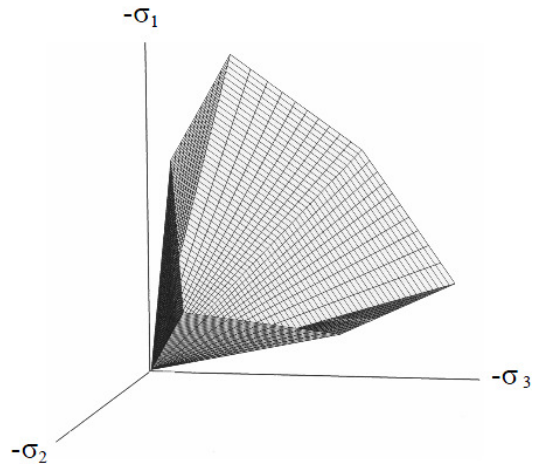

Figure 2.26 The Mohr-Coulomb yield surface in principal stress space for $c = 0$ (Brinkgreve et al., 2007)

The plastic potential functions of Mohr-Coulomb model are defined as below:

$$g_{1a} = \frac{1}{2}(\sigma'_2 - \sigma'_3) + \frac{1}{2}(\sigma'_2 + \sigma'_3)\sin\psi \quad (2.21)$$

$$g_{1b} = \frac{1}{2}(\sigma'_3 - \sigma'_2) + \frac{1}{2}(\sigma'_3 + \sigma'_2)\sin\psi \quad (2.22)$$

$$g_{2a} = \frac{1}{2}(\sigma'_3 - \sigma'_1) + \frac{1}{2}(\sigma'_3 + \sigma'_1)\sin\psi \quad (2.23)$$

$$g_{2b} = \frac{1}{2}(\sigma'_1 - \sigma'_3) + \frac{1}{2}(\sigma'_1 + \sigma'_3)\sin\psi \quad (2.24)$$

$$g_{3a} = \frac{1}{2}(\sigma'_1 - \sigma'_2) + \frac{1}{2}(\sigma'_1 + \sigma'_2)\sin\psi \quad (2.25)$$

$$g_{3b} = \frac{1}{2}(\sigma'_2 - \sigma'_1) + \frac{1}{2}(\sigma'_2 + \sigma'_1)\sin\psi \quad (2.26)$$

Where ψ is the dilatancy angle of the soils. Hence, there are five parameters including c, ϕ and ψ for plasticity and E and ν for elasticity are required for Mohr-Coulomb model.

2.6 Case of Piled Raft in Bangkok Soil

Phongpat Kitpayuck (2009) performs a parameter study for a case of piled raft in Bangkok soil. The properties of Bangkok soil used for his analyses are shown in Table 2.2.

Table 2.2 Properties of Bangkok soil used in analyses of Phongpat Kitpayuck (2009)

Materials	Depth (m)	Unit Weight (kN/m^3)	Cohesion (kN/m^2)	Friction Angle (degree)	Poisson's Ratio	Young Modulus (kN/m^2)	Interface parameters
Soft Clay	0-15	15.5	20	-	0.495	3000	0.9
Stiff Clay	15-25	18.8	90	-	0.495	40500	0.5
1st Sand	25-35	19.8	-	35.8	0.3	80000	0.6
Hard Clay	35-45	20.2	300	-	0.495	150000	0.3
2nd Sand	45-55	20.5	-	36.2	0.25	200000	0.6

A 50-storey building for which the applied load is assumed to be 1 ton/m^2/floor has been considered in the study. Figure 2.27 shows the 3D layout of the piled raft foundation under superstructure. The analysis results show that the stiffness of soil beneath the raft has a significant influence on the behavior of the piled raft. However, his study is performed for normal condition. In this paper, the problem will be analyzed again with considering the effect of ground surface subsidence.

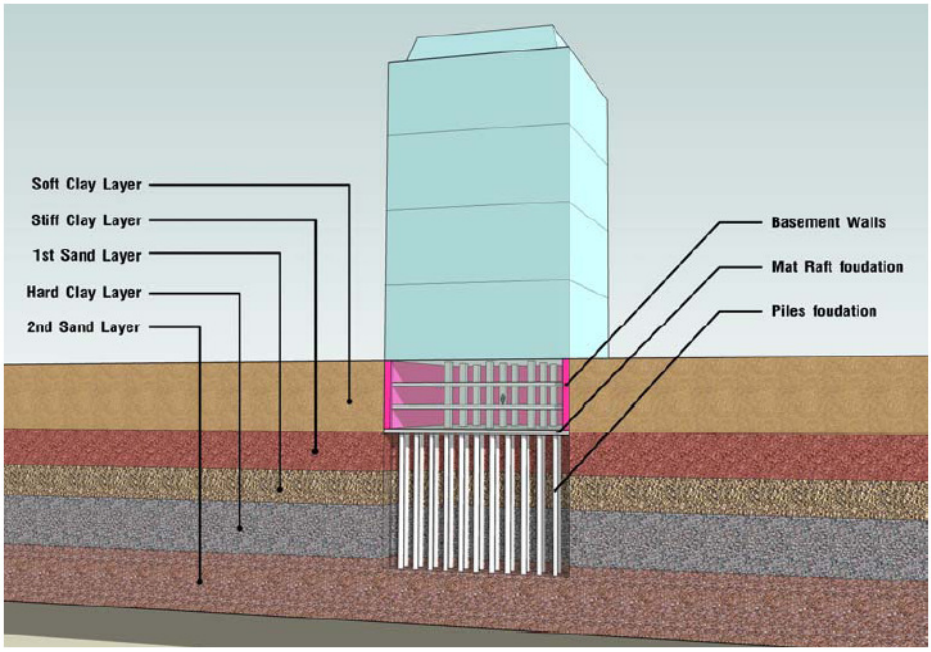

Figure 2.27 3D layout of the piled raft foundation under superstructure (Phongpat Kitpayuck, 2009)

2.7 Conclusions

Extensive research works have been done for piled raft on stiff soils and little papers have been considered on piled raft on soft soils and foundation in ground subsidence condition as well. From the review, it can be seen that, for piled raft in soft soils, the load carried by the raft is small and the average and differential settlements of the foundation are very large.

For piled raft in ground subsidence, such as La Azteca building, the average and differential settlement of foundation are also very large because of not only load of superstructure but also incremental settlement from ground subsidence. The portion of incremental settlements from ground subsidence is determined this study.

CHAPTER III

SIMPLIFIED METHOD FOR ANALYSIS OF PILED RAFT IN NORMAL CONDITION

3.1 Introduction

Simplified method can be used in preliminary design stage for a quick evaluation of behavior of the foundation and to indicate whether use of piled raft is feasible or not. This chaper summarizes the thoery of Poulos-Davis-Randolph (PDR) method and Modifications of Poulos-Davis-Randolph (MPDR) method.

3.2 Solutions for Raft and Single Pile

3.2.1 Solution for raft

Raft foundation is treated as for shallow foundation. For example, vertical capacity, moment capacity and vertical settlement can be treated as below.

Vertical capacity of raft in clay is calculated as

$$q_u = F_{cs} c N_c \tag{3.1a}$$

$$Q_{raft}^{ult} = q_u \times A \tag{3.1b}$$

Where

q_u = ultimate bearing capacity, F_{cs} = shape factor, c = cohesion of soil, N_c = bearing capacity factor, Q_{raft}^{ult} = total ultimate bearing capacity, A = area of raft.

The maximum ultimate moment sustained by the soil below the raft (Poulos, 2000)

$$M_m = \frac{p_{ur} B L^2}{8} \tag{3.2}$$

where

M_m = maximum possible moment that soil can support, p_{ur} = ultimate bearing capacity below raft, B = width of raft (in y-direction), L = length of raft (in x-direction).

Vertical settlement of a rigid circle raft (Poulos and Davis, 1974)

$$\rho = \frac{P_{av} a}{E_s} \times I_\rho \tag{3.3}$$

where ρ = Vertical settlement of raft, P_{av} = uniformly load on circled raft, a = radius

of raft, E_s = Young's modulus of soil, I_ρ = influenced factor for vertical displacement.

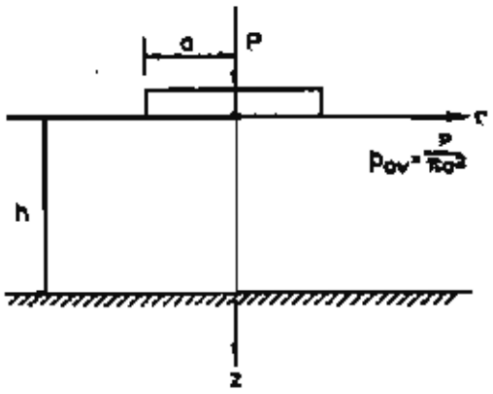

Figure 3.1 Symmetrical vertical load on circled raft (after Poulos and Davis, 1974).

Stiffness of rigid circle raft foundation

From (3.2): $P = [\frac{E_s}{aI_\rho}] \times \rho$ (stress) or $P(\pi a^2) = [\pi a^2 \frac{E_s}{aI_\rho}] \times \rho = [\pi a \frac{E_s}{I_\rho}] \times \rho$ (force)

$$K = \frac{\pi a E_s}{I_\rho} \tag{3.4}$$

h = thickness of soil layer, ν = Poisson's ratio, $\frac{a}{h}$ and ν Figure 3.1 ==> I_ρ

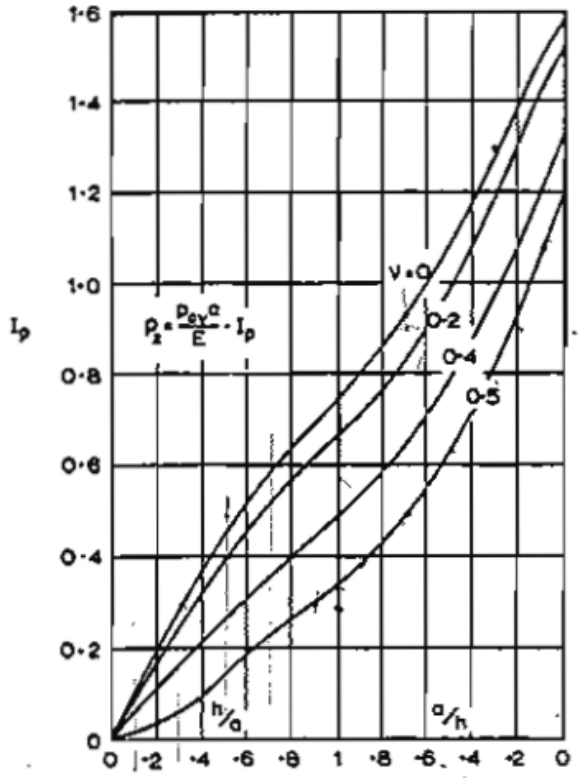

Figure 3.2 Influence factors for vertical displacement of rigid circle (Poulos and Davis,

1974).

3.2.2 Solution for single pile

Randolph et al. (1978) was described an analytical method for analysis of a single vertically loaded pile. The model pile with the soil surrounding the pile is divided into two layers by a line AB is shown in Figure 3.3. A summary of steps in the solutions will be presented here.

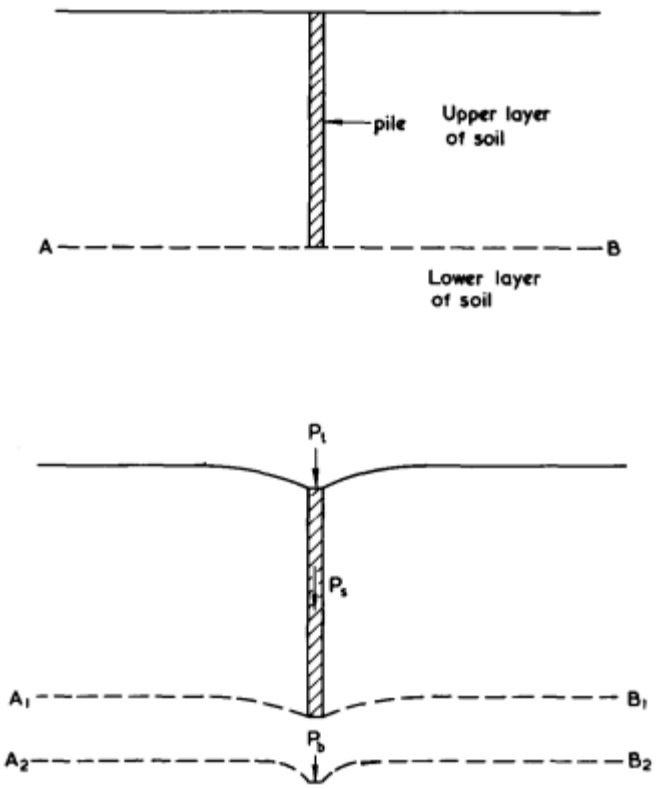

Figure 3.3 Uncoupling of effects due to pile shaft and base: (a) upper and lower soil layers; (b) separate deformation patterns of upper and lower layers (Randolph et al., 1978)

For rigid pile

+ Assumption of a logarithmic displacement field around the piled shaft as

$$\begin{cases} w(r) = \dfrac{\tau_0 r_0}{G} \ln\left(\dfrac{r_m}{r}\right), & r_0 \le r \le r_m \\ w(r) = 0, & r > r_m \end{cases} \tag{3.5}$$

where τ_0 is the shear stress at the pile shaft, r_0 is the radius of the pile and r_m is the

limiting radius of influence of the pile.

+ Deformation of the piled shaft is expressed, using the linear load transfer function, as

$$w_s = \zeta \frac{\tau_0 r_0}{G} \tag{3.6}$$

where

$$\zeta = \ln\left(r_m / r_0\right) \tag{3.7}$$

+ Deformation of the piled base is expressed, using the Boussinesq solution for a rigid punch acting on an elastic half-space, as

$$w_b = \frac{P_b\left(1-\nu\right)}{4 r_0 G} \tag{3.8}$$

+ At some distance from the piled base, the load will appear as a point load. The settlement around a point load decreases inversely with the radius as

$$w(r) = \frac{P_b\left(1-\nu\right)}{2\pi r G} \tag{3.9}$$

The ratio of equation (4.2) and (4.3) gives

$$\frac{w(r)}{w_b} = \frac{2}{\pi}\frac{r_0}{r} \tag{3.10}$$

From St Venant's principle, the settlement caused by the piled base at large radii should equal that due to a point load. Therefore, settlement profile at the top of the lower layer of soil in Figure 3.3 is described by

$$w(r) = w_b \frac{2}{\pi}\frac{r_0}{r} \tag{3.11}$$

+ The overall load – settlement ratio for a rigid pile may be written in dimensionless form

$$\frac{P_t}{G_l r_0 w_t} = \frac{P_b}{G_l r_0 w_b} + \frac{P_s}{G_l r_0 w_s} = \frac{4}{1-\nu} + \rho\frac{2\pi}{\zeta}\frac{l}{r_0} \tag{3.12}$$

For general condition

- Randolph (1994) presented an approximate solution based on separate treatment of the piled shaft and the piled base as below.

+ The piled head response is given by

$$\frac{P_t}{G_l r_0 w_t} = \frac{\dfrac{4\eta}{(1-\nu)\xi} + \rho\dfrac{2\pi}{\zeta}\dfrac{\tanh\mu l}{\mu l}\dfrac{l}{r_0}}{1+\dfrac{1}{\pi\lambda}\dfrac{4\eta}{(1-\nu)\xi}\dfrac{\tanh\mu l}{\mu l}\dfrac{l}{r_0}} \tag{3.13}$$

where P_t and w_t are the load and displacement at the top of the pile

l and r_0 are the length and radius of the pile

G_l is the value of shear modulus at a depth of $z = l$ (see Figure 3.4)

$\eta = r_b/r_0$ (under-reamed piles)

ν = Poisson ratio of soil

$\xi = G_l / G_b$ (end-bearing piles)

G_b = shear modulus of soil below the level of pile base

$\rho = G_{ave} / G_l$ (heterogeneity of soil modulus)

G_{ave} = average shear modulus of soil along pile length

$\lambda = E_p / G_l$ (pile-soil stiffness ratio)

$\zeta = \ln\left(r_m / r_0\right)$ (measure of radius of influence of pile)

$r_m = \left\{0.25 + \xi\left[2.5\rho(1-\nu) - 0.25\right]\right\} l$ (maximum radius of influence)

$= 2.5\rho(1-\nu)l$ for $\xi = 1$ (friction pile)

$\mu l = \sqrt{2/\zeta\lambda}\left(l / r_0\right)$ (pile compressibility)

$$\tanh(\mu l) = \frac{e^{2\mu l} - 1}{e^{2\mu l} + 1}$$

+ The proportion of load reaching the piled base is given by

$$\frac{P_b}{P_t} = \frac{\dfrac{4\eta}{(1-\nu)\xi}\dfrac{1}{\cosh\mu l}}{\dfrac{4\eta}{(1-\nu)\xi} + \rho\dfrac{2\pi}{\zeta}\dfrac{\tanh\mu l}{\mu l}\dfrac{l}{r_0}} \tag{3.14}$$

where $\cosh(\mu l) = \dfrac{e^{2\mu l} + 1}{2e^{\mu l}}$

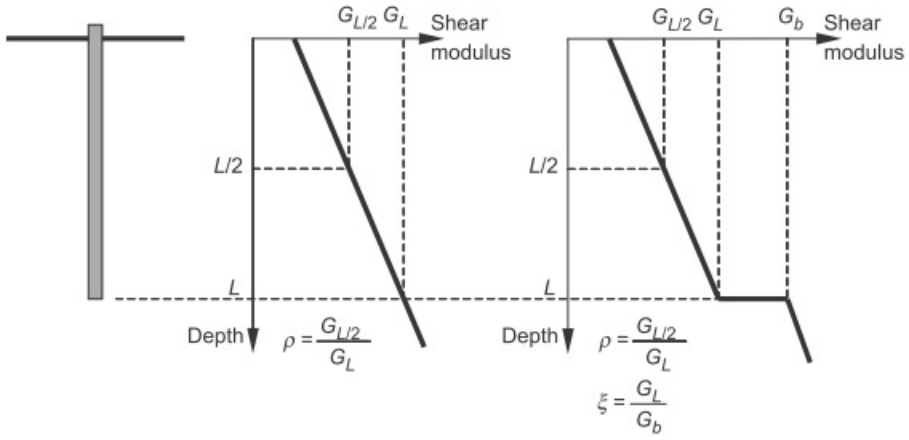

(a) Floating pile (b) End-bearing pile

Figure 3.4 Assumed variation of soil shear modulus with depth (Fleming, 1992)

***Discussion**:

+ Stiffness of single pile is be derived from equation (3.13) as

$$k = G_l r_0 \left\{ \frac{\dfrac{4\eta}{(1-\nu)\xi} + \rho \dfrac{2\pi}{\zeta} \dfrac{\tanh \mu l}{\mu l} \dfrac{l}{r_0}}{1 + \dfrac{1}{\pi\lambda} \dfrac{4\eta}{(1-\nu)\xi} \dfrac{\tanh \mu l}{\mu l} \dfrac{l}{r_0}} \right\} \tag{3.15}$$

+ For piles longer than $l / r_0 = 3 \times \sqrt{E_p / G_l}$ *, the pile head stiffness can be approximated as*

$$\frac{P_t}{G_l r_0 w_t} = \rho\pi\sqrt{2\lambda / \zeta} \tag{3.16}$$

where G_l *taken as the shear modulus at a depth of* $z = l = 3r_0 \times \sqrt{E_p / G_l}$

+ For stubby piles (such as equivalent piers), $l / d < 10$*, the parameter* ζ *should be adjusted as*

$$\zeta = \ln\left[5 + 2.5\rho(1-\nu) l / r_0\right] \tag{3.17}$$

+ For very stiff piles, equation (3.13) reduces to

$$\frac{P_t}{G_l r_0 w_t} = \frac{4\eta}{(1-\nu)\xi} + \rho \frac{2\pi}{\zeta} \frac{l}{r_0} \tag{3.18}$$

This expression applies for single piles where $l/d < 0.25\times\sqrt{E_p/G_l}$ *. For an equivalent pier, the condition is* $l/d_{eq} < 0.1\times\sqrt{E_{eq}/G_l}$

3.3 Poulos-Davis-Randolph (PDR) Method

3.3.1 Estimation of ultimate geotechnical capacity

3.3.1.1 Vertical loading

The ultimate geotechnical capacity of a piled raft is estimated as the lesser of the following two values:

(a) the sum of the ultimate capacities of the raft plus all the piles in the system.

(b) The ultimate capacity of a block containing the piles and raft, plus that of the portion of the raft outside the periphery of the pile group.

Conventional design approaches can be used to estimate the vertical capacity.

3.3.1.2 Lateral loading

The ultimate lateral capacity is the lesser of the sum of the ultimate lateral capacity of the raft plus that of all the piles, or the ultimate lateral capacity of a block containing the piles, raft and the soil, plus the contribution due to that portion of the raft outside the periphery of the pile group. Converntinal foundation design procedures can be used to assess the lateral ultimate capacity.

3.3.1.3 Moment loading

The ultimate moment capacity of the piled raft can be estimated approximately as the lesser of:

(a) the ultimate moment capacity of the raft (M_{ur}) and the individual piles (M_{up})

(b) the ultimate moment capacity of a block containing the piles, raft and soil (M_{ub})

The ultimate moment capacity of the raft can be estimate using the approach used by Poulos (2000):

$$\frac{M_{ur}}{M_m} = \frac{27}{4}\times\frac{V}{V_u}\left(1-\sqrt{\frac{V}{V_u}}\right) \tag{3.19}$$

where M_m = maximum possible moment that soil can support

V = applied vertical load

V_u = ultimate centric load on raft when no moment is applied.

Considering loading in the x-direction only, for a rectangular raft, the maximum moment M_m in the x-direction can be expressed as

$$M_m = \frac{p_{ur} B L^2}{8} \tag{3.20}$$

where p_{ur} = ultimate bearing capacity below raft

B = width of raft (in y-direction)

L = length of raft (in x-direction).

The ultimate moment contributed by the piles can be estimated from

$$M_{up} = \sum_{i=1}^{2} P_{uui} \left| x_i \right| \tag{3.21}$$

where P_{uui} = ultimate uplift capacity of typical pile i

$\left| x_i \right|$ = absolute distance of pile I from centre of gravity of group

n = number of piles.

Poulos and Davis (1980) give the solution for ultimate moment capacity M_{ub} (if no harizontal force is acting) as

$$M_{uB} = \alpha_B \times \overline{p}_u \times B_B \times D_B^2 \tag{3.22}$$

where

B_B = width of block perpendicular direction of loading

D_B = depth of block

$\overline{p}_u$ = average ultimate lateral resistance of soil along block

α_B = factor depending on distribution of ultimate lateral pressure with depth

= 0.25 for constant p_u with depth

= o.20 for linearly increasing p_u with depth from zero at the surface.

3.3.2 Estimation of load-settlement behavior of piled rafts

PDR method includes the following steps:

(c) estimation of the load sharing between the raft and the piles, using the approximate solution of Randolph (1994).

(d) hyperbolic load-deflection relationships for the piles and for the raft, thus providing a more realistic overall load-settlement response for the piled raft system than the original tri-linear approach of Poulos and Davis (1980).

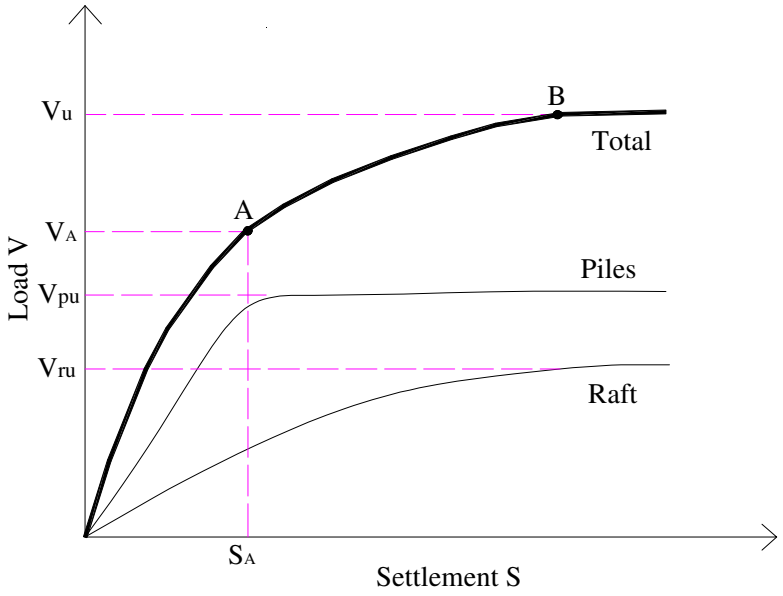

Figure 3.5 Construction of load-settlement curve for piled raft

Figure 3.5 shows diagrammatically the load-settlement relationship for the piled raft. The point A represents the point at which the pile capacity is fully mobilised, when the total vertical applied load is V_A. Up to that point, both the piles and the raft share the load, and the settlement (S) can be expresses as

$$S = \frac{V}{K_{pr}} \tag{3.23}$$

where V = vertical applied load

K_{pr} = axial stiffness of piled raft system.

Beyond point A, additional load must be carried by the raft, and the settlement is given by

$$S = \frac{V_A}{K_{pr}} + \frac{V - V_A}{K_r} \tag{3.24}$$

where V_A = applied load at which pile capacity is mobilized

K_r = axial stiffness of raft.

The load V_A can be estimated from

$$V_A = \frac{V_{pu}}{\beta_p} \tag{3.25}$$

where V_{pu} = ultimate capacity of piles (single pile or block failure mode, whichever is less)

β_p = proportion of load carried by piles.

The approximate expressions described by Randolph (1994) are used for K_{pr} in equation (1) and β_p in equation (2), namely

$$K_{pr} = XK_p \tag{3.26}$$

where K_p denotes the stiffness of pile group alone and, for fairly large numbers of piles,

$$X \approx \frac{1-0.6\left(K_r / K_p\right)}{1-0.64\left(K_r / K_p\right)} \tag{3.27}$$

$$\beta_p = 1/(1+\alpha) \tag{3.28}$$

$$\alpha \approx \frac{0.2}{1-0.8(K_r / K_p)}\left(\frac{K_r}{K_p}\right) \tag{3.29}$$

If it is assumed that the pile and raft load-settlemnt relationships are hyperbolic, then the secant stiffnesses of the piles (K_p) and the raft (K_r) can be expressed as

$$K_p = K_{pi}\left(1-R_{fp}V_p / V_{pu}\right) \tag{3.30}$$

$$K_r = K_{ri}\left(1-R_{fr}V_r / V_{ru}\right) \tag{3.31}$$

where

K_{pi} = initial tangent stiffness of pile group, R_{fp} = hyperbolic factor for pile group, V_p = load carried by piles, V_{pu} = ultimate capacity of piles, K_{ri} = initial tangent stiffness of raft, R_{fr} = hyperbolic factor for raft, V_r = load carried by raft, V_{ru} = ultimate capacity of raft.

The load carried by the piles is given by

$$V_p = \beta_p \times V \le V_{pu} \tag{3.32}$$

and the load carried by the raft is

$$V_r = V - V_p \tag{3.33}$$

where V denotes the total vertical applied load.

Substituting equation (3.25) – (3.33) in equations (3.23) and (3.24), the following expressions are obtained for the load-settlement relationship of the piled raft system.

- $V \le V_A$: $$S = \frac{V}{XK_{pi}\left(1-\frac{R_{fp}\beta_p V}{V_{pu}}\right)} \tag{3.34}$$

- $V > V_A$: $$S = S_A + \frac{V - V_A}{K_{ri}\left[1-R_{fr}\frac{\left(V-V_{pu}\right)}{V_{ru}}\right]} \tag{3.35}$$

where

$$S_A = \frac{V_A}{XK_{pi}\left(1-R_{fp}\right)} \tag{3.36}$$

with V_A given by equation (3.25).

Equations (3.34) – (3.36) are used to estimate the average load-settlement relationship for the piled raft.

3.3.2.1 Immediate and final settlements

The immediate and final settlements of piled raft in clay can be estimated by using the above procedure.

For immediate settlements, the pile and raft stiffnesses are those relevant to the undrained case, if using elastic-based theory, are estimated by using undrained values of modulus and Poisson's ratio of the soil.

For long-term settlements (immediate plus consolidation settlements, but excluding creep), Poulos and Davis (1980) suggested the calculation of overall total final settlement S_{TF} as

$$S_{TF} = \frac{V}{K_u} + V\left(\frac{1}{K'_e} - \frac{1}{K_{ue}}\right) \tag{3.37}$$

where V = applied vertical load on foundation, K_u = undrained foundation stiffness (from non-linear analysis), K_{ue} = undrained foundation stiffness (from elastic undrained analysis), K'_e = drained foundation stiffness (from elastic drained analysis).

3.3.2.2 Differential settlements

Randolph (1994) proposed an approximate procedure to estimate the maximum differential settlement of a uniformly loaded raft foundation, by relating the ratio of differential settlement to the overall settlement, to the relative rigidity of the raft. This ratio can be used for piled raft foundation. Horikoshi and Randolph (1997) provided conventional charts for the estimation of differential settlement as in Figure 3.3.

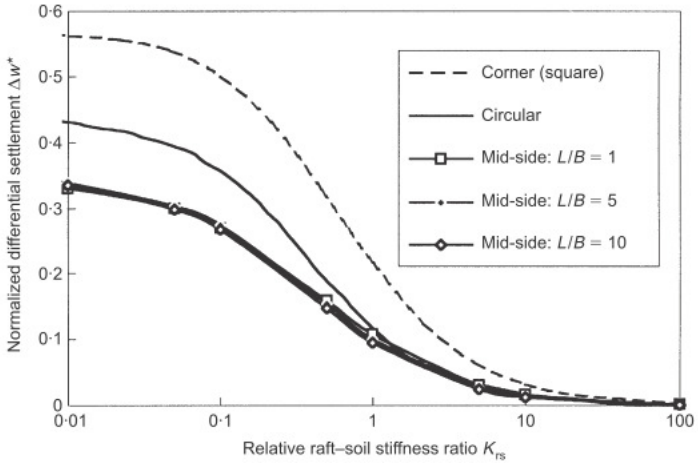

Figure 3.6 Variation of normalized differential settlement with raft-soil stiffness ratio K_{rs} (Horikoshi and Randolph, 1997)

3.3.3 Estimation of piled loads

The axial force P_i in any pile i in the foundation system can be estimated from

$$P_i = \frac{V\beta_p}{n_p} + \frac{M_x^* x_i}{I_y} + \frac{M_y^* y_i}{I_x} \tag{3.38}$$

with

$$M_x^* = \frac{M_x - M_y I_{xy}/I_x}{1 - I_{xy}^2/(I_x I_y)} \quad , \quad M_y^* = \frac{M_y - M_x I_{xy}/I_y}{1 - I_{xy}^2/(I_x I_y)} \tag{3.39}$$

where V = Total vertical load acting at centroid of foundation

n_p = number of piles in group

M_x, M_y = moments about centroid of pile group in direction of x- and y-axes, respectively

β_p = proportion of load carried by piles

I_x, I_y = moment of inertia of pile group with respect to x- and y-axes, respectively

I_{xy} = product of inertia of pile group about centroid

x_i,y_i = distance of pile i from y-and x-axes, respectively

M_x^* , M_y^* = effective moments in x- and y-directions, respectively, taking symmetry of pile layout into account.

For a symmetrical pile group layout, $I_{xy} = 0$ and $M_x^* = M_x$, $M_y^* = M_y$. Equation (3.38) then reduces to

$$P_i = \frac{V\beta_p}{n_p} \pm \frac{M_x x_i}{\sum_{i=1}^{n_p} x_i^2} \pm \frac{M_y y_i}{\sum_{i=1}^{n_p} y_i^2} \tag{3.40}$$

3.3.4 Estimation of raft moments and shears

The piled raft is considered as a series of piled strip foundations (Poulos, 1991) and use the solutions for a trip on an elastic foundation, with the piles being treated as supports (or negative loads).

3.4 Modification of PDR Method

3.4.1 Solution for piled group

3.4.1.1 Interaction method (Randolph et al., 1979; Randolph, 1994)

- Interaction between similarly loaded rigid piles

+ Group of two piles

The settlement of one pile is the sum of the settlement due to its own loading plus that due to the neighbouring piles displacement field. Thus

The settlement of the piled shaft at the piled mid-depth

$$w = w_1 + w_2 = \frac{\tau_0 r_0}{G}\left[\ln\left(\frac{r_m}{r_0}\right) + \ln\left(\frac{r_m}{s}\right)\right] \tag{3.41}$$

The load – settlement ratio for each pile shaft is

$$\frac{P_s}{G_l r_0 w_s} = \frac{2\pi\rho}{\zeta + \ln\left(r_m / s\right)} \frac{l}{r_0} \tag{3.42}$$

The settlement of the piled base is

$$w_b = w_1 + w_2 = \frac{P_b(1-\nu)}{4r_0 G_l}\left(1+\frac{2}{\pi}\frac{r_0}{s}\right) \tag{3.43}$$

The load – settlement ratio for each pile base is

$$\frac{P_b}{G_l r_0 w_b} = \frac{4}{1-\nu}\frac{s}{\frac{2}{\pi}r_0 + s} \tag{3.44}$$

The overall load – settlement ratio for each of two similarly loaded piles is

$$\left(\frac{P_t}{G_l r_0 w_t}\right)_2 = \frac{4}{1-\nu}\frac{s}{\frac{2}{\pi}r_0 + s} + \frac{2\pi\rho}{\zeta + \ln(r_m/s)}\frac{l}{r_0} \tag{3.45}$$

The interaction factor between two similar piles is

$$\left(\frac{G_l r_0 w_t}{P_t}\right)_2 = (1+\alpha_v)\left(\frac{G_l r_0 w_t}{P_t}\right)_1 \tag{3.46}$$

$$\text{where} \quad \alpha_v = \frac{\text{additional settlement due to adjacent pile}}{\text{settlement of pile under its own load}}$$

+ Group of three piles (at the corners of an equilateral triangle of side s)

$$\left(\frac{P_t}{G_l r_0 w_t}\right)_3 = \frac{4}{1-\nu}\frac{s}{\frac{4}{\pi}r_0 + s} + \frac{2\pi\rho}{\zeta + 2\ln(r_m/s)}\frac{l}{r_0} \tag{3.47}$$

+ Group of four piles (at the corners of a square of side s)

$$\left(\frac{P_t}{G_l r_0 w_t}\right)_4 = \frac{4}{1-\nu}\frac{s}{\frac{5.414}{\pi}r_0 + s} + \frac{2\pi\rho}{\zeta + \ln\left[\frac{r_m^3}{\sqrt{2}s^3}\right]}\frac{l}{r_0} \tag{3.48}$$

- Analysis of rigid piled groups

+ For the j^{th} pile of a group of n piles (each pile may take a different load share of total load and may also be of different radius), the shaft settlement is

$$(w_s)_j = \sum_{i=1}^{n}(w_s)_{ij} = \frac{1}{G}\sum_{i=1}^{n}(\tau_0)_i (r_0)_i \ln\left(\frac{r_m}{s_{ij}}\right) \tag{3.49}$$

where $s_{ij} = r_0$ for i = j. The n different values of w_s may be related to the n values of τ_0 by equation (3.49) to give a matrix equation

$$w_s = [F_s]\tau_0 \tag{3.50}$$

Similarly, the base settlements may be estimated by

$$(w_b)_j = \sum_{i=1}^{n}(w_b)_{ij} = \frac{2}{\pi}\frac{1-\nu}{4G_l}\sum_{i=1}^{n}\frac{(P_b)_i}{s_{ij}} \tag{3.51}$$

where $s_{ij} = (2/\pi)r_0$ for i = j. This leads to a second matrix equation, relating the base settlements w_b to the base loads P_b

$$w_b = [F_b]P_b \tag{3.52}$$

For rigid pile ($w_s = w_b$) and for a rigid cap ($(w_s)_i = (w_s)_j$), equations (3.50) and (3.52) may be solved to get values of τ_0 and P_b for a given piled cap displacement. From these values, the overall and average load – settlement ratio for the pile group may be calculated.

- For general condition

Randolph (1994) presents equations, based on modifying the shaft and base stiffnesses for a single pile accordance with the total interaction effect, for calculating the interaction effects between piles in a general piled group as below.

+ For shaft stiffness, the load transfer parameter (ζ^*) should be modified by

$$\zeta^* = n\zeta - \sum_{i=2}^{n}\ln(s_i / r_0) \tag{3.53}$$

+ For base stiffness, the parameter (ξ^*) should be modified by

$$\xi^* = \xi\left[1 + \frac{2}{\pi}\sum_{i=2}^{n}\frac{r_b}{s_i}\right] \tag{3.54}$$

where n = the number of piles in the group

s_i = the spacing of the i^{th} pile from pile 1

r_b = the piled base radius of the i^{th} pile

r_0 = the piled middle radius of the i^{th} pile

- The stiffness of each pile in piled group

Equations (3.53) and (3.54) may then be used in equation (3.13) and (3.14) to calculate the overall stiffness and the proportion of load reaching the piled base of each pile in piled group.

- The stiffness of piled group with n piles (assumed rigid cap) can be calculated by

$$k_p = \sum_{i=1}^{n} k_i \tag{3.55}$$

where k_i is stiffness of the i^{th} pile in piled group

k_p is the stiffness of the piled group

***Discussion**:

+ The stiffness of piled group with n piles can be calculated by

$$k_p = \sum_{i=1}^{n} k_i = nk_1 \tag{3.56}$$

where k_1 is stiffness of the typical pile in piled group

k_p is the stiffness of the piled group

3.4.1.2 Group efficiency (Randolph, 1994): the efficiency approach described by Fleming et al. (1992), based on analyses using the PIGLET program.

The group efficiency is defined as the inverse of the group settlement ratio, R_s:

$$\eta = \frac{1}{R_s} = \frac{k_p}{nk_1} \tag{3.57}$$

where η is the group efficiency

k_1 is the piled head stiffness of a single pile

k_p is the stiffness of the complete group (in terms of average settlement).

The group efficiency may be taken as

$$\eta = n^{-e} \tag{3.58}$$

where n is the number of piles in the group

the exponent e = 0.3 – 0.5 (friction piles)

= 0.6 – higher (end-bearing piles)

For friction piles, the exponent e can be defined as

$$e = e_1(l/d).c_1(E_p/G).c_2(s/d).c_3(\rho).c_4(\nu) \tag{3.59}$$

The values of e_1, c_1, c_2, c_3 and c_4 are determined from Figure 3.7.

The stiffness of piled group is calculated as

$$k_p = n^{1-e} k_1 \tag{3.60}$$

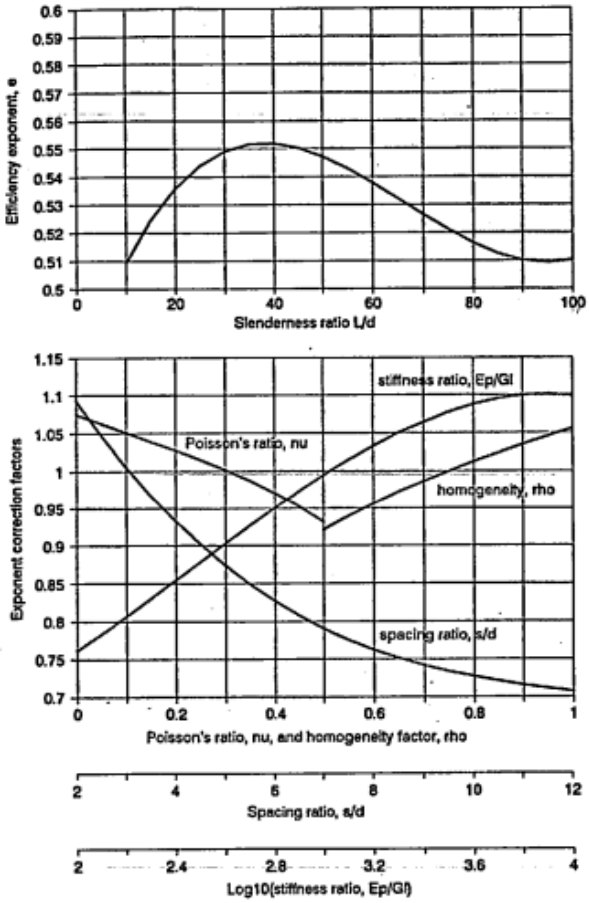

Figure 3.7 Design charts for group efficiency (after Fleming et al., 1992)

3.4.1.3 Equivalent Pier or Raft Approach (Randolph,1994; Horikoshi et al., 1999)

- The appropriate parameter to categorize pile groups is

$$R = \sqrt{ns / l} \tag{3.61}$$

where n = number of piles

s = piled spacing

l = piled length

- For values of R which are greater than 4, ($R \geq 4$), an equivalent raft should be used for the analysis.

- For values of R smaller than 4, (R < 4), and certainly for values less than 2, the equivalent pier approach is suitable.

Diameter of the equivalent pier:

$$d_{eq} = \sqrt{\frac{4}{\pi} A_g} \tag{3.62}$$

Young's modulus of the pier:

$$E_{eq} = E_s + \left(E_p - E_s\right)\left(\frac{A_p}{A_g}\right) \tag{3.63}$$

where d_{eq} = diameter of the pier

A_g = plan area of the piled group as a block

E_{eq} = Young's modulus of the equivalent pier

E_s = Average Young's modulus of the soil penetrated by the piles

E_p = Young's modulus of the piles

A_p = total cross sectional area of the piles in the group.

- The stiffness of piled group can be calculated as

$$k_p = G_l r_0 \left\{ \frac{\frac{4\eta}{(1-\nu)\xi} + \rho \frac{2\pi}{\zeta} \frac{\tanh \mu l}{\mu l} \frac{l}{r_0}}{1 + \frac{1}{\pi\lambda} \frac{4\eta}{(1-\nu)\xi} \frac{\tanh \mu l}{\mu l} \frac{l}{r_0}} \right\} \tag{3.64}$$

where P_t and w_t are the load and displacement at the top of the pier

l and is the length of the pier

G_l is the value of shear modulus at a depth of $z = l$

$r_0 = d_{eq}/2$ (radius of the pier)

$\eta = r_b/r_0$ (under-reamed pier)

ν = Poisson ratio of soil

$\xi = G_l / G_b$ (end-bearing pier)

G_b = shear modulus of soil below the level of pier base

$\rho = G_{ave} / G_l$ (heterogeneity of soil modulus)

G_{ave} = average shear modulus of soil along pile length

$\lambda = E_{eq} / G_l$ (pier-soil stiffness ratio)

$\zeta = \ln\left[5 + 2.5\rho(1-\nu) l / r_0\right]$ (stubby pier of friction pile)

$\zeta = \ln\left\{5 + \left[0.25 + (2.5\rho(1-\nu) - 0.25)\xi\right] l / r_0\right\}$ (stubby pier of end-bearing pile)

$$\mu l = \sqrt{2/\zeta\lambda}\,(l/r_0)$$

$$\tanh(\mu l) = \frac{e^{2\mu l}-1}{e^{2\mu l}+1}$$

+ The proportion of load reaching the pier base is given by

$$\frac{P_b}{P_t} = \frac{\dfrac{4\eta}{(1-\nu)\xi}\dfrac{1}{\cosh\mu l}}{\dfrac{4\eta}{(1-\nu)\xi} + \rho\dfrac{2\pi}{\zeta}\dfrac{\tanh\mu l}{\mu l}\dfrac{l}{r_0}} \tag{3.65}$$

where $\cosh(\mu l) = \dfrac{e^{2\mu l}+1}{2e^{\mu l}}$

3.4.1.4 Poulos (2002)

The stiffness of piled group is calculated as

$$k_{pi} = k_1 \times n^w \tag{3.66}$$

where k_1 = stiffness of single pile

n = number of piles

w = group exponent, typically in the range of 0.3 – 0.5, but varying with piled spacing.

3.4.2 Solution for piled raft

3.4.2.1 Randolph (1994) and Poulos (2002)

- The settlement of each component (raft and piled group) may be expressed as

$$\begin{Bmatrix} w_p \\ w_r \end{Bmatrix} = \begin{bmatrix} 1/k_p & \alpha_{pr}/k_r \\ \alpha_{rp}/k_p & 1/k_r \end{bmatrix} \begin{Bmatrix} P_p \\ P_r \end{Bmatrix} \tag{3.67}$$

where α_{pr} and α_{rp} are the interaction factors

P and *k* are the loads and stiffnesses relating to each component

- The interaction factors are related by

$$\alpha_{pr} = \alpha_{rp}\frac{k_r}{k_p} \tag{3.68}$$

- Since the (average) settlement of piles and raft are identical, the overall stiffness, k_{pr},

can be calculated as

$$k_{pr} = \frac{P_p + P_r}{w_{pr}} = \frac{1+(1-2\alpha_{rp})(k_r / k_p)}{1-\alpha_{rp}^2 (k_r / k_p)} k_p \tag{3.69}$$

- The proportion of load carried by the piles can be calculated as

$$\frac{P_p}{P_p + P_r} = \frac{1}{1+\frac{P_r}{P_p}} = \frac{k_p - \alpha_{rp} k_r}{k_p + \left(1-2\alpha_{rp}\right) k_r} \tag{3.70}$$

- The proportion of load carried by the raft can be calculated as

$$\frac{P_r}{P_p + P_r} = \frac{1}{\frac{P_p}{P_r}+1} = \frac{\left(1-\alpha_{rp}\right) k_r}{k_p + \left(1-2\alpha_{rp}\right) k_r} \tag{3.71}$$

- The estimation of interaction factor, α_{rp}, is based on the solution of single piles with circular caps of radius, r_c, as shown in Figure 3.8.

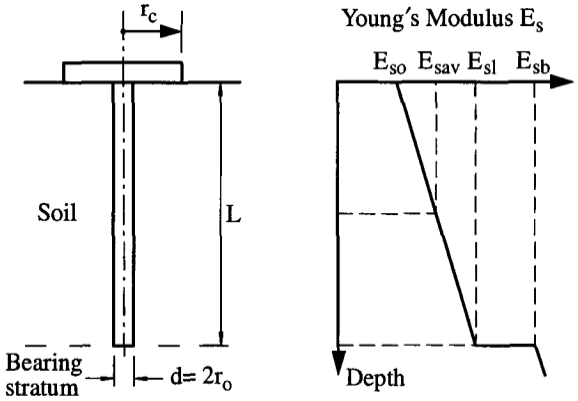

Figure 3.8 Simplified representation of piled raft unit (Poulos, 2002)

The value of α_{rp} can be calculated by

$$\alpha_{rp} = \frac{\ln\left(r_m / r_c\right)}{\ln\left(r_m / r_0\right)} = 1 - \frac{\ln\left(r_c / r_0\right)}{\zeta} \tag{3.72}$$

where r_m = the radius of influence of the piles, r_c = average radius piled cap (corresponding to an area equal to the raft area divided by number of piles), r_0 = radius of piles.

$$\zeta = \ln\left(\frac{r_m}{r_0}\right) \text{ and } r_m = \{0.25 + \xi[2.5\rho(1-\nu) - 0.25]\} \times l$$

$\xi = E_{sl} / E_{sb}$, $\rho = E_{sav} / E_{sl}$, ν = Poisson's ratio of soil, l = piled length, E_{sl} = soil Young's modulus at the level of piled tip, E_{sb} = soil Young's modulus of the bearing stratum below the piled tip, E_{sav} = average soil Young's modulus along piled shaft.

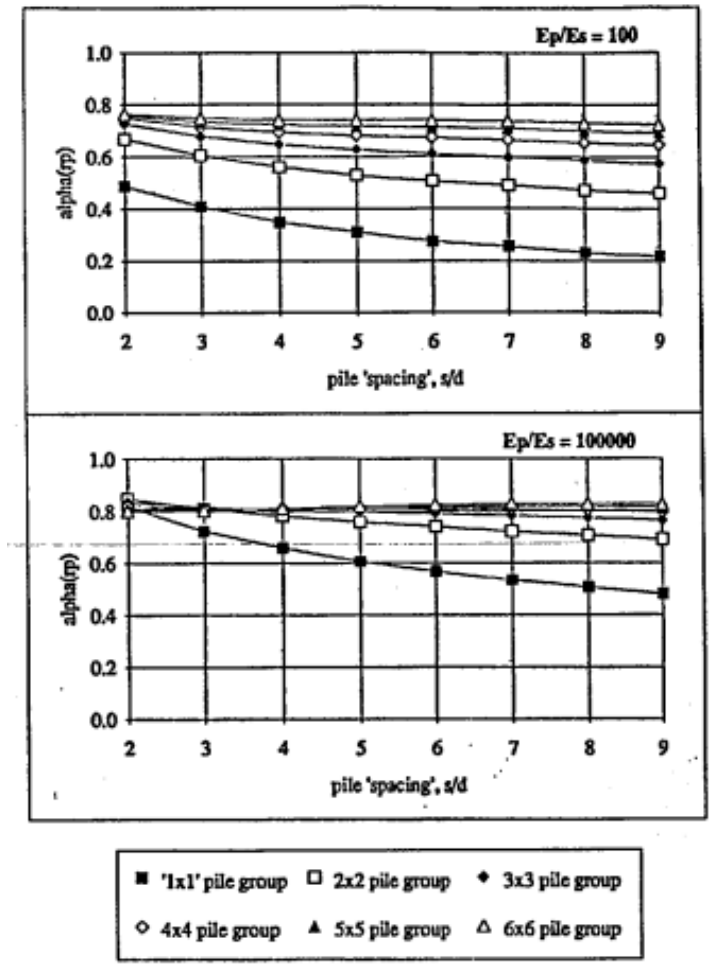

Figure 3.9 Values of interaction factor, α_{rp}, for groups of varying size (Randolph, 1994)

This relationship is extended for larger piled groups, where an equivalent radius, r_c, is calculated from the area of raft associated with each pile. However, as mentioned in Randolph (1994), when the group size increases, the value of α_{rp} tends toward a constant value of about 0.8, independent of the piled spacing, slenderness ratio or stiffness ratio. Figure 3.9 shows the relationship between interaction factor, α_{rp}, and piled spacing, s/d.

***Discussion**:

- *For* $\alpha_{rp} = 0.8$, the equation of stiffness of piled raft is reduced to

$$k_{pr} = \frac{P_p + P_r}{w_{pr}} = \frac{1 - 0.6(k_r / k_p)}{1 - 0.64(k_r / k_p)} k_p \tag{3.73}$$

This equation is same as the equation presented in Poulos (2000), and the combined stiffness of piled raft is close to that of the piled group alone.

- The ratio of loads carried by the raft and piled group is

$$\frac{P_r}{P_p} = \frac{0.2}{1 - 0.8(k_r / k_p)} \frac{k_r}{k_p} \tag{3.74}$$

This equation is same as the equation of X presented in Poulos (2000), and the value of X typically lie in the range 0.3 – 0.5 times (k_r/k_p).

3.4.2.2 Equivalent pier approach

The stiffness of piled raft can be calculated from the stiffness of pier including complete piled raft (piled group plus raft). The steps of the calculations are same for pier of piled group (*see 3.4.1.3*).

3.4.2.3 Poulos (2005)

α_{rp} = 0.6 – 0.8 (the larger value being relevant for larger numbers of piles)

3.4.3 Solution for differential settlement

Randolph (1994) and Poulos (2002) present method for estimation of differential settlement of piled raft foundation. As shown in Poulos (2002), most analyses of pile group settlement make one of the two following extreme assumptions:

1. The pile cap is perfectly rigid so that all piles settle equally (under centric load) and hence there is no differential settlement.
2. The pile cap is flexible, so that the distribution of load onto the piles is known; in this case, the differential settlements within the group can be computed, ignoring the effect of the raft.

In reality, the situation is usually between these two extremes. Randolph (1994) has developed useful design guidelines for assessing the differential settlement

within a uniformly loaded pile group.

+ For a perfectly flexible pile cap, Randolph has related the ratio of differential settlement ΔS to the average group settlement, S_{av}, to a ratio R, as follows:

$$\Delta S/S_{av} = fR/4 \qquad \text{for } R \leq 4 \qquad (3.75a)$$

$$\Delta S/S_{av} = f \qquad \text{for } R > 4 \qquad (3.75b)$$

where f = 0.3 for center-to-midside, and 0.5 for center-to-corner;

$$R = (ns/L)^{0.5} \qquad (3.75c)$$

n = number of piles; s = pile center-to-center spacing; L = pile length.

For pile caps with a finite rigidity, the differential settlements will reduce from the above values (which are for perfectly flexible pile caps), and Randolph suggests that the approach developed by Randolph and Clancy (1993) be adopted. This approach relates the normalized differential settlement to the relative stiffness of the pile cap (considered as a raft). Mayne and Poulos (1999) have developed a closed-form approximation for the ratio of comer to center settlement of a rectangular foundation, and from this approximation, a rigidity correction factor, f_R can be derived:

$$f_R \approx 1 / (1+2.17\ K_F) \qquad (3.76a)$$

$$\text{where } K_F = (E_r/E_{sav})\ (2t/d)^3 \qquad (3.76b)$$

K_F = foundation flexibility factor; E_r = Young's modulus of pile cap; E_{sav} = representative soil Young's modulus beneath the cap (typically within a depth of about half the equivalent diameter of the cap); t = thickness of pile cap; d = equivalent diameter of pile cap (to give equal area with the actual cap).

The factor f_R from equation (3.76a) is then applied to the maximum differential settlement estimated from equations (3.75).

3.5 Conclusions

In normal condition, PDR method can be used to estimate the overall behavior of piled raft foundation, but it shows a limitation on estimate of piled loads for the piles and bending moments for the raft. MPDR with some modifications on solutions for interaction between piles in piled group, interaction between raft and piled group in piled raft, and differential settlement gave some improvement to PDR method.

However, in both PDR and MPDR methods, the interaction between raft and piled group is used of the result from interaction between a circular cap and one pile and it is still a limitation.

Extending the solution of simplified methods to piled raft in ground subsidence condition is limited because of the complicated interaction between raft, piles and soil. FE analysis with full interaction between raft, piles and soil are taken into account should be used for estimating full behavior of piled raft foundation, especially in ground subsidence condition.

CHAPTER IV

CENTRIFUGAL ANALYSIS OF MODEL PILED RAFT IN GROUND SUBSIDENCE CONDITION

4.1 Introduction

This chapter presents the centrifugal analysis of model piled raft in ground subsidence condition. The centrifugal modeling including testing cases, testing apparatus, foundation models, instrumentations, soil preparations, soil properties, foundation installation and loading stages were presented in details. Six cases of model piled rafts including group 1 (soil condition 1) and group 2 (soil condition 2) were conducted in this study. The testing results and some discussions were also given for model foundations in ground subsidence condition.

4.2 Centrifugal Modeling

4.2.1 Testing Cases

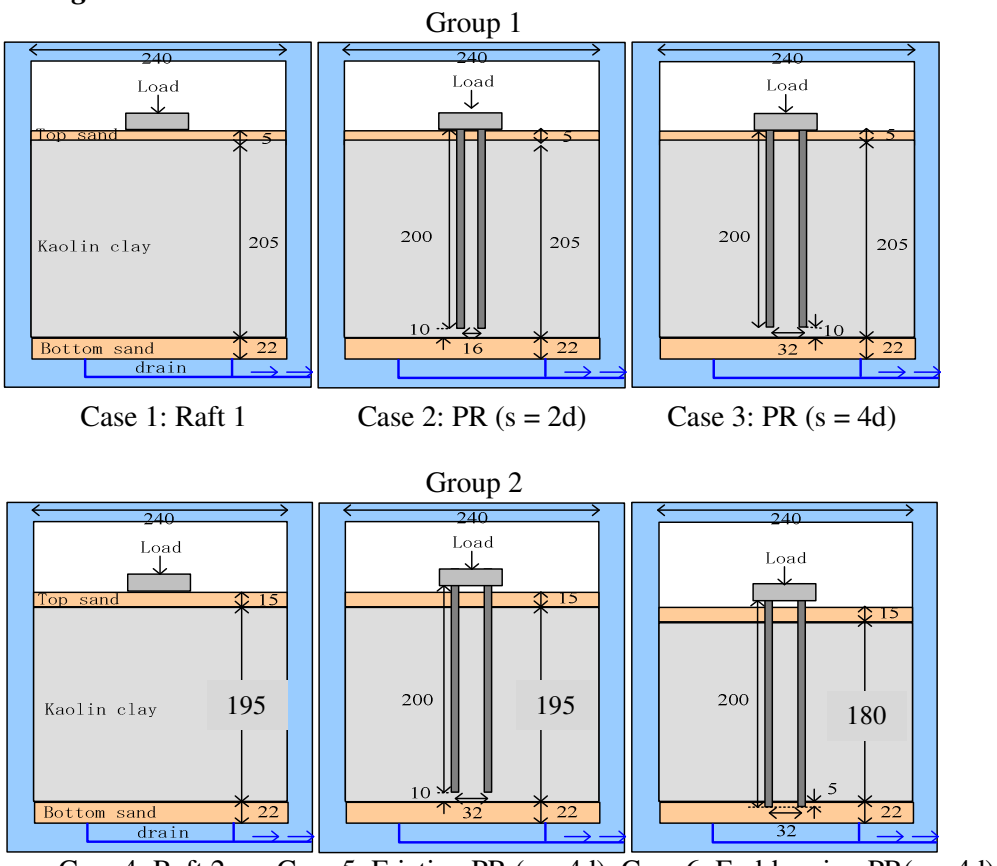

Figure 4.1 Six cases of model foundations in centrifugal tests (PR = piled raft)

In order to evaluate the effectiveness of piles, effect of piled spacing and effect of piled base as well as to estimate the effects of ground subsidence causing by groundwater pumping on raft and piled raft foundations, six cases were conducted in this study. Figure 4.1 shows the six cases of model foundations in centrifugal tests. Case 1 and case 4 was plain raft foundations and the difference between these cases was the thickness of top sand layer and Kaolin clay layer. Case 2 and case 4 were friction piled rafts with piled spacing of 2d and 4d, respectively. Case 5 and case 6 were to compare the response between friction and end-bearing piled rafts. All piled raft models were squared 2 x 2 piled raft foundation with the length of pile of 200 mm. Two ground water conditions including undrained (without groundwater pumping) and drained (with groundwater pumping) were considered in centrifugal tests.

4.2.2 Testing Apparatus

The centrifugal testing equipment of the Disaster Prevention Research Institute (DPRI) in Kyoto University was used for this study. Total allowable weight is 140 kg. The effective radius of the centrifuge is 2.5 m and the maximum payload is 24 G-ton. Figure 4.2 shows a photo of testing apparatus used in this study (T. V. Tran et al., 2012).

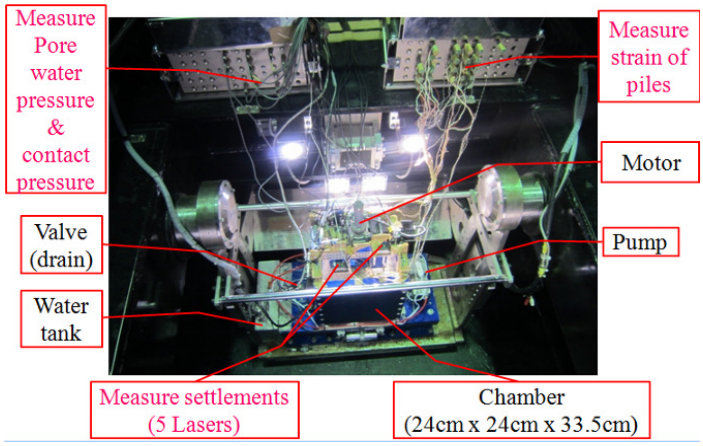

Figure 4.2 Photo of testing apparatus used in this study

The soil chamber had the inside dimension of 240 mm x 240 mm x 335 mm, and the thickness of 30 mm. The acceleration applied to the testing models was 50g. The models were scaled down to ratio of 1/50. Scaling laws presented in Table 4.1 were applied for the relationship between the model and the prototype.

Table 4.1 Scaling laws

Parameters	Scale*	Parameters	Scale*
Acceleration	*N*	Density	*1*
Length	*1/N*	Mass	$1/N^3$
Stress	*1*	Force	$1/N^2$
Strain	*1*	Time (diffusion)	$1/N^2$
Stiffness	*1/N*	Strain rate	N^2

**Scale: model/prototype. N: scale factor*

4.2.3 Foundation Models

Raft and piled raft models are shown in Figure 4.4a. The raft model was made of aluminum alloy and was designed to be a stiff raft. The size of the raft for both cases was 56 mm long, 56 mm wide and 15 mm thick. The dimension of the raft was chosen to satisfy the allowable weight, to minimize boundary effects of the chamber wall, and also to reduce the consolidation time. The ratio between the edge of chamber and the equivalent edge of raft was about 4.3 beyond the effect of rigid wall which was estimated to be at 3 to 4 (Vincenzo, 1998). The model pile was made of closed-end aluminum pipe, which had an outside diameter of 8 mm and the thickness of 1 mm. The length of the pile was 200 mm, taken with the slenderness ratio of 25. The pile diameter was chosen to ease the attachment of strain gauges on its surface. Young's modulus of piles was about 68 GPa and Poisson ratio was taken as 0.34 while the unit weight was about 2.7 g/cm3.

4.2.4 Instrumentations

Figure 4.3 and Figure 4.4 show the details of the instrumentation on the foundation. Figure 4.5 shows the instrumentation of ground model. Strain gauges were attached along pile shaft to measure axial load distribution. A motor was set on the top of the chamber to apply vertical load for foundations via a con rod (Figure 4.5). A load cell was attached at the tip of the con rod to measure applied load. Five laser transducers were used for the test. Two laser transducers were installed to measure the settlement of foundations while other two laser transducers were used to measure of ground surface settlement.

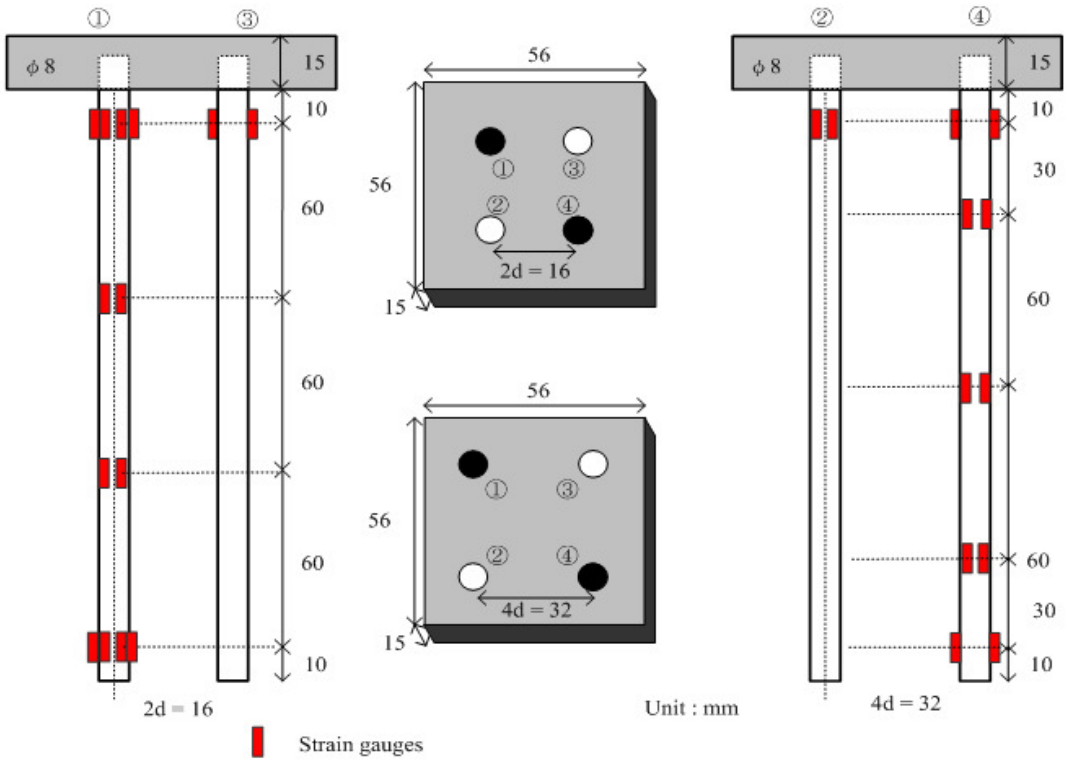

Figure 4.3 Instrumentation of strain gauges in Case 2 & 3

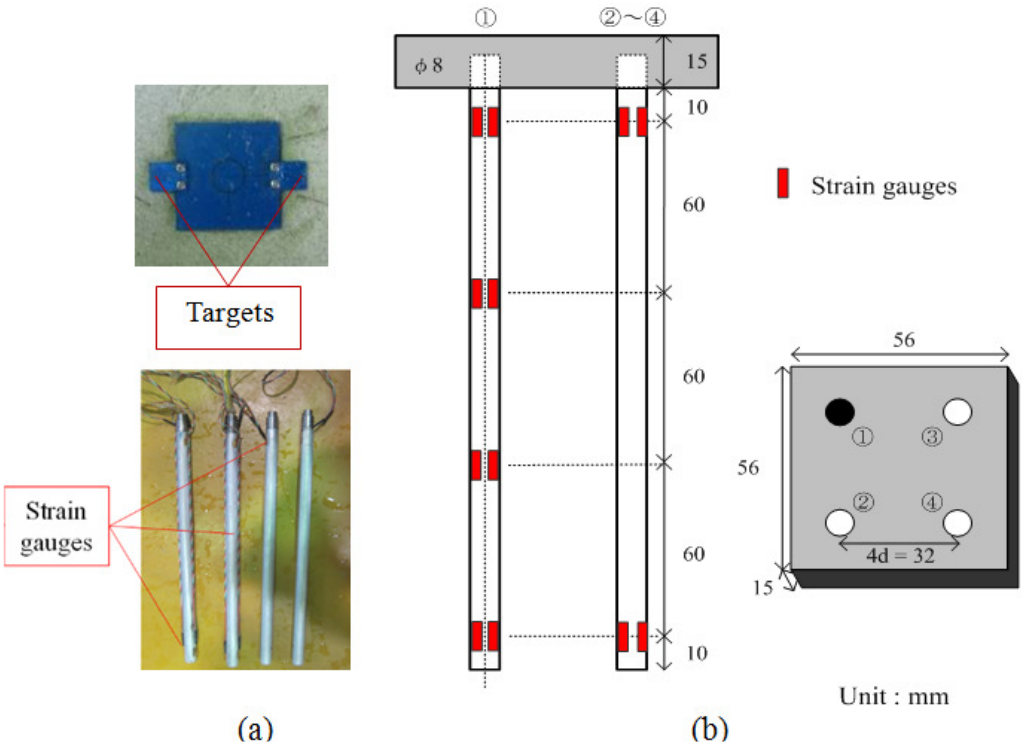

Figure 4.4 Model raft and piles (a) and instrumentation of strain gauges in Case 5 & 6 (b)

The final laser transducer was used to record settlement at the middle of the ground via a telltale. Eight pore pressure transducers were buried in the ground to measure the change of water pressure during loading process. Six of them were embedded below the pile tip and other two were installed at the middle of pile shaft.

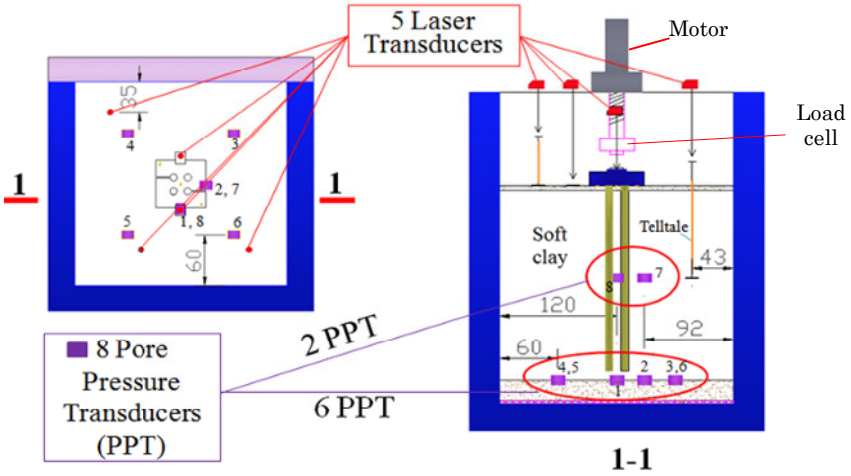

Figure 4.5 Instrumentations of ground model

4.2.5 Soil Preparation

Method of soil preparation is shown in Figure 4.6. Three layers of soil including bottom sand, Kaolin clay and top sand were used in the chamber. Bottom sand was silica sand (grade 6) which was pluviated on the bottom of chamber till it got the thickness of 22mm.

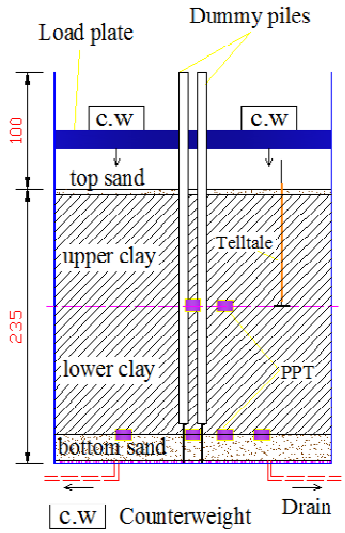

Figure 4.6 Method of soil preparation

This layer was considered as stiff layer (Dr ≈ 80 ÷ 85). Kaolin clay was prepared in 2 layers with the total thickness of 205 mm. Lower layer of clay was preconsolidated at 50g with drained condition for 2 hours. Then upper layer of clay was poured on the lower layer and preconsolidated at 1g with drained condition for 12 hours before preconsolidating at 50g with undrained condition for 8.5 hours. Top sand was a 5 mm thickness of silica sand (grade 6). The effectiveness of this layer was to prevent the clay surface from softening to a slurry condition during the centrifuge tests and to facilitate the contact between the raft and the pile heads. It was poured on the surface of upper layer of clay after installing the testing piles which had been done at the end of preconsolidation. No scale effect was remarked for using top sand layer in the tests (Horikoshi et al., 1996). Grease was used to reduce friction of chamber walls. It is noticed that dummy piles were set into the chamber before preparing of bottom sand layer in case of test with piled raft foundation.

4.2.6 Soil Properties

Figure 4.7 shows a cone penetration test (CPT) and a vane shear test which were used for evaluating undrained shear strength S_u of soil. CTP and vane shear test were immediately performed after completing each centrifugal test. Diameter of the cone was 20 mm and it was penetrated into the soil at a rate of 10 mm/s. Capacity of vane shear tester (FTD20CN-S) was limited to 20 kPa and a vane factor of 0.8 was used for calculating vane shear test result. Figure 4.8 and Figure 4.9 show the result of undrained shear strength S_u of soil models.

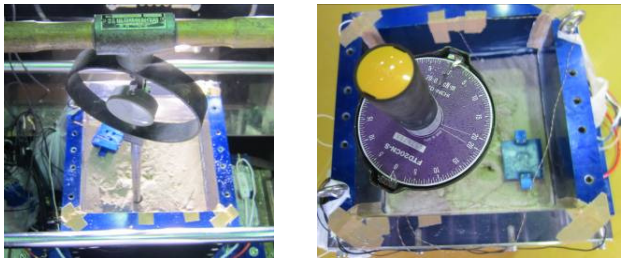

(a) CPT (b) Vane shear test

Figure 4.7 Evaluation of shear strength of soil models

Tests for physical properties and consolidation test were conducted to determine properties of kaolin clay. Soil samples used for these tests were taken from the

chamber after finishing preconsolidation. Results of consolidation test of kaolin clay are shown in Figure 4.10 and Figure 4.11. Table 4.2 summarizes the physical properties of kaolin clay.

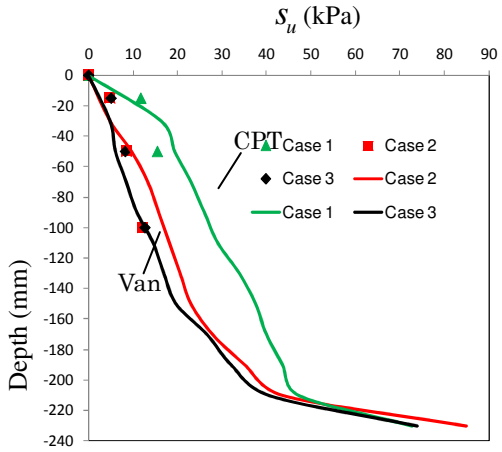

Figure 4.8 Shear strength of soil model in case 1, 2 & 3

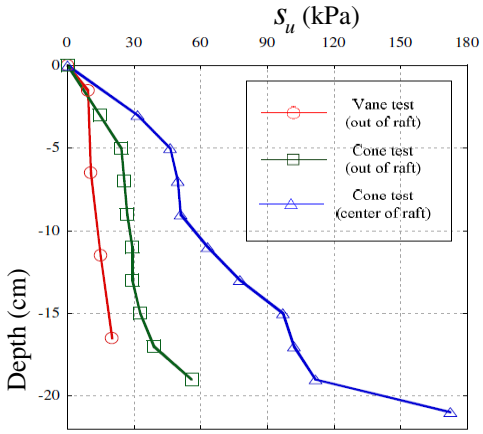

Figure 4.9 Shear strength of soil model in case 4, 5 & 6

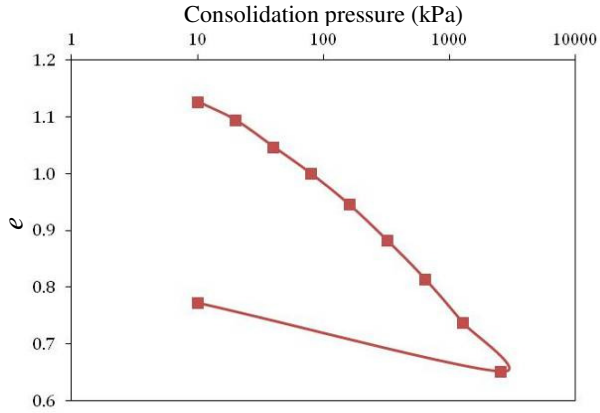

Figure 4.10 e-logP curve of clay case 1, 2 & 3

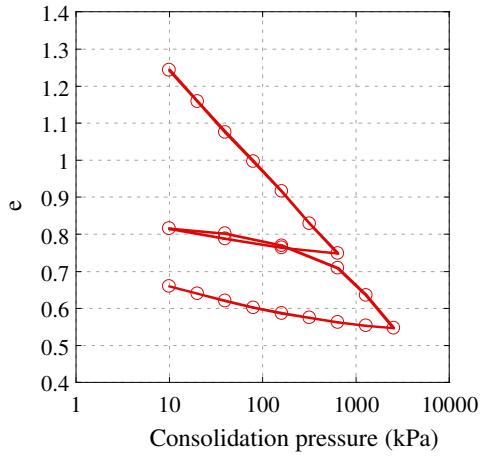

Figure 4.11 e-logP curve of clay case 4, 5 & 6

Table 4.2 Physical properties of kaolin clay

Description	Unit	Kaolin clay
Liquid limit: LL	%	45.54
Plastic limit: PL	%	33.72
Plasticity Index: PI	%	11.82
Water content	%	43.43
Specific gravity: G_s	-	2.634
Density: γ	$kN.m^{-3}$	17.18

Properties of silica sand were determined from specific gravity test and sieve test. The specific gravity G_s of silica sand was 2.65. Figure 4.12 shows the result of sieve test of silica sand. Average particle size *d50* of 0.22 mm and coefficient ununiformity C_u of 1.67 were deduced from Figure 4.12.

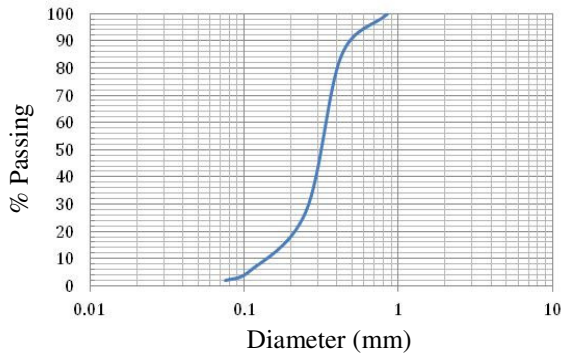

Figure 4.12 Sieve analysis result of silica sand

4.2.7 Foundation Installation

Figure 4.13 shows the method used for installing piled raft model. The piles was installed one by one on the soil (at 1g) at the end of the preconsolidation, after removing dummy piles with external diameter of 8 mm. Piled heads were carefully aligned to avoid inclined piles, different spacing and different embedded length as well. The raft was adjusted to ensure that its surface was horizontal by using water level.

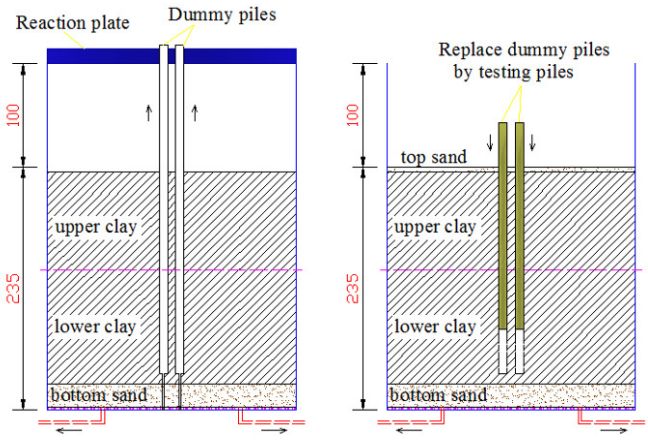

(a) Set up dummy piles (b) Install testing piles

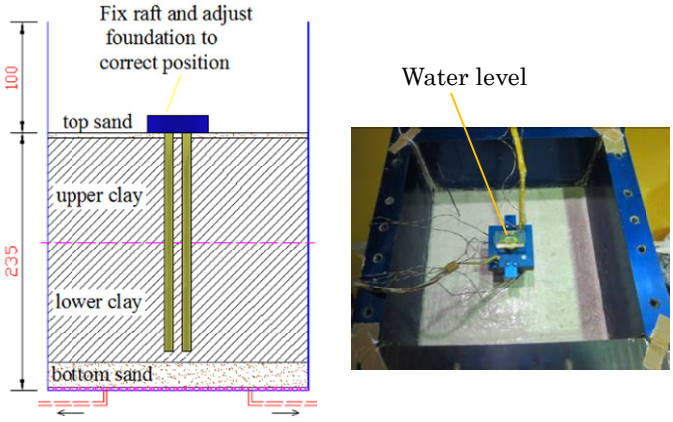

(c) Fix raft with pile head (d) Check raft surface by water level

Figure 4.13 Installation of piled raft model

As discussed in Horikoshi et al. (1996), the piles should be installed in-flight for an accurate simulation of prototype behavior (at 50g). The following stress increase due to self-weight could overcome the initial increase in horizontal stress around piles due

to installation if the piles were installed at lower accelerations. This could lead to remarkable reduction in pile capacity. However, the results of current study were focused on the comparison of undrained and drained conditions for raft and piled raft foundations. Effects of methods of piled installation can be neglected.

4.2.8 Loading Stages

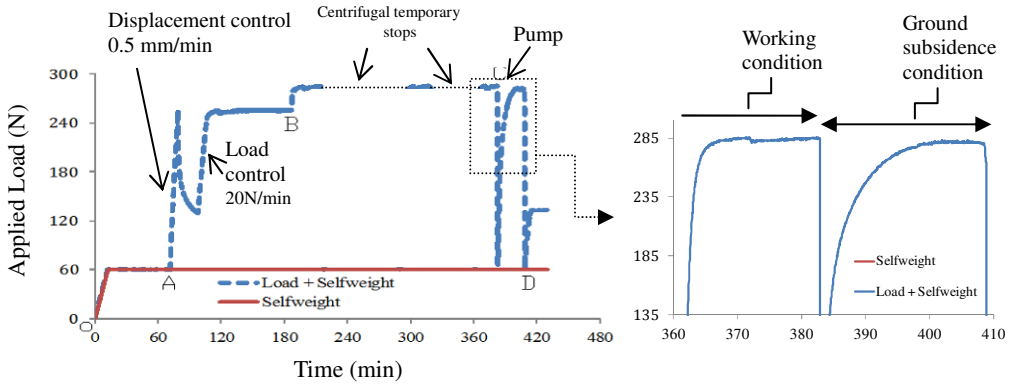

Figure 4.14 Development of applied load with time in case 1

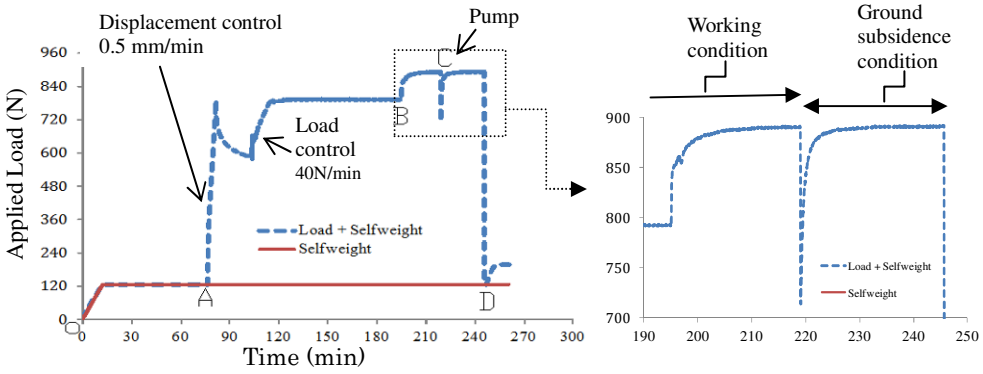

Figure 4.15 Development of applied load with time in case 2

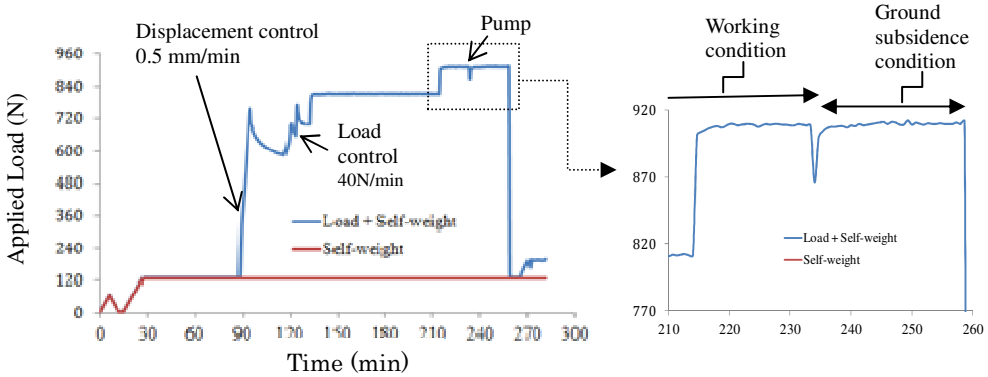

Figure 4.16 Development of applied load with time in case 3

Because of low capacity of raft foundation, value of load used in case 1 was taken about 33 % value of load used in case 2. Loading stages including a prepared stage and two main stages are shown in Figure 4.14, Figure 4.15 and Figure 4.16. Prepared stage (OA): Both case 1, case 2 and case 3 were consolidated under selfweight of the foundations before applying vertical load. Stage 1(AB): The loads were firstly applied to the foundations up to designed values (200 N for case 1 and 660 N for case 2) by displacement control (0.5mm/min) and waited for the dissipation of excess pore water pressure. During that process, the applied loads were decreased because of settlement of soil. Then the loads were increase to the designed values by loading control (20N/min for case 1 and 40N/min for case 2) and waited till the settlements of foundations were almost completed. Stage 2(BCD): The loads were increased about 15 % current values in order to sure that the rafts were fully contacted with the soil surface. Then total loads were kept constantly till finishing the test. To simulate groundwater pumping condition, the soil was drained (point C) by a magnetic valve at the bottom of chamber. Unfortunately, two unexpected stops of centrifugal machine causing the remove of applied load occurred during this stage in case 1(Figure 4.14).

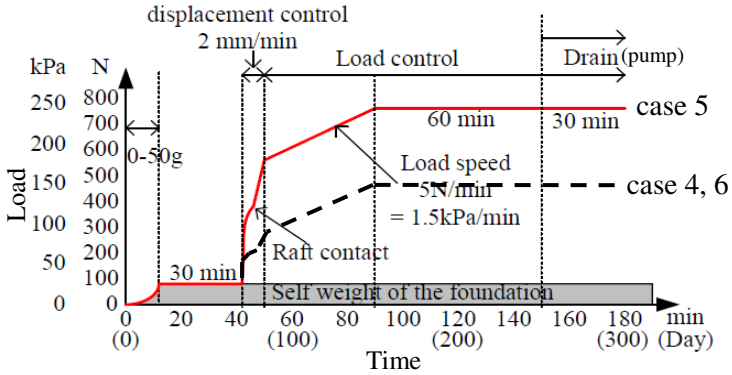

Figure 4.17 Applied loads for case 4, 5 & 6

Figure 4.17 shows type of load used for case 4, case 5 and case 6. The foundations was applied a distribution load of 245 kPa (case 5: friction piled raft) and 145 kPa (case 4: raft and case 6: end-bearing piled raft) and then the water table was pumped (drained) for 30 min.

4.3 Results and Discussions

Comparison of case 1 case 2

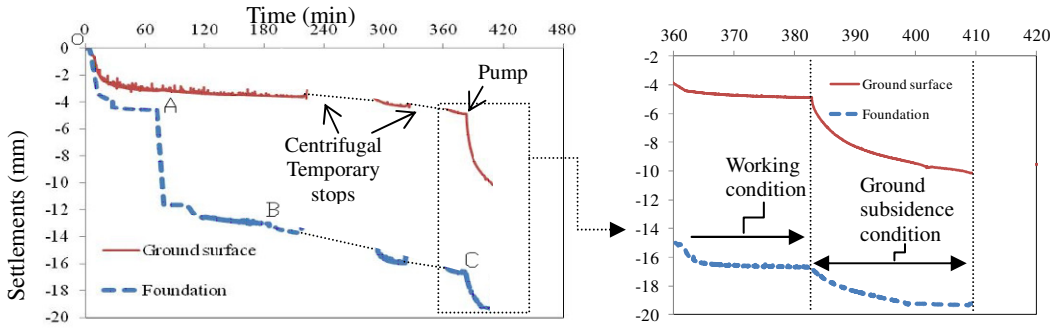

(a) original (b) View

Figure 4.18 Settlements of foundation and ground surface with time in case 1

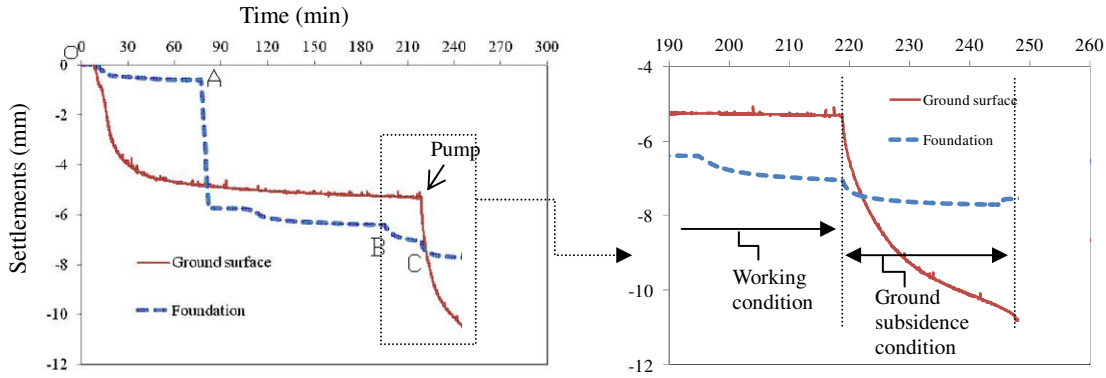

(a) original (b) View

Figure 4.19 Settlements of foundation and ground surface with time in case 2

Figure 4.18 shows settlements of raft foundation and ground surface with time in case 1. Raft foundation settled 4.5 mm and the ground surface settled 2.8 mm after prepared stage (OA). In stage 1 (AB), the settlement of the foundation increased remarkably because of applied load and it got the value of 13 mm at point B. However, ground surface showed a small settlement and it got a value of 3.5 mm at the end of stage 1. In stage 2, the settlement of foundation increased lightly when the applied load was increased 15 % current load of stage 1. The soil swelled largely when the centrifugal machine stopped (BC). At point C, the total settlement of foundation was 16.5 mm while the total settlement of ground surface was 5 mm. During drained condition (CD), the settlements of foundation and ground surface increased significantly. At the end of experiment (point D), the final settlement of foundation was 19.3 mm while a value of 10 mm was measured from the final settlement of ground surface. It is noted that the settlement of raft foundation increased about 2.8

mm and the settlement of ground surface increased about 5 mm in a period of 25 minutes of pumped (drained) condition.

Figure 4.19 presents settlements of piled raft foundation and ground surface with time in case 2. After prepared stage (OA), settlement of foundation was 0.7 mm and the settlement of ground surface was 4.8 mm. In stage 1 (AB), the settlement of foundation increased largely under the applied load. At the end of stage 1 (point B), the settlement of foundation was 6.5 mm and the settlement of ground surface was 5.3 mm. In stage 2 (BCD), the applied load was increased 15 % current load of stage 1. In undrained condition (BC), the settlement of foundation increased 0.5 mm and the settlement of ground surface increased lightly. At point C, the total settlement of foundation was 7 mm while the total settlement of ground surface was 5.4 mm. However, in pumped (drained) condition (CD), the increase of ground surface settlement was larger than the increase of foundation settlement. For example, ground surface settlement increased about 5.5 mm while the settlement of raft foundation increased about 0.7 mm in a period of 25 minutes of pumped (drained) condition. At the end of test (point D), the final settlement of foundation was 7.7 mm and the settlement of ground surface was 10.9 mm.

Figure 4.20 shows the relationship between foundation settlement which was normalized by raft thickness T_r and applied load which was normalized by undrained shear strength S_u for both cases 1 and case 2. It is noticed that the settlement of the foundation caused by prepared stage was ignored in Figure 4.20 and Figure 4.21. When the piles were added to the foundation, the settlement of the foundation decreased significantly. In other words, the bearing capacity of piled raft foundation increased remarkably. As shown in Figure 4.20, at a settlement of 32 % raft thickness (4.8mm), the bearing capacity of piled raft foundation was 4.2 times larger than the bearing capacity of raft foundation. It confirms the effective of piles in reducing settlement for piled raft foundation in normal (undrained) condition (Burland, 1995).

In pumped (drained) condition, the bearing capacity of the foundation was also improved appreciably. For example, at the settlement of 45 % raft thickness (6.8 mm), the bearing capacity of piled raft foundation was 5.1 times larger than the bearing capacity of raft foundation.

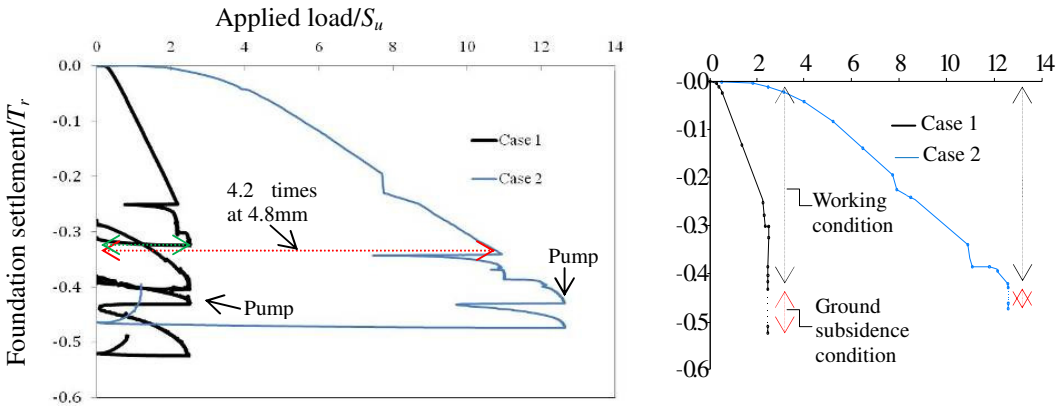

(a) original (b) simplification

Figure 4.20 Found. settlements/raft thickness vs applied load/undrained shear strength

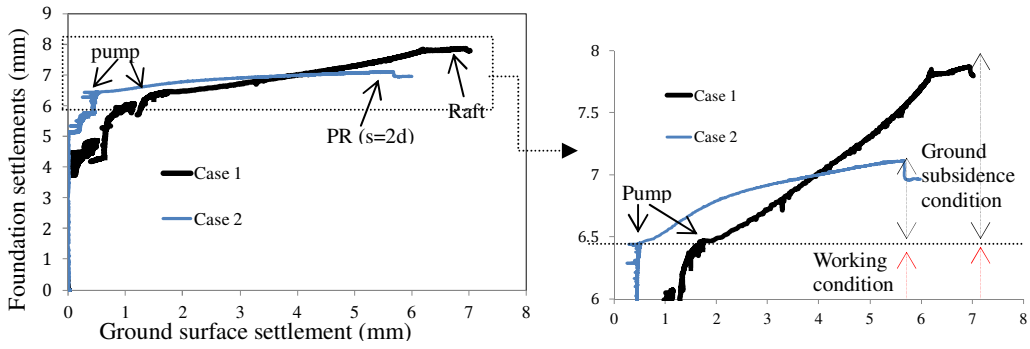

(a) original (b) View of small rectangular

Figure 4.21 Foundation settlements versus ground surface settlement

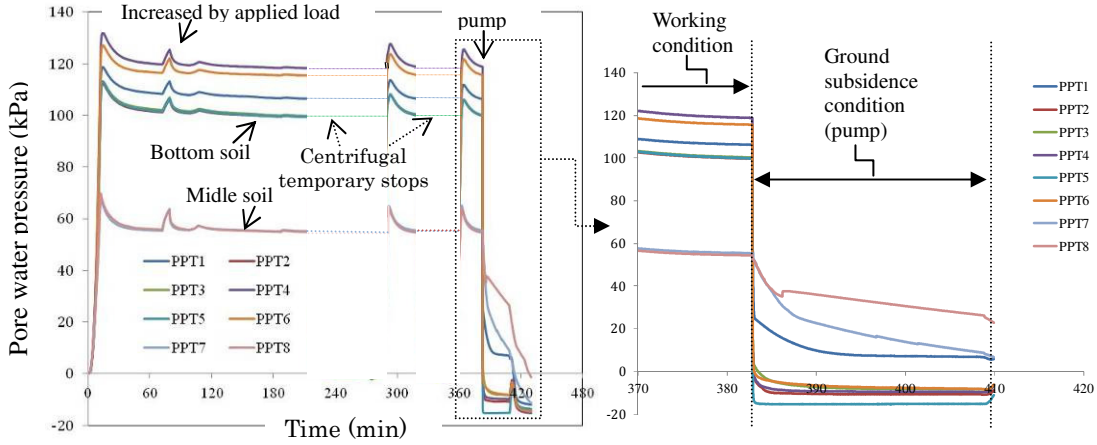

(a) original (b) View with simplification

Figure 4.22 Change of pore water pressure with time in case 1

Figure 4.21 presents the relationship between foundation settlement and ground surface settlement. It revealed that both raft and piled raft foundations continued to

settle as ground surface settlement increased. However, regarded to the effect of ground surface settlement, settlement of raft foundation was more affected than settlement of piled raft foundation.

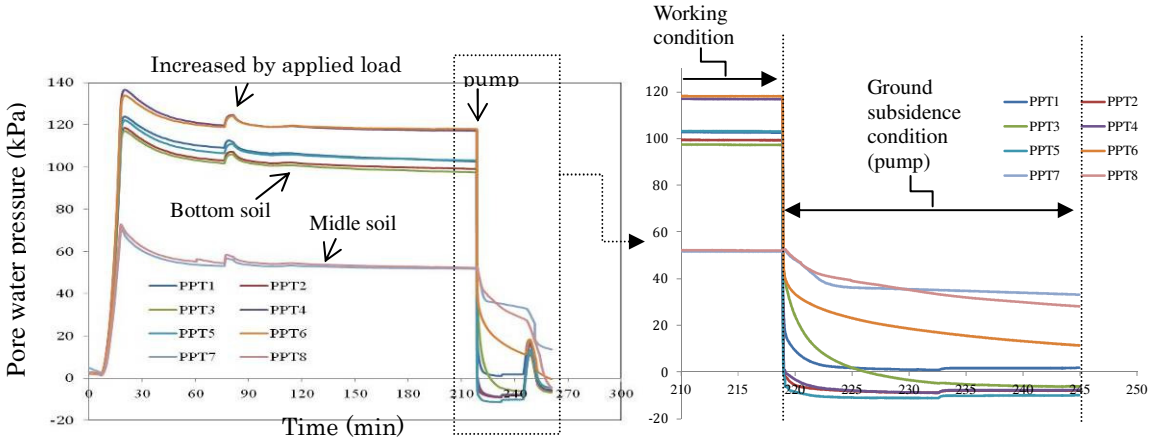

(a) original (b) View with simplification

Figure 4.23 Change of pore water pressure with time in case 2

Figure 4.22 and Figure 4.23 present the change of pore water pressure with time in case 1 and case 2, respectively. The values of pore pressure transducers at the bottom soil were around 2 times the values at the middle soil in both case 1 and case 2. When the applied load was applied by displacement control method, the load was firstly carried by the water in the soil. Then the applied load was transferred to the soil structures during dissipation of excess pore water pressure and the settlement of the soil increased.

For checking soil conditions during the test, additional results are also presented in this chapter. These results consist of change of pore water pressure in the soil, variation of air pressure in water tank and distribution of contact pressure under the raft during centrifuge tests.

Figure 4.24 and Figure 4.25 show the variation of air pressures in water tank in cases 1 and case 2 respectively. The air pressure in the water tank increased up to the values of 6 kPa because of increasing gravity in prepared stage and was constantly kept at that value during stage 1 and stage 2.

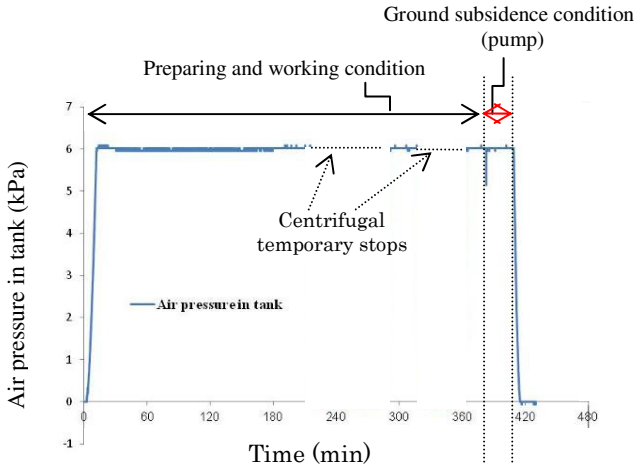

Figure 4.24 Variation of air pressure in tank with time in case 1

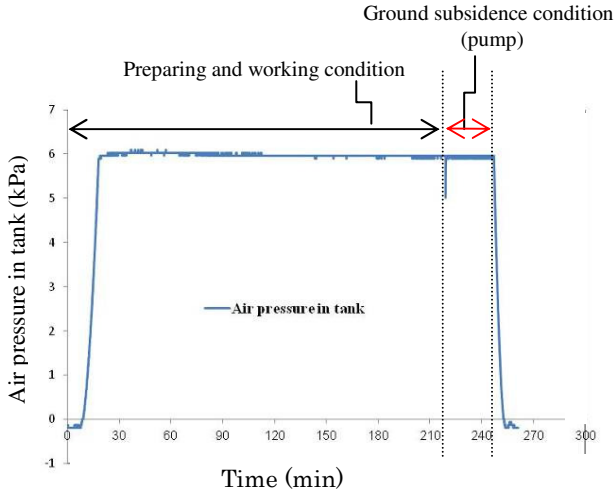

Figure 4.25 Variation of air pressure in tank with time in case 2

Comparison of case 2 case 3

Case 2: s = 2d

Case 3: s = 4d

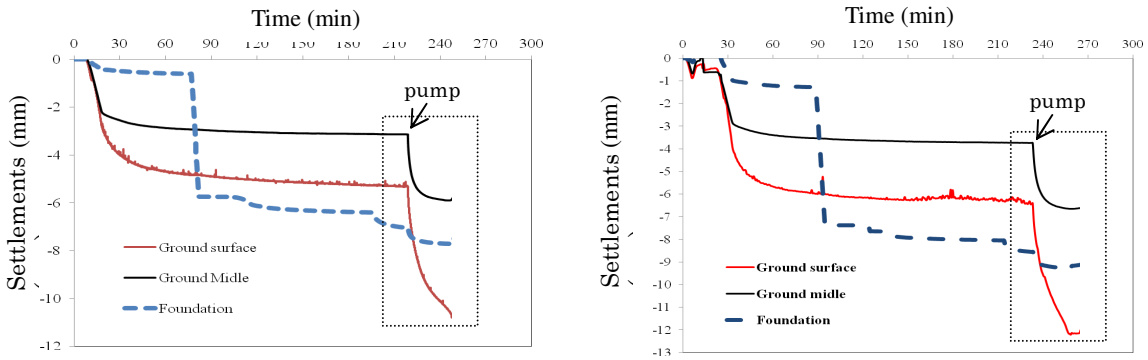

(a) original

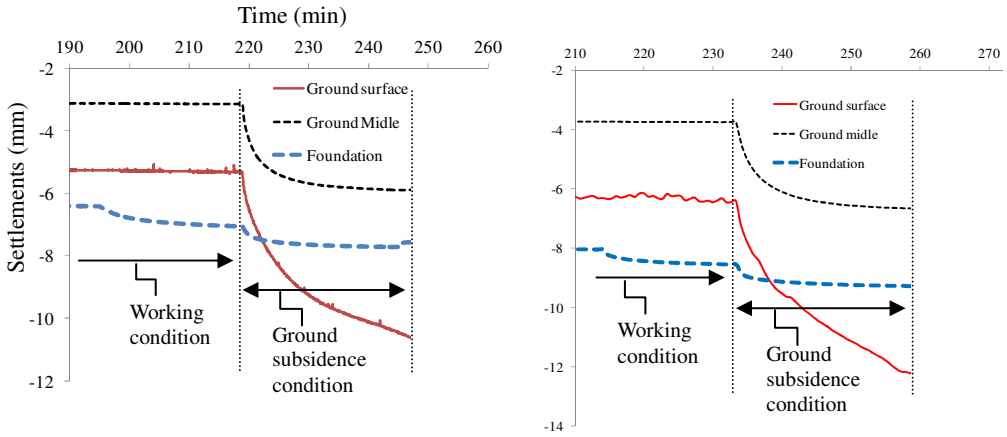

(b) View of small rectangulars

Figure 4.26 Settlements of ground surface, ground middle and foundation with time

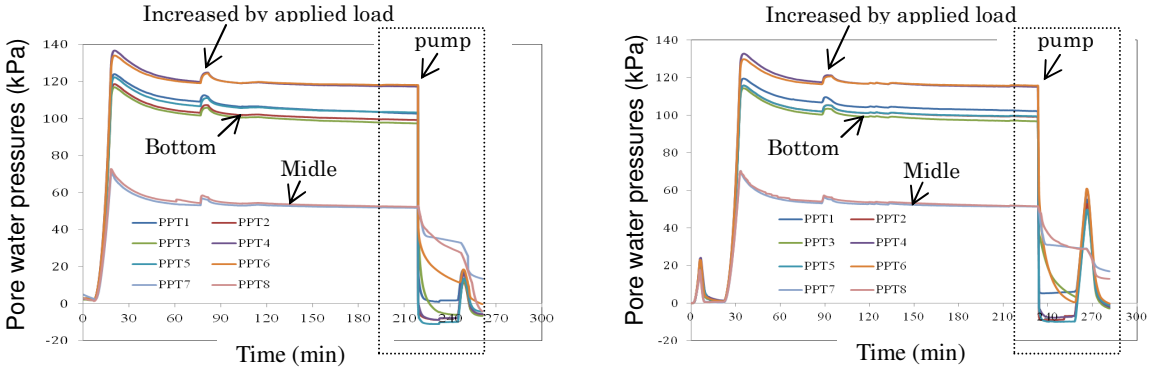

(a) original

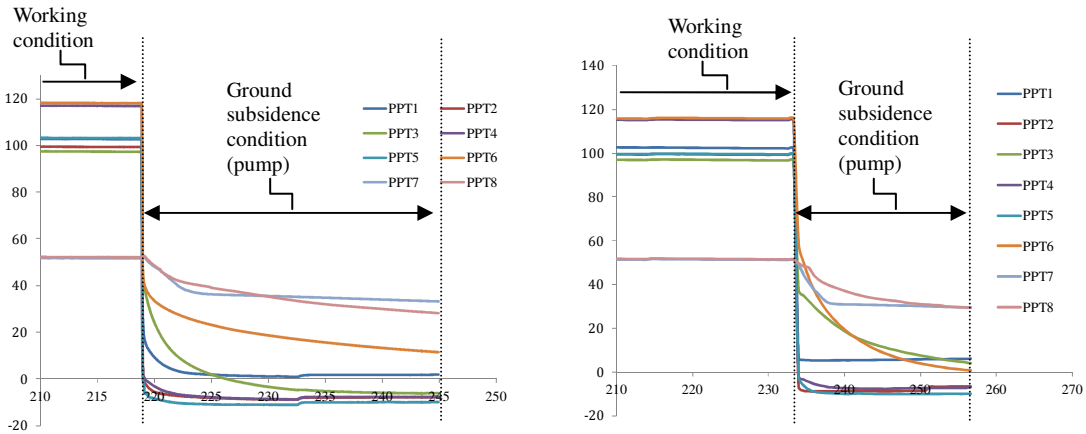

(b) View of small rectangulars

Figure 4.27 Variation of pore water pressures with time

Figure 4.26 shows settlements of ground surface, ground middle and foundation with time in case 2 and case 3. The settlements behavior of both tow cases are in the same

way. When ground subsidence condition occurred (pumped condition), the settlement of the piled raft foundation was increased. The increments of the settlement are nearly same for case 2 and case 3. Settlements of ground middle are around 50% compared to settlement of ground surface.

Figure 4.27 presents the variations of pore water pressures during the centrifugal tests. When the applied load was applied by displacement control method, the load was firstly carried by the water in the soil. Then the applied load was transferred to the soil structures during dissipation of excess pore water pressure and the settlement of the soil increased. Values of pore pressure transducers at the bottom soil were around 2 times the values at the middle soil in both case 2 and case 3.

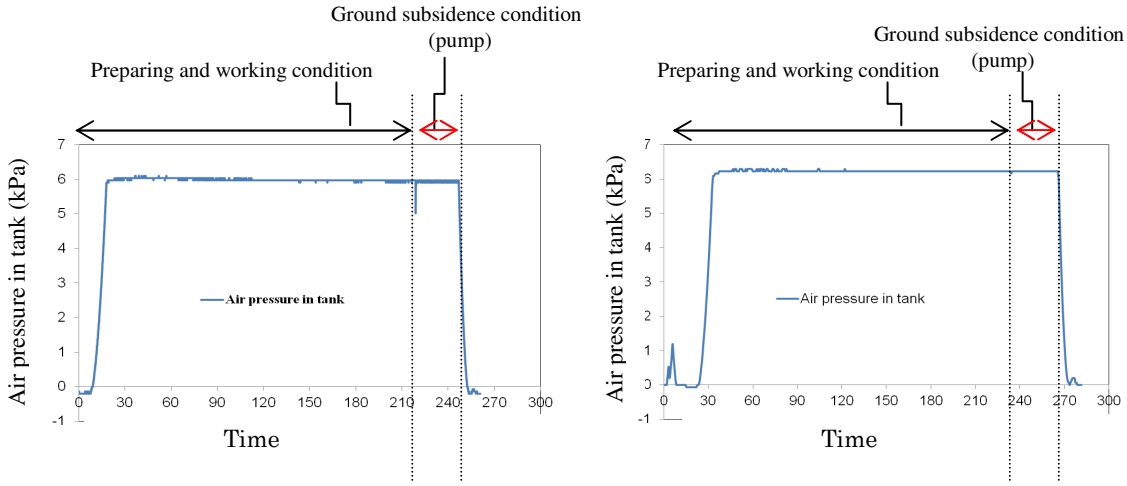

(a) case 2 (b) case 3

Figure 4.28 Variation of air pressure in water tank with time

Variation of air pressures in water tank in cases 2 and case 3 are shown in Figure 4.28. The air pressure in the water tank increased up to the values of 6 kPa because of increasing gravity in prepared stage and was constantly kept at that value during the centrifugal tests.

Figure 4.29 presents a comparison of load-settlement curves between case 2 and case 3. The foundation settlements was normalized by the width of raft (56mm) and the applied load was normalized by average undrained shear strength S_u for both case 2 and case 3. It is noticed that the settlement of the foundation caused by seflweight was ignored in Figure 4.29. The changing tendency of load-settlement

curves is nearly same for both two cases. When pumped (drained) condition is applied to the soil, the settlement is largely increased under constant loads.

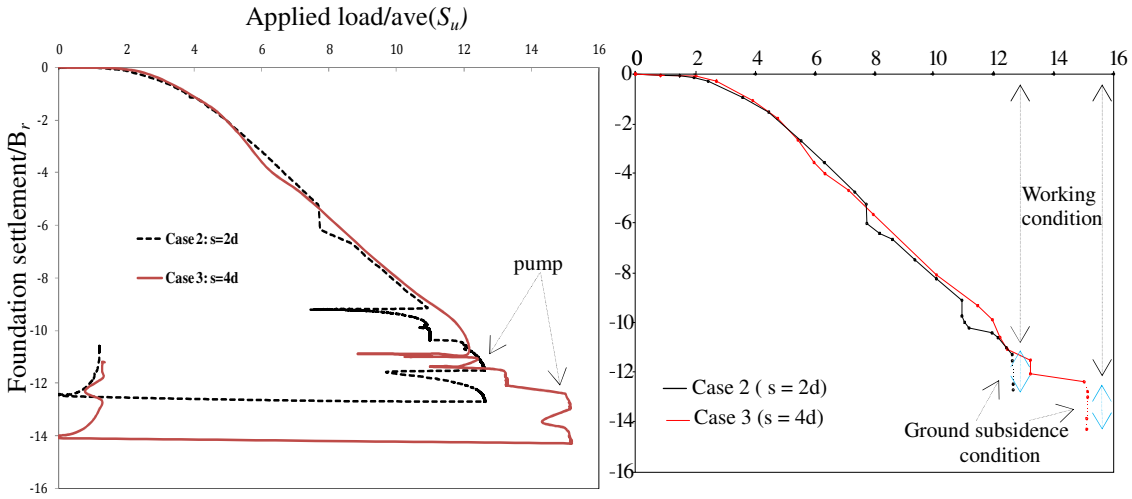

(a) original (b) simplification

Figure 4.29 Comparison of load – settlement curves

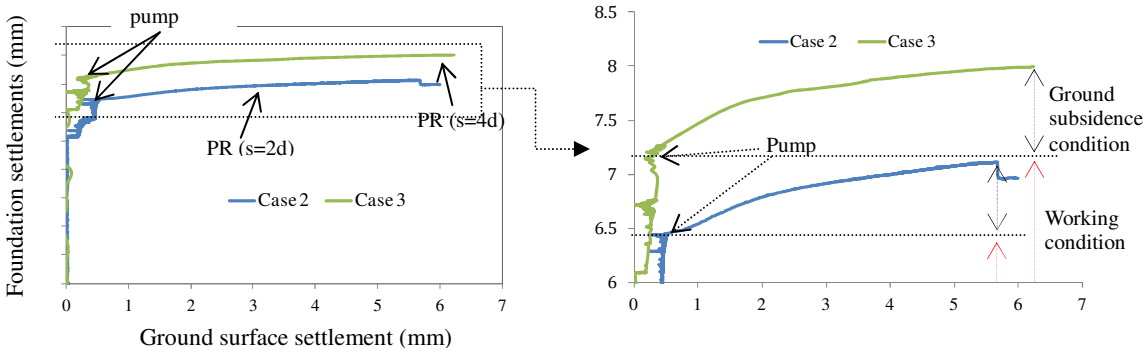

(a) original (b) View with simplification

Figure 4.30 Comparison of ground subsidence – foundation settlement curves

Relationship between foundation settlement and ground surface settlement is presented Figure 4.30. It can be seen that both case 2 and case 3 continued to settle as ground surface settlement increased. Regarding to the piled spacing, the effect of piled spacing on the settlement of the foundations is remarkable for case 3 (s = 4d).

Comparison of case 4, case 5 and case 6

The comparison of load - displacement curves of case 4, case 5 and case 6 are shown in Figure 4.31. For all of the results, settlement from self weight was ignored. From

the settlement of around 0.2 mm, the settlement of case 5 increased rapidly due to slip of piles but the settlement of case 6 increased gradually due to bearing resistance from bearing ground. The settlement stiffnesses were about 35 N/mm and 370 N/mm for case 5 and case 6 respectively. From settlement of around 3.5 mm, the applied load of case 5 and total axial force of pile top made a difference gradually because the raft started to share the applied load (raft started to contact with ground surface). The settlement stiffness of case 5 was also increased to around 130 N/mm from the settlement of around 3.5 mm. This increment of stiffness in case 5 came from the support of the raft. Less settlement was found on end-bearing piled raft in both normal (undrained) and pumped (drained) conditions. However, larger settlements were seen on raft and friction piled raft in both normal and pumped conditions. After pumping about 30 min, the total axial force of pile top became equal to applied load due to larger ground settlement than raft settlement.

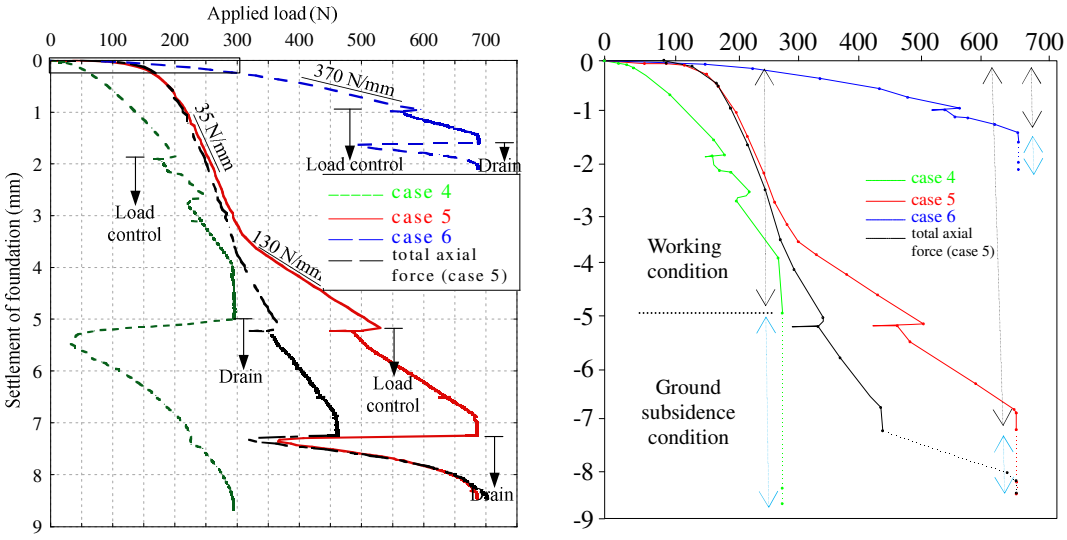

(a) original (b) simplification

Figure 4.31 Load-settlement curves of case 4, 5 & 6

Figure 4.32 show the distribution of axial force with depth in ground subsidence condition for case 5 and case 6. In ground subsidence condition, the axial force in piles (both friction and end-bearing piles) was increased with depth to neutral plans because of negative skin friction. The neutral plans were occurred at depths of around 140 mm and 180 mm for friction piles and end-bearing piles, respectively. The increment of axial force in end-bearing piles was larger than in friction piles.

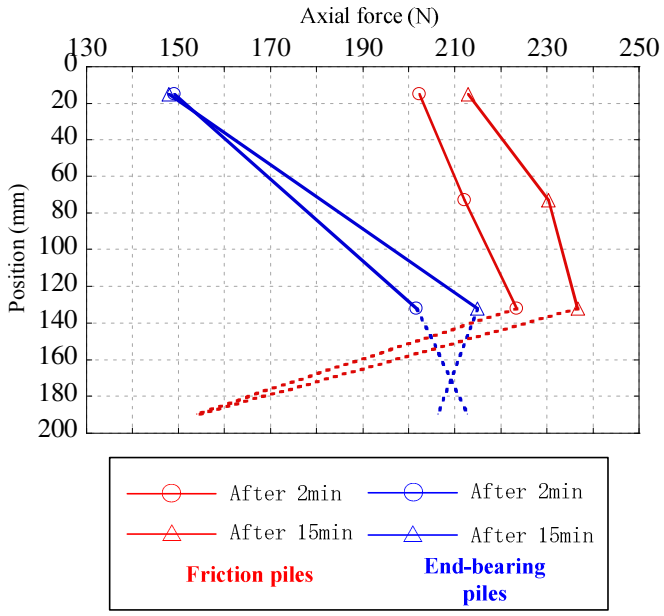

Figure 4.32 Distribution of axial force with depth in ground subsidence condition (case 5 & 6)

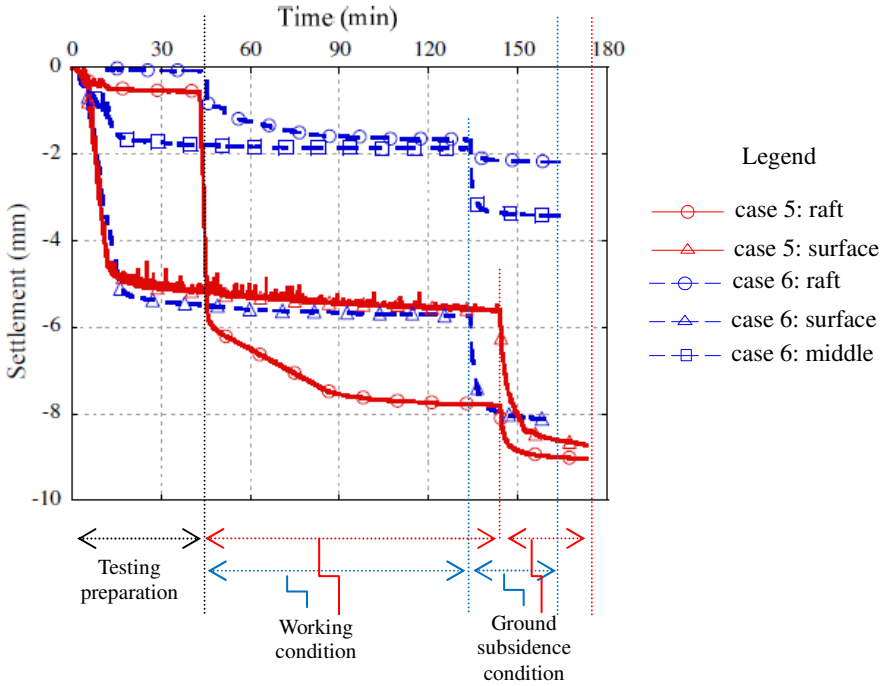

Figure 4.33 Settlement with time of case 5 & 6

Time settlement results of case 5 and case 6 are shown in Figure 4.33. When acceleration of centrifuge increased from 1g to 50g, compared with ground surface settlement of around 5.5 mm, rafts settled 0.5 mm in case 5 and less than 0.1 mm in

case 6, respectively. These differences made a difficulty for loading of the foundation so that the raft always contact with the ground surface.

4.4 Conclusions

Based on experimental results, the settlement of foundations increased nearly linear with ground subsidence. In ground subsidence condition, when piled spacing increased (2d to 4d), the settlement of foundation increased and axial load of the piles increased. After pumping ground water for about 30 min, the total axial force of pile top became equal to applied load due to larger ground settlement than raft settlement. Negative skin friction of end-bearing piled raft was very larger than that of friction piled raft in ground subsidence condition.

CHAPTER V

NUMERICAL ANALYSES OF PILED RAFT IN GROUND SUBSIDENCE CONDITION

5.1 Introduction

This chapter presents the geotechnical parameter assessment, verification of analysis, and parameter study of model piled rafts and piled rafts in Bangkok soil. The work was conducted by three-dimensional finite element analysis using Plaxis 3D. The purpose of these analyses was to find the trend of variation of load-settlement curves, load distribution between group of piles and raft, and the change in axial force of the pile under effect of ground subsidence. For piled raft in Bangkok soil, three cases including 30-storey building with 6 basements, 6-storey building with 3 basements and 5-storey building under the effect of ground subsidence were considered. Numerical analysis was performed for different levels of ground water table and different piled configurations.

5.2 Geotechnical Parameter Assessment

The design of piled raft requires an assessment of a number of geotechnical and performance parameters, including:

(a) Raft bearing capacity
(b) Piled capacity
(c) Soil modulus for raft stiffness
(d) Soil modulus for piled stiffness

Correlations from SPT (Poulos, 2000)

Raft ultimate bearing capacity: $p_{ur} = K_1 N_r \quad (kPa)$ (5.1)

Pile ultimate shaft resistance: $f_s = a\left(2.8N_s + 10\right) \quad (kPa)$ (5.2)

Pile ultimate base resistance: $f_b = K_2 N_b \quad (kPa)$ (5.3)

Soil Young's modulus below raft: $E_{sr} = 2N_r \quad (MPa)$ (5.4)

Soil Young's modulus along pile: $E_s = 3N_s \quad (MPa)$ (5.5)

Soil Young's modulus below piled tip: $E_s = 3N_b \quad (MPa)$ (5.6)

where N_r = average SPT-value (corrected to 60% energy ratio) within a depth of one-half of raft width.

N_s = average SPT-value along piled shaft

N_b = average SPT-value close to piled tip

K_1, K_2 = factors shown in Table 4.1

a = 1 for displacement piles in all soils and non-displacement piles in clay

= 0.5 – 0.6 for non-displacement piles in granular soil.

Table 5.1 Correlation factors K_1 and K_2 for ultimate bearing capacity

Soil type	K_1: Raft	K_2: Displacement piles	K_2: Non-displacement piles
Sand	90	325	165
Sandy silt	80	205	115
Clayey silt	80	165	100
Clay	65	100	80

Correlations from CPT

For sand, the friction angle (φ = φ') was calculated from cone resistance by equation from Kalhawy and Mayne (1908, as referenced in Townsend et al., 2001).

$$\phi'_{tc} = 17.6 + 11.0 \times \log\left[\left(q_c / p_a\right) / \left(\sigma'_{v0} / p_a\right)^{0.5}\right] \tag{5.7}$$

Where σ'_{v0} is average effective overburden stress (kPa) and p_a is atmospheric pressure (100kPa).

For clay, the cohesion ($c_u = S_u$) was calculated from cone resistance by the following equation (Lunne et al., 1997):

$$S_u = \frac{q_c - \sigma_{v0}}{N_k} \tag{5.8}$$

Where σ_{v0} is total in situ vertical stress (kPa) and N_k is an empirical cone factor. Based on the work of Lunne et al. (1997), N_k was taken a value of 10 for this study.

Correlations from Experiments

Many researchers proposed typical ranges of Young modulus and Poisson's ratio for

different soils in literatures. A summary of well-known authors conducted by Phongpat Kitpayuck (2009) was referenced in this study.

(a) Young modulus

Clay		
Normally consolidated clay	(200-500) × S_u	(Bowles, J.E., 1988)
Lightly overconsolidated clay	(750-1200) × S_u	(Bowles, J.E., 1988)
Very soft clay	200-1500 t/m^2	(Bowles, J.E., 1988)
Soft clay	500-2500 t/m^2	(Bowles, J.E., 1988)
Soft clay	180-350 t/m^2	(Das, B.M., 2001)
Soft Bangkok clay	150 × S_u	(Bergado et al.,1990)
Medium clay	1500-5000 t/m^2	(Bowles, J.E., 1988)
Medium Bangkok clay	(300-600) × S_u	(NAVFAC.DM.7.1,1982)
Hard clay	5000-25000 t/m^2	(Bowles, J.E., 1988)
Hard clay	600-1400 t/m^2	(Das, B.M., 2001)
Medium Bangkok clay	(240-1200) × S_u	(NAVFAC.DM.7.1, 1982)
Sand		
Silty sand	500-2000 t/m^2	(Bowles, J.E., 1988)
Dense sand	5000-8100 t/m^2	(Bowles, J.E., 1988)
Dense sand	3500-7000 t/m^2	(Das, B.M., 2001)

(b) Poisson's ratio

Clay		
Saturated	0.4-0.5	(Bowles, J.E., 1988)
Medium Clay	0.25-0.4	(Das, B.M., 2001)
Sandy Clay	0.2-0.3	(Bowles, J.E., 1988)
Sand		
Sand	0.1-1.00	(Bowles, J.E., 1988)
Medium Sand	0.25-0.4	(Das, B.M., 2001)
Silty Sand	0.2-0.4	(Das, B.M., 2001)

Based on typical range, Young modulus and Poisson ratio was selected for model soils.

Effective Young modulus was determined from equation (Brinkgreve et al., 2007):

$$E' = \frac{2}{3}(1+\nu')E_u \tag{5.9}$$

ν' is effective poinsson's ratio. It is around 1/3 for most soils, and was taken as 0.3 for sand and 0.33 for Kaolin clay in this study.

Senneset et al. (1989, as referenced in Lunne et al., 1997) summarized typical values of effective cohesion and effective friction angle for various soil types.

Soil types	c' (kPa)	φ' (degree)
Clay, soft	5-10	19-24
Clay, medium	10-20	19-29
Clay, stiff	20-50	27-31
Silt, soft	0-5	27-31
Silt, medium	5-15	29-33
Silt, stiff	15-30	31-35
Sand, loose	0	29-33
Sand, medium	10-20	31-37
Sand, dense	20-50	35-42
Hard, stiff soil, OC, cemented	> 50	38-45

Effective strength parameters were also selected for model soils based on the typical values recommended above.

Coefficients of permeability (k) of model soils were determined as below:

For sand, the coefficient of permeability in cm/sec was calculated from the following empirical expression (Zeevaert, 1973):

$$k = C \times D_{10}^2 \tag{5.10}$$

in which C is a coefficient that has a range of 50 to 150. The average value of 100 was taken for this calculation. D_{10} in centimeters is the diameter at which 10% of the

material passes this diameter. It was defined from the sieve analysis test which was presented in Chapter 3. D_{10} is around 0.015 cm and coefficient of permeability is around 4×10^{-4} m/s or 34.56 m/day.

For clay, coefficient of permeability was taken from the work of Danno et al. (2009) and Das (2007). It was about 1.366×10^{-7} m/s or 11.8×10^{-3} m/day for Kaolin clay and range of typical values as in Table 5.2

Table 5.2 Range of typical values of coefficient of permeability, k (cm/s)

Type of soil	Coefficient of permeability, k (cm/s)
Medium to coarse gravel	Greater than 10^{-1}
Coarse to fine sand	10^{-1} to 10^{-3}
Fine sand, silty sand	10^{-3} to 10^{-5}
Silty, clayey silt, silty clay	10^{-4} to 10^{-6}
Clays	10^{-7} or less

5.3 Verification of Analysis and Parameter Study for Model Piled Rafts

5.3.1 Raft in ground subsidence (compared with centrifugal model test)

Geometry of Foundation

In order to evaluate effect of ground subsidence on the settlement of square raft, a following case was considered in FE analysis.

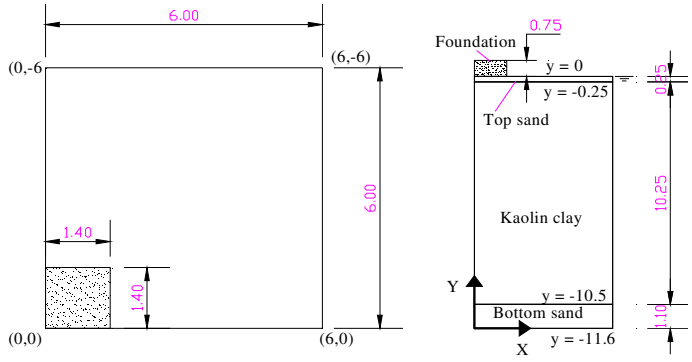

Figure 5.1 Geometry of foundation and soil in FE analysis (unit: m)

A 2.8 x 2.8 x 0.75 m raft was considered in this study. To enable any possible mechanism in Kaolin clay and to avoid any influence of the outer boundary, the model was extended in both horizontal directions to a total width of 6.0 m. Figure 5.1 shows the geometry of foundation and soil in FE analysis.

Properties of Soil and Raft

Table 5.3 Parameters of model soils for FE analysis

Description	Top Sand	Kaolin Clay	Bottom Sand
Depth (m)	0-0.25	0.25–10.5	10.5-11.6
Unit Weight, γ_{sat} (kN/m^3)	18.1	17.2	18.1
Material Model	MC	MC	MC
Permeability, k (m/day)	34.56	0.000118	34.56
Interfaces, R_{inter} (-)	0.7	0.6	0.7
Dilatancy angle, ψ' (degree)	0.0	0.0	0.0
Poisson's ratio, ν' (-)	0.3	0.33	0.3
c' (kN/m^2)	1.0	5.0	1.0
φ' (degree)	28	20	37
E' (kN/m^2)	4333	300	8667

MC: Mohr-Coulomb

Three layers of soil including top sand, kaolin clay and bottom sand were simulated in this analysis. The calculation was done by consolidation analysis with effective parameters. The thickness and properties of each layer of soil are shown in Table 5.3. Young modulus of Kaolin clay was increased with depth, starting at y_{ref} = -0.25m, and the increment was 300kN/m2/m. The properties of raft foundation are presented in Table 5.4.

Table 5.4 Material properties of raft (floor)

Description	Raft
Type of behaviour	Linear, isotropic
Thickness, *t* (m)	0.75
Weight, γ (kN/m^3)	27
Young's modulus, *E* (kN/m^2)	6.8×10^7
Poisson's ratio, ν (-)	0.15

Type of Load

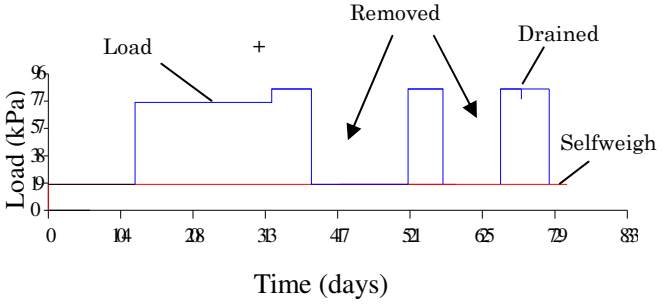

Figure 5.2 Applied load with time in FE analysis

Figure 5.2 shows type of load used in FE analysis. The foundation was firstly consolidated under its selfweight (19.1 kPa). Then it was applied a load of about 64 kPa (or 200N) and after that the load was increased about 15% the current value of load. The load was removed two times during the test and before pumped (drained) condition was conducted.

Details of Simulation

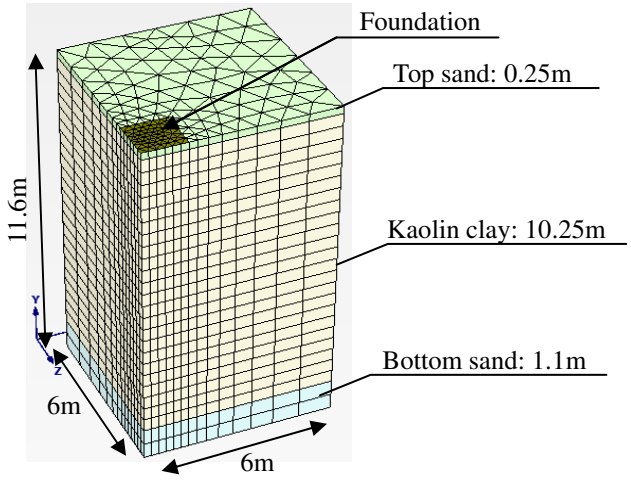

Figure 5.3 Simulation of raft foundation on soft clay

A borehole was used to assign information of soil layers and location of water table. The properties and location of soil layers in Table 5.3 were inputted to material data set and the location of water table was defined at the ground surface (y = 0). The raft was simulated by floor element and the properties were given in Table 5.4.

Figure 5.3 shows the simulation of raft foundation in FE analysis. The global coarseness of the mesh in horizontal as well as vertical directions was set to fine. 2D finite element mesh was generated before generating a full 3D mesh. The 2D mesh generation process was based on a robust triangulation principle that searched for optimized triangle and which resulted in unstructured mesh. Large displacement gradients were expected around and under the raft. Hence, refine cluster was done for the raft to have finer mesh. The 3D mesh composed of 15-node wedge elements was created by connecting the corners of the 2D triangular elements to the corresponding points of the corresponding elements in the next work plane. A total of 6656 elements and 18805 nodes were created after generating the mesh.

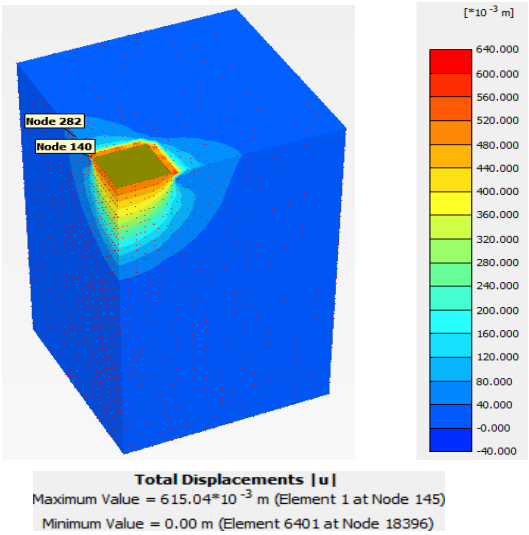

Figure 5.4 Total displacements at the end of test

The interfaces (R_{inter}) were taken as 0.6 for Kaolin clay while 0.7 for top sand and bottom sand. Initial stresses were generated by using K0 Procedure in which the default value of K0 was based on Jaky's formula. Construction stages was followed the type of load (Figure 5.2) and consolidation was used for calculation type. Pumped (drained) at bottom of the model was selected when simulating ground water pumping condition. Centrifugal analysis of this model raft was case 1 in Chapter 4. A comparison between FE analysis results and centrifugal testing results is presented for discussions.

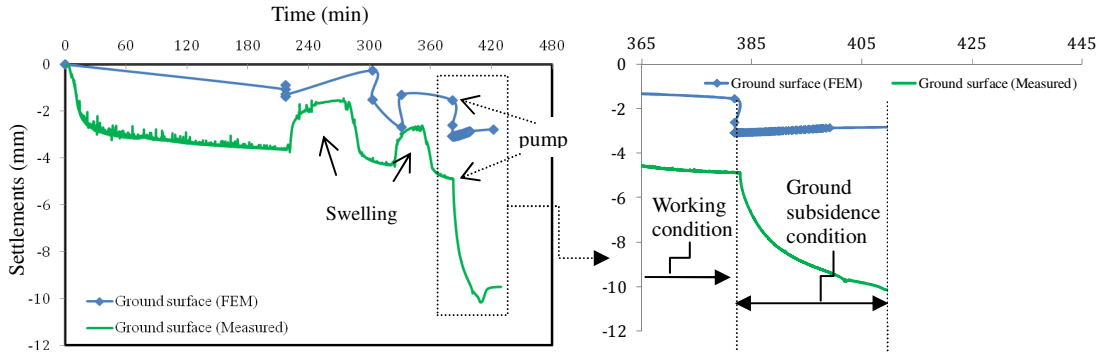

(a) original (b) view and simplification

Figure 5.5 Settlement of ground surface with time (in model scale)

Figure 5.4 shows total displacement at end of test. Displacement is concentrated around the central of the foundation. The maximum value of total displacement is about 62 cm at the end of test. For comparison, settlement of ground surface with time is plotted (Node 282 in Figure 5.4) in Figure 5.5. The manner of settlement of ground

surface in FEM is same as in measurement. However, the measured values are larger than those values in FEM. When pumped (drained) condition was applied, ground surface settled about 5mm (measured) and about 2.1mm (FEM). Figure 5.6 shows the settlement of foundation with time which was plotted at Node 140 in Figure 5.4 (ignored the settlement casing by foundation selfweight). The settlement of foundation was increased about 2.8mm after draining the soil for 25min. The result of FEM agreed well with measured results.

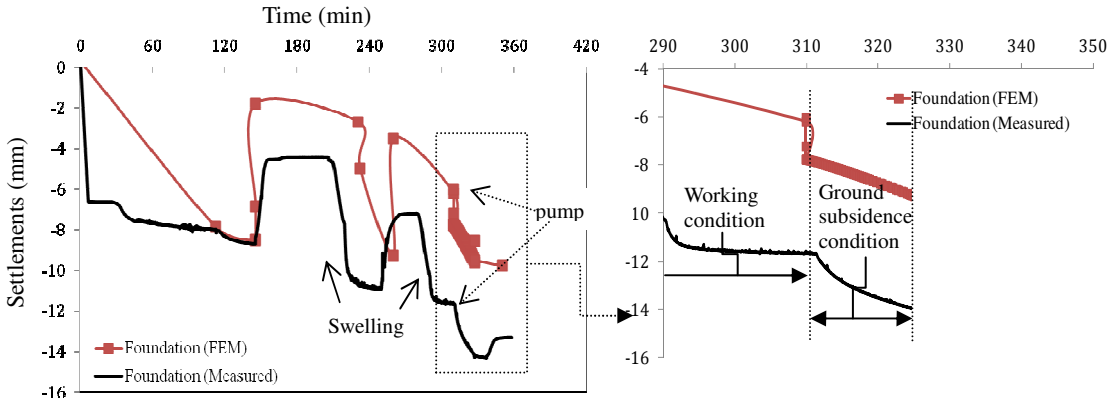

(a) original (b) view and simplification

Figure 5.6 Settlement of foundation with time after ignoring effect of selfweight (in model scale)

5.3.2 Piled raft in ground subsidence (compared with centrifugal model tests)

Geometry of Foundation

In order to evaluate effect of ground subsidence on the changing of axial force of piles in piled raft foundation, two cases of 2.8 x 2.8 x 0.75 m piled raft with 4 piles (friction piled raft and end-bearing piled raft) were considered in this study.

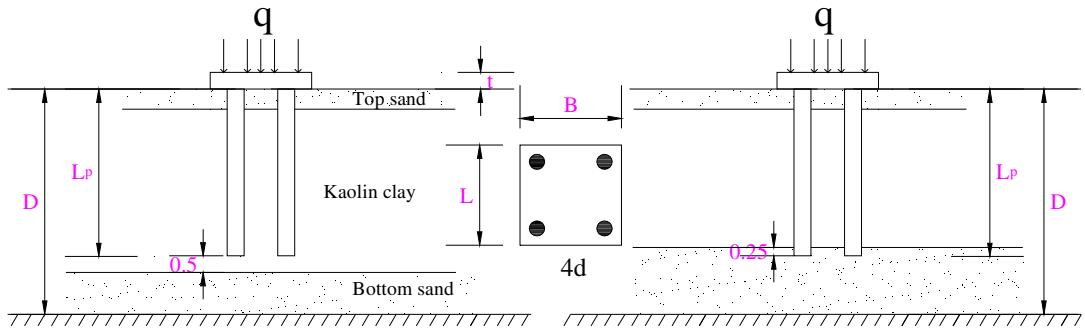

(a) friction piled raft (b) end-bearing piled raft

Figure 5.7 Geometry of foundations and soil (unit: m)

The model was extended in both horizontal directions to a total width of 12 m (or 240 mm in model scale) and a depth of 11.6 m (or 232 mm) for friction piled raft and 10.85 m (or 217 mm) for end-bearing piled raft. Figure 5.7 shows the geometry of foundations in soil and Figure 4.1 shows the simulation of piled raft in FE analysis.

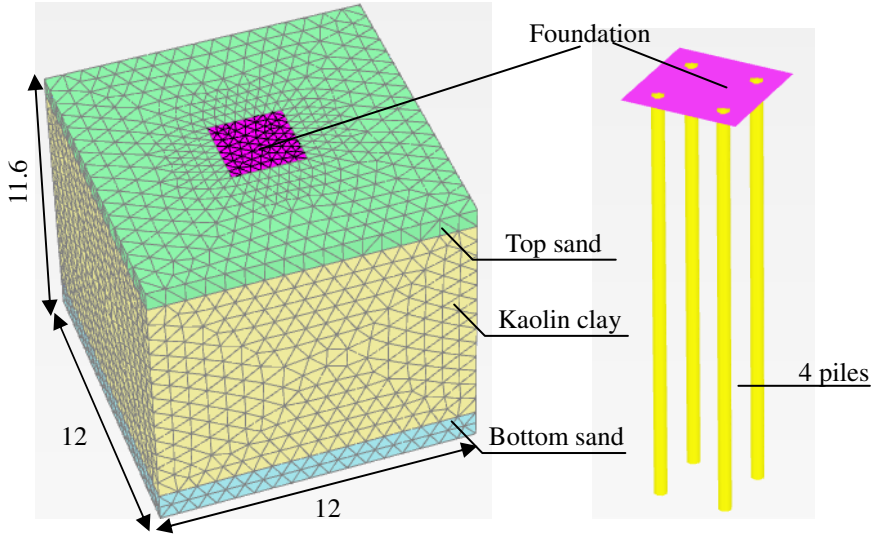

Figure 5.8 Model of friction piled raft and soil in FE analysis (unit: m)

Properties of Soil and Foundation

Table 5.5 Parameters for model soils

Description	Top Sand	Kaolin Clay	Bottom Sand
Depth (m): friction piled raft	0–0.75	0.75–10.5	10.5–11.6
Depth (m): end-bearing piled raft	0–0.75	0.75–9.75	9.75–10.85
Unit Weight, γ_{sat} (kN/m^3)	18.1	17.2	18.1
Material Model	MC	MC	MC
Permeability, k (m/day)	34.56	0.000118	34.56
Interfaces, R_{inter} (-)	0.6	0.7	0.6
Dilatancy angle, ψ' (degree)	0.0	0.0	0.0
Poisson's ratio, ν' (-)	0.3	0.33	0.3
c' (kN/m^2)	1.0	5.0	1.0
φ' (degree)	28	20	33
E' (kN/m^2)	4333	300	8667

Three layers including top sand, Kaolin clay and bottom sand were simulated in this analysis. The calculation was done by consolidation analysis with effective parameters. Table 5.5 shows the properties of soils. Young modulus of Kaolin clay

was increased with depth, starting at y_{ref} = -0.75m, and the increment was 300kN/m^2/m. The properties of raft and piles are presented in Table 5.6 and Table 5.7 respectively.

Table 5.6 Parameters for model raft

Description	Raft
Type of behaviour	Linear, isotropic
Thickness, t (m)	0.75
Weight, γ (kN/m^3)	27
Young's modulus, E (kN/m^2)	68 × 10^6
Poisson's ratio, ν (-)	0.15

Table 5.7 Parameters for model piles

Description	Pile
Material model	Linear elastic
Young's modulus, E (kN/m^2)	68 × 10^6
Poisson's ratio, ν (-)	0.15
Weight, γ (kN/m^3)	9.35
Properties type	Massive circular pile
Diameter, d (m)	0.4
Length of pile, L_p (m)	10

Type of Load

Figure 5.9 shows type of load used in FE analysis which was done the same manner with centrifugal test (case 5 and case 6 in Chapter 4).

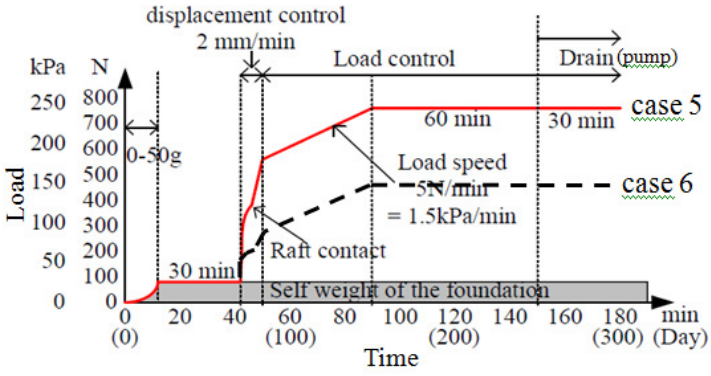

Figure 5.9 Applied loads with time in FE analysis (case 5: friction piled raft, case 6: end-bearing piled raft)

The foundations was applied a distribution load of 245 kPa (friction piled raft) and

145 kPa (end-bearing piled raft) and then the water table level was lowered to -7.725 m (or 155 mm after pumping 15 min in model scale).

Details of Simulation

A borehole was used to assign information of soil layer and location of water table. The properties of soil layers in Table 5.5 were inputted to material data set and the location of water table was defined at the ground surface (z = 0 m) and was lowered to other depths in analysis. The raft was simulated by plate element and the properties were given in Table 5.6. The piles were simulated by embedded pile element and the properties in Table 5.7 were used.

The global coarseness of the mesh in horizontal as well as vertical directions was set to medium. Full 3D finite element mesh was generated. The 3D mesh composed of 15-node wedge elements was created by connecting the corners of the 2D triangular elements to the corresponding points of the corresponding elements in the next work plane. The total of 29737 elements and 44037 nodes for friction piled raft and 27361 elements and 40699 nodes for end-bearing piled raft were created after generating the mesh. The interfaces (R_{inter}) were taken as 0.7 for Kaolin clay while 0.6 for top sand and bottom sand. Initial stresses were generated by using K0 procedure. Plastic was used for calculation type.

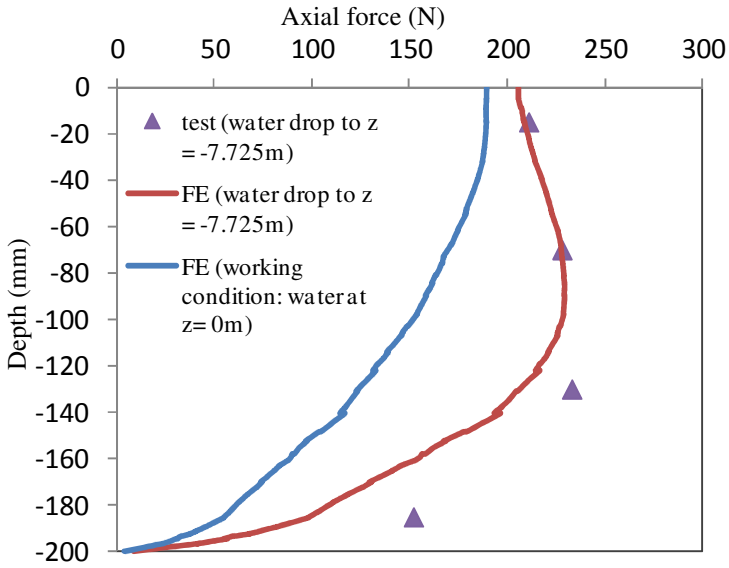

Figure 5.10 Distribution of axial force with depth of friction piled raft (case 5 in chapter 4: in model scale)

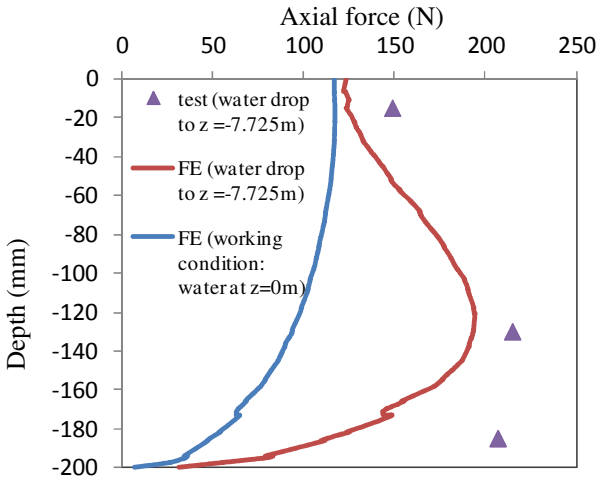

Figure 5.11 Distribution of axial force with depth of end-bearing piled raft (case 6 in chapter 4: in model scale)

Centrifugal analyses of these model piled rafts were presented in Chapter 4. A comparison between FE analysis results and centrifugal testing results is presented in Figure 5.10 and 5.11. The results of FEM agreed well with measured results.

5.3.3 Parameter study of model piled rafts

Size of foundation was taken from centrifugal models. Effect of piled spacing, Young's modulus of Kaolin clay and level of ground water on distribution of axial force of piled in piled raft.

+ Effect of piled spacing

Piled rafts with s = 2d and s = 4d were considered in this analysis; ground water level: z = -7.725 m (or 155 mm in model scale).

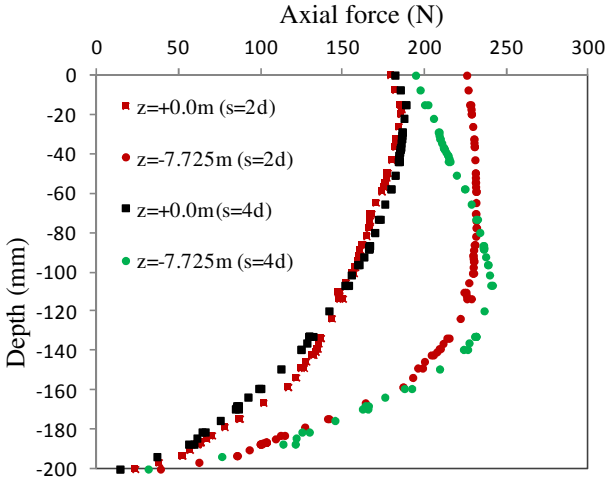

Figure 5.12 Friction piled raft

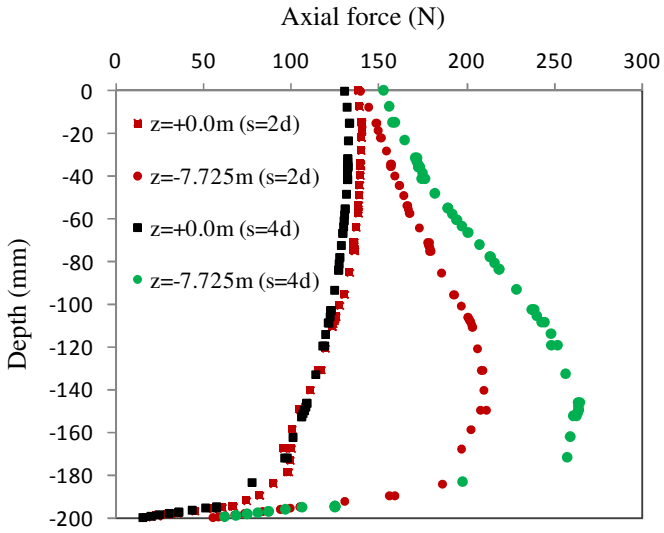

Figure 5.13 End-bearing piled raft

+ Effect of Young's modulus of Kaolin clay

s = 4d; ground water level: z = -7.725 m (or 155 mm in model scale); E1 = 300 kPa, E_{incr} = 300 kPa/m ; E2 = 2660 kPa, E_{incr} = 300 kPa/m

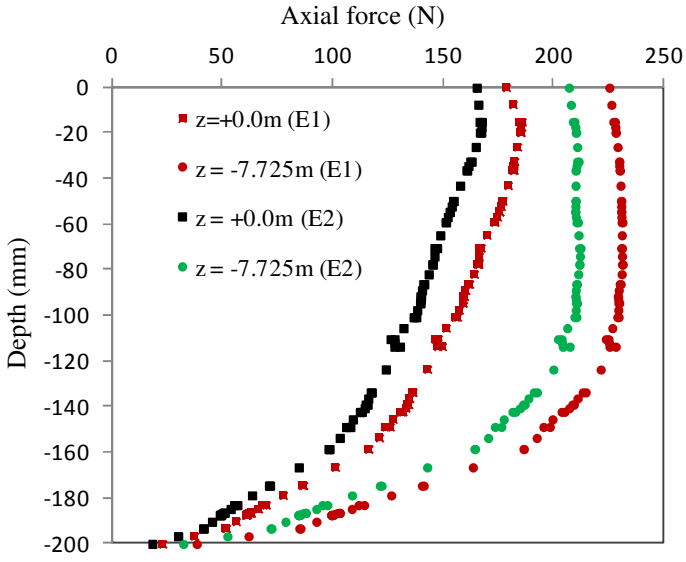

Figure 5.14 Friction piled raft

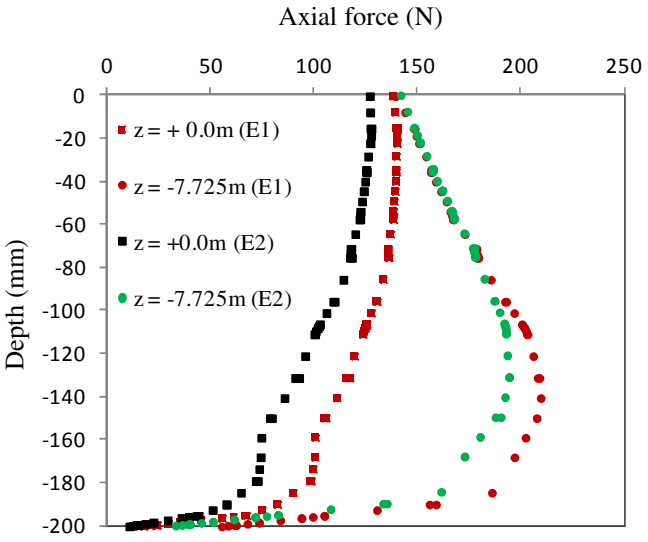

Figure 5.15 End-bearing piled raft

+ *Effect of level of ground water*

Levels of ground water table: z = +0.0 m (0.0 mm), z = -7.725 m (155 mm) and z = -10 m (200 mm in model scale).

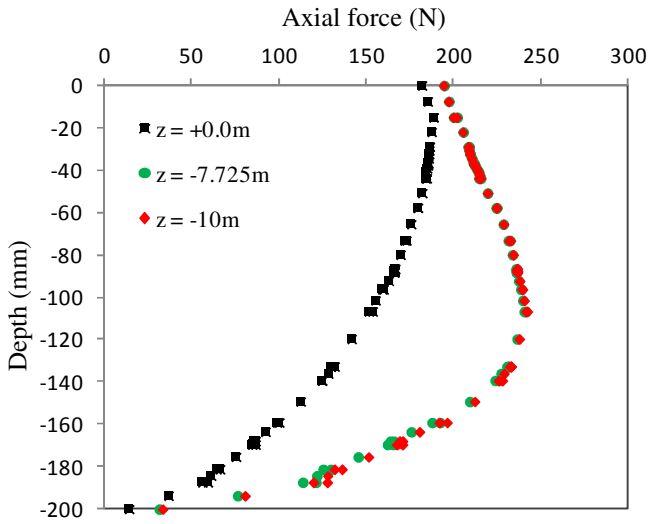

Figure 5.16 Friction piled raft

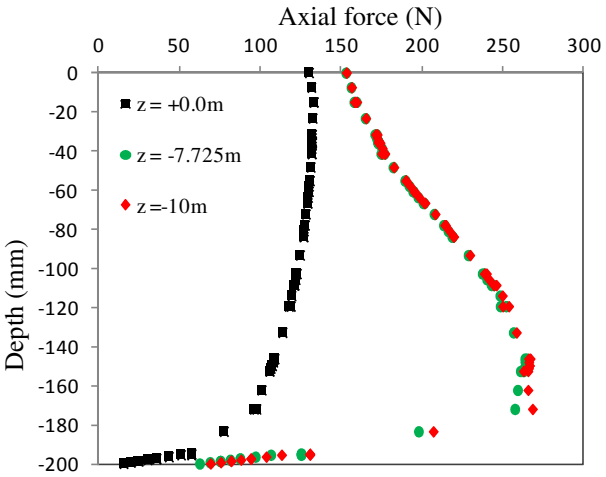

Figure 5.17 End-bearing piled raft

From the results of parameter study of model piled rafts, some discussions were given as below.

When piled spacing increases, the maximum axial force of the piles increase. For friction piled raft, maximum axial forces increased 45 N and 60 N for piled spacings of 2d and 4d, respectively. For end-bearing piled raft, when piled spacings increased from 2d to 4d, the maximum axial forces increased 65 N and 125 N, respectively.

When Young's modulus of the soil increases (E2 = 8.9 E1), the maximum axial force decreases because of increase of load carried by the raft. For friction piled raft, maximum axial forces were 185 N and 160 N for E1 and E2 in normal condition while the maximum axial forces increased 50 N for both E1 and E2 in ground subsidence condition. For end-bearing piled raft, maximum axial forces were 145 N and 130 N for E1 and E2 in normal condition while maximum axial forces increased 65 N and 55 N for E1 and E2, respectively in ground subsidence condition.

When ground water levels decrease from +0.0 m to -7.725 m, maximum axial forces were increased 70 N and 145 N for friction and end-bearing piled rafts, respectively. However, the axial forces were constant when ground water levels decreased from -7.725 m to -10 m.

For all cases of parameter study, negative skin friction of end-bearing piled raft is larger than that of friction piled raft in ground water pumping condition.

5.4 Analysis of Piled Raft in Bangkok Soil

5.4.1 Geometry of foundation

Apartments with 3 to 6 basements were popular in Bangkok city. In order to evaluate effect of ground subsidence, depth of raft and piled configuration on the load-settlement curves, load distributions and axial force of the piles of square piled raft foundation, three cases were considered in numerical analysis (Figure 4.18). Figure 4.18a shows the plain view of the foundation and Figure 4.18b shows three cases of foundations and soils in numerical analysis. The depths of raft are -15 m (case 1: 6 basements), -7.5 m (case 2: 3 basements) and + 0.0 m (case 3). In each case, the foundation was analyzed with raft alone and 4 piled configurations (A, B, C and D) as shown in Figure 5.18. Table 5.8 summarizes the cases of analysis for Bangkok soil.

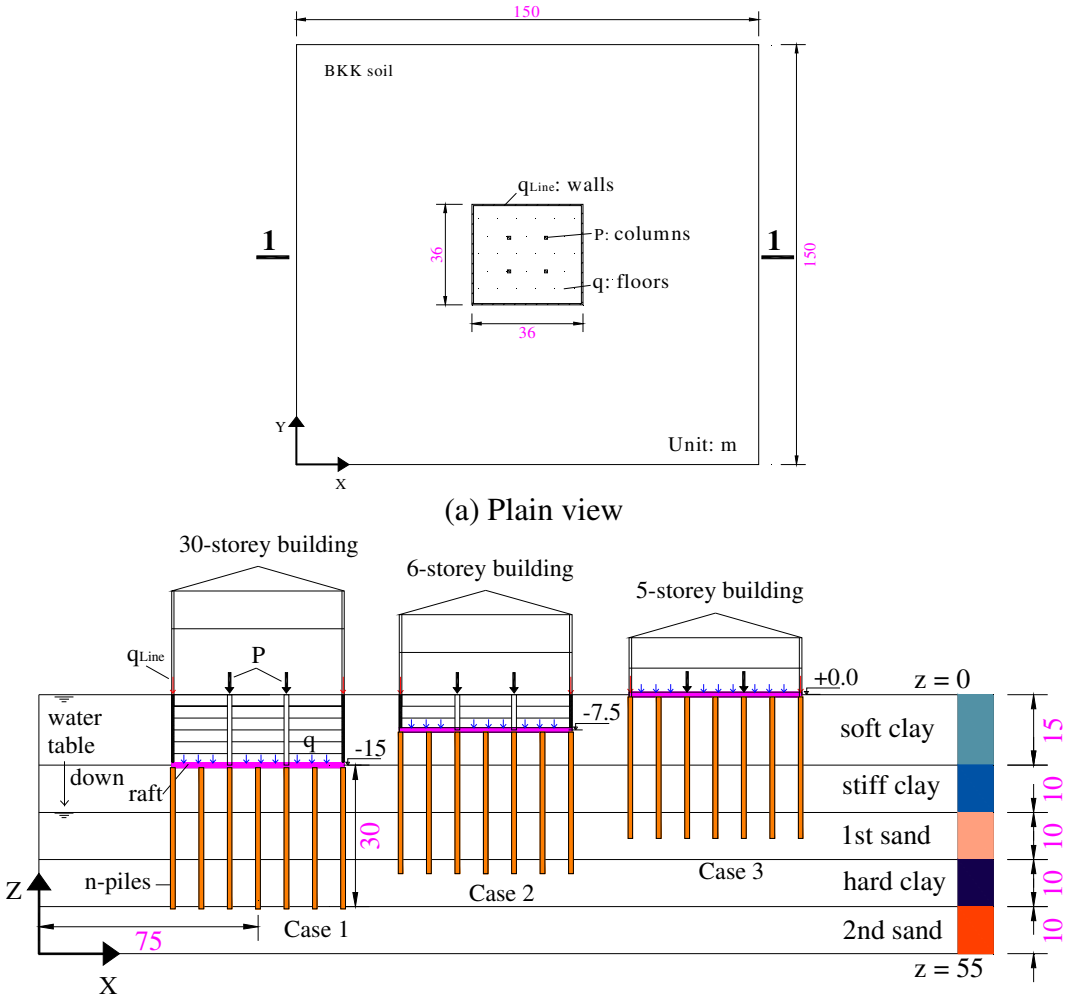

(a) Plain view

(b) Section 1-1

Figure 5.18 Three cases of foundations and soils in numerical analysis (unit: m)

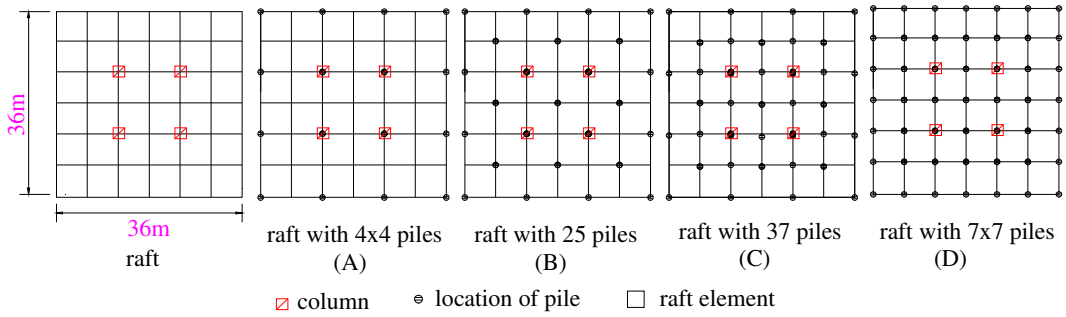

Figure 5.19 Raft and 4 piled configurations (A, B, C and D) considered in each case

A 36 m × 36 m squared raft with a thickness of 1 m, supported by 16 piles (A), 25 piles (B), 37 piles (C) and 49 piles (D), was considered in this study. The length of piles was 30 m and diameter of piles was 1 m. The piled spacing was varied from 6 m to 12 m depending on piled configurations.

Table 5.8 Summary of main cases of analysis for Bangkok soil

Cases i (i = 1,2,3)	Numbers of pile	Piled Configuration	Smallest piled spacing: s (m)	Factors of study
i-1	Raft	-	-	Effect of numbers of pile and piled configuration .
i-2	Raft with 16 piles	A	12	
i-3	Raft with 25 piles	B	8.5	
i-4	Raft with 37 piles	C	6	
i-5	Raft with 49 piles	D	6	

Case 1: depth of raft at -15m; case 2: depth of raft at -7.5m; case 3: depth of raft at +0.0m

Table 5.9 Parameter study for piled raft in Bangkok soil

Cases (j = 1 to 5)	Parameters	Unit	Comparisons	Factors of study
4-j	E_1 = 5320	kN/m^2	**3**, 4, 5	Effect of Young's modulus
5-j	E_1 = 7980	kN/m^2		
6-j	q = 84	kN/m^2	**3**, 6	Effect of pattern of loads
7-j	t = 0.5	m	**3**, 7, 8	Effect of raft thickness
8-j	t = 1.5	m		
9-j	q = 67.2	kN/m^2	**6**, 9, 10	Effect of level of loads
10-j	q = 50.4	kN/m^2		
11-5	s = 6d = 6	m	**11**, 12, 13	Effect of piled spacing (raft without beams, q = 84 kPa)
12-5	s = 5d = 3	m		
13-5	s = 3d = 2	m		

j = 1: Raft, j = 2: Raft with 16 piles (A), j = 3: Raft with 25 piles (B), j = 4: Raft with 37 piles (C), j = 5: Raft with 49 piles (D).

Case 3 was also used for comparison in parameter study (case 4 to case 13) which was

done for evaluating the effect of Young's modulus of soft clay layer, pattern of loads, raft thickness, level of loads and piled spacing on distribution of loads and settlements in piled raft. Table 5.9 shows cases of parameter study for piled raft in Bangkok soil.

For all cases, the ground water table was firstly located at the ground surface (+0.0 m) and it was gradually decreased to the levels of -15 m and -25 m in order to simulate ground subsidence. Full foundation was modeled in the analysis. To enable any possible mechanism in soft clay and to avoid any influence of the outer boundary, the model was extended in both horizontal directions to a total width of 150 m.

5.4.2 Properties of soil and foundation

Table 5.10 Properties of Bangkok subsoil (effective parameters)

Description	Name	Soft clay	Stiff clay	1st Sand	Hard clay	2nd Sand	Unit
Material model	Model	MC	MC	MC	MC	MC	-
Drainage type	Type	Drained	Drained	Drained	Drained	Drained	-
Unit weight above phreatic level	γ_{unsat}	14.2	17.4	18.4	18.8	19.1	kN/m^3
Unit weight below phreatic level	γ_{sat}	15.2	18.4	19.4	19.8	20.1	kN/m^3
Young's modulus	E'	2660	35910	69333	133000	173333	kN/m^2
Poisson's ratio	ν'	0.33	0.33	0.3	0.33	0.3	-
Cohesion	c'_{ref}	5	15	1	25	1	kN/m^2
Friction angle	φ'	24	27	35	30	36	o
Dilatancy angle	ψ	0	0	0	0	0	o
Soil type	-	Very fine	Very fine	Medium	Very fine	Medium	-
Permeability	k	0.0001	0.0001	1	0.0001	1	m/day
Interfaces	R_{inter}	0.7	0.7	0.6	0.7	0.6	-
Initial condition	-	K0	K0	K0	K0	K0	-

MC = Mohr Coulomb

The properties of Bangkok soil were determined from the works of Phongpat Kitpayuck (2009) in section 2.6 and formulations in section 5.2. Five layers of soil including soft clay, stiff clay, 1st sand, hard clay and 2nd sand were simulated in this analysis. The thickness of each soil layer is shown in Figure 5.18b. The calculation was done by drained, plastic analysis with effective parameters. Properties of each layer of soil are shown in Table 5.10. Young modulus of soil is constant with depth in each layer. The properties of foundation are presented in Table 5.11, Table 5.12 and Table 5.13 below.

Table 5.11 Material properties of raft, basement floors and basement walls

Description	Name	Raft	Basement floor	Basement wall	Unit
Thickness	d	1	0.3	0.5	m
Weight	γ	24	24	24	kN/m^3
Type of behaviour	Type	Linear, isotropic	Linear, isotropic	Linear, isotropic	-
Young's modulus	E_1	35×10^6	35×10^6	35×10^6	kN/m^2
Poisson's ratio	ν_{12}	0.2	0.2	0.2	-

Table 5.12 Material properties of basement columns and basement beams

Description	Name	Basement column	Basement beam	Unit
Cross section area	A	1	1.5	m^2
Volumetric weight	γ	24	8.8	kN/m^3
Type of behaviour	Type	Linear	Linear	-
Young's modulus	E_1	35×10^6	35×10^6	kN/m^2
Moment of inertia	I_3	0.083	0.281	m^4
	I_2	0.083	0.125	m^4

Column: bxh = 1mx1m, beams: bxh = 1m x 1.5m

Table 5.13 Material properties of embedded pile

Description	Name	Embedded piles	Unit
Young's modulus	E	35×10^6	kN/m^2
Unit weight	γ	8.8	kN/m^3
Pile type	-	Predefined	-
Predefined pile type	-	Massive circular pile	-
Diameter	Diameter	1	m
Skin resistance	Type	Linear	-
Max. traction allowed at the top of embedded pile	$T_{top,max}$	200	kN/m
Max. traction allowed at the bottom of embedded pile	$T_{bot,max}$	500	kN/m
Base resistance	F_{max}	1×104	kN

5.4.3 Type of load

Three types of load including surface load, point load and line load was applied for piled raft. Surface load (distribution load) was applied on raft and basement floors.

Table 5.14 Summary of applied loads for analysis of piled raft in Bangkok soil

Load	Name	Case 1	Case 2	Case 3	Unit
q	Surface load (raft, floor)	5.3	5.3	5.3	kN/m^2
P	Point load (column)	69874	13975	11650	ken
q_L	Line load (wall)	2547	471	385	kN/m
Total	Sum of loads (q, P, q_L)	687.444	144.338	108.9	MN
Building	Assumed load: 16.8 kPa/storey	30 storeys + 6 basements	6 storeys + 3 basements	5 storeys + 0 basements	-

Point load (concentrated load) was applied to the locations of columns. Line load was applied to the basement walls. The calculation of these loads was based on the work of Brinkgreve et al. (2007). Table 5.14 summarizes the three types of load which was applied the numerical analysis.

5.4.4 Details of simulation

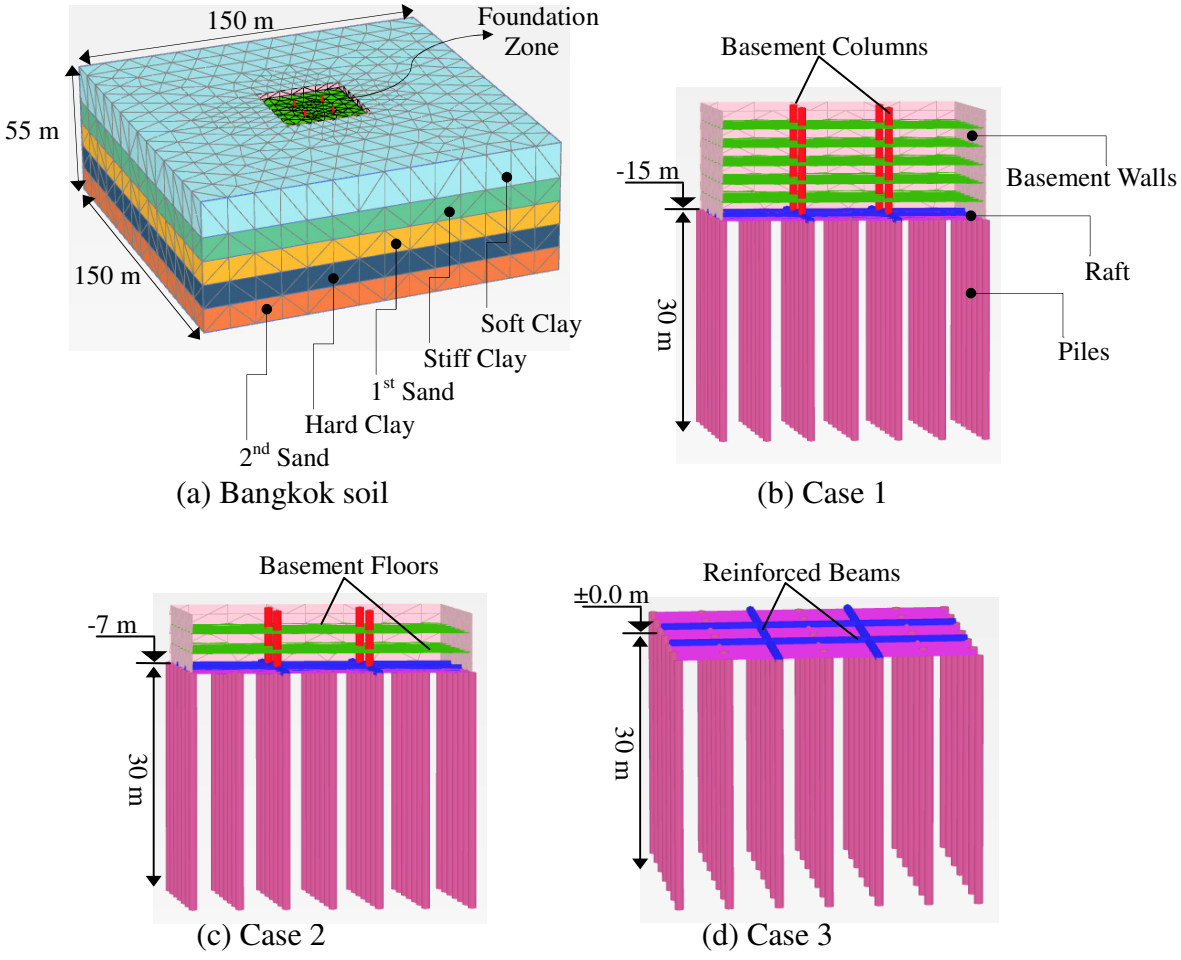

Figure 5.20 Simulation of piled raft foundation on Bangkok soil

A borehole was used to assign information of soil layers and location of water table. The properties and location of soil layers in Table 5.10 were inputted to material data set and the location of water table was defined at the ground surface (z = 0). In each case ij (i = 1 to 3, j = 1 to 5), the level of water table was decreased to z = -15 m and z = - 25 m in separated phases after loading phase. The raft, basement floors and basement walls were simulated by plate element and the properties were given in Table 5.11. The basement columns and basement beams were simulated by beam

element and the properties were given in Table 5.12. The embedded piles were simulated by embedded pile element and the properties were shown in Table 5.13.

Figure 5.20 shows the simulation of piled raft foundations in numerical analysis. The global coarseness of the mesh in horizontal as well as vertical directions was set to medium. Full 3D mesh was generated after completing structures tab. The mesh generation process was based on a robust triangulation principle that searched for optimized triangle and which resulted in unstructured mesh. Large displacement gradients were expected around and under the raft. Hence, refine cluster was done for the raft to have finer mesh. The 3D mesh composed of 15-node wedge elements was created by connecting the corners of the triangular elements to the corresponding points of the corresponding elements in the next work plane. The total of 12171 elements and 18907 nodes for case 1, 11674 elements and 18799 nodes for case 2 and 9881 elements and 16279 nodes for case 3 were created after generating the mesh.

The interfaces (R_{inter}) were taken as 0.7 for clay while 0.6 for sand. Initial stresses were generated by using K0 Procedure in which the default value of K0 was based on Jaky's formula. Construction stages were included 4 stages (build foundation, loading foundation: used Table 5.14, decrease water table to -15 m and decrease water table to -25 m) and plastic was used for calculation type. Drained condition was selected for all soils and incorporating with drawdown of water table to simulate ground subsidence condition.

5.4.5 Results and Discussions

5.4.5.1 General information

Four positions on raft were selected for investigation as shown in Figure 4.21 below. The center, corner and middle edge of the raft were considered for that curve. The point under the column was also an interesting position for investigation. The point at 1/3 edge of raft was chosen for plotting axial force of the pile at that position.

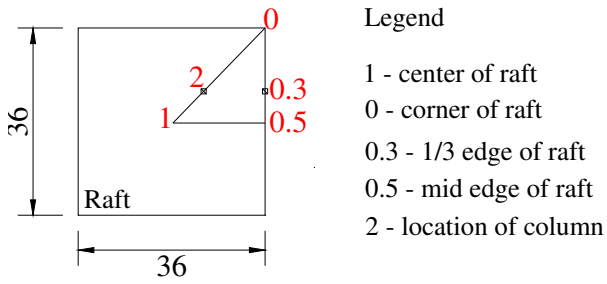

Figure 5.21 Selection of points for investigation

Settlement of foundation and differential settlements between two points were written as

S = total settlement of foundation. $\Delta S = 0 - 2$ = differential settlement between corner to location of column of raft.

Ground subsidence

For all cases, the distribution of ground subsidence under decreasing of ground water table was firstly analyzed. Ground water at levels of 0.0 m, -7.5 m, -15 m and -25 m were investigated and shown in Figure 4.22.

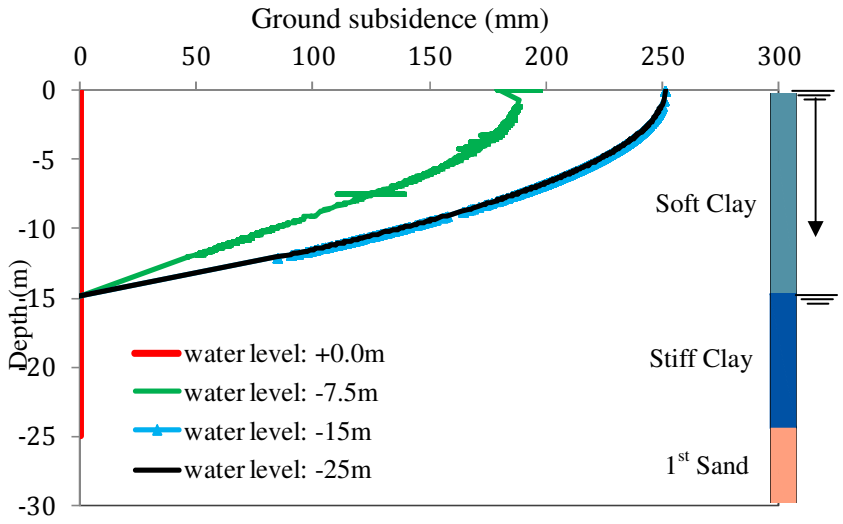

Figure 5.22 Distribution of ground subsidence with depth causing by decrease of ground water levels (for all cases)

When ground water decreased to -7.5 m and -15m, the ground surface settled around 195 mm and 250 mm, respectively. The distribution of ground subsidence in soft clay layer was nearly linear (max value at surface and equal to zero at bottom) and it was

agreed well with assumption of Poulos (2008) as well as results of centrifugal test (Figure 4.26 in Chapter 4). The mechanism of ground surface subsidence arising from groundwater extraction may be explained as shown in part 2.3.3 of Chapter 2. Ground subsidence did not occur when ground water decreased from -15m to -25m and it was not considered in the comparisons below.

Capacities of raft alone and single pile

+ Raft alone

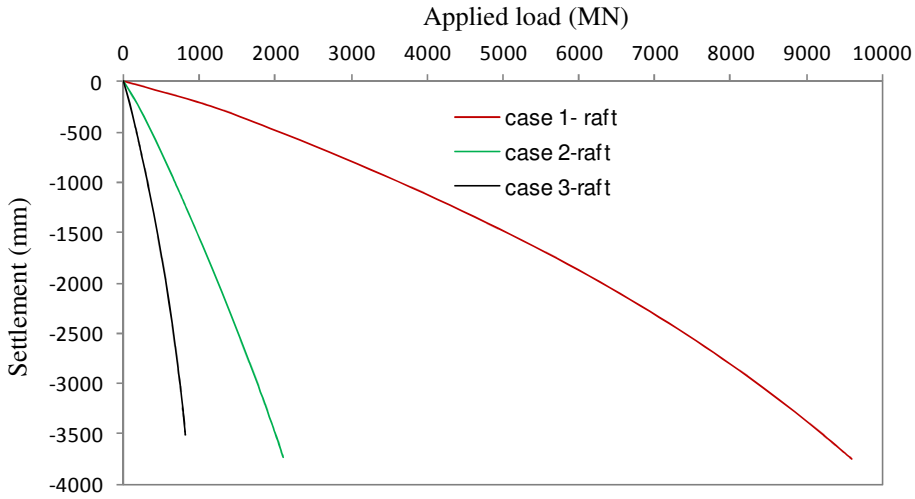

Figure 5.23 Load – settlement curves of raft foundations (at around 10% width of raft) in normal condition (for cases 1, 2 & 3)

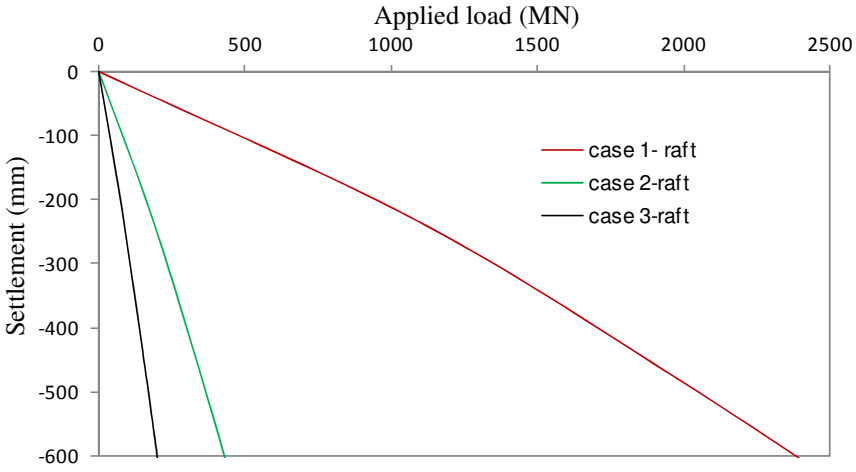

Figure 5.24 Load – settlement curves of raft foundations (at around 1.7% width of raft) in normal condition (for cases 1, 2 & 3)

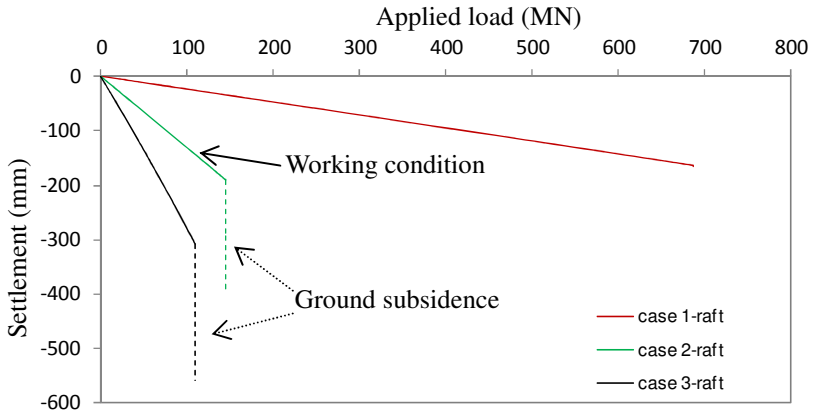

Figure 5.25 Load – settlement curves of raft foundations (at working loading) in ground subsidence (for case 1, 2 & 3)

+ *Single pile*

The pile at point 2 (for all cases: pile under column) was considered for comparison.

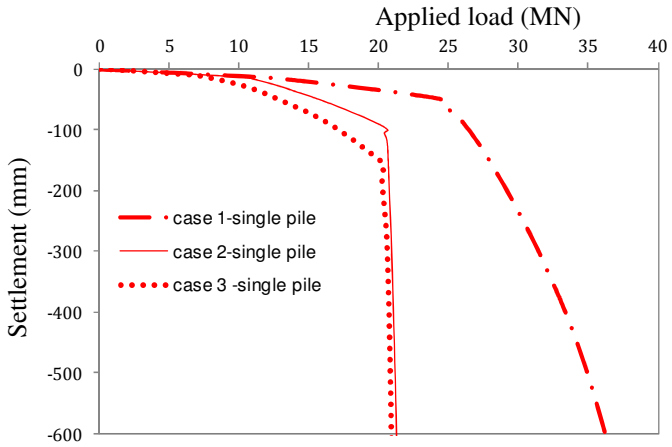

Figure 5.26 Load – settlement curves of single pile (at ultimate load) in normal condition (for cases 1, 2 & 3)

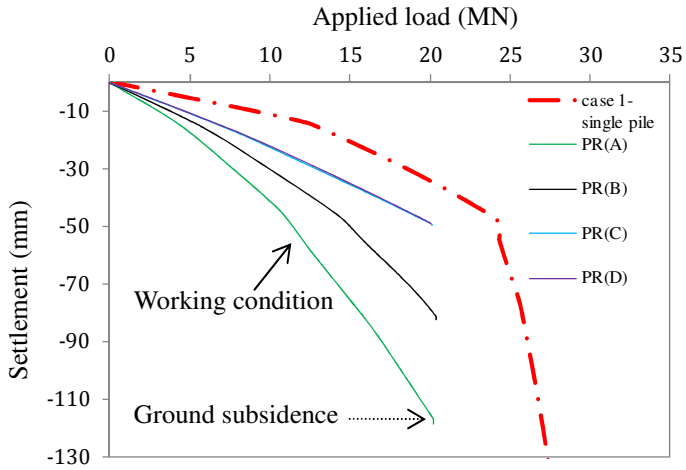

(a) Case 1

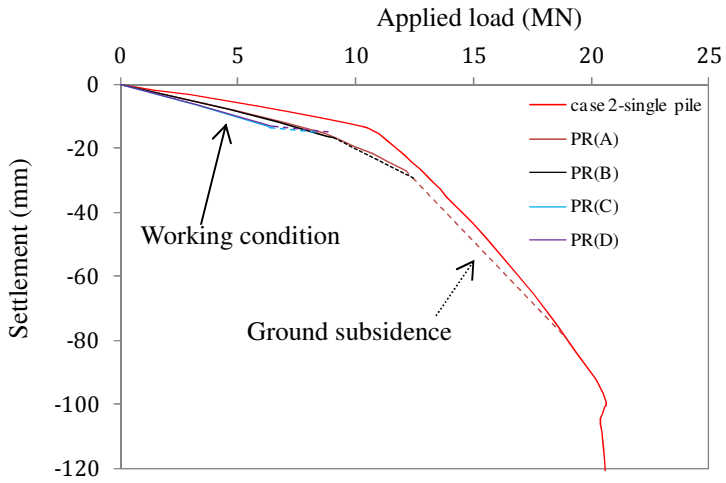

(b) Case 2

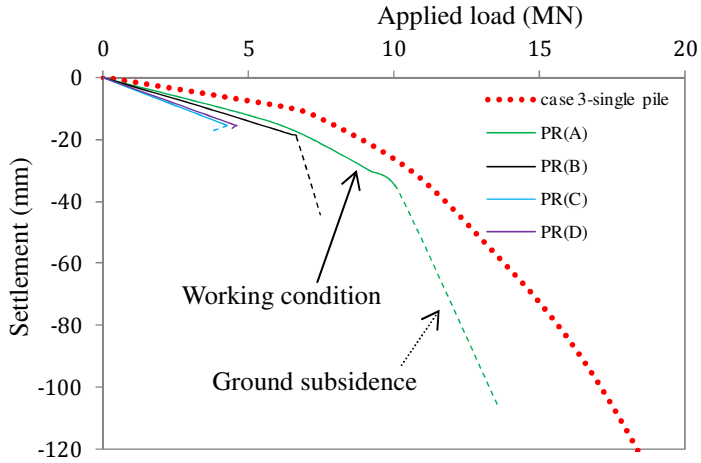

(c) Case 3

Figure 5.27 Load – settlement curves of single pile (at ultimate load) and pile in piled raft (at working loading) in ground subsidence (case 1, 2, 3)

Figure 4.23 and 4.24 shows the load-settlement curves of raft alone for the settlements at 10% and 1.7% raft width, respectively. The capacities of raft (at settlement of 1.7% raft width = 600 mm) were around 2400 MN, 400 MN and 220 MN for, in turn of that order, cases 1, 2 and 3. Figure 4.25 shows the load-settlement curve of raft alone (at working loads) in ground subsidence condition for cases 1, 2 and 3. In ground subsidence condition, large settlements of foundations can be found (around 200 mm and 255 mm) for cases 2 and 3 while very small of settlement of foundation (nearly 0 mm) occurred in case 1. The reasons are the raft in case 1 was set on stiff clay layer

while the rafts in cases 2 and 3 were set at middle and surface of soft clay layers. However, the total settlements of both cases 1, 2 and 3 were less than 600 mm.

Figure 4.26 shows the load – settlement curves of single pile (at ultimate load) in normal condition for cases 1, 2 and 3. The ultimate bearing capacities of single piles were around 26 MN, 20 MN and 19.7 MN for cases 1, 2 and 3 respectively. Load – settlement curves of pile in piled raft (at working loading) in ground subsidence for case 1, 2, 3 is shown in Figure 4.27. For comparison purpose, the load-settlement curve of single pile (at ultimate load) was also plotted in Figure 4.27 in red lines. It can be seen that the capacities of piles in piled rafts (PR(A)) were mobilized (under working loads) around 77 % in case 1, 90% in case 2 and 74% in case 3. These piles may be called as creep piling, based on the discussion of Randolph (1994) in which 70-80% of piles' ultimate bearing capacity was mobilized under working load. Large settlements of piles were also found (for case 2 and 3) in ground subsidence condition. The settlement of piles in case 1 was very small in ground subsidence condition. The values of settlement in cases 2 and 3 (piles at point 2 in Figure 4.21) causing by ground subsidence were around 57 mm and 75 mm, respectively. The reason because more load was induced on the piles (drag force) and the piles need to settle more to support the imposed load. It can be explained in the same manner for PR(B), PR(C) and PR(D). For those types of piled raft, the numbers of piles were increased and, therefore, the total capacity of all piles in a piled raft was increased. The applied load was constant while increasing the capacity of foundation would make the settlements of foundation decreased. In generally, the effect of ground subsidence on settlement of foundation was decreased in case of increasing numbers of piles as seen in Figure 4.27. The reason may be that the interaction between of piles affected on the effective of drag force. The overlap of stresses zone around the piles maybe made a portion of decrease in the magnitude of drag force.

***Load distribution, average and differential settlements:** *(effect of raft thickness)*

Case 3: **t = 1m**, case 7: **t = 0.5 m**, case 8: **t = 1.5 m**; PG(0) = piled group (ground water at +0.0 m), PG(-15) = piled group (ground water at -15 m). Differential settlement = S2 (at point 2) – S0 (at point 0).

+ Case 3

Load distribution

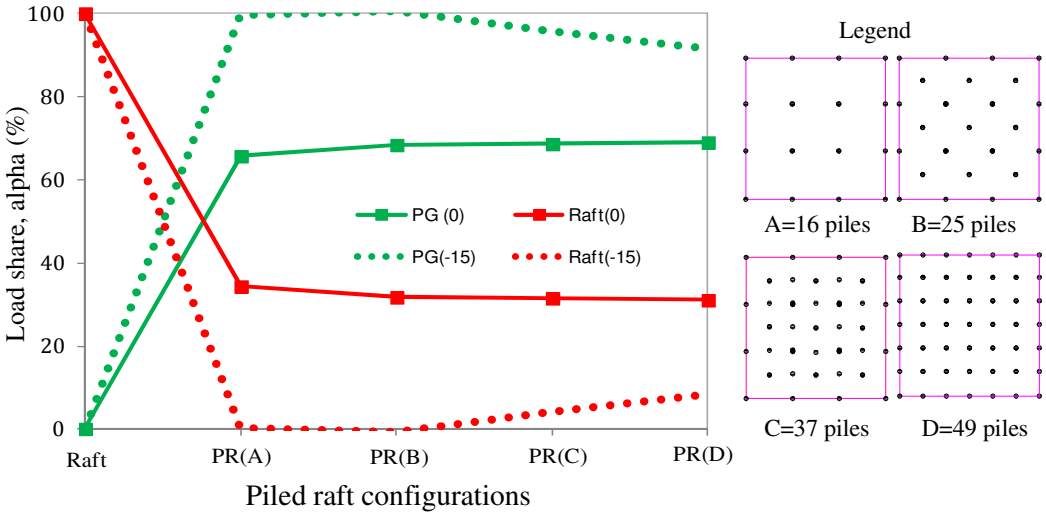

Figure 5.28 Load distributions in piled rafts before and after ground subsidence in case 3

Settlements

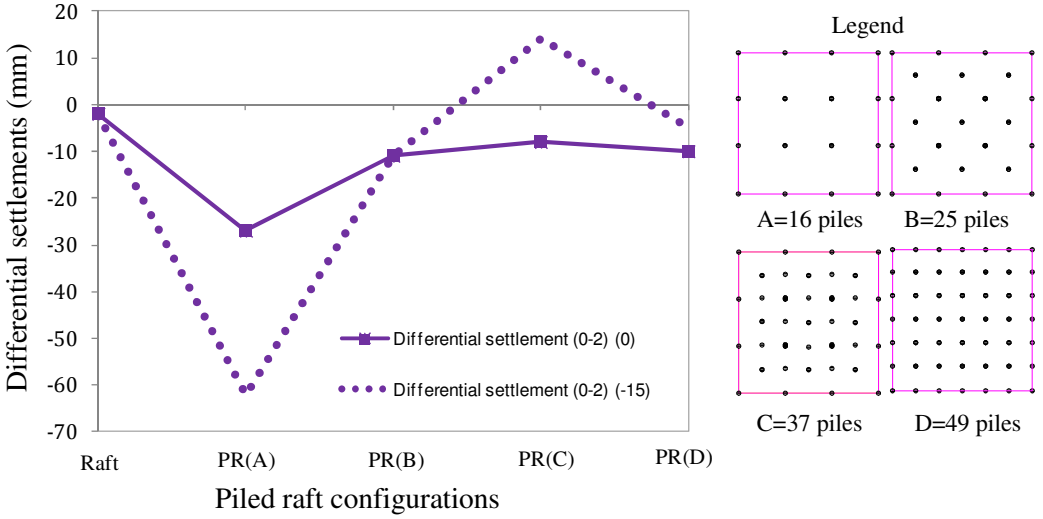

Figure 5.29 Differential settlements (0-2) in piled rafts before and after ground subsidence in case 3

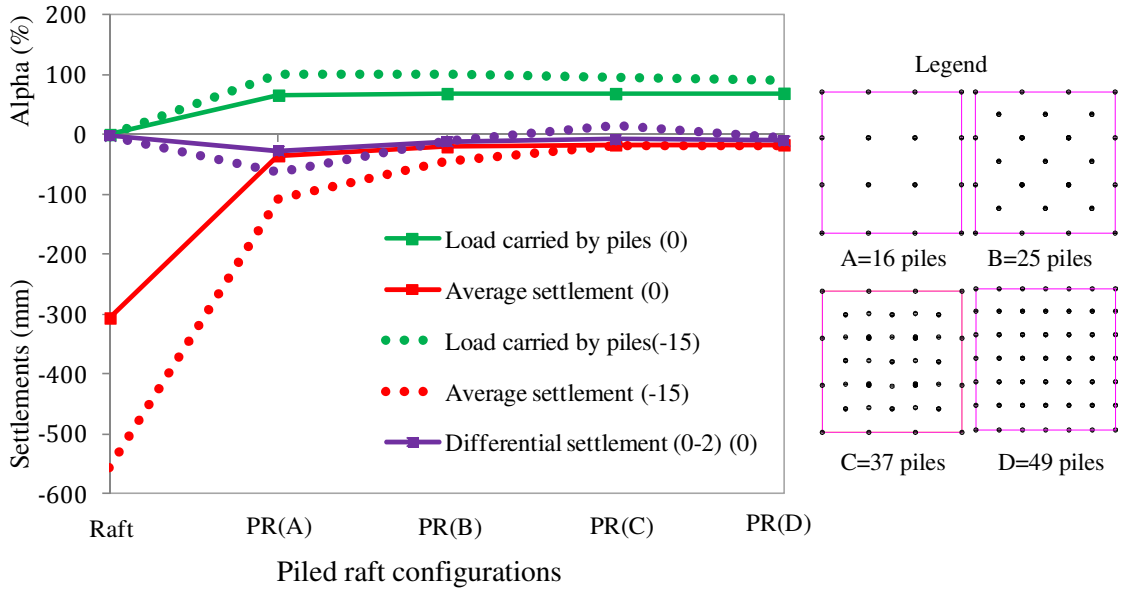

Figure 5.30 Average settlement, differential settlements and piled load share in piled rafts before and after ground subsidence in case 3

Figure 5.28 shows the load distributions between raft and group of piles in piled rafts before and after ground subsidence in case 3. The loads sharing by raft and piles in normal condition (water level at +0.0 m) and ground subsidence condition (water level at -15 m) were presented by the continuous lines and dash lines, respectively. For normal condition, the load carried by the piles was around 65% (PR(A: 16 piles)) and the raft shared 35% applied load. Although numbers of piles were increase in PR(B: 25 piles), PR(C: 37 piles) and PR(D: 49 piles), the load shared by the piles was increased very little (less than 5 %). For ground subsidence condition, the load shared by the piles was increased up to around 100% (PR(A) and PR(B)), 95% (PR(C)) and 90% (PR(D)). The reason was that the soil under the raft settled and reduced the contact between ground surface and raft. Therefore, the load shared by raft was reduced largely and this load was transfer to the piles. Beside the applied load, the piles had also to support the weight of the raft when the contact between the raft and ground surface decreased. A little load shared by the raft in PR(C) and PR(D) because the large settlement of those types of piled raft, compared to PR(A) and PR(B), made the raft little contacted with ground surface.

Figure 5.29 shows differential settlements between the position under the column (2) and corner of raft (0) in piled rafts before and after ground subsidence in

case 3. For normal condition (continuous line), the differential settlement was large for PR(A) and was decreased when more piles added to the raft (PR(B), PR(C) and PR(D)). The values for differential settlements were 25 mm, 11 mm, 9 mm and 10 mm for PR(A), PR(B), PR(C) and PR(D), respectively. Because the additional piles distributed under the raft made the applied loads became more uniform than before adding piles. The piles added along the perimeter of the raft (under the walls) also reduced the settlements at those points which results the reduction of differential settlements. This shows that the effectiveness of piles in reducing differential settlements is evident. For ground subsidence condition (dash line), the differential settlements were increased in PR(A) and PR(C) while they were not varied in PR(B) and PR(D). The values of differential settlements were around 60 mm and 15 mm for PR(A) and PR(C), respectively. The reason was that the piled at point 2 settled to mobilize the capacity for supporting imposed load (from drag force). The differential settlements of raft alone were -2 mm for both normal condition and ground subsidence condition. It means that the raft was thick enough for distribution of applied loads into uniform load.

Figure 5.30 presents average settlement, differential settlements and piled load share in piled rafts before and after ground subsidence in case 3. For normal condition, the average settlement of raft was 306 mm and this average settlement decreased with the increased of numbers of piles. The reductions of average settlement were around 88 %, 93 %, 94% and 94% for PR(A: 16 piles), PR(B: 25 piles), PR(C: 37 piles) and PR(D: 49 piles), respectively. For ground subsidence condition, the average settlement of raft was increased up to 557 mm and the reductions of settlement were 81%, 91%, 96% and 96% for PR(A: 16 piles), PR(B: 25 piles), PR(C: 37 piles) and PR(D: 49 piles), respectively. The reason, for both conditions, was that the piled shared the load of the raft and therefore reduced the average settlement of the foundation. Ground subsidence affected on PR(A) and PR(B) in reducing average settlement (and also differential settlement). However, ground subsidence showed little effect on reducing settlements (average and differential settlements) for fully piled raft (PR(D)).

+ Case 3, 7 & 8

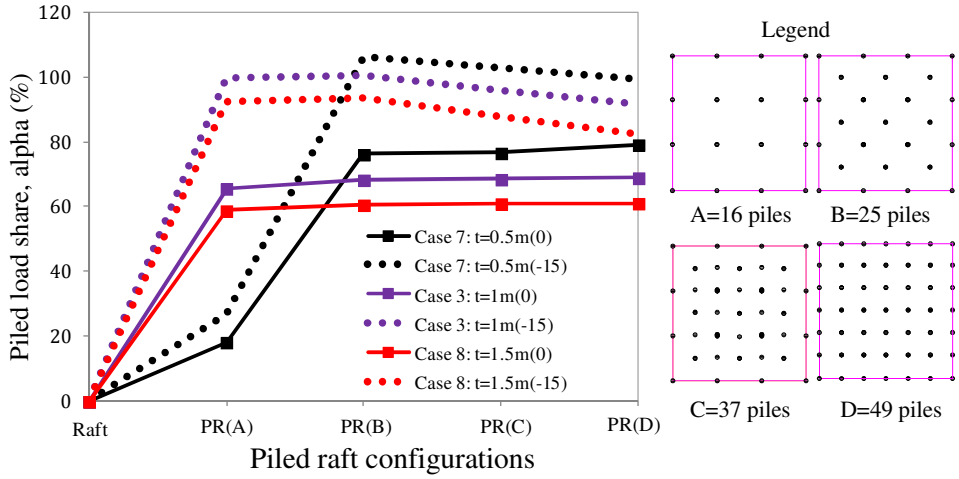

Figure 5.31 Piled load shares in piled rafts with different configurations in case 3, 7 & 8 (t = thickness of raft)

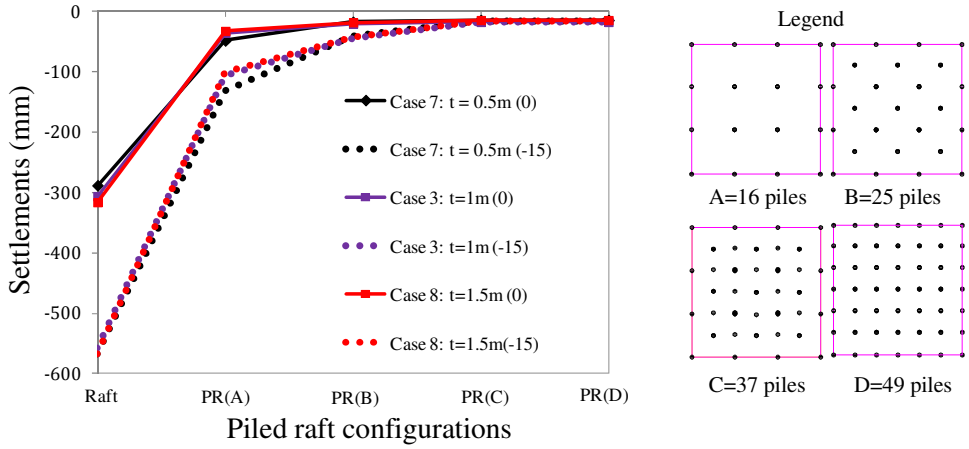

Figure 5.32 Average settlements in piled rafts before and after ground subsidence in case 3, 7 & 8 (t = thickness of raft)

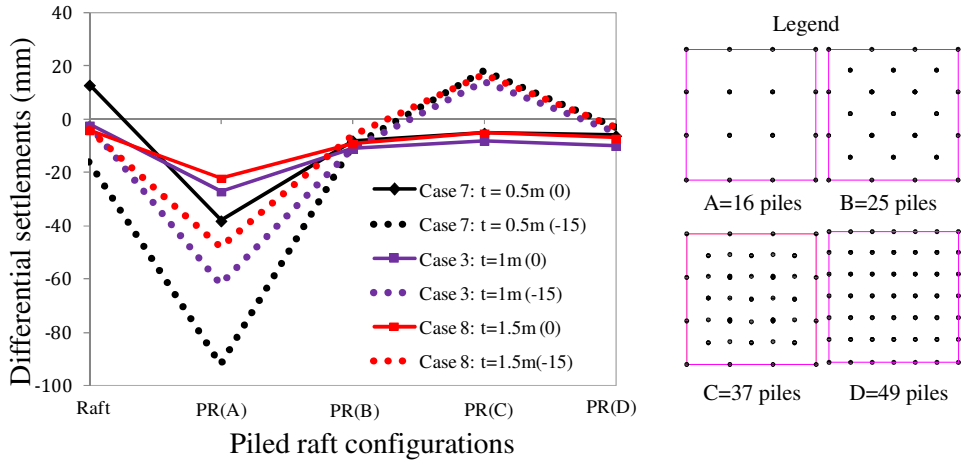

Figure 5.33 Differential settlements (0-2) in piled rafts before and after ground subsidence in case 3, 7 & 8 (t = thickness of raft)

Figure 5.31 shows the piled load shares in piled rafts with different configurations in case 3, 7 and 8. It was noted that the only difference between these three cases was the thickness of the raft. The thicknesses of the rafts were 0.5 m, 1 m and 1.5 m for case 7, case 3 and case 8, respectively. For normal condition, at the same piled raft configuration, the loads shared by the piles were different when the raft thicknesses were different. For example, at PR(A), the loads shared by the piles were 18%, 66% and 59% for the raft thicknesses of 0.5 m, 1 m and 1.5 m respectively. The reason might be come from the contact between the raft and ground surface which located between the piles. More deflection should be found for the raft which had the less raft – soil stiffness. However, when the raft-soil stiffness was large (the load on the raft should be redistributed into uniform), the deflection of the raft between piles was decrease and, therefore, decrease the contact between raft and ground surface in that zone. The result was more load should be transferred to the piles and the load carried by the piles should be increased. For case 3 (t =1 m) and case 8 (t = 1.5 m), at type of PR(A), when the thickness of the raft large enough to make the raft-stiffness became strong enough, the piled load shared was decreased with the increase of raft thickness. For the types of PR(B), PR(C) and PR(D), more piles were inserted between the piles in PR(A) and it resulted that the raft-soil stiffness was increased. The distribution of load became more uniform. At the same piled raft configure, the load shared by the piles was decreased with the increase of raft thickness. For ground subsidence condition, in both cases, the piled load shares increased, as discussed in previous part. The increases of piled load shares were around 50% for PR(A) in both cases. The increases of piled load shares (PR(B)) were 39%, 49% and 54% for the raft thicknesses of 0.5 m, 1 m and 1.5 m in ground subsidence. For PR(C) and PR(D), the increase of piled load shares were around 5% and 10% lower than PR(B).

Figure 5.32 presents the average settlements in piled rafts before and after ground subsidence in case 3, 7 and 8. In normal condition, the average settlements of foundation were decreased with the increase of number of piles. For example, the settlements of raft was reduced by 90%, 94%, 95% and 95% for PR(A: 16 piles), PR(B: 25 piles), PR(C: 37 piles) and PR(D: 49 piles), respectively. The reason was that the piles shared a major part of applied load when they were added to the

foundation. The average settlements were increased around 79%, 200% 139%, 7% and 7% for raft alone, PR(A), PR(B), PR(C) and PR(D) in ground subsidence condition. The range of average settlements with different raft thicknesses in both normal condition and ground subsidence condition were quite narrow. Therefore, the effect of raft thickness on the average settlement was small in the considered situation.

Figure 5.33 a comparison of differential settlements (0-2) in piled rafts before and after ground subsidence in case 3, 7 and 8. The differential settlements were largely increased for raft alone, PR(A) and PR(C) in ground subsidence condition. Little change in differential settlements for PR(B) and PR(D) in ground subsidence condition as discussed previous. The stiffness of the raft had a strong effect on differential settlement in both normal condition and ground subsidence condition. In normal condition, for PR(A), the differential settlements were 22 mm, 27 mm and 38 mm for raft thicknesses of 1.5 m, 1 m and 0.5 m, respectively. When more piles were inserted into the raft area (PR(B), PR(C) and PR(D)), the differential settlements were decreased. The fully piled raft (PR(D: 49 piles)) reduces the average settlement by about 95% (see Figure 5.32), but showed virtually small change in differential settlements compared with the raft alone (about 25%) (see Figure 5.33).

**** Piles as settlement reducer***

Case 1:

- Q_{ult} = 2400 MN, $P_{working}$ = 687.444 MN: SF = 2400/687.444 = 3.49
- S = 166 mm

Case 2:

- Q_{ult} = 400 MN, $P_{working}$ = 144.338 MN: SF = 400/144.338 = 2.77
- S = 393 mm

Case 3:

- Q_{ult} = 220 MN, $P_{working}$ = 108.9 MN: SF = 220/108.9 = 2.02
- S = 557 mm

==> Need piles to reduce settlement of raft foundations (all cases) to 50 mm and to increase SF in case 3 to 2.5

5.4.5.2 Comparison of parameter study for piled raft in Bangkok soil

For piled raft in Bangkok soil, the parameter study was focused on the effect of ground subsidence on *load – settlement curves, load distribution between group of piles and raft, the change in axial force of the pile and variations in maximum bending moment and maximum shear force in the raft*. Ground water decreased from level of +0.0 m (surface) to level of -15 m. For the purpose of this study, the length and diameter of the piles were kept constant and the effect of ground subsidence was investigated under some specific piled raft foundations. The following conclusions were drawn.

1) <u>Numbers of piles and piled configuration</u>

Figures 5.34 – 5.36 show the effect of numbers of piles and piled configuration on the load-settlement curves of foundations. The role of numbers of piles in reducing settlement of rafts in cases 1, 2 and 3 was obvious. As discussed previous, when more piles were added to the foundation such as in PR(A: 16 piles), PR(B: 25 piles), PR(C: 37 piles) and PR(D: 49 piles, it shared a major part of applied and, therefore, reduced large settlement of foundations. For example, in case 1, the settlement of foundation was reduced from 166 mm (raft) to 117 mm (16 piles), 82 mm (25 piles), 50 mm (37 piles) and 49 mm (49 piles).

Ground subsidence was not effect on case 1 while had a strong effect on case 2 and case 3 where the rafts were set in or on soft clay layer. In normal condition, the settlement of raft was reduced from 188 mm (raft) to 27 mm (16 piles), 16 mm (25 piles), 13 mm (37 piles) and 13 mm (49 piles) for case 2 while the settlement of raft was reduced from 306 mm (raft) to 35 mm (16 piles), 20 mm (25 piles), 17 mm (37 piles) and 17 mm (49 piles) for case 3.

In ground subsidence condition, the settlement of raft was reduced from 393 mm (raft) to 79 mm (16 piles), 29 mm (25 piles), 15 mm (37 piles) and 15 mm (49 piles) for case 2 while the settlement of raft was reduced from 557 mm (raft) to 106 mm (16 piles), 45 mm (25 piles), 18 mm (37 piles) and 18 mm (49 piles) for case 3.

Load-settlement curves

Settlement at central of raft was considered for all load-settlement curves.

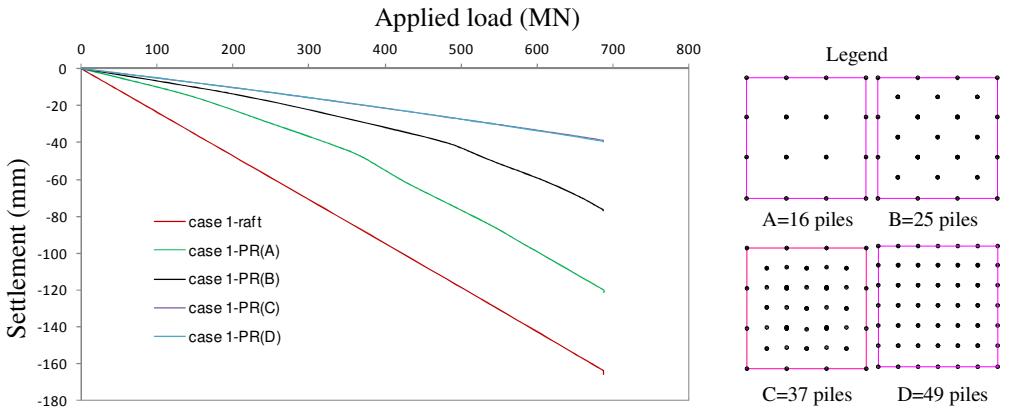

Figure 5.34 Effect of numbers of piles and piled configuration in case 1

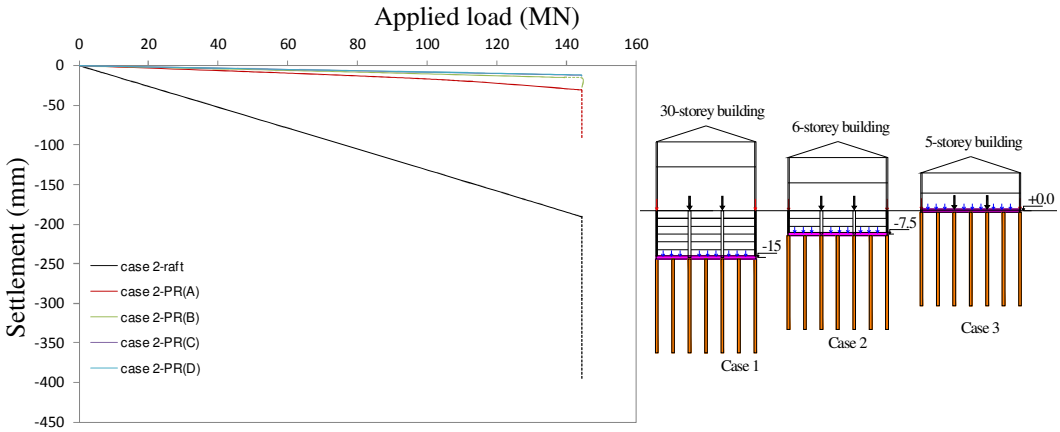

(a)

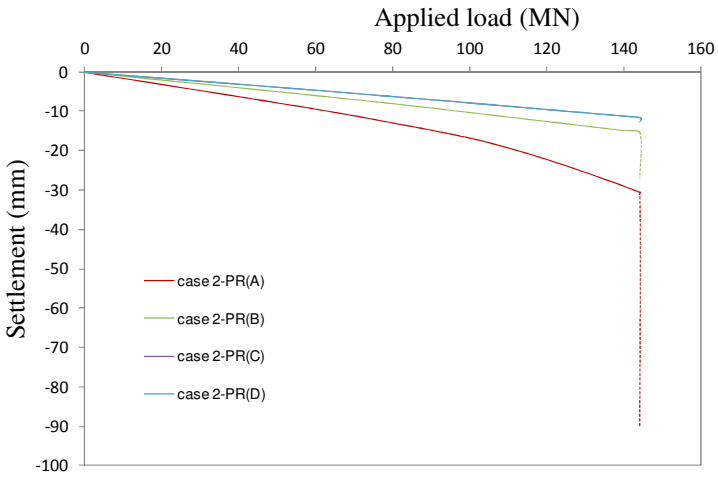

(b)

Figure 5.35 Effect of numbers of piles and piled configuration in case 2

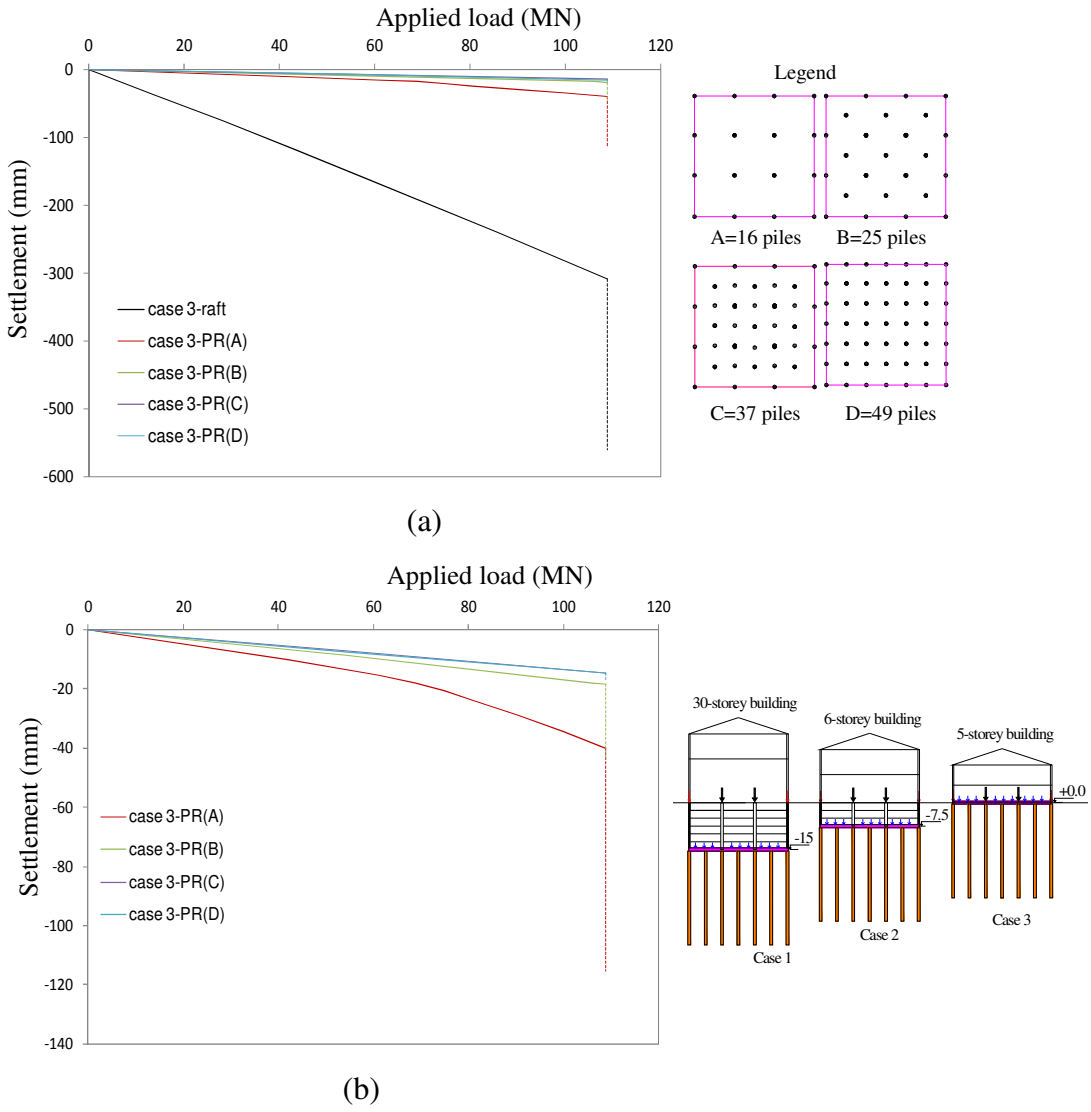

Figure 5.36 Effect of numbers of piles and piled configuration in case 3

Axial force in piles

PR(A)(0) = piled raft, configuration A, ground water level at +0.0 m (normal condition).

PR(A)(-15) = piled raft, configuration A, ground water level at -15 m (ground subsidence condition)

Figure 5.37 – 5.39 present the distribution of axial forces with depth for ground water level at +0.0 m (normal condition) and at -15 m (ground subsidence condition) in cases 1, 2 and 3. In both cases, the axial forces increased when ground subsidence occurred.

In case 1, as seen in Figure 5.37, the maximum axial forces (positions 2, 0 and 0.3) were at the top of piles and were not increased in ground subsidence condition. Negative skin friction was not affected in case 1. The difference in piled raft configurations was quite narrow, excepting for PR(D) where fully piled raft was used and axial force in each piles was small.

In case 2, see Figure 5.38, the maximum axial forces were at the different positions on the piles and were largely increased in ground subsidence condition. For example, the pile at point 2 (under the column) (see Figure 5.38a), the maximum axial force of piles in PR(A) (red lines) was at the top of the piles and was increased around 7 MN (from 12.5 MN to 19.5MN). As discussed previous, the increase came from the applied load, weight of structure carried by water and negative skin friction on the walls which was transferred to the piles. For the pile at point 0 (corner of raft) (see Figure 5.38b), the maximum axial force of piles in PR(A) (red lines) was at depth of around 6.5 m from the top of the piles (neutral plane at around -6.5 m from the top of the pile) and was increased around 8 MN (from 6 MN to 14MN). The increase came from the applied load, weight of structure carried by water which was transferred to the piles and the negative skin friction (on the walls and on the piles) of soft clay layer. For the pile at point 0.3 (1/3 edge of raft) (see Figure 5.38c), the maximum axial force of piles in PR(A) (red lines) was at depth of around 6.5 m from the top of the piles (neutral plane at around -6.5 m from the top of the pile) and was increased around 12 MN (from 4.5 MN to 16.5MN). The increase came from the applied load, weight of structure carried by water which was transferred to the piles and the negative skin friction (on the walls and on the piles) of soft clay layer. When numbers of piles increased (PR(B), PR(C) and PR(D)), the axial forces was decreased and the axial lines were moved to the left. For example, comparing axial fore of the same pile (point 0) in PR(A) and PR(D) gave an interesting results. When ground subsidence occurred, the axial force of the pile was increased around 8MN and 2.2 MN (from 3.8 MN to 6 MN) for PR(A) and PR(D), respectively.

In case 3, see Figure 5.39, the increase axial force in the same manner in case 2. It was noted that the raft in case 3 was set on surface of soft clay layer. Therefore, a larger part of piled length was in negative skin friction zone and a larger increment of

axial force should be appeared. For example, the pile at point 0.3 (1/3 edge of raft) (see Figure 5.39c), the maximum axial force of piles in PR(A) (red lines) was at depth of around 14 m from the top of the piles (neutral plane at around -14 m from the top of the pile) and was increased around 6.8 MN (6.2 MN to 13 MN). The loaded increment came from the applied load and the negative skin friction of soft clay layer.

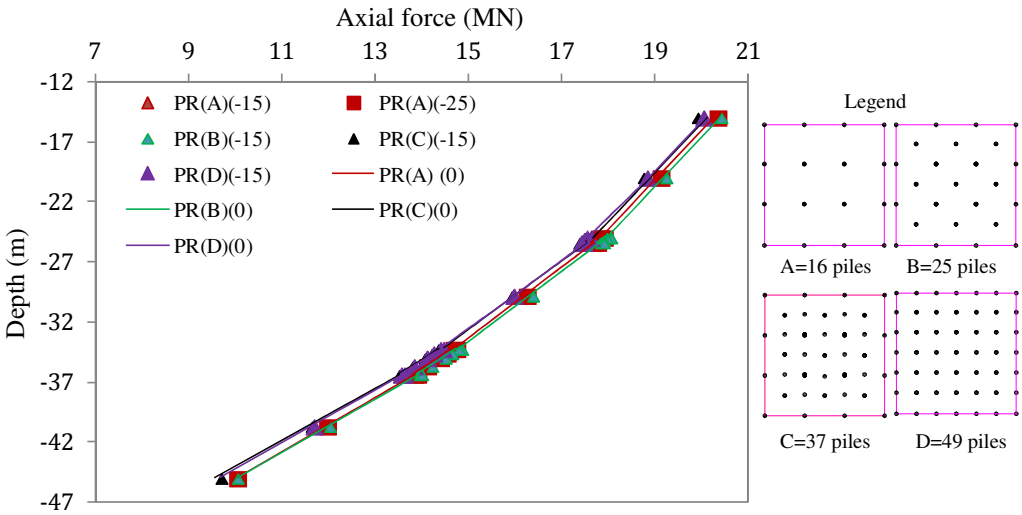

(a) Pile at position 2

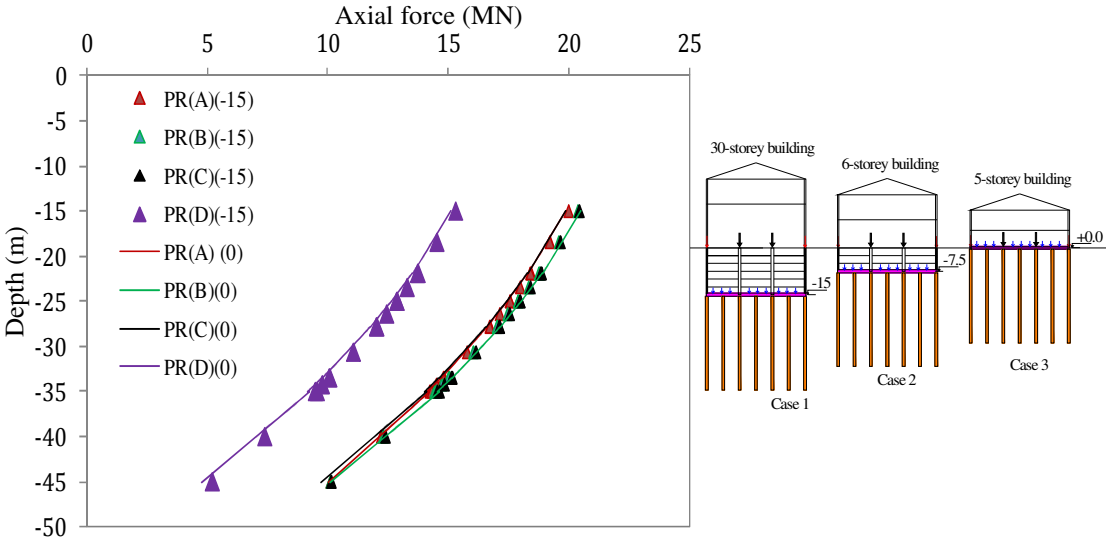

(b) Pile at position 0

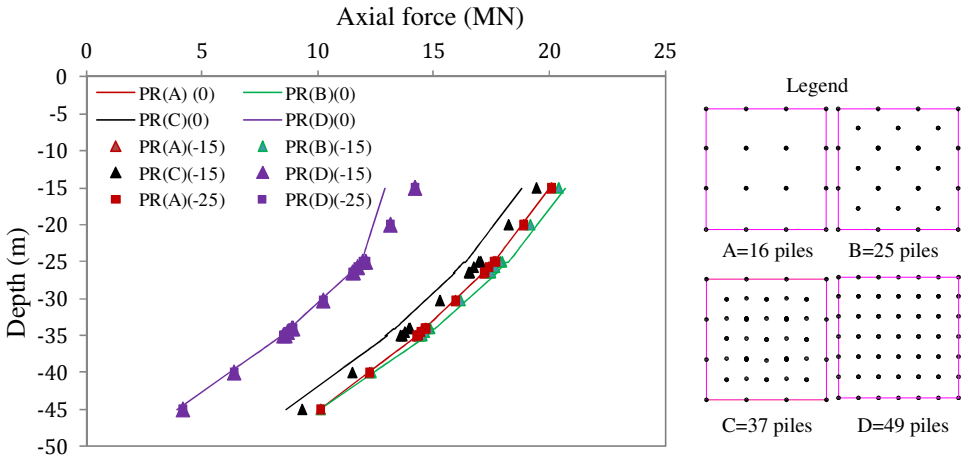

(c) Pile at position 0.3

Figure 5.37 Effect of numbers of piles and piled configuration in case 1

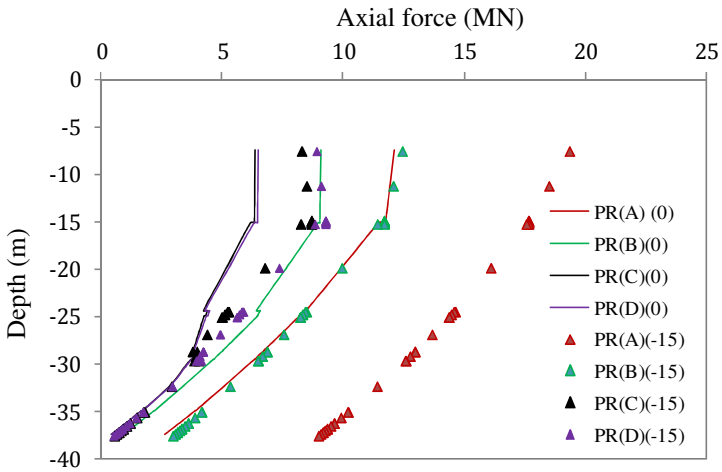

(a) Pile at position 2

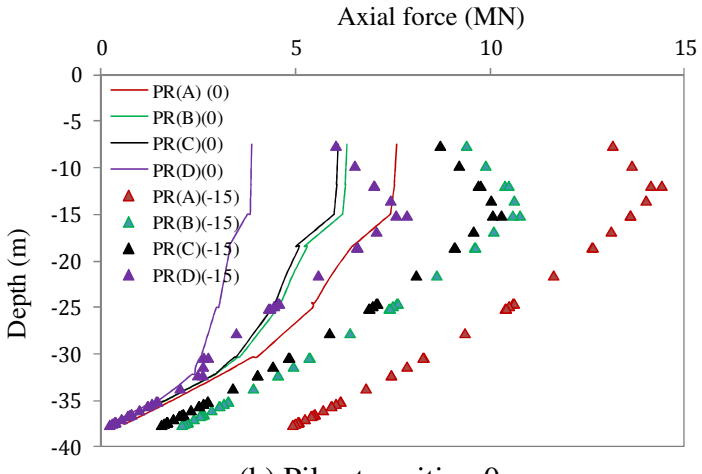

(b) Pile at position 0

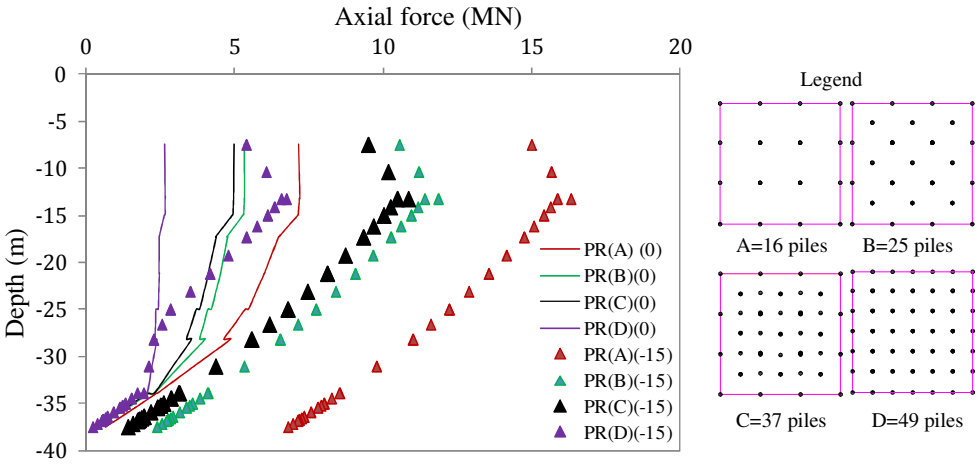

(c) Pile at position 0.3

Figure 5.38 Effect of numbers of piles and piled configuration in case 2

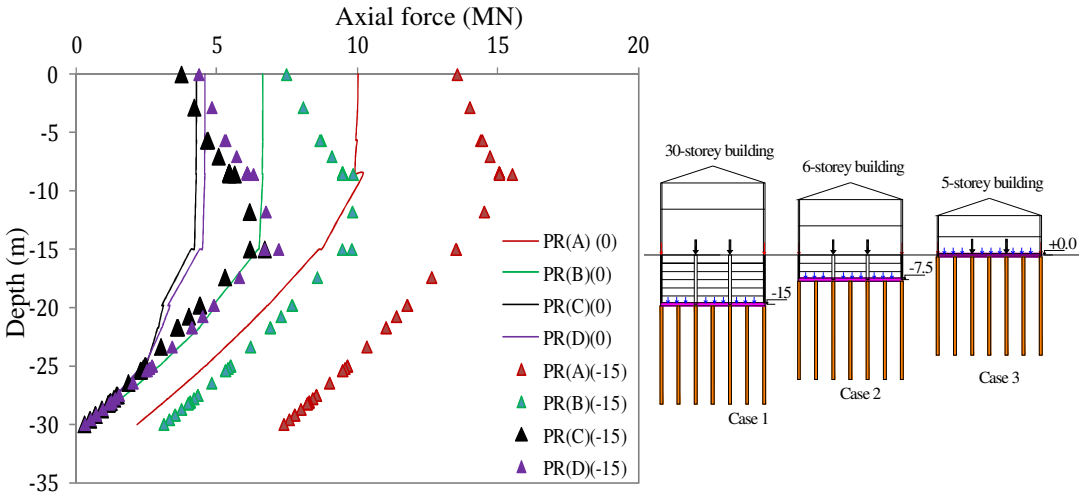

(a) Pile at position 2

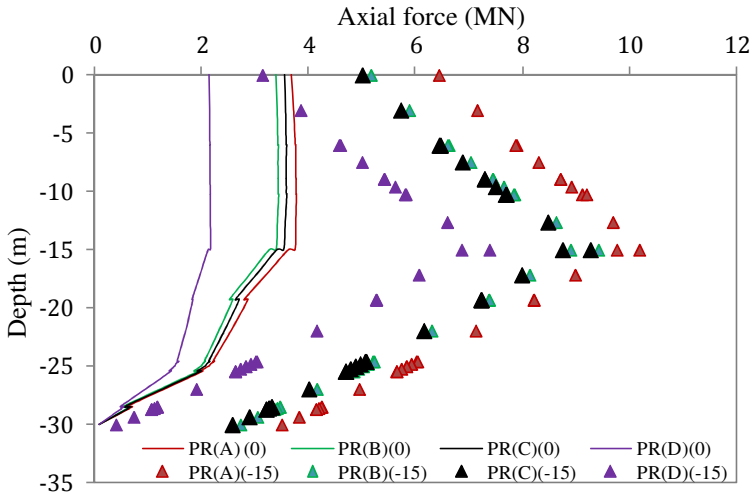

(b) Pile at position 0

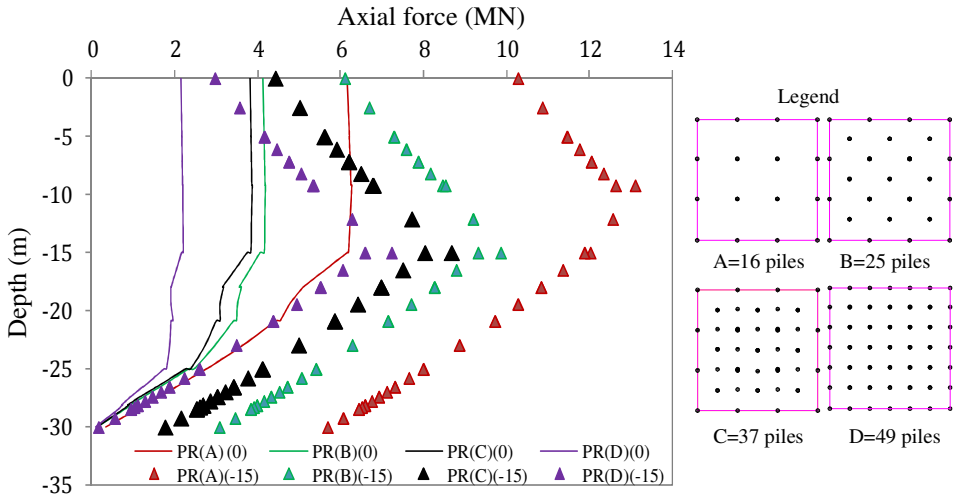

(c) Pile at position 0.3

Figure 5.39 Effect of numbers of piles and piled configuration in case 3

Load distribution and settlement

The settlement at point 2 (under column) was chosen for plotting load distribution-settlement curves. Continuous lines were for normal condition and dash lines were for ground subsidence condition.

Figure 5.40 shows the relationship between the load carried by the piles (piled load share: %) and the settlement of the foundation. Figure 5.40a presents a full view of variation of piled load share with settlement while Figure 5.40b shows the view of small rectangular in Figure 5.40a. These figures show that, in ground subsidence condition, the settlement of foundations increased and the piled load share also increased.

For case 1 (red lines), piled load shares were not affected in ground subsidence condition. Piled load share of PR(A =16 piles) and PR(B = 25 piles) increased around 1% while these values were around 5% for PR(C =37piles) and PR(D= 49piles).

For case 2 (green lines), the piles carried all applied load and self-weight of raft, floors, wall, beam and columns (> 100%) in ground subsidence condition. Piled load share of PR(A =16 piles) increased around 50% with the increment settlement of foundation of around 50 mm. Piled load share of PR(B =16 piles), PR (C = 37piles) and PR(D = 49piles) increased around 57% with the increment settlement of foundation of around 5 mm.

For case 3 (black lines), the piles also carried most of applied load (~100%) in ground subsidence condition. The increments in piled load shares were around 30 % for PR(A), PR(B) and PR(C), and around 25 % for PR(D).

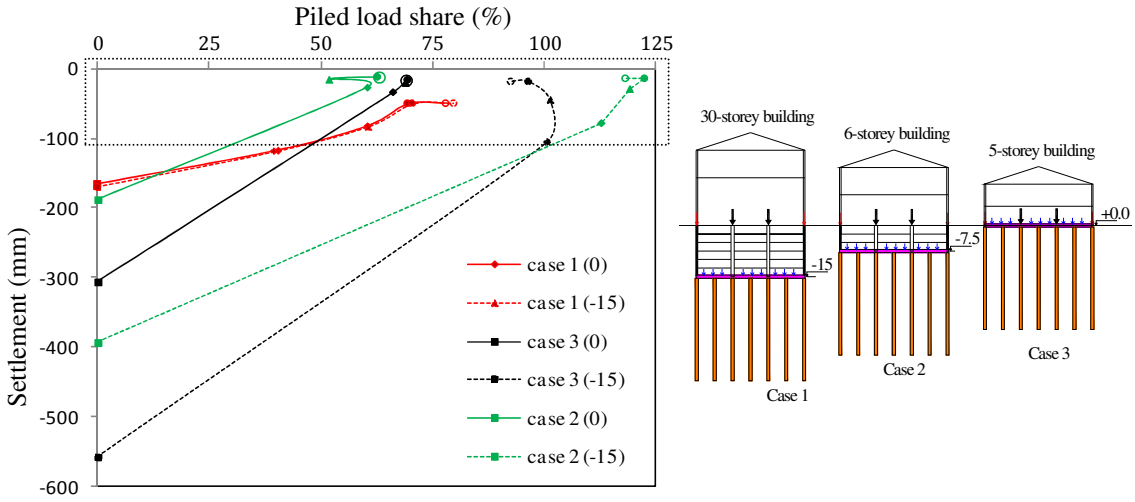

(a) Full

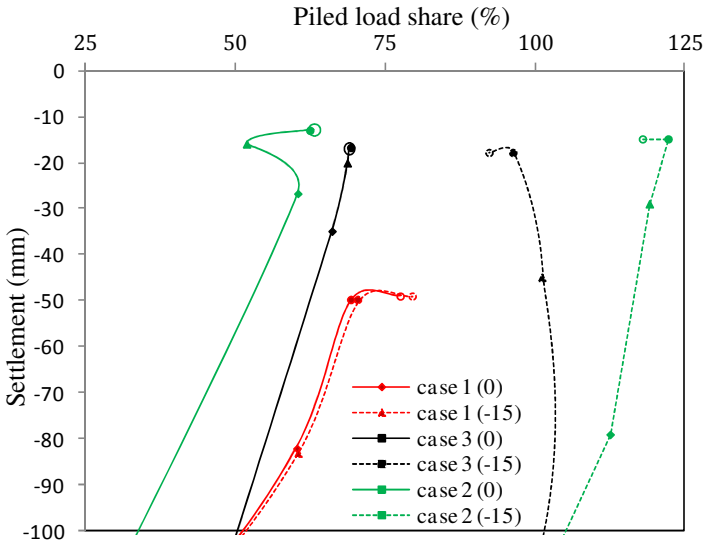

(b) View of small rectangular

(0) – water level at ground surface; (-15) - water level at depth of 15m

Figure 5.40 Comparison of load distribution and settlement for case 1, 2 & 3 (Unit used in legend figure: m)

Raft bending moments and shear

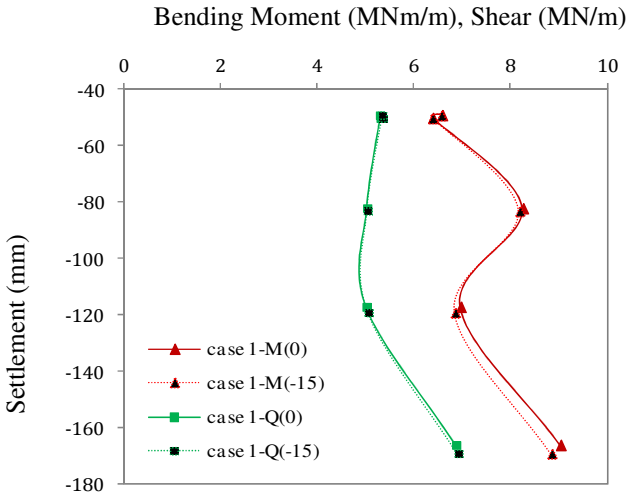

Figure 5.41 Bending moment, shear force and settlement for case 1

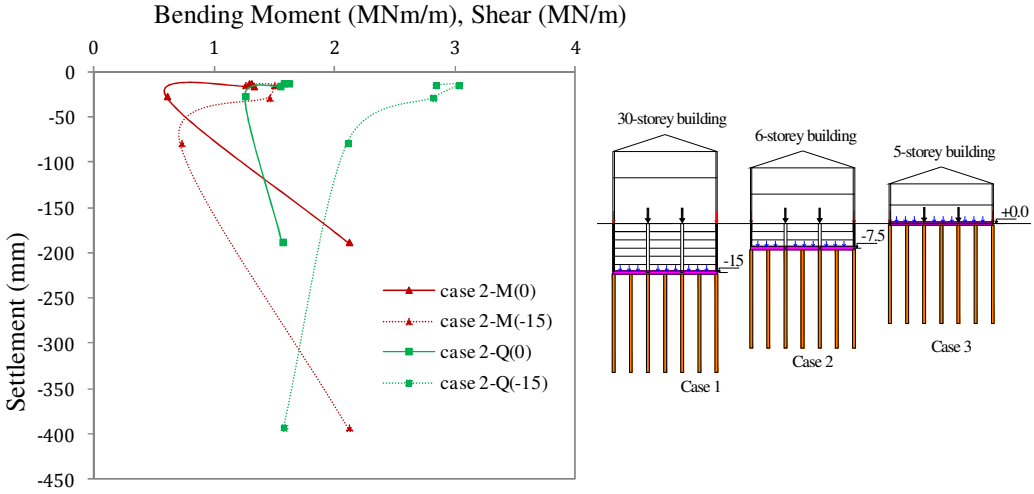

Figure 5.42 Bending moment, shear force and settlement for case 2

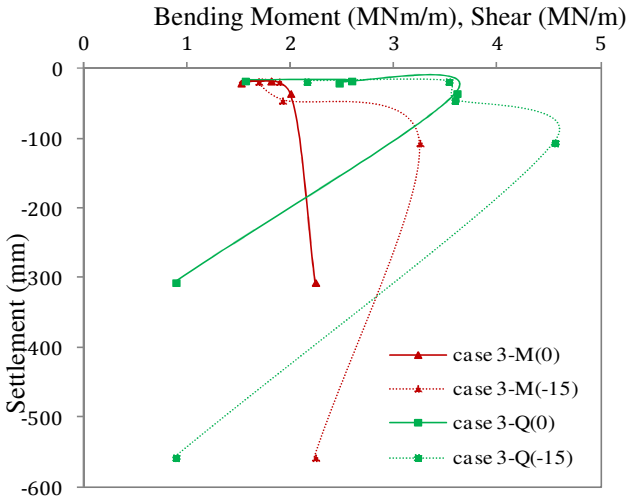

Figure 5.43 Bending moment, shear force and settlement for case 3

Figures 5.41-5.43 present the variation of raft bending moment and shear for case 1, case 2 and case 3, respectively.

Bending moment and shear in raft of case 1 were changed very little (decreasing less than 1.5 MN.m/m for bending moment and 0.5 MN/m for shear) in ground subsidence condition.

For case 2 (Figure 5.42), bending moment was constant (around 1.7 MN.m/m) for PR(A) although large settlement was found (around 200 mm) in ground subsidence condition. PR(B) had an increment of around 0.9 MN.m/m with an increment in settlement of around 50 mm. PR(C) and PR(D) had an increment of around 1.2 MN.m/m with an increment in settlement of around 5 mm. For variation of shear in cases 2, shear was constant (around 2.3 MN/m) for PR(A) although large settlement was found (around 200 mm) in ground subsidence condition. PR(B) had an increment of around 0.2 MN/m with an increment in settlement of around 50 mm. PR(C) and PR(D) had an increment of around 0.2 MN/m with an increment in settlement of around 3 mm.

For case 3 (Figure 5.43), bending moment was constant (around 2.2 MN/m) for PR(A) although large settlement was found (around 300 mm) in ground subsidence condition. PR(B) had an increment of around 1.2 MN/m with an increment in settlement of around 100 mm. PR(C) and PR(D) had an increment of around 0.2 MN/m with an increment in settlement of around 5 mm. Shear was constant (around 0.9 MN.m/m) for PR(A) although large settlement was found (around 300 mm) in ground subsidence condition. PR(B) had an increment of around 1 MN.m/m with an increment in settlement of around 100 mm. PR(C) and PR(D) had an increment of around 0.6 MN.m/m with an increment in settlement of around 10 mm.

2) <u>Effect of Young's modulus</u>

Case 3: $E_3' = 2660\ kPa$ *; Case 4:* $E_4' = 2E_3' = 5320\ kPa$ *; Case 5:* $E_5' = 3E_3' = 7980\ kPa$

Applied load P3 = P4 = P5 = 108.9 MN

Load-settlement curves

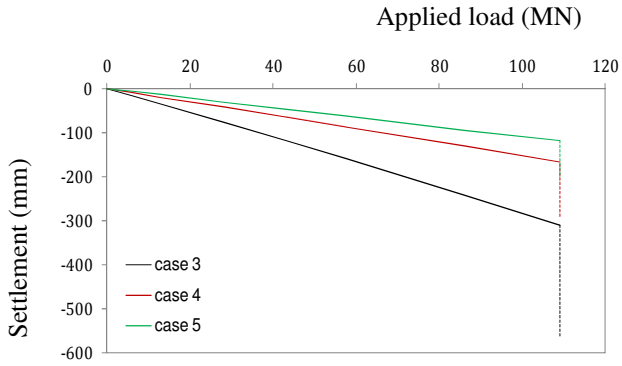

Figure 5.44 Effect of Young's modulus on raft foundations

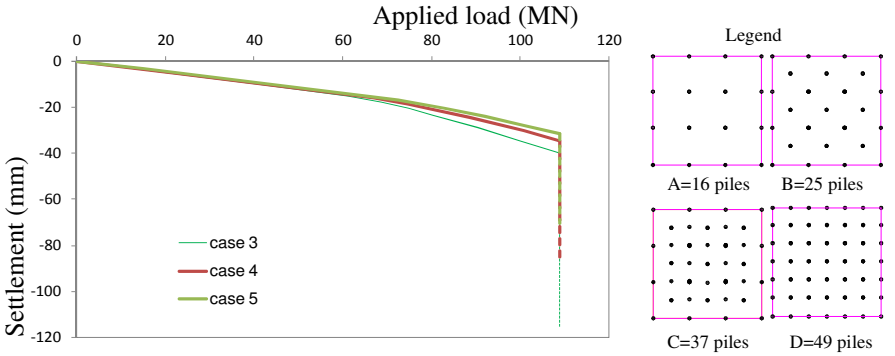

Figure 5.45 Effect of Young's modulus on piled raft with 4x4 piles (A)

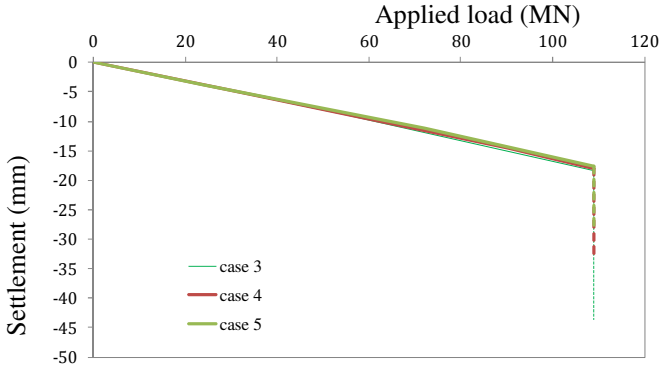

Figure 5.46 Effect of Young's modulus on piled raft with 25 piles (B)

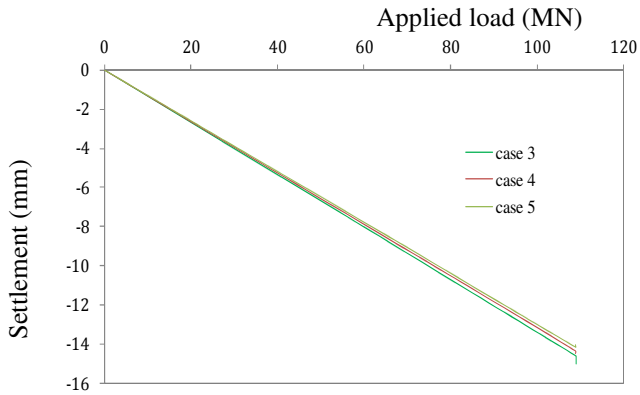

Figure 5.47 Effect of Young's modulus on piled raft with 37 piles (C)

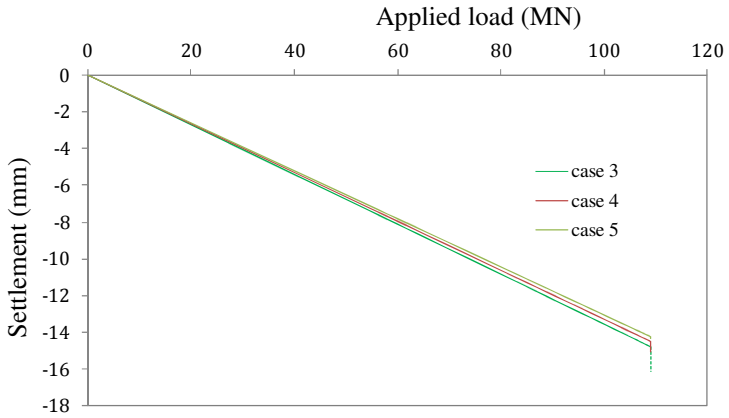

Figure 5.48 Effect of Young's modulus on piled raft with 7x7 piles (D)

Figures 5.44 – 5.48 show the effect of Young's modulus of soil on the load-settlement curves of foundations.

Figure 5.44 shows that the settlements of raft foundation decreased around 50 % or 70 % when Young's modulus of soil increases 2 times ($E_4 = 2E_3$) or 3 times ($E_5 = 3E_3$) in ground subsidence condition. The settlement of foundation decreased around 40% ($E_4 = 2E_3$) and 60% ($E_5 = 3E_3$) for PR(A) while these values were around 50% ($E_4 = 2E_3$) and 65% ($E_5 = 3E_3$) for PR(B). Very little settlements occurred in PR(C) and PR(D) in ground subsidence condition when Young's modulus of soil increased because almost the load carried by the piles.

Axial force in piles

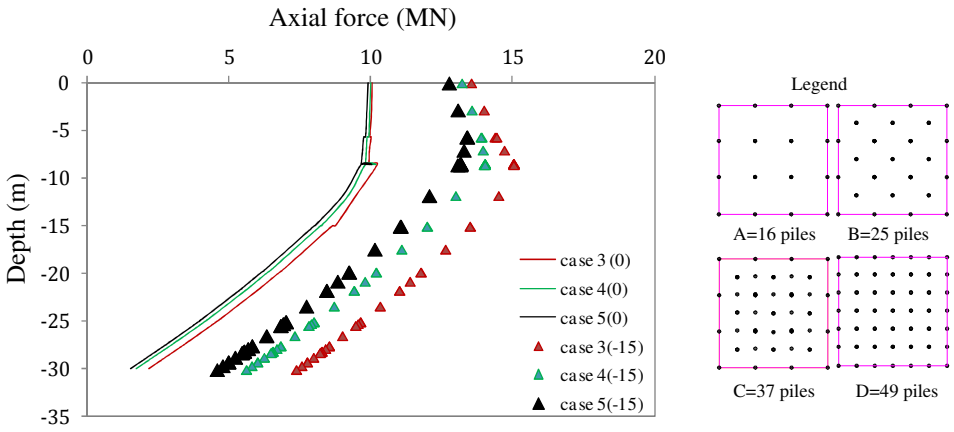

(a) Pile at position 2

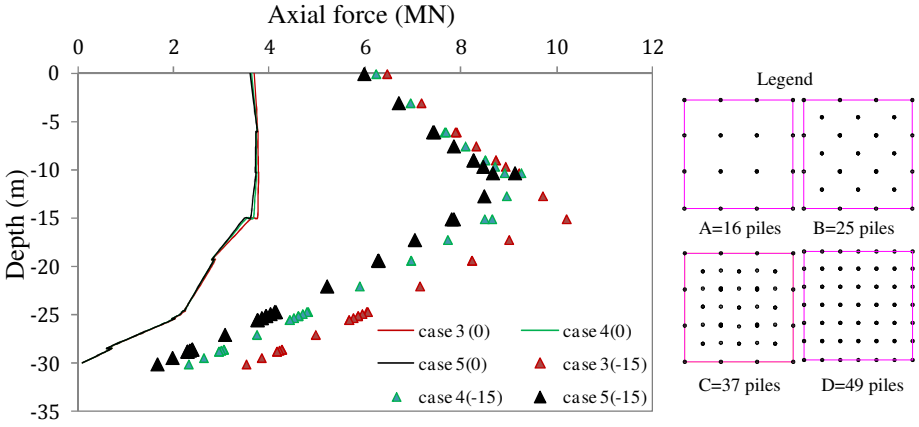

(b) Pile at position 0

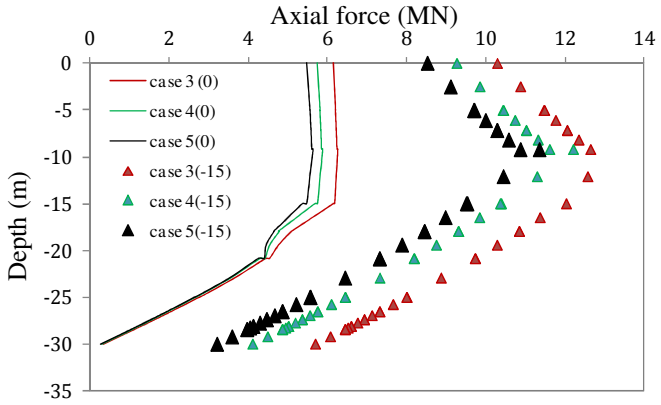

(c) Pile at position 0.3

Figure 5.49 Effect of Young's modulus on piled raft with 4x4 piles (A)

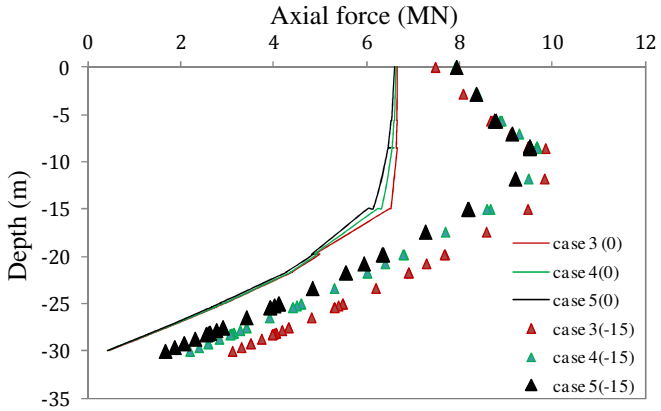

(a) Pile at position 2

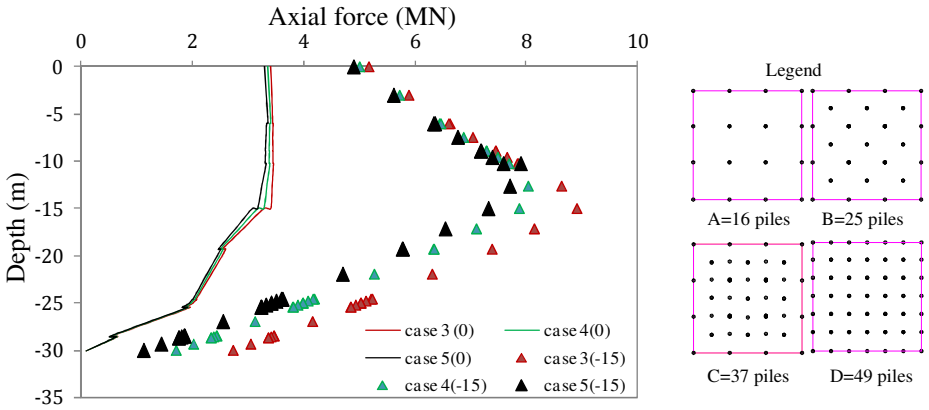

(b) Pile at position 0

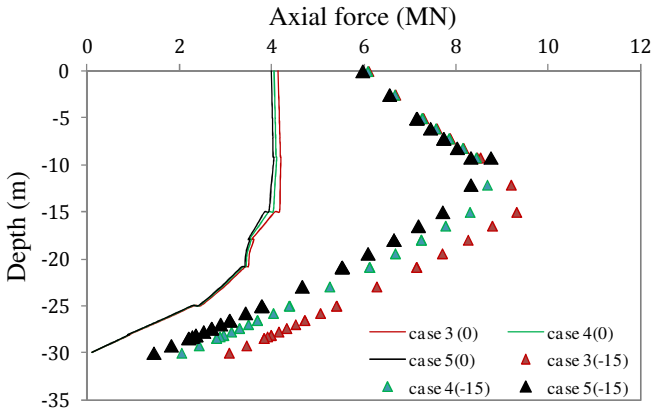

(c) Pile at position 0.3

Figure 5.50 Effect of Young's modulus on piled raft with 25 piles (B)

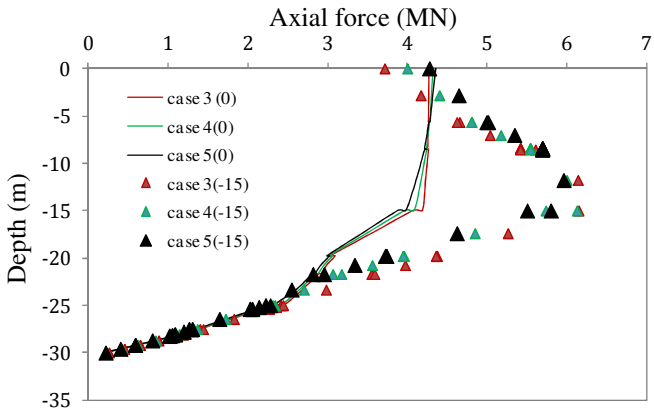

(a) Pile at position 2

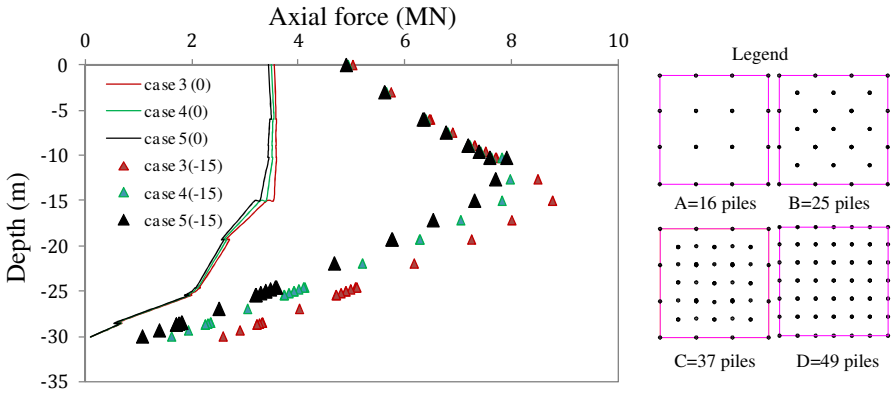

(b) Pile at position 0

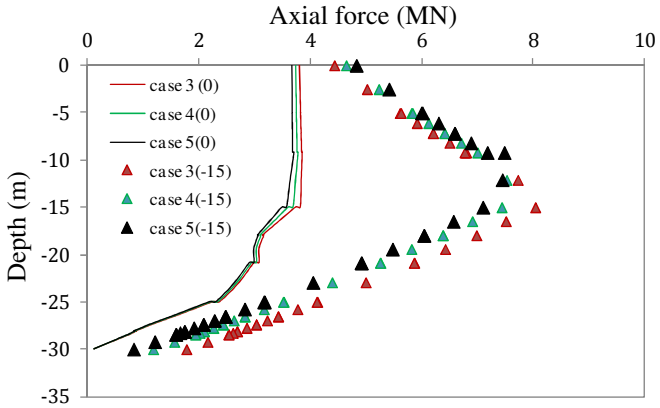

(c) Pile at position 0.3

Figure 5.51 Effect of Young's modulus on piled raft with 37 piles (C)

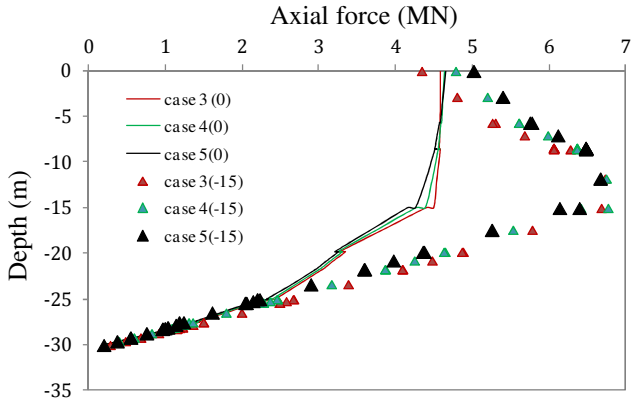

(a) Pile at position 2

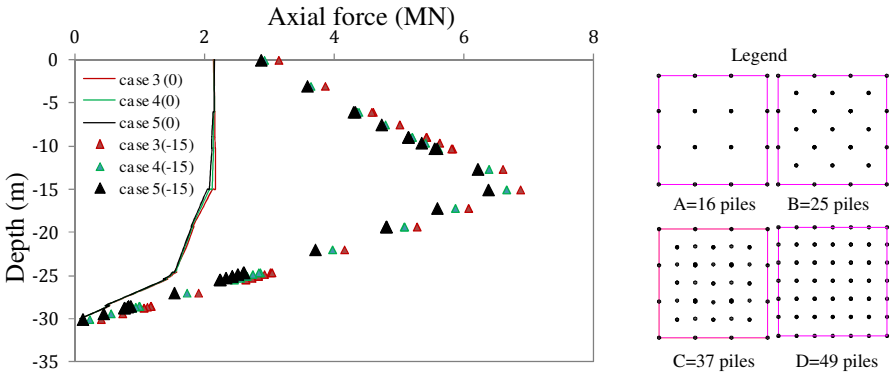

(b) Pile at position 0

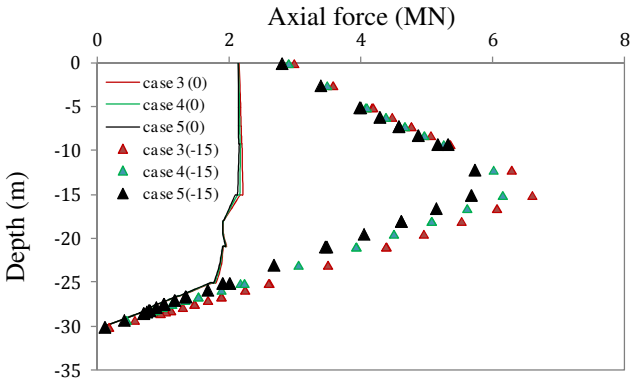

(c) Pile at position 0.3

Figure 5.52 Effect of Young's modulus on piled raft with 7x7 piles (D)

PR(A)(0) = piled raft, configuration A, ground water level at +0.0 m (normal condition). PR(A)(-15) = piled raft, configuration A, ground water level at -15 m (ground subsidence condition)

Figure 5.49 – 5.52 present the distribution of axial forces with depth for ground water level at +0.0 m (normal condition) and at -15 m (ground subsidence condition) in cases 3 (E_3), case 4 ($E_4 = 2E_3$) and case 5 ($E_5 = 2E_3$). When Young's modulus of soil increased ($E_4 = 2E_3$ and $E_5 = 2E_3$), the maximum axial forces in piles increased largely with depth in ground subsidence condition.

For example, in PR(A) and at point 2 (under column) (Figure 5.49a), the maximum axial forces increased around 3 MN, 4 MN and 6 MN for E_3, $E_4 = 2E_3$ and $E_5 = 2E_3$, respectively. In PR(B) (Figure 5.50a), the maximum axial forces increased around 3 MN, 3.2 MN and 3.5 MN for E_3, $E_4 = 2E_3$ and $E_5 = 2E_3$, respectively. In PR(D) (Figure 5.52a), the maximum axial forces increased around 2.3 MN for E_3, $E_4 = 2E_3$ and $E_5 = 2E_3$.

Load distribution and settlement

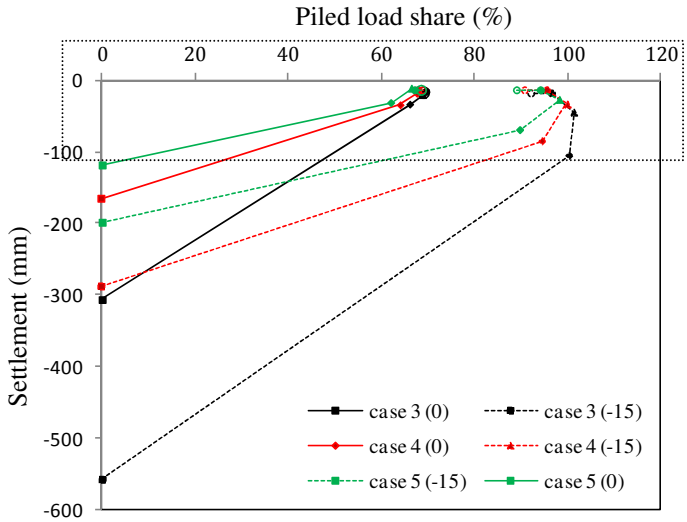

(a) Full view

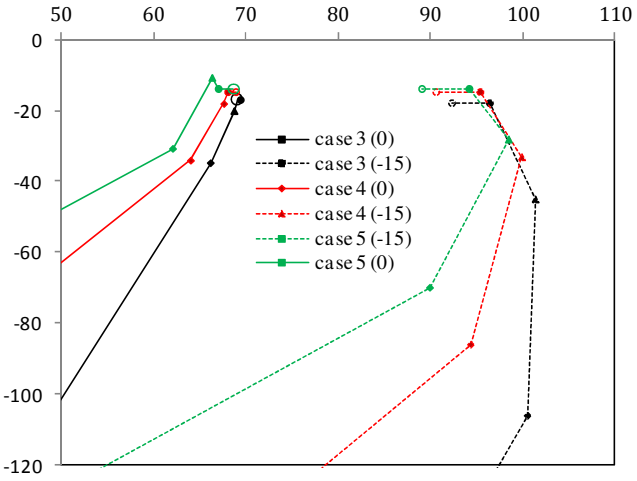

(b) View of small rectangular

Figure 5.53 Comparison of load distribution and settlement for case 3, 4 and 5

Figure 5.53 shows variations of piled load share with settlement for different Young's moduli of soil in normal condition and ground subsidence condition. When Young's modulus of soil increased, the piled load share in ground subsidence condition decreased. For example, for PR(A), the piled load shares were decreased 36 %, 30 % and 27 % for E_3, $E_4 = 2E_3$ and $E_5 = 3E_3$, respectively. For PR(D), the piled load shares were decreased 23 %, 21 % and 18 % for E_3, $E_4 = 2E_3$ and $E_5 = 3E_3$, respectively.

Raft bending moments and shear

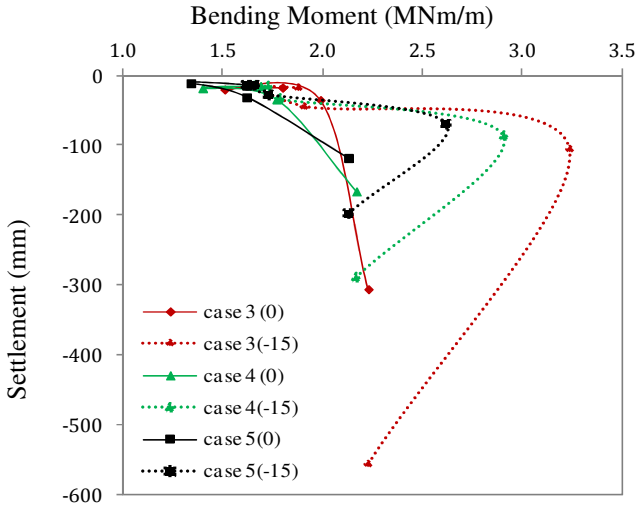

Figure 5.54 Comparison of bending moments and settlements in case 3, 4 & 5

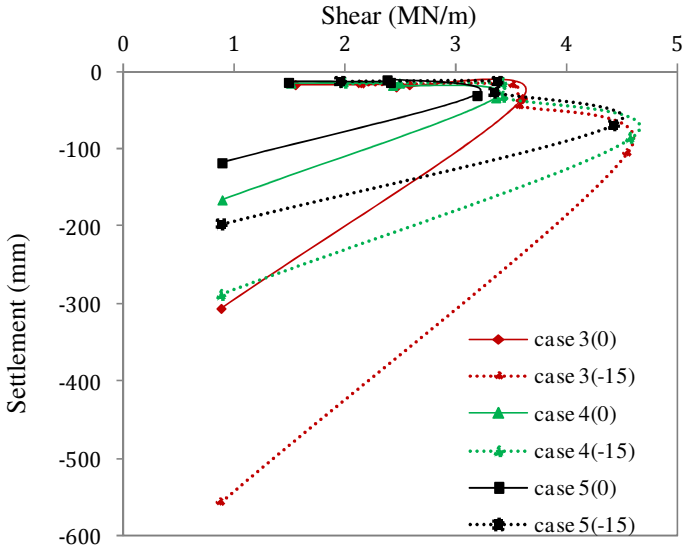

Figure 5.55 Comparison of shear forces and settlements in case 3, 4 & 5

Figure 5.54 and Figure 5.55 present the comparison of bending moments and shear force with settlements in different values of Young's modulus of soil. When Young's modulus of soil increased, the bending moment of raft in ground subsidence condition decreased while shear force of raft increased. For example, for PR(A), bending moment were decreased 1.5 MN.m/m, 1 MN.m/m and 0.95 MN.m/m for E_3, $E_4 = 2E_3$ and $E_5 = 3E_3$, respectively. For PR(A), shear force were increased 0.95 MN/m, 1.22 MN/m and 1.25 MN/m for E_3, $E_4 = 2E_3$ and $E_5 = 3E_3$, respectively.

3) Effect of pattern of loads

Case 3: combined loads and Case 6: uniform load q = 84 kPa.

Load-settlement curves

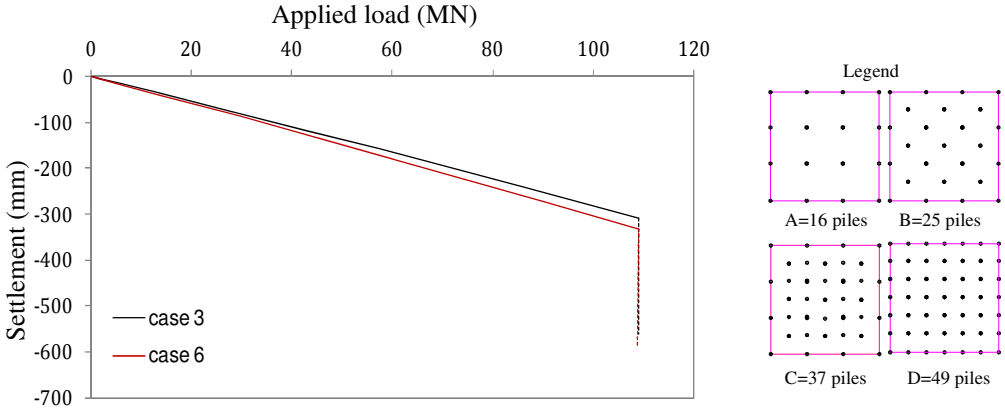

Figure 5.56 Effect of load patterns on raft foundations

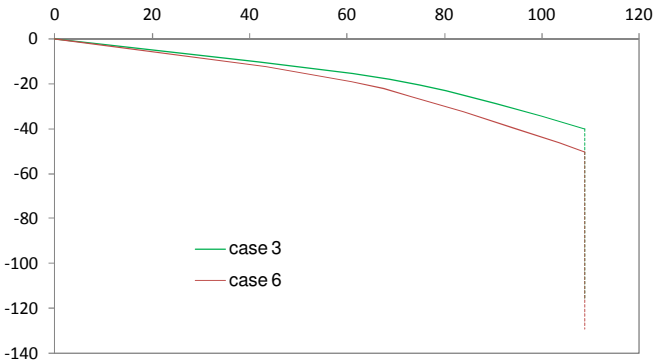

Figure 5.57 Effect of load patterns on piled raft with 4x4 piles (A)

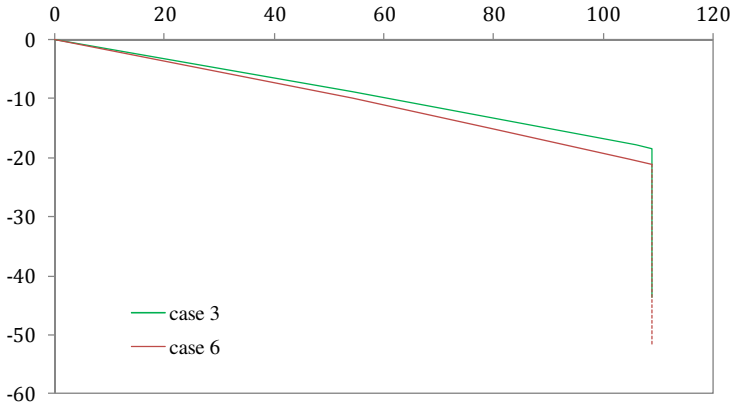

Figure 5.58 Effect of load patterns on piled raft with 25 piles (B)

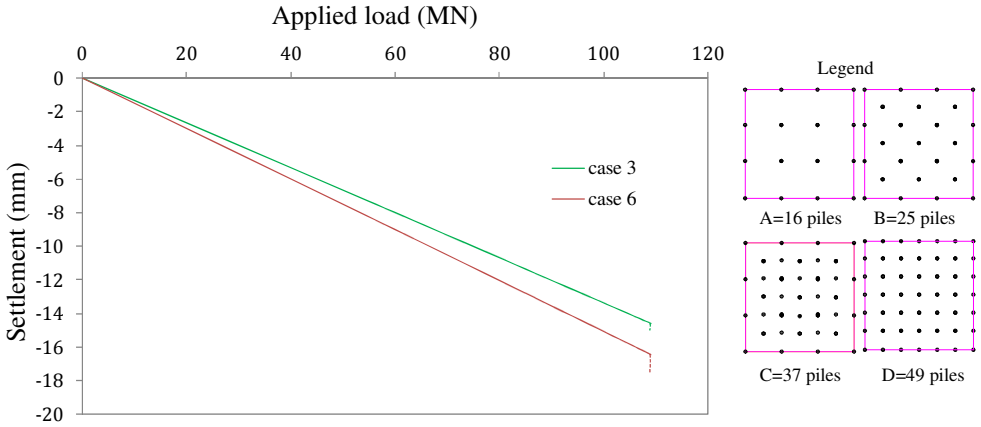

Figure 5.59 Effect of load patterns on piled raft with 37 piles (C)

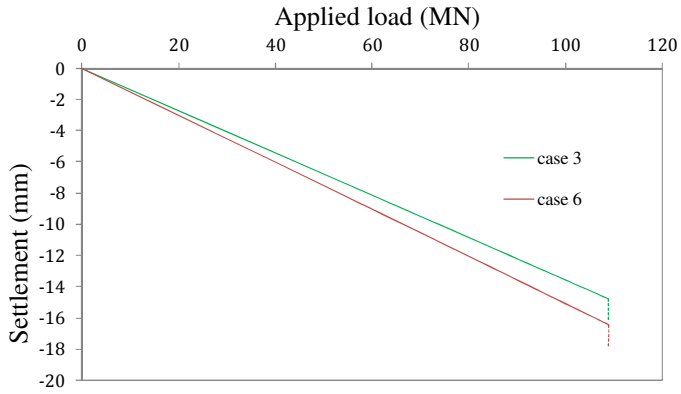

Figure 5.60 Effect of load patterns on piled raft with 7x7 piles (D)

Figures 5.56 - 5.60 present the effect of pattern of load on load-settlement curves of foundation in normal condition and ground subsidence condition. More settlement was found for case of uniform load, compared to combined load. For example, for PR(A), settlements of foundation were around 120 mm and 130 for combined load (case 3) and uniform load (case 6), respectively.

Axial force in piles

Figures 5.61 – 5.64 show the effect of load patterns on maximum axial force of piles in piled raft in normal condition and ground subsidence condition.

Compared to combined load (case 3), more load concentrated around the centre of raft while lesser load at the corner of raft and the same load at the edge of raft for uniform applied load (case 6).

For example, in PR(A) and at point 2 (under column, around the centre of raft)

(Figure 5.61a), the maximum axial forces increased to values of 15 MN and 16 MN for combined load and uniform load, respectively. In PR(B) (Figure 5.62a), the maximum axial forces increased to values of 9 MN and 10.5 MN for combined load and uniform load, respectively. In PR(D) (Figure 5.64a), the maximum axial forces increased to values of 6.2 MN and 6.7 MN for combined load and uniform load, respectively.

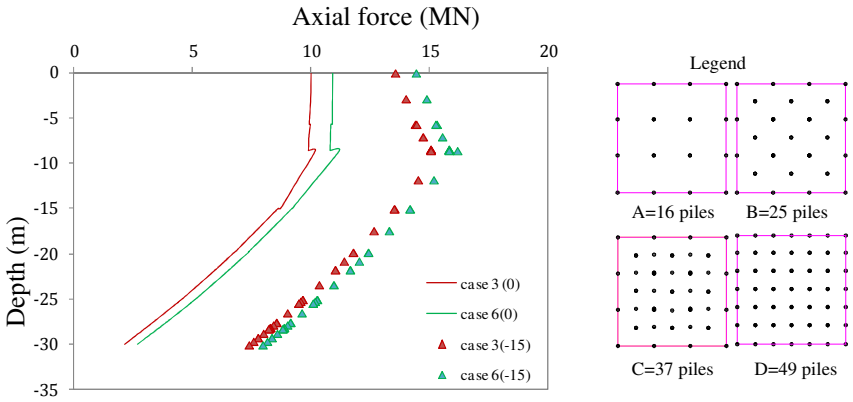

(a) Pile at position 2

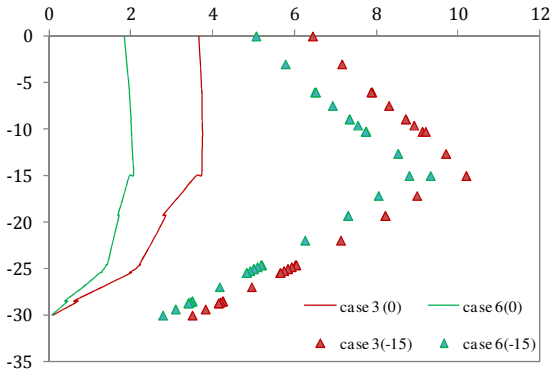

(a) Pile at position 0

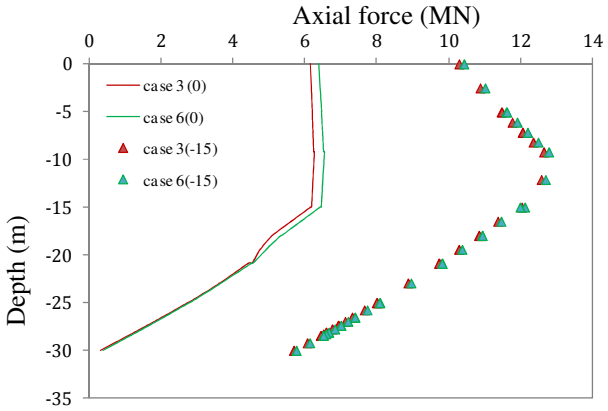

(a) Pile at position 0.3

Figure 5.61 Effect of load patterns on piled raft with 4x4 piles (A)

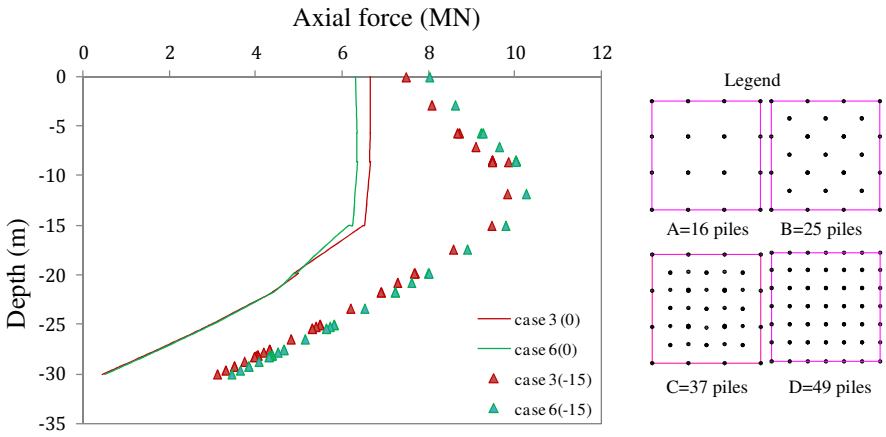

(a) Pile at position 2

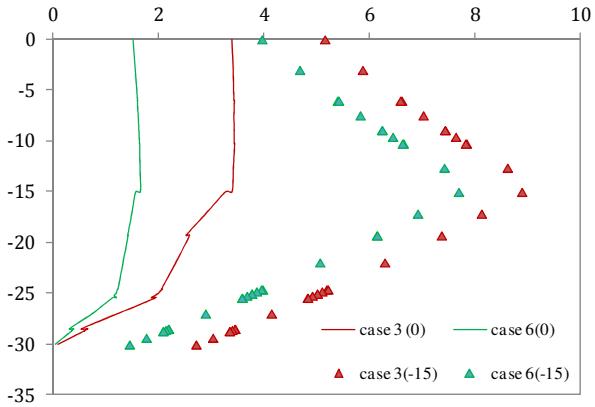

(a) Pile at position 0

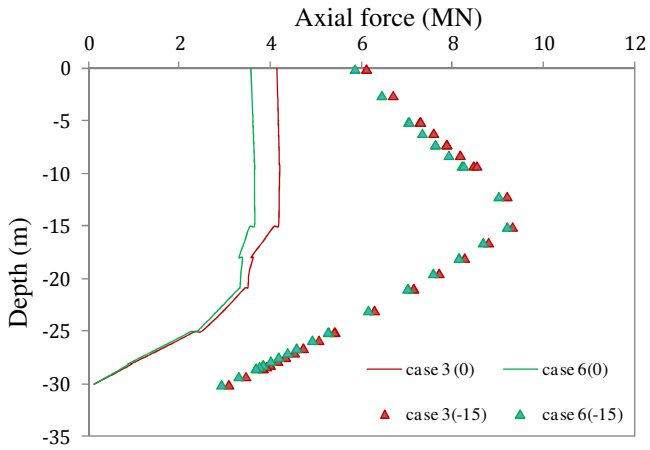

(a) Pile at position 0.3

Figure 5.62 Effect of load patterns on piled raft with 25 piles (B)

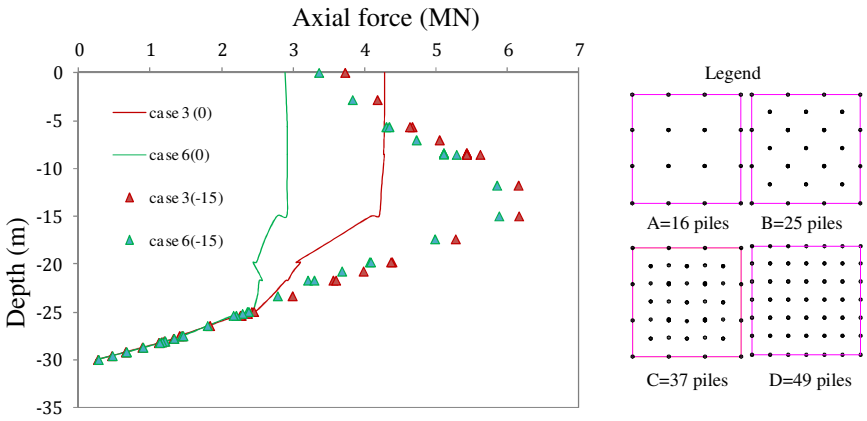

(a) Pile at position 2

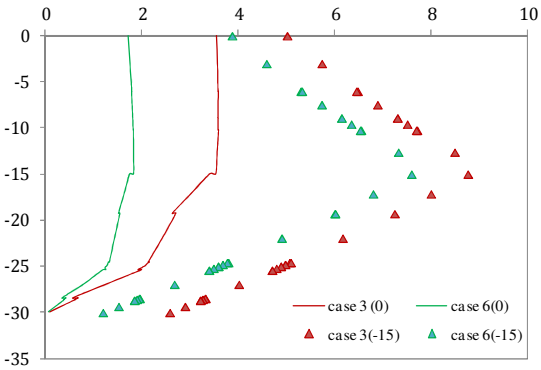

(b) Pile at position 0

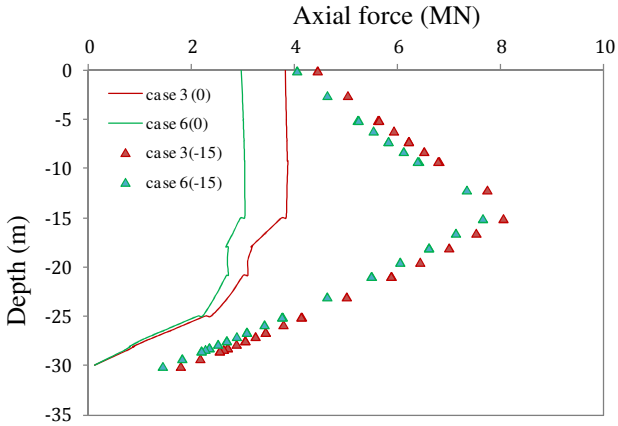

(c) Pile at position 0.3

Figure 5.63 Effect of load patterns on piled raft with 37 piles (C)

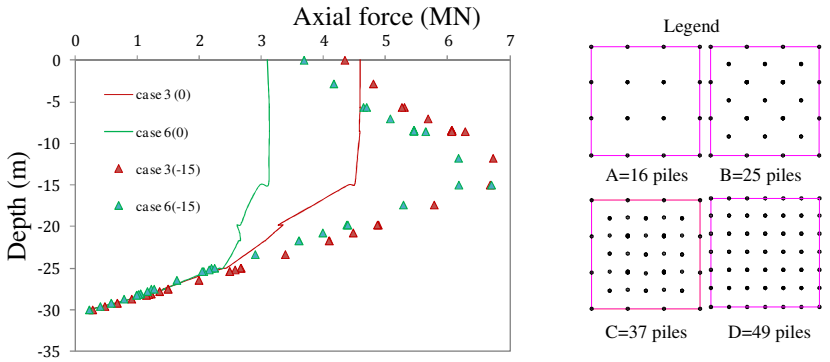

(a) Pile at position 2

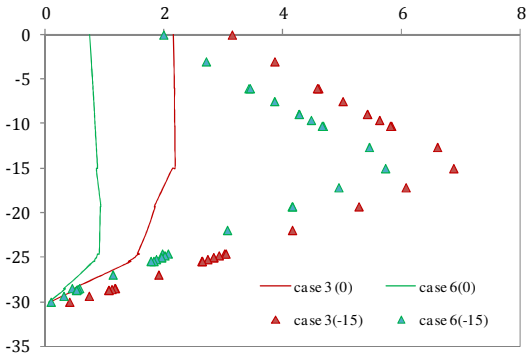

(a) Pile at position 0

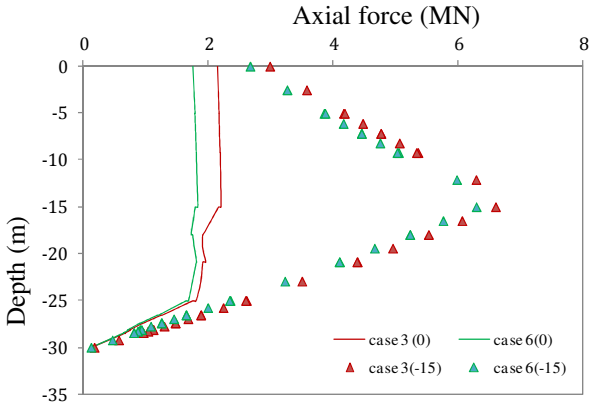

(a) Pile at position 0.3

Figure 5.64 Effect of load patterns on piled raft with 7x7 piles (D)

Load distribution and settlement

Figure 5.65 shows relationship of piled load share with foundation settlement under effect of load patterns in normal and ground subsidence conditions. Compared to combined load, in ground subsidence, the same value of piled load share (but larger

settlement) was found for PR(A=16piles). However, smaller values of piled load share were found when numbers of piles increase in ground subsidence condition. For example, in PR(C), the values of piled load shares were 97% and 96.6 % for combined load and uniform load in ground subsidence condition.

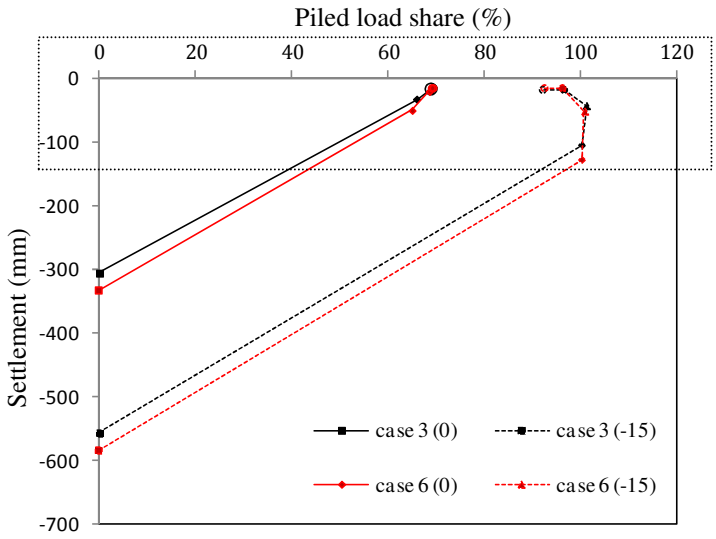

(a) Full view

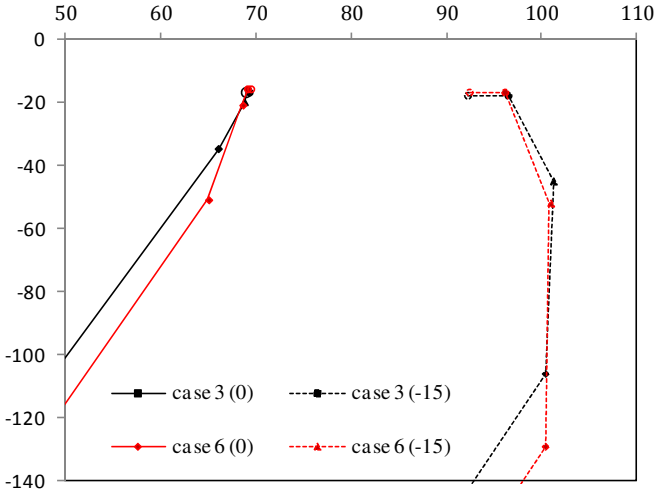

(b) View of small rectangular

Figure 5.65 Comparison of load distribution and settlement for case 3 and case 6

Raft bending moments and shear

Figure 5.66 and Figure 5.67 show the effect of pattern of load on bending moment and shear of raft in normal condition and ground subsidence condition.

As seen in Figure 5.66, larger values of maximum bending moment occurred for uniform load for both normal and ground subsidence conditions. For example, in PR(A), maximum bending moment were 3.4 MN.m/m and 3.8 MN.m/m for combined load and uniform load in ground subsidence condition.

Figure 5.67 shows that smaller values of maximum shear force occurred for uniform load for both normal and ground subsidence conditions. For example, in PR(A), maximum shear force were 4.5 MN/m and 4.4 MN/m for combined load and uniform load in ground subsidence condition.

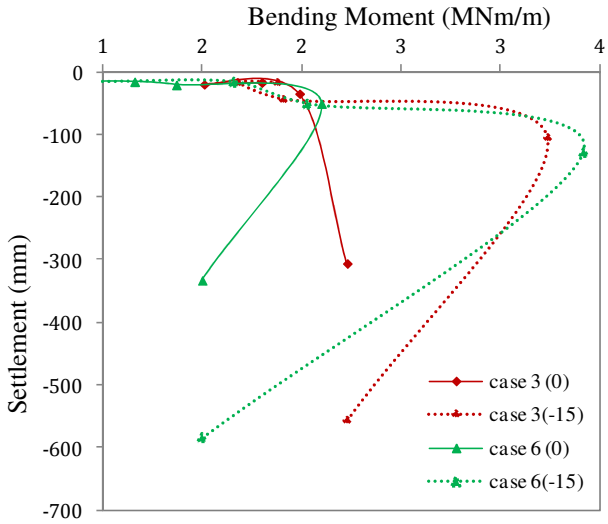

Figure 5.66 Comparison of bending moments and settlements in case 3 and case 6

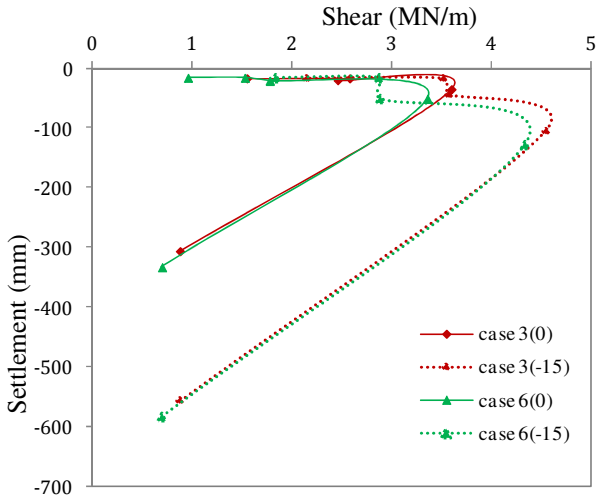

Figure 5.67 Comparison of shear forces and settlements in case 3 and case 6

4) <u>Effect of raft thickness</u>

Case 3: ***t = 1m****, case 7:* ***t = 0.5 m****, case 8:* ***t = 1.5 m***

Effects of raft thickness on load distribution, average and differential settlements were described in details in part ***5.4.5.1*** of this chapter.

Load-settlement curves

Figures 5.68 - 5.72 present the effect of raft thickness on load-settlement curves of foundations in normal and ground subsidence conditions.

For PR(A), less settlement was found for case of thicker raft in both normal and ground subsidence conditions. In ground subsidence, the settlements of foundation were around 130 mm, 120 mm and 110 for the raft thicknesses of 0.5 m, 1 m and 1.5 m, respectively.

However, with larger numbers of piles, the settlements of piled raft were nearly same for PR(B), PR(C) and PR(D) although there was a small part of settlement in case of raft thickness of 0.5 m which was smaller than others. For example, for PR(D) in ground subsidence condition, the settlements of foundations were 15.5 mm, 16 mm and 115.9 mm for raft thicknesses of 0.5 m, 1 m and 1.5 m.

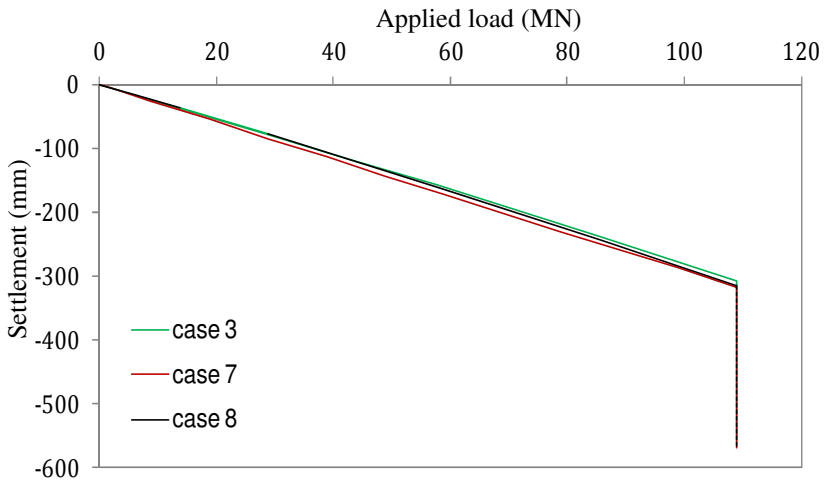

Figure 5.68 Effect of raft thickness on raft foundations

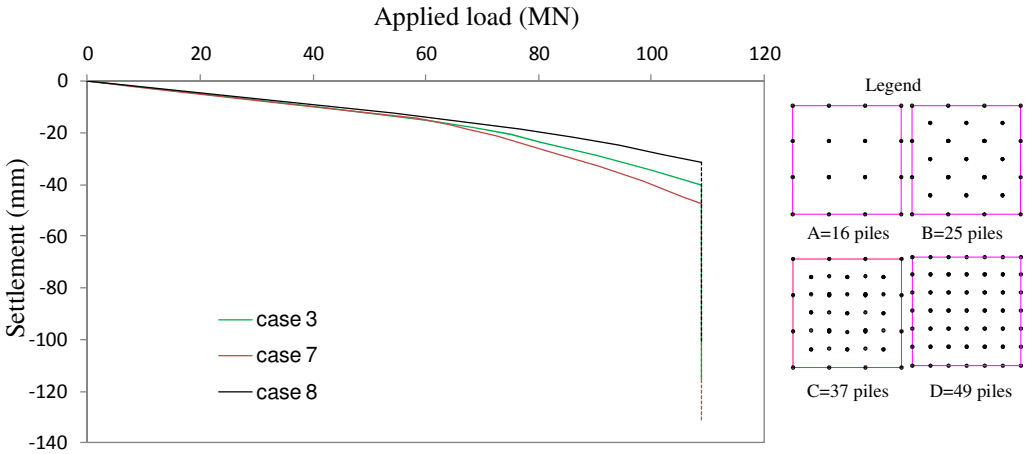

Figure 5.69 Effect of raft thickness on piled raft with 4x4 piles (A)

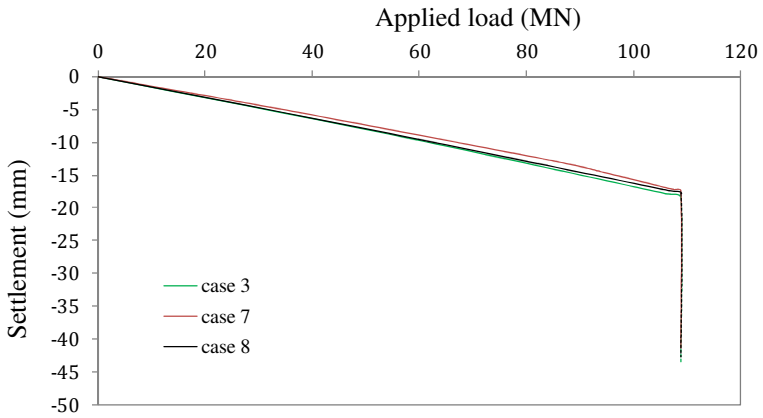

Figure 5.70 Effect of raft thickness on piled raft with 25 piles (B)

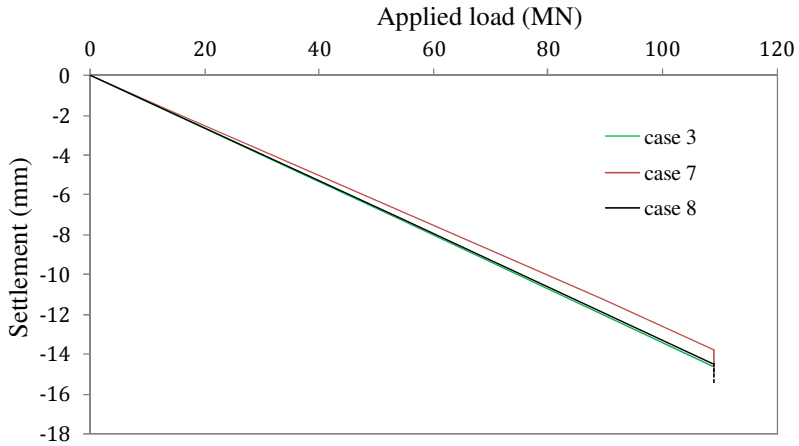

Figure 5.71 Effect of raft thickness on piled raft with 37 piles (C)

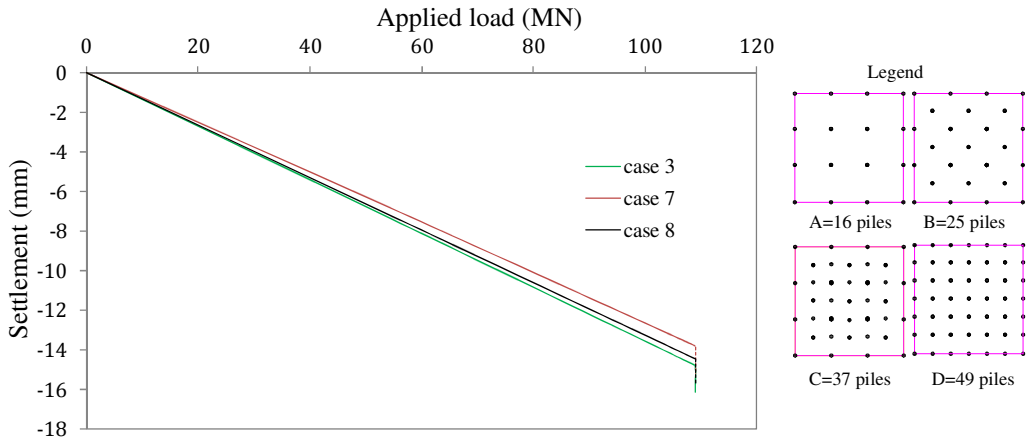

Figure 5.72 Effect of raft thickness on piled raft with 7x7 piles (D)

Axial force in piles

Figures 5.73 – 5.76 show the effect of raft thicknesses on the maximum axial force of piles in piled raft in normal and ground subsidence conditions.

For piles around centre of raft, larger axial force occurred on lesser thickness of raft while lesser values of were found on lesser thickness of raft for piles at the corner and edge of raft in ground subsidence condition. For example, as seen on Figures 5.73a, the value of maximum axial force at point 2 was 16 MN, 15 MN and 14 MN for raft thicknesses of 0.5 m, 1 m and 1.5 m, respectively. Figure 5.74c shows that the values of maximum axial forces were 8.5 MN, 8.6 MN and 8.8 MN for raft thicknesses of 0.5 m, 1 m and 1.5 m, respectively.

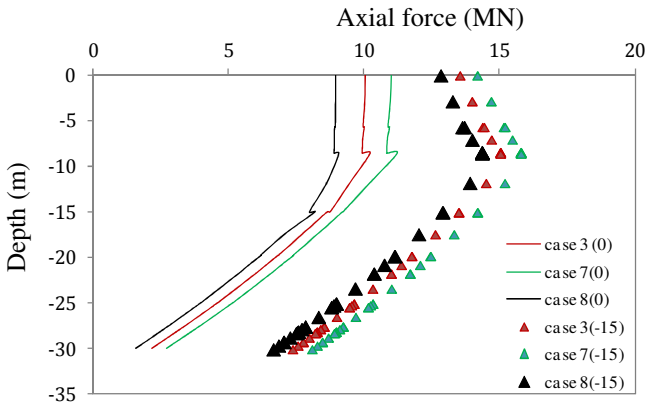

(a) Pile at position 2

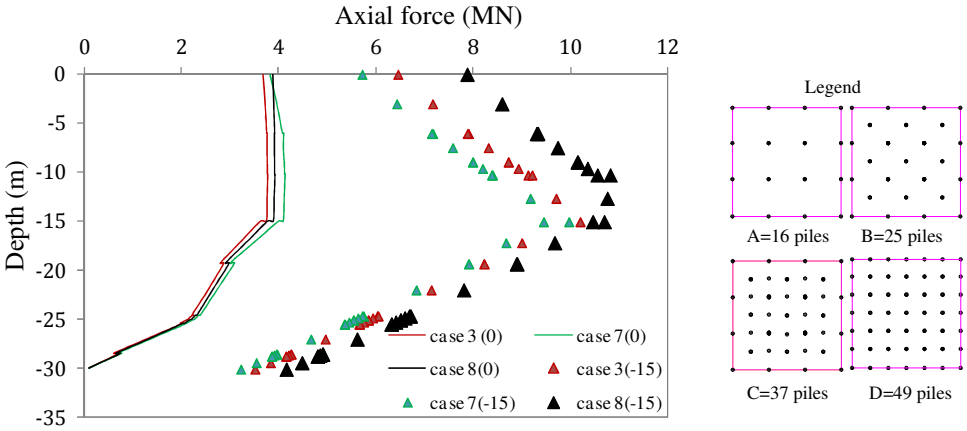

(b) Pile at position 0

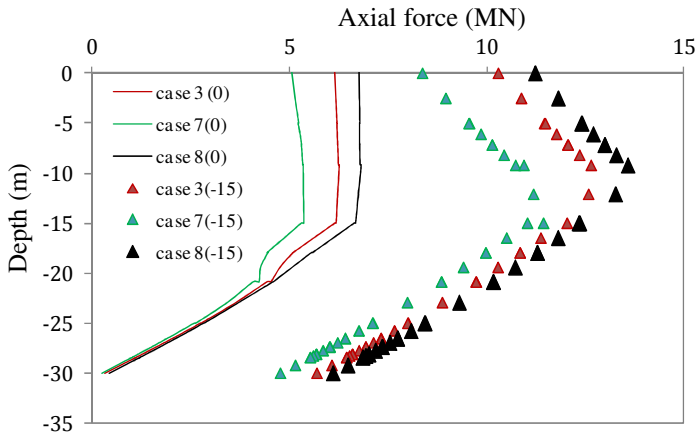

(c) Pile at position 0.3

Figure 5.73 Effect of load patterns on piled raft with 4x4 piles (A)

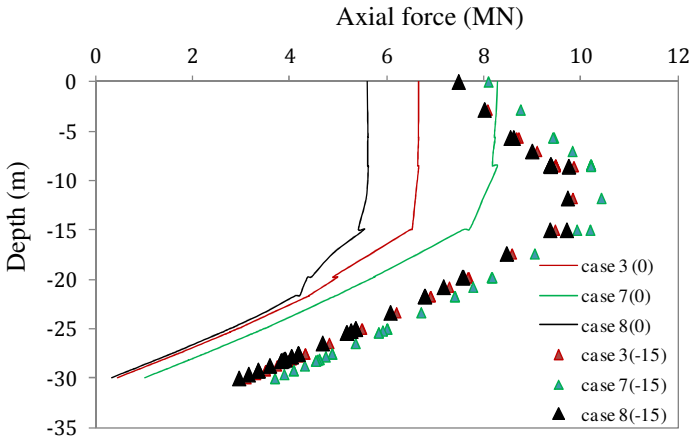

(a) Pile at position 2

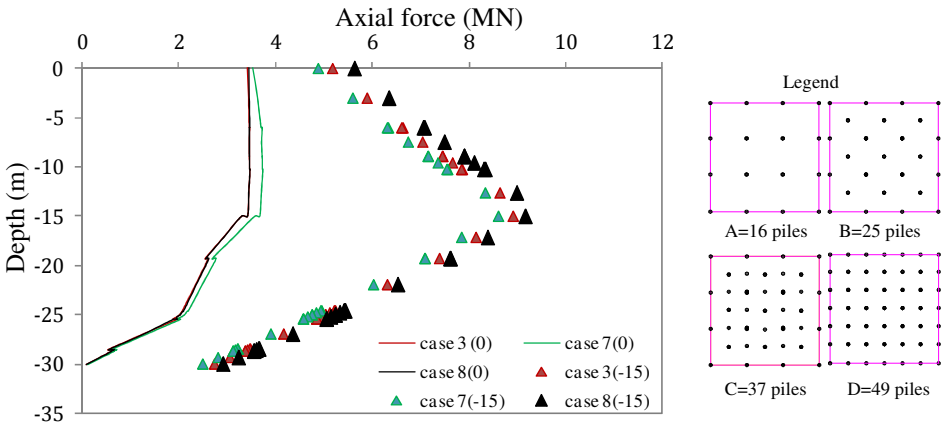

(b) Pile at position 0

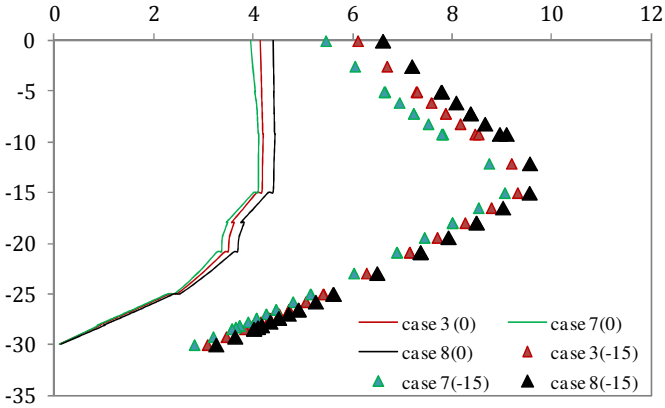

(c) Pile at position 0.3

Figure 5.74 Effect of load patterns on piled raft with 25 piles (B)

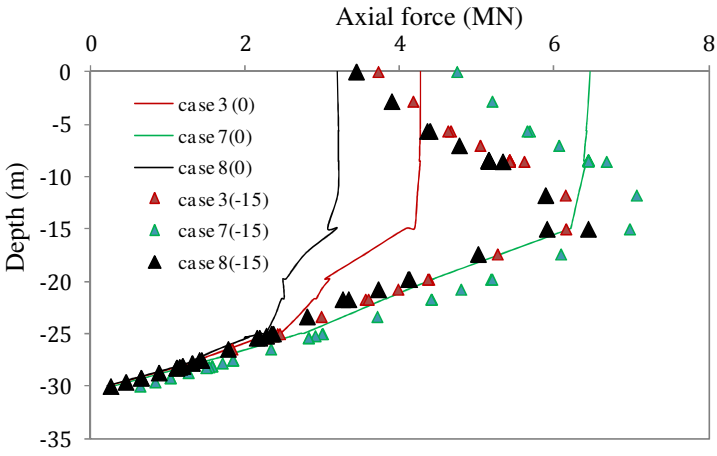

(a) Pile at position 2

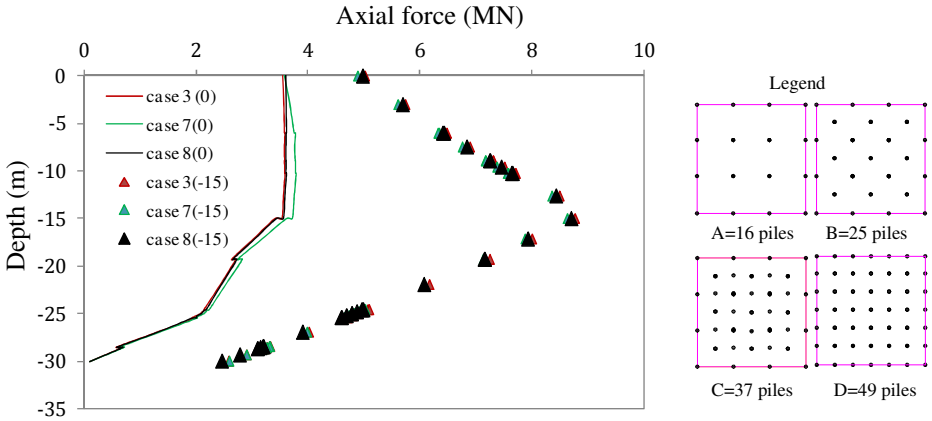

(b) Pile at position 0

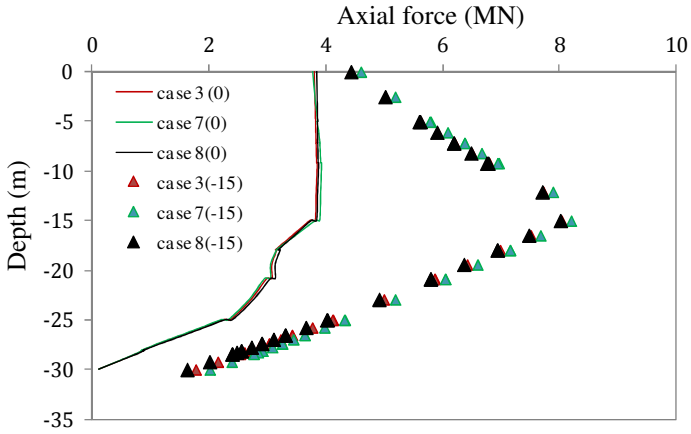

(c) Pile at position 0.3

Figure 5.75 Effect of load patterns on piled raft with 37 piles (C)

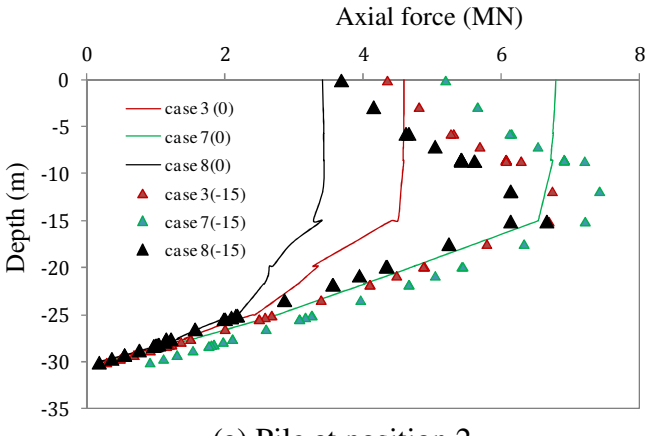

(a) Pile at position 2

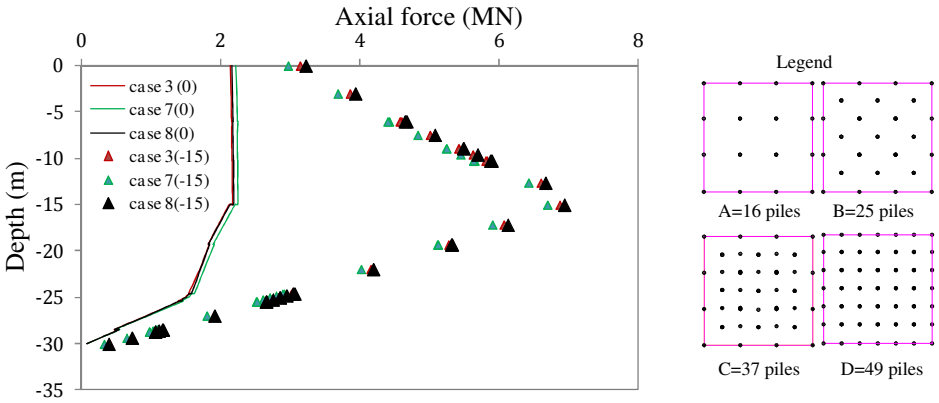

(b) Pile at position 0

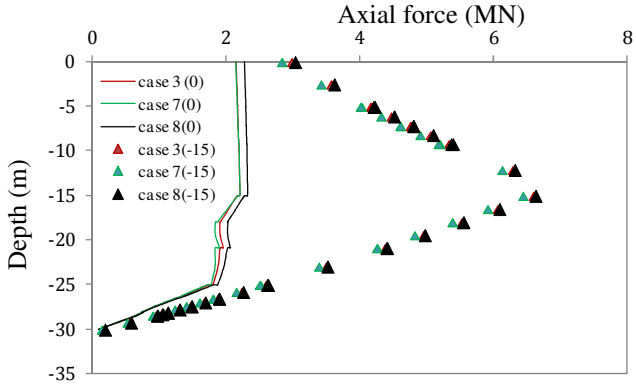

(c) Pile at position 0.3

Figure 5.76 Effect of load patterns on piled raft with 7x7 piles (D)

Load distribution and settlement

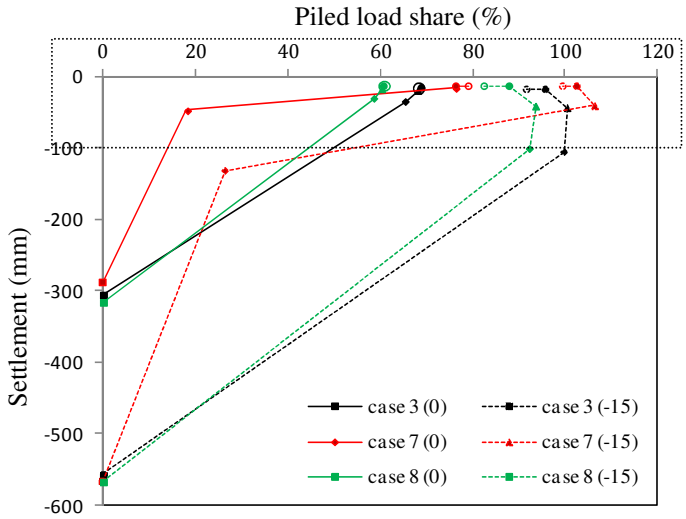

(a) Full view

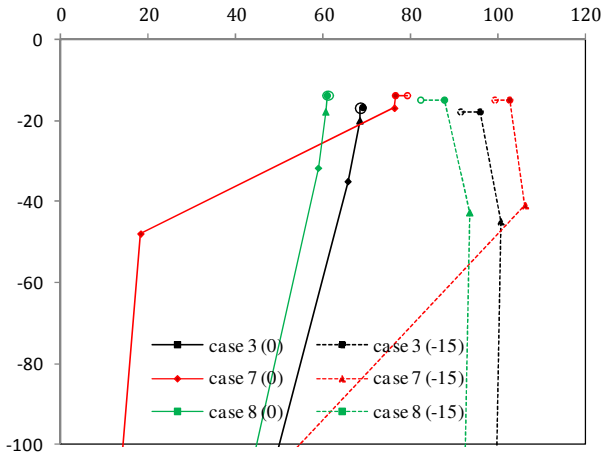

(b) View of small rectangular

Figure 5.77 Comparison of load distribution and settlement for case 3, 7 & 8

Figure 5.77 presents the effect of raft thickness on the relationship between piled load share and settlement in normal and ground subsidence conditions.

Pied load share decreased when raft thickness increased. For example, for PR(D) in ground subsidence, the piled load shares were around 99 %, 90 % and 80 % for raft thicknesses of 0.5 m, 1 m and 1.5 m. The raft carried more load when the thickness of raft increased.

Raft bending moments and shear

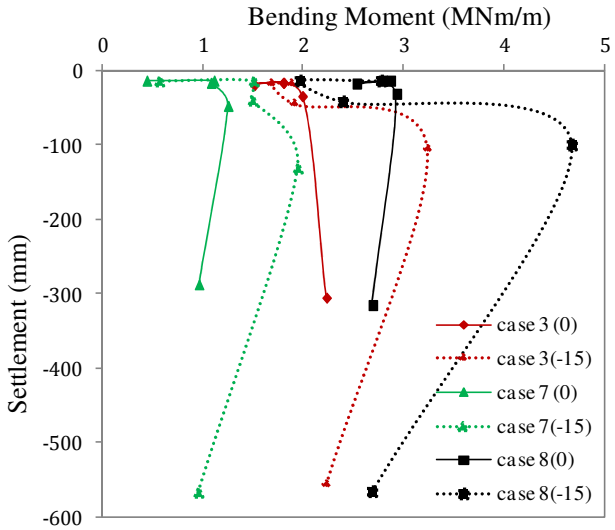

Figure 5.78 Comparison of bending moments and settlements in case 3, 7 & 8

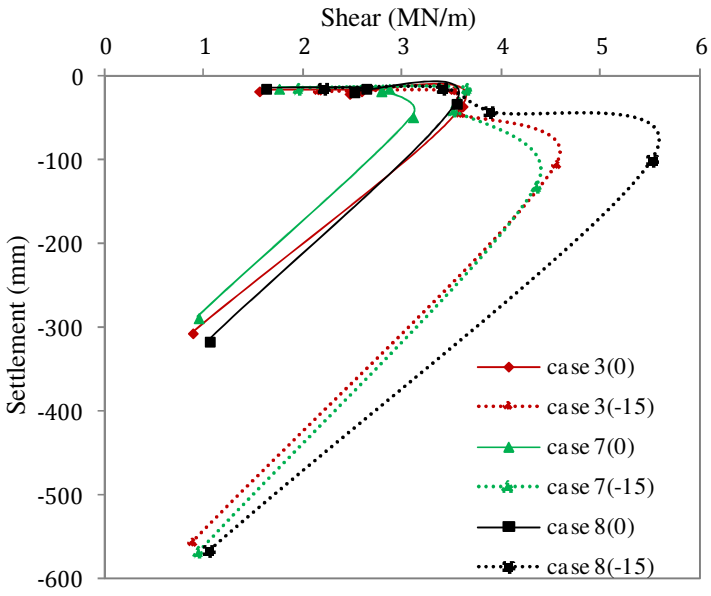

Figure 5.79 Comparison of shear forces and settlements in case 3, 7 & 8

Figure 5.78 and Figure 5.79 show the effect of raft thicknesses on maximum bending moments and shear forces of the raft.

As seen on Figure 5.78, the maximum bending moments of raft increased when the thicknesses of raft increased. For example, for PR(A) in ground subsidence condition, the values of bending moment of raft were around 2 MN.m/m, 3.3 MN.m/m and 4.8 MN.m/m for raft thicknesses of 0.5 m, 1 m and 1.5 m, respectively.

As seen on Figure 5.79, the maximum shear forces of raft increased when the thicknesses of raft increased. For example, for PR(A) in ground subsidence condition, the values of shear forces of raft were around 4.2 MN/m, 4.3 MN/m and 5.6 MN/m for raft thicknesses of 0.5 m, 1 m and 1.5 m, respectively.

5) <u>Effect of levels of load</u>

Case 6: **q = 84 kPa** (5 floors building); case 9: **q = 67.2 kPa** (4 floors building), case 10: **q = 50.4 kPa** (3 floors building).

Load-settlement curves

Figures 5.80 – 5.84 show the effect of levels of load on load – settlement relationship of foundations in normal and ground subsidence conditions. The effectiveness of the piles in reducing settlements of foundations was obvious when the foundation was

applied different levels of load.

For PR(C) (Figure 5.83), when the levels of applied load increased 33 % (case 9) and 66 % (case 10), the settlements of foundations were reduced around 24 % and 41 % in ground subsidence condition, respectively. The reduction of settlement was nearly linear with the increase of applied load.

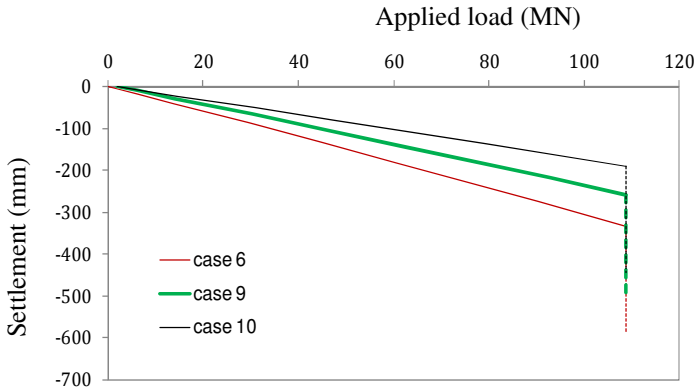

Figure 5.80 Effect of level of loads on raft foundations

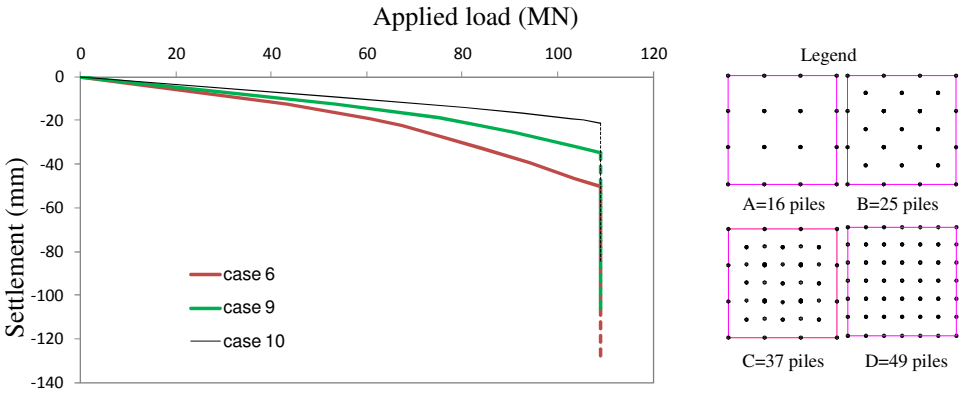

Figure 5.81 Effect of level of loads on piled raft with 4x4 piles (A)

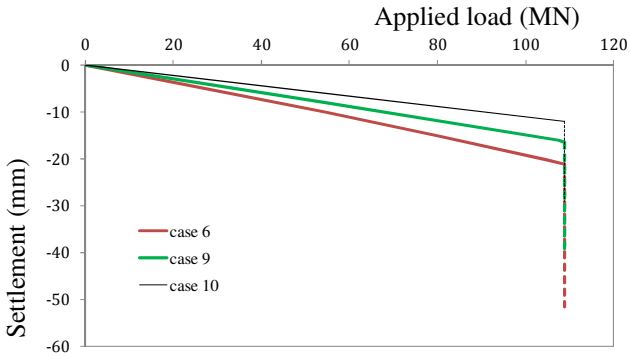

Figure 5.82 Effect of level of loads on piled raft with 25 piles (B)

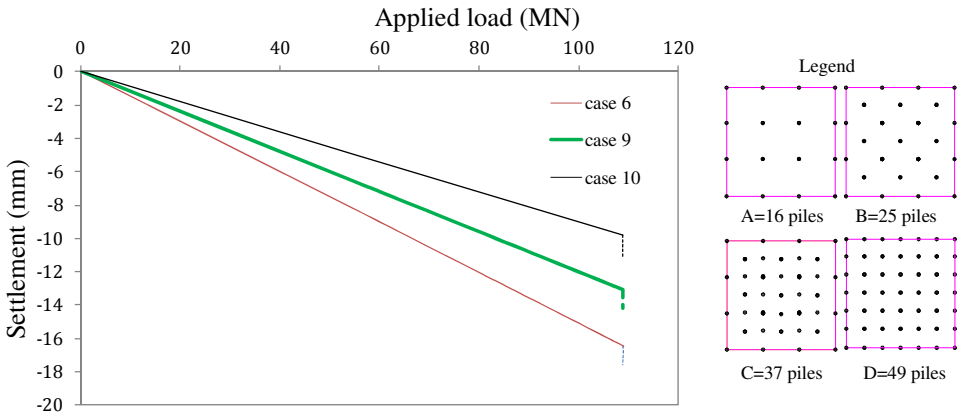

Figure 5.83 Effect of level of loads on piled raft with 37 piles (C)

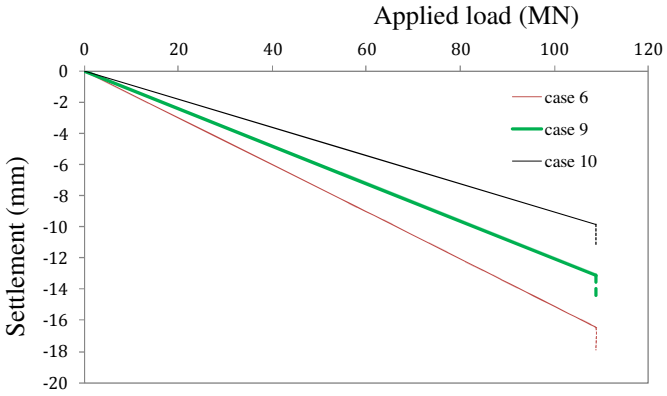

Figure 5.84 Effect of level of loads on piled raft with 7x7 piles (D)

Axial force in piles

Figures 5.85 – 5.88 present the effect of levels of load on the maximum axial forces of piles in piled raft in normal and ground subsidence conditions.

The lines for axial forces in ground subsidence condition were parallel. For example, for point 2 of PR(A) (Figure 5.85a), when applied levels increased 33 % and 66 %, the maximum axial forces increased 14 % and 28 % in ground subsidence, respectively.

For piles at the corner or the edge of raft, the different increments of maximum axial forces with different levels of load were small. For example, for point 0 of PR(D) (Figure 5.88b), the differences of maximum axial force were less than 5 % although levels of load were increased 33 % and 66 %.

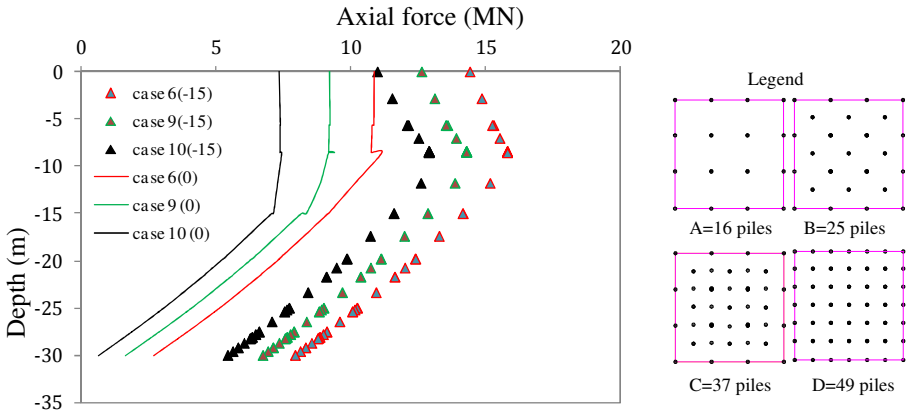

(a) Pile at position 2

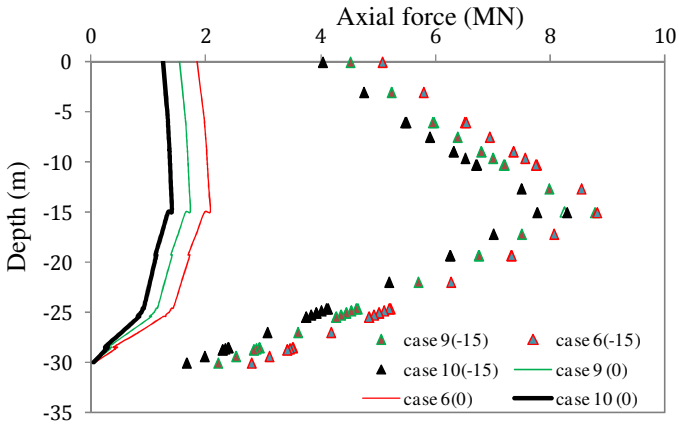

(b) Pile at position 0

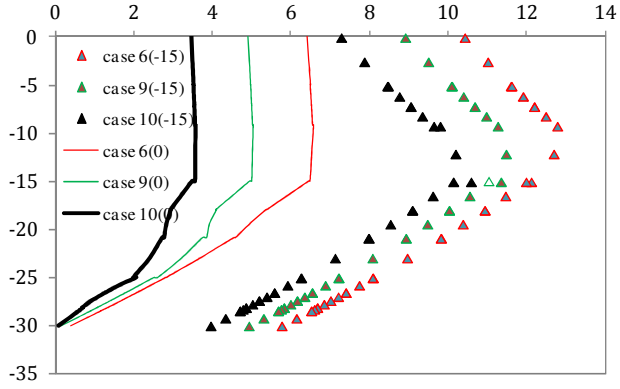

(c) Pile at position 0.3

Figure 5.85 Effect of levels of loads on piled raft with 4x4 piles (A)

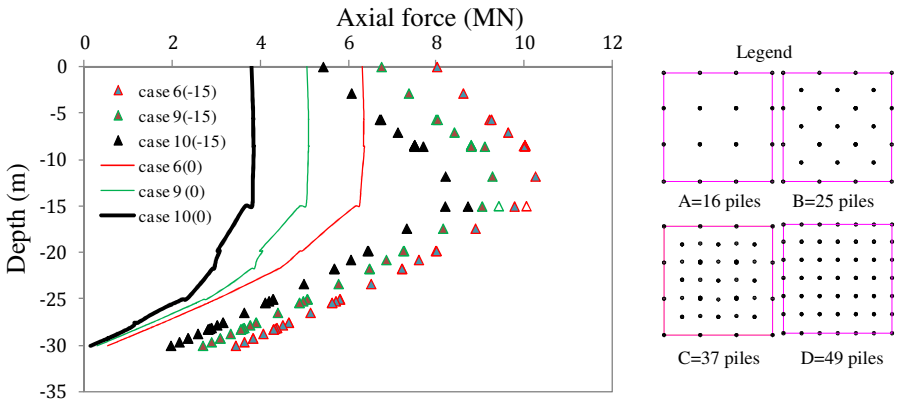

(a) Pile at position 2

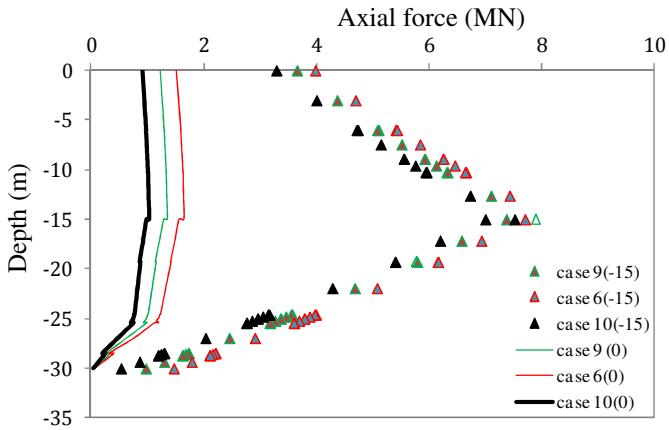

(b) Pile at position 0

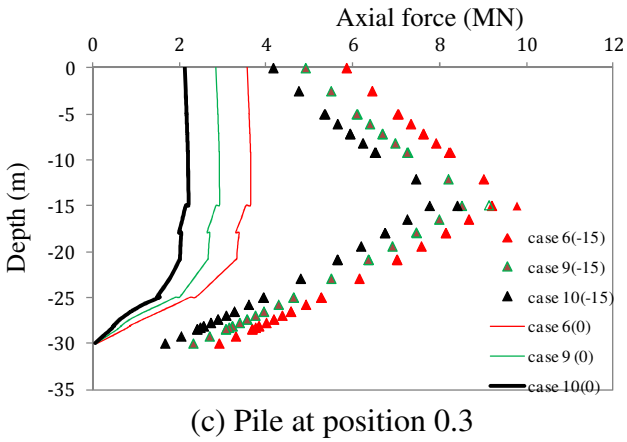

(c) Pile at position 0.3

Figure 5.86 Effect of levels of loads on piled raft with 25 piles (B)

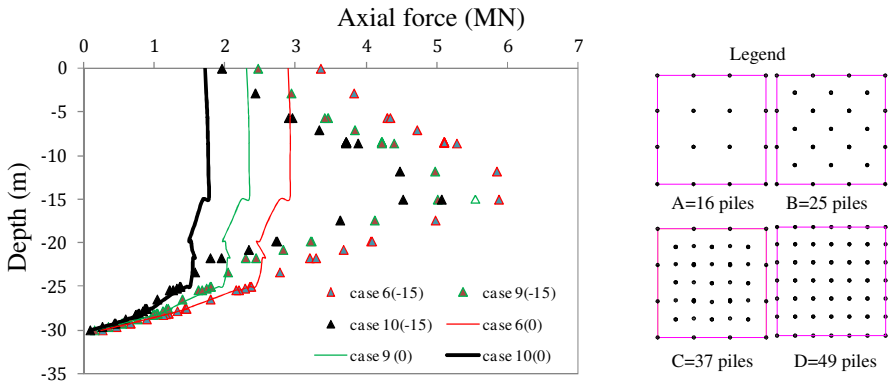

(a) Pile at position 2

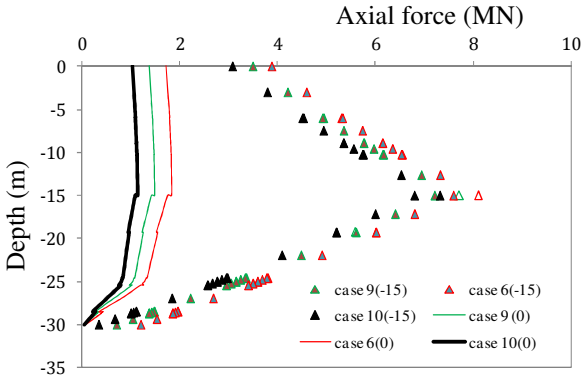

(b) Pile at position 0

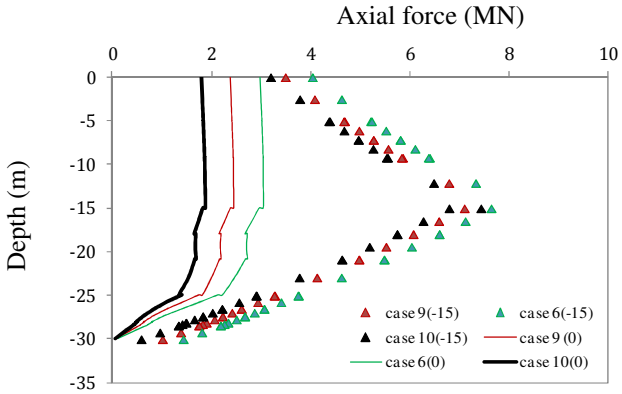

(c) Pile at position 0.3

Figure 5.87 Effect of levels of loads on piled raft with 37 piles (C)

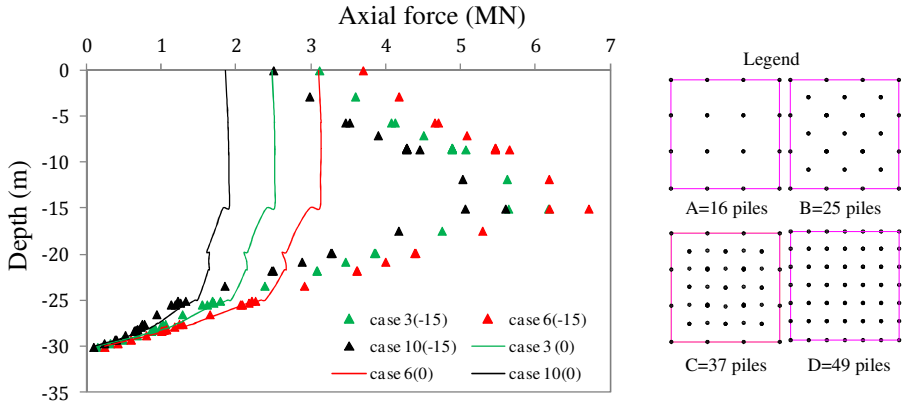

(a) Pile at position 2

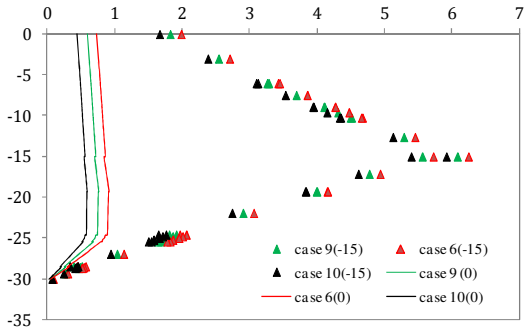

(b) Pile at position 0

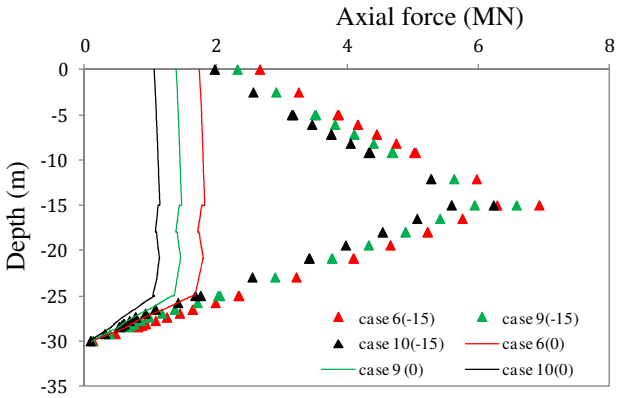

(c) Pile at position 0.3

Figure 5.88 Effect of levels of loads on piled raft with 49 piles (D)

Load distribution and settlement

Figure 5.89 shows the effect of levels of load on the relationship between piled load share and settlement of foundation in normal and ground subsidence conditions.

When levels of load increased 33 % and 66 %, the piled load share increased 20 % and 33 %, respectively, for PR(A) in ground subsidence condition. When numbers of piles increased (PR(B), PR(C) and PR(D)), the piled load share vary

complicatedly in ground subsidence condition. For example, for PR(D) in ground subsidence, the piled load share increased 17 % and 43 % when level of load increased 33 % and 66 %.

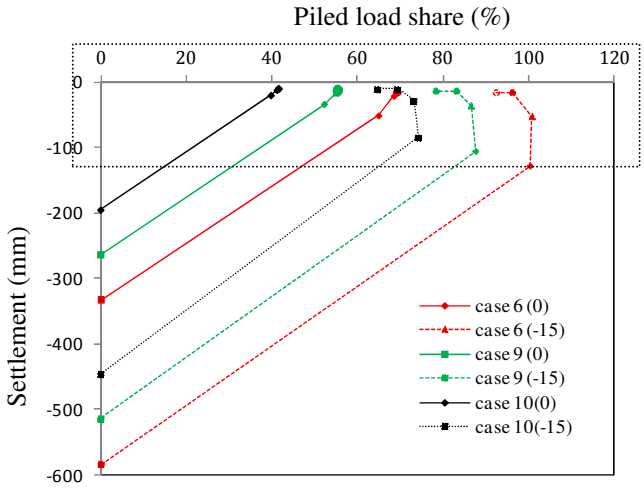

(a) Full view

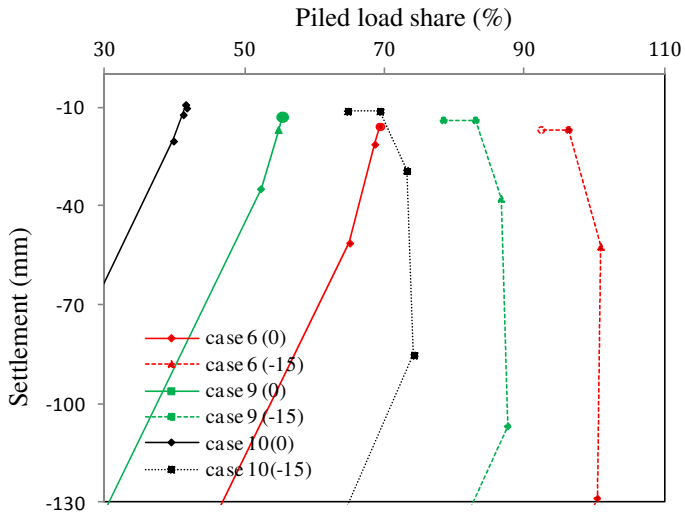

(b) View of small rectangular

Figure 5.89 Comparison of load distribution and settlement for case 6, 9 & 10

Raft bending moments and shear

Figure 5.90 and Figure 5.91 present the effect of levels of load on the maximum bending moment and shear force of raft in normal and ground subsidence conditions.

As seen in Figure 5.90, when applied load increased 33 % and 66 %, the maximum bending moment increased 15 % and 33 % for PR(A) in ground subsidence condition. For PR(B), PR(C) and PR(D) increased in the same manner with PR(A).

For maximum shear force in raft, when applied load increased 33 % and 66 %, the maximum shear force increased 16 % and 30 % for PR(A) in ground subsidence condition. For PR(B), PR(C) and PR(D) increased in the same manner with PR(A).

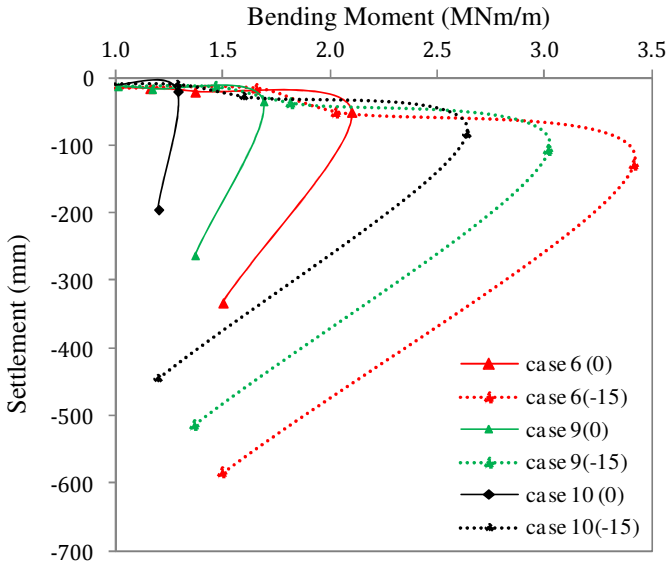

Figure 5.90 Comparison of bending moments and settlements in case 6, 9 & 10

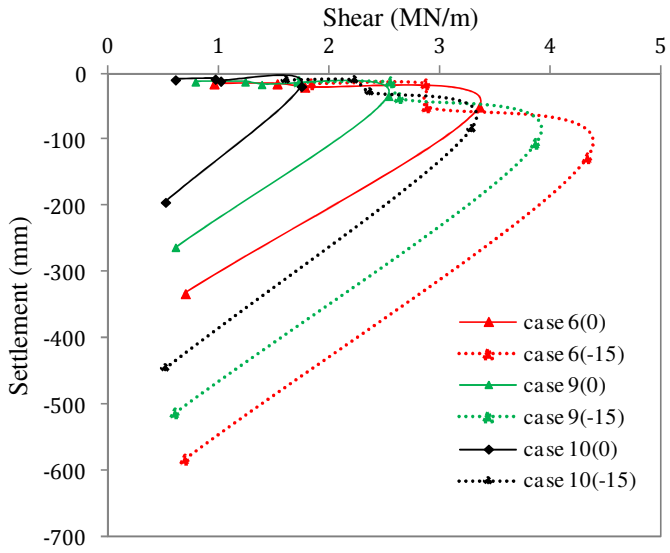

Figure 5.91 Comparison of shear forces and settlements in case 6, 9 & 10

6) <u>Effect of piled spacing</u>:

Case 11: ***s = 6 m****, case 12:* ***s = 3 m****, case 13:* ***s = 2 m.*** *Raft without beams, q = 84 kPa, t = 2 m.*

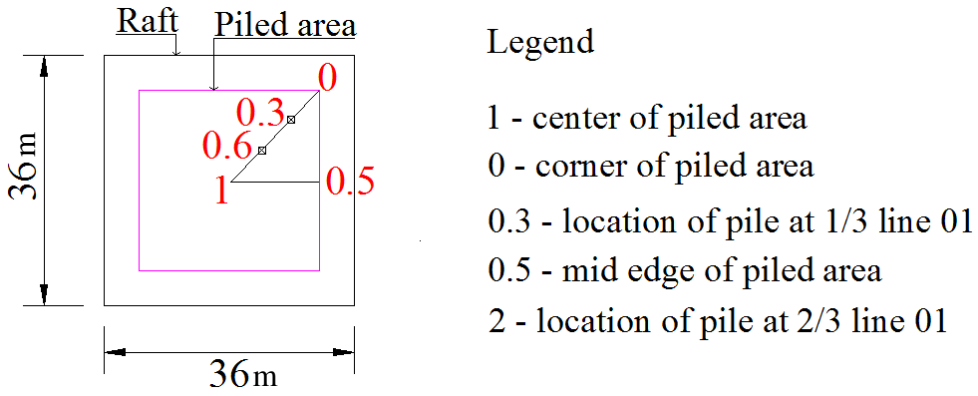

Figure 5.92 Positions of piles were considered in case 11, 12 & 13

Load-settlement curves

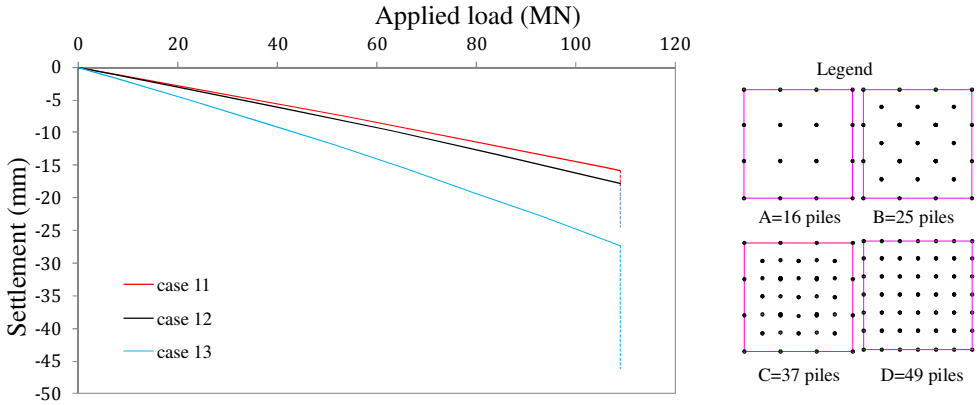

Figure 5.93 Effect of piled spacings on piled raft with 7x7 piles (D)

Figure 5.93 shows the effect piled spacing on load-settlement curves of piled raft in normal and ground subsidence conditions.

As seen on the Figure 5.93, for these models, when piled spacings increased (s = 2 m, 3 m and 6 m), the settlement of foundation decreased in both normal and ground subsidence conditions. When piled spacing increased 50 % (s = 3 m) and 200 % (s = 6 m), the settlement of foundation reduced 47 %, 63 %, respectively.

When piled spacing larger than around 3d, the effectiveness of piles in reducing settlement of raft was nearly same in normal condition but different in ground subsidence condition. For example, for piled spacings of 2d, 3d and 6d, the settlements of piled raft were around 27 mm, 17 mm and 15 mm, respecitively, in

normal condition while the settlements of piled raft were around 46 mm, 24 mm and 17 mm, respectively, in ground subsidence condition.

Axial force in piles

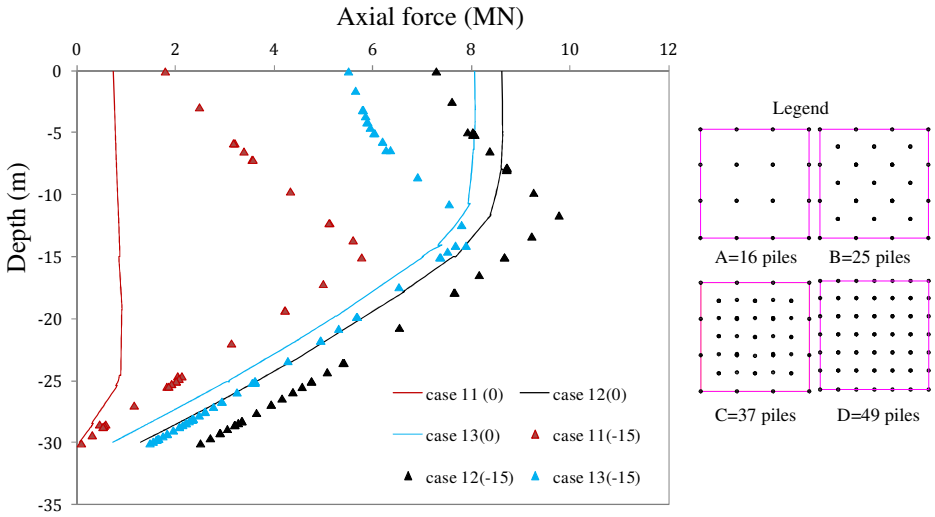

(a) Pile at position 0

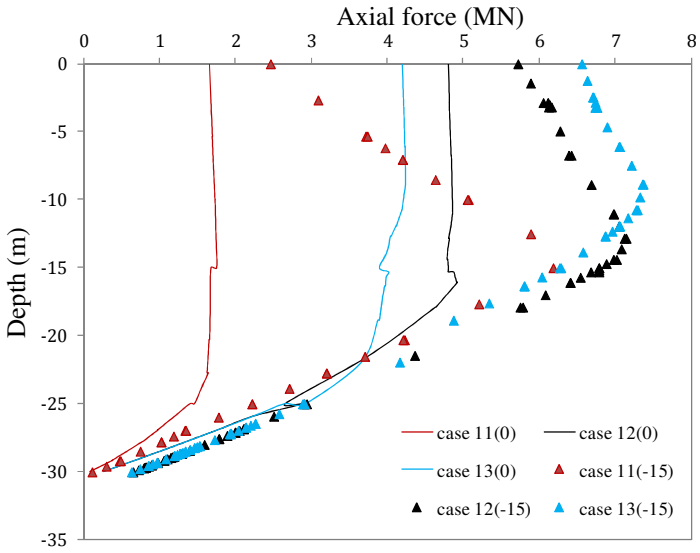

(b) Pile at position 0.5

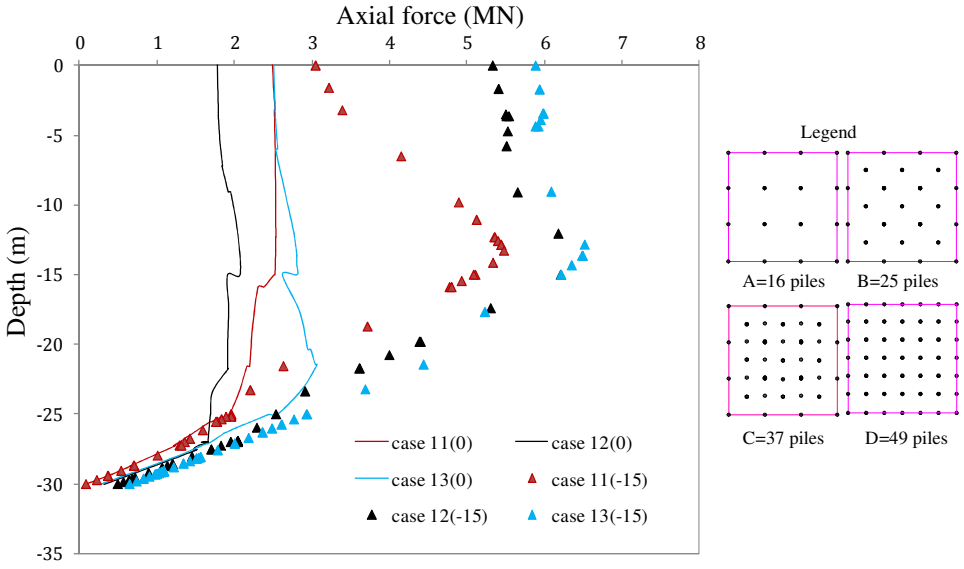

(c) Pile at position 0.3

Figure 5.94 Effect of piled spacings on piled raft with 49 piles (D)

Figure 5.94 shows the effect of piled spacing on maximum axial forces of piles in piled raft in normal and ground subsidence conditions.

For pile at point 0 (corner of raft), in ground subsidence condition, the maximum axial force increased when piled spacing increased. For example, in ground subsidence, the increments of maximum axial forces were 1.3 %, 18 % and around 566 % (from 0.9 MN to around 6 MN) for piled spacings of 2d, 3d and 6d, respectively.

Interactions between piles may be a reason for decrease of negative skin friction on piles resulting decrease of maximum axial forces for small spacing (2d). However, for larger piled spacing (3d or 6d), the interactions between piles decreased and, therefore, increased effect of negative skin friction on piles which made the maximum axial forces increased.

Load distribution and settlement

Figure 5.95 shows the effect of piled spacing on the relationship between piled load share and settlement of foundation in normal and ground subsidence conditions. Line with square points was for piled rafts in normal condition and line with rectangular points was for piled rafts in ground subsidence condition.

In normal condition, piled load shares increased when piled spacing increased.

However, in ground subsidence, piled load shares decreased with the increase of piled spacings. For example, in normal condition, when piled spacings increased from 2d to 3d and 6d, piled load shares increased from 77 % to 83 % and 88 %, respectively. However, in ground subsidence condition, the values of piled shares were 99 %, 97 % and 96 % for piled spacings of 2d, 3d and 6d, respectively. The increments of piled load shares were 22 %, 14 % and 8 % for piled spacings of 2d, 3d and 6d.

Piled load shares decreased with the increase of piled spacing may be explained by considering the interaction between piles in piled raft. As discussed in previous part, interaction between piled reduced the effect of negative skin friction on the piles.

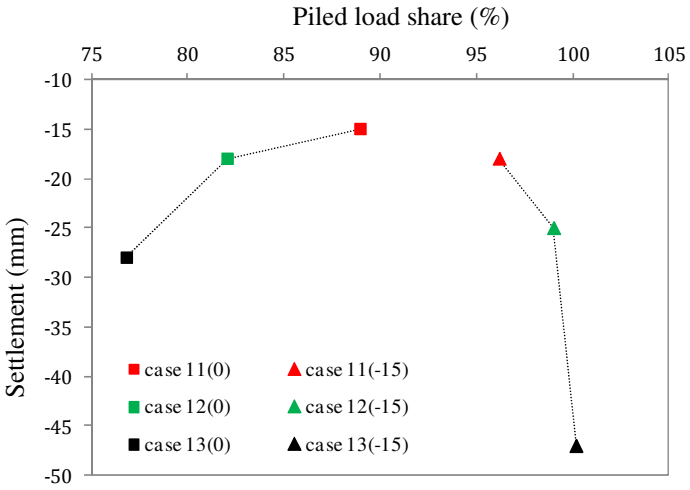

Figure 5.95 Comparison of load distribution and settlement for case 11, 12 & 13

Raft bending moments and shear

Figures 5.96 and Figure 5.97 present the effect of piled spacings on the maximum bending moment and shear force in the raft in normal and ground subsidence conditions. Line with square points was for piled rafts in normal condition and line with rectangular points was for piled rafts in ground subsidence condition.

In normal condition and ground subsidence condition, maximum bending moment increased when piled spacing increased (Figure 5.96). For example, in normal condition, values of bending moments were 1 MN.m/m, 1.35 MN.m/m and 2.05 MN.m/m for piled spacings of 2d, 3d and 6d, respectively. In ground subsidence condition, the values of bending moments increased to 1.5 MN.m/m, 1.7 MN.m/m and

1.95 MN.m/m for piled spacings of 2d, 3d and 6d, respectively. For piled raft with piled spacings of 2d and 3d, the bending moment increased 50 % and 26 % in ground subsidence condition. However, for piled raft with piled spacing of 6d, the bending moment decreased around 5 % in ground subsidence condition.

As seen in Figure 5.97, the maximum shear force in raft decreased when piled spacing increased for both normal and ground subsidence conditions. Compared to normal condition, shear forces increased around 14 %, 8 % and 6 % for piled raft with piled spacings of 2d, 3d and 6d, respectively, in ground subsidence condition. Larger area distributed by the piles which made load more uniform distribution on the raft and, therefore, it may be make the decrease of shear forces in the raft.

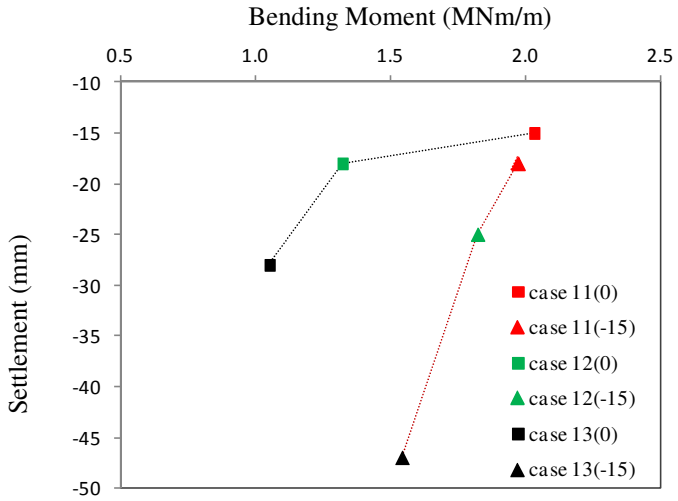

Figure 5.96 Comparison of bending moments and settlements in case 11, 12 & 13

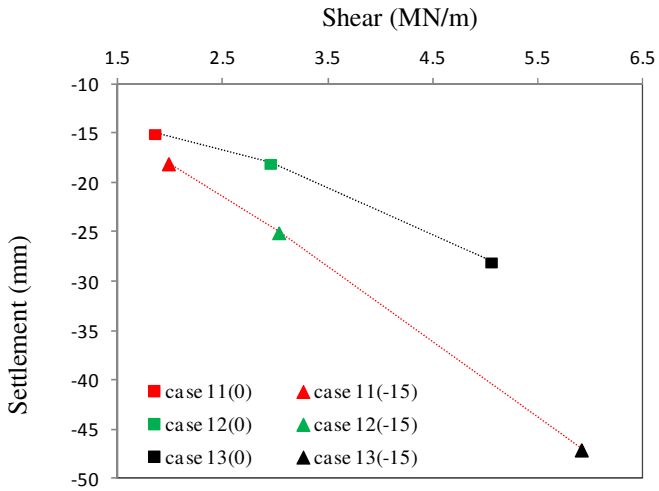

Figure 5.97 Comparison of shear forces and settlements in case 11, 12 & 13

5.5 Conclusions

From the results of parameter study of model piled raft and piled raft in Bangkok soil, some discussions were given as below.

For parameter study of model piled raft (size of foundation was taken from centrifugal models)

When piled spacing increases, the maximum axial force of the piles increase. For friction piled raft, maximum axial forces increased 45 N and 60 N for piled spacings of 2d and 4d, respectively. For end-bearing piled raft, when piled spacings increased from 2d to 4d, the maximum axial forces increased 65 N and 125 N, respectively.

When Young's modulus of the soil increases (E2 = 8.9 E1), the maximum axial force decreases because of increase of load carried by the raft. For friction piled raft, maximum axial forces were 185 N and 160 N for E1 and E2 in normal condition while the maximum axial forces increased 50 N for both E1 and E2 in ground subsidence condition. For end-bearing piled raft, maximum axial forces were 145 N and 130 N for E1 and E2 in normal condition while maximum axial forces increased 65 N and 55 N for E1 and E2, respectively in ground subsidence condition.

When ground water levels decrease from +0.0 m to -7.725 m, maximum axial forces were increased 70 N and 145 N for friction and end-bearing piled rafts, respectively. However, the axial forces were constant when ground water levels decreased from -7.725 m to -10 m.

For all cases of parameter study, negative skin friction of end-bearing piled raft is larger than that of friction piled raft in ground water pumping condition.

For parameter study of piled raft in Bangkok soil

For piled rafts in Bangkok soil, considering the ground subsidence condition when ground water levels decreases from +0.0 m to -7.5 m, -15 m and -25 m.

Numbers of piles and piled configuration: when more piles were added to the foundation such as in PR(A: 16 piles), PR(B: 25 piles), PR(C: 37 piles) and PR(D: 49 piles, it shared a major part of applied load and, therefore, reduced large settlement of

foundations, reduced bending moment and shear force in the raft in ground subsidence condition.

Young's modulus of soil: when Young's modulus of soil increases 2 times ($E_4 = 2E_3$) or 3 times ($E_5 = 3E_3$), the settlements of raft foundation decreased around 50 % or 70 %, the piled load share decreased, the maximum axial forces in piles increased largely with depth, and the bending moment of decreased while shear force of raft increased in ground subsidence condition.

Pattern of loads: more settlement was found for case of uniform load, compared to combined load. More load concentrated around the centre of raft while lesser load at the corner of raft and the same load at the edge of raft for uniform applied load. The same value of piled load share (but larger settlement) was found for PR(A=16piles). Larger values of maximum bending moment occurred for uniform load for both normal and ground subsidence conditions. Maximum shear force occurred for uniform load for both normal and ground subsidence conditions.

Raft thickness: for piles around centre of raft, larger axial force occurred on lesser thickness of raft while lesser values of axial forces were found on lesser thickness of raft for piles at the corner and edge of raft in ground subsidence condition. When raft thickness increased, pied load share decreased, the maximum bending moments of raft increased, the maximum shear forces of raft increased.

Levels of loads: the effectiveness of the piles in reducing settlements of foundations was obvious when the foundation was applied different levels of load. The reduction of settlement was nearly linear with the increase of applied load. When levels of load increased 33 % and 66 %, the piled load share increased 20 % and 33 %, respectively, for PR(A), the maximum bending moment increased 15 % and 33 % for PR(A), the maximum shear force increased 16 % and 30 % for PR(A) in ground subsidence condition. For PR(B), PR(C) and PR(D) increased in the same manner with PR(A).

Piled spacing: for these models, when piled spacings increased (s = 2 m, 3 m and 6 m), the settlement of foundation decreased in both normal and ground subsidence conditions. When piled spacing larger than around 3d, the effectiveness of piles in reducing settlement of raft was nearly same in normal condition but different

in ground subsidence condition. In normal condition, piled load shares increased when piled spacing increased. However, in ground subsidence, piled load shares decreased with the increase of piled spacings. In both normal condition and ground subsidence condition, maximum bending moment increased when piled spacing increased, the maximum shear force in raft decreased when piled spacing increased.

In summary, the analyses show that the load – settlement curves, load distribution between group of piles and raft, axial force of the pile, average and differential settlements, the maximum bending moment and maximum shear force are significantly affected by above parameters.

CHAPTER VI

CONCLUSIONS AND RECOMMENDATIONS

6.1 Conclusions

The primary objective of this thesis was to investigate the effect of ground subsidence on load distributions, average and differential settlements, and raft bending moment and shear of piled raft foundation by using centrifugal test and FE analysis.

For centrifugal test, six cases of model foundations were conducted at the centrifugal accelerate of 50g order to evaluate the effects of ground subsidence on the behavior of foundations. Group 1 (soil condition 1) with case 1: raft alone, case 2: piled raft (s = 2d), case 3: piled raft (s = 4d) and group 2 (soil condition 2) with case 4: raft alone, case 5: friction piled raft (s = 4d) and case 6: end-bearing piled raft (s = 4d) were studied. Three layers of soils including bottom dense sand, middle soft clay and top medium sand were considered in all cases. The results of centrifugal test show that, settlement of foundations increased nearly linear with ground subsidence. In ground subsidence condition, when piled spacing increased (2d to 4d), the settlement of foundation increased and axial load of the piles increased. After pumping ground water for about 30 min, the total axial force of pile top became equal to applied load due to larger ground settlement than raft settlement. Negative skin friction of end-bearing piled raft was very larger than that of friction piled raft in ground subsidence condition.

For FE analysis, parameter study for model piled rafts and three cases of piled raft in Bangkok soil were performed in this study. FE analysis was done by Plaxis 3D Version 2011. The factors including piled spacing, Young's modulus of soil and ground water levels were considered in parameter study for model piled rafts and the factors including number of piles, Young's modulus of soil, pattern of loads, raft thickness and piled spacing were considered in parameter study for three cases of piled rafts on Bangkok soil (case 1, case 3 and case 3 with levels of raft at -15 m, -7.5 m and + 0.0 m, respectively). Three layers of soils including bottom sand, middle clay and top sand were considered for model piled rafts while all 5 layers in Bangkok soil were simulated in the analyses. The calculation was done by drained, plastic analysis

with effective parameters. The results of parameter study of model piled raft and piled raft in Bangkok soil show that

For model piled rafts, size of foundation was taken from centrifugal model tests, when piled spacing increases, the maximum axial force of the piles increase. For friction piled raft, maximum axial forces increased 45 N and 60 N for piled spacings of 2d and 4d, respectively. For end-bearing piled raft, when piled spacings increased from 2d to 4d, the maximum axial forces increased 65 N and 125 N, respectively. When Young's modulus of the soil increases (E2 = 8.9 E1), the maximum axial force decreases because of increase of load carried by the raft. For friction piled raft, maximum axial forces were 185 N and 160 N for E1 and E2 in normal condition while the maximum axial forces increased 50 N for both E1 and E2 in ground subsidence condition. For end-bearing piled raft, maximum axial forces were 145 N and 130 N for E1 and E2 in normal condition while maximum axial forces increased 65 N and 55 N for E1 and E2, respectively in ground subsidence condition. When ground water levels decrease from +0.0 m to -7.725 m, maximum axial forces were increased 70 N and 145 N for friction and end-bearing piled rafts, respectively. However, the axial forces were constant when ground water levels decreased from -7.725 m to -10 m. For all cases of model piled rafts, negative skin friction of end-bearing piled raft is larger than that of friction piled raft in ground water pumping condition.

For piled rafts in Bangkok soil, when more piles were added to the foundation, it shared a major part of applied load and, therefore, reduced large settlement of foundations, reduced bending moment and shear force in the raft in ground subsidence condition. When Young's modulus of soil increases 2 times ($E_4 = 2E_3$) or 3 times ($E_5 = 3E_3$), the settlements of raft foundation decreased around 50 % or 70 %, the piled load share decreased, the maximum axial forces in piles increased largely with depth, and the bending moment of decreased while shear force of raft increased in ground subsidence condition. More settlement was found for case of uniform load, compared to combined load. More load concentrated around the centre of raft while lesser load at the corner of raft and the same load at the edge of raft for uniform applied load. The same value of piled load share (but larger settlement) was found for PR(A=16piles).

Larger values of maximum bending moment occurred for uniform load for both normal and ground subsidence conditions. Maximum shear force occurred for uniform load for both normal and ground subsidence conditions. For piles around centre of raft, larger axial force occurred on lesser thickness of raft while lesser values of axial forces were found on lesser thickness of raft for piles at the corner and edge of raft in ground subsidence condition. When raft thickness increased, pied load share decreased, the maximum bending moments of raft increased, the maximum shear forces of raft increased. The effectiveness of the piles in reducing settlements of foundations was obvious when the foundation was applied different levels of load. The reduction of settlement was nearly linear with the increase of applied load. When levels of load increased 33 % and 66 %, the piled load share increased 20 % and 33 %, respectively, for PR(A), the maximum bending moment increased 15 % and 33 % for PR(A), the maximum shear force increased 16 % and 30 % for PR(A) in ground subsidence condition. For PR(B), PR(C) and PR(D) increased in the same manner with PR(A). For these models, when piled spacings increased (s = 2 m, 3 m and 6 m), the settlement of foundation decreased in both normal and ground subsidence conditions. When piled spacing larger than around 3d, the effectiveness of piles in reducing settlement of raft was nearly same in normal condition but different in ground subsidence condition. In normal condition, piled load shares increased when piled spacing increased. However, in ground subsidence, piled load shares decreased with the increase of piled spacings. In both normal condition and ground subsidence condition, maximum bending moment increased when piled spacing increased, the maximum shear force in raft decreased when piled spacing increased.

In summary, the results from centrifugal tests and FE analyses show that, in ground subsidence condition, load – settlement curves, load distributions, axial force of piles, average and differential settlements, raft moment and shear are significantly affected by factors considered in parameter study.

6.2 Recommendations

More research works including experimental tests and FE analysis for piled raft in ground subsidence condition are recommended for further researches. The research

should be focused on 4 types of interaction between raft, piles and soil which are of major importance in the behavior of piled raft. The interaction between piles plays an important role among four types of interaction presented in piled raft.

REFERENCES

Brinkgreve, R. B. J. et al. (2007). **Plaxis user's manual**, Version 2.0. Rotterdam: Balkema.

Brown, P.T. and Wiesner, T.J. (1975). The behaviour of uniformly loaded piled strip footings. **Soils and Foundations** 15(4): 13-21.

Burland, J.B. (1995). Piles as settlement reducers. Keynote Address, **18th Italian Congress on Soil Mechanics**. Pavia, Italy.

Butterfield, R., and Banerjee, P. K. (1971). The elastic analysis of compressible piles and pile groups. **Geotechnique** 21(1): 43-60.

Chun-yi Cui, Mao-tian Luan, Mu-guo Li, Ying-hua Zhao (2009). Time-dependent behavior of piled-raft on soil foundation with reference to creep and consolidation. **Electronic Journal of Geotechnical Engineering** 14, Bund. A, Ppr0908.

Conte, G., Madolini, A., Randolph, M. F. (2003). Centrifuge modeling to investigate the performance of pile rafts. **Proceedings of 4th international geotechnical seminar on deep foundation on bored and auger piles**, Ghent, Millpres: 359-366.

Cooke, R. W. (1986). Piled raft foundations on stiff clays: a contribution to design philosophy. **Geotechnique** 36 (2): 169–203.

Danno K. and Kimura M. (2009). Evaluation of long-term displacements of pile foundation using FEM and centrifuge model test. **Soil and Foundations** 49 (6): 941 – 958.

Das, B. M. (2007). **Principles of foundation engineering**. 6th Edition. Toronto: Thomson Learning.

Fellenius, B. H (1998). Recent advances in the design of piles for axial loads, dragloads, downdrag, and settlement. **Urban Geotechnology and Rehabilitation, Seminar sponsored by ASCE Metropolitan Group**, New York: 22–23.

Fellenius, B. H. (2006). Results from long-term measurements in piles of drag loads and downdrag. **Canadian Geotechnical Journal** 43 (4): 409–430.

Fleming, W. G. K., et al. (1992). **Piling Engineering**. 2nd Ed. Blackie A & P, John Wiley & Sons, Inc.

Franke E., EL-Mossallamy Y., Wittmann P. (2000). Calculation methods for raft foundations in Germany. **Design applications of raft foundations**. Hemsley J. A., editor. London: Thomas Telford.

Gobinath, B., Juneja, A. and Agarwal, A. (2010). Numerical modelling of piled raft foundation in soft clays. **Indian Geotechnical Conference**. Bombay, India. Dec. 16-18: 985-988.

Goudreault and Fellenius, B. H., P. A. (1995). Design of piles and pile groups considering capacity, settlement and negative skin friction. **Background and User Manual to Unipile**, Users Manual, Unisoft Ltd.

Gupta, S. C. (1997). **Raft foundation: design and analysis with a practical approach**. New age international (P) limited, Publishers. India.

Hain, S. J. and Lee, I.K. (1978). The analysis of flexible raft-pile systems. **Geotechnique** 28 (1): 65-83.

Hemsley, J. A. (2000). Developments in raft analysis and design. **Design applications of raft foundations**. Hemsley J. A., editor, London: Thomas Telford.

Horikoshi, K. & Randolph, M. F. (1996). Centrifuge modelling of piled raft foundations on clay. **Geotechnique** 46 (4): 741-752.

Horikoshi, K. & Randolph, M. F. (1997). On the definition of raft-soil stiffness ratio for rectangular rafts. **Geotechnique** 47 (5): 1055-1061.

Horikoshi, K. & Randolph, M. F. (1998). A contribution to the optimum design of piled rafts. **Geotechnique** 48 (3): 301-317.

Horikoshi, K. & Randolph, M. F. (1999). Estimation of overall settlement of piled rafts. **Soils and Foundations** 39 (2): 59-68.

JinHyung Lee, Youngho Kim, Sangseom Jeong (2010). Three-dimensional analysis of bearing behavior of piled raft on soft clay. **Computers and Geotechnics** 37: 103–114.

Kang G., Tobita T., Tomisaka K. and Iai S. (2009). Centrifuge modeling for uplift of buried structures by liquefaction: a new measure for uplift. **Annuals of Disas. Prev. Res. Inst., Kyoto Univ.,** No. 52 B: 395–402.

Katzenbach, R., Arslan, U., and Moormann, C. (2000). Piled raft foundations projects in Germany. **Design applications of raft foundations**. Hemsley J. A., editor. London: Thomas Telford.

Katzenbach R., Schmitt A., Turek J. (2005). Assessing settlement of high-rise structures by 3d simulations. **Computer-Aided Civil and Infrastructure Engineering** 20: 221–229.

Le V. T. and Ho T. M. D. (2008). Measuring ground subsidence in Ho Chi Minh city using differential inSAR techniques. **Science & Technology Development** 11 (12): 121 – 130.

Lee C. J, Chen H. T. & Wang W. H. (1998). Negative skin friction on a pile due to excessive groundwater withdrawal. **Centrifuge 98**, Kimura al. el., Editor. Rotterdam: Balkema, Vol.1: 513–518.

Lisa J. Novak, Lymon C. Reese, Honorary Member, ASCE, and Shin-Tower Wang (2005). Analysis of pile-raft foundations with 3d finite-element method. **Proceedings of the 2005 structures congress and the 2005 forensic engineering symposium (ASCE)** 171 (93): 1-12.

Leung, C. F., Liao, B. K., Chow, Y. K., Shen, R. F. & Keg, Y. C. (2004). Behavior of pile groups subject to negative skin friction and axial load. **Soil and Foundations** 44(6): 17-26.

Lunne T., Robertson P. K. and Powell J. J. M. (1997). **Cone penetration testing in geotechnical practice**. New York: Blackie Academic/Routledge Publishing.

Mendonca, A. V., and Paiva, J. B. (2003). An elastostatic FEM/BEM analysis of vertically loaded raft and piled raft foundation. **Engineering Analysis with Boundary Elements** 27: 919 - 933.

Ningombam Thoiba Singh, Baleshwar Singh (2008). Interaction analysis for piled rafts in cohesive soils. **The 12th International Conference of IACMAG**, 3289-3296.

Phienwej N., Thepparak S., Giao P. H. (2004). Prediction of differential settlement of buildings induced by land subsidence from deep well pumping. **15th Southeast Asian Geotechnical Society Conference**, 165 – 170, Bangkok, Thailand.

Phongpat Kitpayuck (2009). An analysis of behavior of piled-raft foundation in Bangkok subsoils. **Master thesis**, AIT, Thailand.

Poulos, H. G. and Davis, E. H. (1974). **Elastic solutions for soil and rock mechanics**. New York: John Wiley.

Poulos, H. G. and Davis, E. H. (1980). **Pile foundation analysis and design**. New York: John Wiley.

Poulos, H. G. (1991). Analysis of piled strip foundations. **Computer Methods and Advances in Geomechanics**, 183-191, Rotterdam.

Poulos, H. G. (2000). Practical design procedures for piled raft foundations. **Design applications of raft foundations**. Hemsley J. A., editor. London: Thomas Telford.

Poulos, H. G. (2001a). Methods of analysis of piled raft foundations. **A report prepared on behalf of technical committee TC18 on piled foundations**. ISSMGE.

Poulos, H. G. (2001b). Piled raft foundations: Design and applications. **Geotechnique** 51 (2): 95–113.

Poulos, H. G. (2002). Simplified design procedure for piled raft foundations. **Geotechnical Special Publication (ASCE)** 116: 441- 458.

Poulos, H. G. (2005). Piled raft and compensated piled raft foundations for soft soil sites. Advances on designing and testing deep foundations. **Geotech Spec. Publ. (ASCE)** 129: 214–35.

Poulos, H. G. (2008). A practical design approach for piles with negative friction. Proceedings of the Institution of Civil Engineers. **Geotechnical Engineering** 161: 19-27.

Prakoso, W.A. and Kulhawy, F.H. (2001). Contribution to piled raft foundation design. **Jnl. Geot. and Geoenv. Eng., ASCE** 127(1): 17-24.

Rabiei, M. (2009). Parametric study for piled raft foundation. **Electronic Journal of Geotechnical Engineering** 14: Bund. A, Ppr0906.

Randolph, M. F. and Wroth, C. P. (1978). Analysis of deformation of vertically loaded piles. **J. Geotech. Engng Div., (ASCE)** 104 (12):1465-1488.

Randolph, M. F. and Wroth, C. P. (1979). An analysis of the vertical deformation of pile groups. **Geotechnique** 29(4): 423–439.

Randolph, M. F. (1994). Design methods for pile groups and piled rafts. **State of the Art Rep., Proc., 13th ICSMFE** 5: 61–82.

Reul O., Randolph M. F. (2003). Piled rafts in overconsolidated clay-comparison of in situ measurements and numerical analyses. **Geotechnique** 53(3): 301–315.

Reul O. (2004). Numerical study of the bearing behavior of piled rafts. **Int J. Geomech (ASCE)** 4(2): 59–68.

Reul O., Randolph M. F. (2004). Design strategies for piled rafts subjected to nonuniform vertical loading. **J. Geotech Geoenviron Eng. (ASCE)** 130(1): 1–13.

Russo, G. (1998). Numerical analysis of piled rafts. **International Journal for Numerical and Analytical Methods in Geomechanics** 22: 477- 493.

Sales M. M., Small J. C., Poulos H. G. (2010). Compensated piled rafts in clayey soils: behavior, measurements, and predictions. **Can. Geotech. J**. 47: 327 – 345.

Sanctis, L. de, Mandolini, A. (2006). Bearing capacity of piled rafts on soft clay soils. J. **Geotechnical and Geoenvironmental Engineering** 132 (12): 1600–1610.

Seo, Y., Choi, K. and Jeong, S. (2003). Design charts of piled raft foundations on soft clay. **Proceedings of 13th International Offshore and Polar Engineering Conference**, 753-755. Honolulu, Hawaii, USA, May 25–30.

Sinha, J. (1997). Piled raft foundations subjected to swelling and shrinking soils. **PhD Thesis**, Univ. of Sydney, Australia.

Small, J. C., Liu, H. L. S. (2008). Time-settlement behavior of piled raft foundations using infinite elements. **Computers and Geotechnics** 35: 187-195.

Small, J. C., and Zhang, H. H. (2002). Behavior of piled raft foundations under lateral and vertical loading. **The International Journal of Geomechnics** 2(1): 29-45.

T. V. Tran, S. Teramoto, M. Kimura, T. Boonyatee & Le Ba Vinh (2012). Effect of ground subsidence on load sharing and settlement of raft and piled raft foundations. **International journal of civil and environmental engineerining**. WASET 6: 177 – 184.

Ta, L. D., and Small, J. C. (1996). Analysis of piled raft systems in layered soils. **International Journal for Numerical and Analytical Methods in Geomechanics** 20: 57-72.

Tan, Y.C., Chow, C. M. and Gue, S.S. 2004. Piled raft with short piles for low-rise buildings on very soft clay. **Proceedings 15th SEAGC**, 171-176. Bangkok, Thailand.

Tan Y. C, Cheah S. W, Taha M. R. (2006). Methodology for design of piled raft for 5-story buildings on very soft clay. **Foundation analysis and design: innovative methods**. **Geotech Spec .Publ. (ASCE)** 153: 226–233.

Townsend F. C., Anderson J. B. and Rahelison L. (2001). Evaluation of FEM engineering parameters from in situ tests. Final report. Submitted to: Florida department of transportation. **Downloaded from vulcanhammer.net**.

Vincenzo Fioravante (1998). Load transfer mechanism of piled raft foundation. **Centrifuge 98**, Kimura al. el., Editor. Rotterdam: Balkema.

Vincenzo Fioravante, Daniela Giretti and Michele Jamiolkowski (2008). Physical modeling of raft on settlement reducing piles. **From Research to Practice in Geotechnical Engineering Congress (ASCE)** 325(2): 206 - 229.

Y. El-Mossallamy, associate Prof., Ain shams University, Cairo, Egypt c/o ARCADIS, Berliner allee 6, D - 64295 Darmstadt, Germany (2008). **Plaxis Bulletin issue 23 / March 2008**, pp.10-13.

Zeevaert, L. (1957). Compensated friction-pile foundation to reduce the settlement of buildings on the highly compressible volcanic clay of Mexico City. **Proc. 4th Int. Conf. Soil Mech. Foundn Engng**, 81−86. London, Aug. 1957.

Zeevaert, L. (1973). **Foundation engineering for difficult subsoil conditions**. New York: Van Nostrand Reinhold.

BIOGRAPHY

Mr. Tran Van Tuan was born in Long My, Hau Giang, Vietnam on 10th May 1983. He received his Bachelor of Engineering in Rural Engineering from Can Tho University of Vietnam in 2006. From 2007 to 2008, he continued his study to earn the degree of Master of Engineering in Geotechnical Engineering at Ho Chi Minh City University of Technology of Vietnam and Toyohashi University of Technology of Japan via Twinning Program.

In 2009, he applied for AUN/SEED-Net (JICA) scholarship to study PhD sandwich programme in Geotechnical Engineering at the Department of Civil Engineering of Chulalongkorn University, Thailand. His advisor was Associate Professor Tirawat Boonyatee (Chulalongkorn University) and his co-advisor was Professor Makoto Kimura (Kyoto University). He spent 8 months of his PhD sandwich program in Infrastructure Innovation Engineering Laboratory at Kyoto University as a trainee.

He has published 2 international journals (International journal of civil and environmental engineering, WASET (2012) and Open Journal of Civil Engineering (2012)), 1 national journal (Journal of Science and Technology, Vietnam (2012)) and 3 proceedings (The 22nd KKCNN Symposia on Civil Engineering (2009), The 24th KKCNN Symposia on Civil Engineering (2011) and 1st International Conference on Sustainable Civil Engineering Structures and Construction Materials (2012)).

His main research theme was to evaluate the behavior of piled raft foundation under the effects of ground subsidence and piled spacing by using simplified method, FE analyses and centrifugal model tests. His dissertation is completed on 2nd semester of 2012.